LABORATORY AND NUMERICAL INVESTIGATIONS OF SOIL RETENTION CURVES

by

MONICA LUCIA MELGAREJO CORREDOR
BSc, MSc

June 2004

A thesis submitted to the University of London
(Imperial College of Science, Technology & Medicine)
in partial fulfillment of the requirements for the degree of
Doctor of Philosophy in the Faculty of Engineering

To my father,
who I miss

ABSTRACT

This thesis discusses a key component of partly saturated soil, the Soil Water Retention Curve (SWRC). As a soil dries from a slurry, its suction increases and its degree of saturation and water content decrease. On subsequent wetting the soil from a dry state it does not follow the same path but is hysteretic, thus forming the principal drying and wetting curves of the SWRC. All drying-wetting curves for that soil, e.g. in its natural in-situ state, lie between these principal curves.

Eight different soil types were investigated to assess changes in the shape and position of the SWRC for different soil characteristics. Comprehensive drying and wetting paths were followed experimentally to model a number of conditions that occur in nature, particularly with relation to cyclic seasonal fluctuations.

Suction is notoriously difficult to measure. In this study the filter paper method was primarily used, for which a thorough appraisal and suggested improvements have been made. A modified pressure plate apparatus was also designed for the improved measurements of very low suctions. The experimental data revealed some distinct characteristics of the SWRC related to the soil type and to these relations are described in a qualitative sense. Various mathematical formulations have been proposed in the past to model the SWRC, its hysteresis and different components. These were reviewed and the van Genuchten equation and Luckner formulation selected to model the experimental data. The ultimate intention is to implement these formulations in numerical analyses.

The van Genuchten equation was found to model the principal curves of the SWRC well in most cases. Relationships were investigated between the van Genuchten parameters (α, n, m) and soil characteristics such as the Atterberg Limits. Reasonable trends were evident but it was not possible to establish accurate and reliable quantitative relationships. It is likely that factors, such as the particle size distribution, also need to be considered. The Luckner formulation was found to model the scanning curves within the boundary curves reasonably well in most cases.

Numerical analyses were performed implementing the SWRC, to model field tests in a residual soil, using the van Genuchten equation (without taking hysteresis into account). Appropriate parameters were established using a curve-fitting technique, which then were applied to other field test data at the same location. Very good agreement was found between the numerical analysis and the field data. A numerical parametric study indicated that the factors that have the greatest influence are the van Genuchten n value, controlling the slope of the SWRC, and the saturated permeability.

ACKNOWLEDGEMENTS

I would like to express my gratitude to the Soil Mechanics Section at Imperial College and to the ORS for their financial support. The assistance given by the National University of Colombia is acknowledged.

I would like to thank to my supervisors Professor David Potts and Dr. Andrew Ridley for their helpful suggestions and assistance throughout my PhD. I want especially to recognise the collaboration and support given by Prof. Potts during all these years – they are much appreciated!

Particular gratitude I want to express to Dr. Lidija Zdravkovic for her technical help, especially during the period I worked in F.E., for her friendship since I came to London and for that hug she gave me when I needed it most. Special gratitude is also expressed to Dr. Jamie Standing for his enormous collaboration correcting my grammar and understanding my first drafts of the thesis, for his time, friendship and positive thoughts. I am very grateful to Graham, Alan and Steve for their technical support in the laboratory. I want to reserve special thanks to Steve for his friendship, teaching about laboratory work, equipment and advice during all these years.

I appreciate very much Matthew for all those conversations about life and the universe, for his trust and for his lessons about Soil Mechanics and laboratory work.

Particular thanks to Liana for those funny and enjoyable days at College and to Beatrice for her relaxing friendship, her understanding and for being always there. I am very grateful to Michele for her support and love specially in all those difficult days, I will never forget these two phrases 'a horse is a horse' and 'I can not be more complicated'! I would like also to thank very much to Pedro because of his patience, care and strong support, also for his help when I was stressed, I am sorry for being so stressful sometimes!

My deepest gratitude goes to Daniela, Natalia and David for all those kisses through the phone, they made my life sweeter in London, to Yolanda, Gabriel and German for their enthusiastic support and belief in me. There are no words to thank my mother for her help and love during all these years. I love all of you.

I want also to express my deepest gratitude to Julio for his faith, support and love during our period here in London. Thanks for sharing life with me.

TABLE OF CONTENTS

LIST OF FIGURES

LIST OF TABLES

LIST OF ABREVIATIONS

α_3	Maximum suction difference between the main wetting and drying curves at the same moisture content
α, n, m	van Genuchten parameters
β'	Bounding factor (Croney et al.)
χ	Bishop parameter
$\left(\Delta\upsilon/\Delta\varepsilon_s\right)_f$	Dilatancy index at failure
ε_s	Shear strain defined as $\varepsilon_s = 2(\varepsilon_1 - \varepsilon_3)/3$
ϕ	Porosity
ϕ'	Friction angle
ϕ^b	Slope of the failure envelope in the shear strength matrix suction plane
γ_t	Total unit weight
γ_d	Dry unit weight
κ	Elastic compressibility coefficient (slope of the swelling line)
λ	Elasto-plastic compressibility coefficient (slope of the normal compression line)
λ_p	Pore size distribution index
λ_a	Mass rate of air flow
π	Osmotic suction
π_c	Capillary pressure
θ	Volumetric water content
θ_a	Volumetric water content at the residual air content
θ_f	Terminal residual or final volumetric water content
θ_i	Volumetric water content at point i
θ_r	Initial residual volumetric water
θ_s	Volumetric water content at saturation point
θ_{mdc}	Volumetric water content on the main drying curve
θ_{mwc}	Volumetric water content on the main wetting curve
θ^{n+1}	Volumetric water content of the new point of the predicted scanning curve
$\theta^{n+1}{}_{mdc}$	Volumetric water content at a starting point of a predicted scanning curve from a main drying curve

$\theta^{n+1}{}_{mwc}$	Volumetric water content at a starting point of a predicted scanning curve from a main wetting curve.
Θ	Normalised volumetric water content
ρ_w	Density of water
σ	Total stress
σ'	Effective stress
$\sigma'_a, \sigma'_b, \sigma'_c$	The principal effective stresses
$(\sigma_1 - \sigma_3)$	Deviator stress at failure
$(\sigma_1 - u_a), (\sigma_3 - u_a)$	Major and minor net total stresses,
σ'_{nf}	Effective normal stress at failure
τ	Shear strength
τ_f	Shear stress at failure
ν	Angle of dilation
v_a	Velocity of air flow
v_{w0}	Inverse of the density of water
v_w	Velocity of the water flow
ϖ	Slope term line
Ω	Parameter governing the water flow resulting from a change in the soil volume
ψ	Total suction
ψ_{tr2}	Transition suction pressure at which the soil changes from drying to wetting
ψ_{tr1}	Transition suction pressure at which the soil changes from wetting to drying
ψ_a	Matrix suction at the residual air content
ψ_{AEV}	Suction at the graphic air-entry value
ψ_{des}	Suction at desaturation point
ψ_c	Suction where the hysteresis curves merge
ψ_f	Terminal residual or final matrix suction
ψ_i	Suction at the i point
ψ_r	Initial residual matrix suction
ψ^{n+1}	Suction at a new point of a predicted scanning curve
ψ_u	Suction at which the main curves separate
a, n	Dimensionless material constants (relation to Gardner's equation)
AEV	Air-entry value

c'	Effective cohesion
d	Particle diameter
d_m	Minimum particle diameter (mm)
d_r	Residual particle diameter (mm)
D	Transmission constant of proportionality for the air phase
$e=\left(V_v/V_s\right)$	Void ratio
e_w	Equivalent void ratio
$f(s)$	Intercept of the failure lines on the axis $(p-u_a)$
g	Gravitacional accelaration
g_a	Fitting parameter corresponding to the initial change in the slope in the particle-size distribution curve
g_m	Fitting parameter corresponding to the curvature of the particle-size distribution curve
g_n	Fitting parameter corresponding to the maximum slope of the particle-size distribution curve
G_s	Specific Gravity
h_w	Total head in the water phase
H	Elastic modulus for the soil structure with respect to the matrix suction (ICFEP input parameter)
k_s	Saturated permeability also $k_{\max}$
k_w	Coefficient of permeability with respect to the water phase for unsaturated soil
M_a, M_w, M_s	Soil parameters that depend on degree of saturation, total stress and suction ratio
M'	Inclination of the failure lines
MDC, MWC	Main drying and main wetting curve respectively
p	Total mean stress (confining stress) $\left(1/3(\sigma_1+\sigma_2+\sigma_3)\right)$
p''	Pore water deficiency (Atkhinson,1961)
$(p-u_a)$	Net mean total stress
$P_p(d)$	Percent passing a particular grain-size distribution, *d*
PDC, PWC	Principal drying and principal wetting curve respectively
PSC	Primary scanning curve
(PSC)1D	Primary scanning curve, first drying path
(PSC)1W	Primary scanning curve, first wetting path
q	Deviator stress

R	Universal gas constant ($8.314 Jmol^{-1}K^{-1}$)
R	Gradient of the SWRC governing the change in the water storage within the soil due to a change in suction (ICFEP input parameter)
s	Matrix suction
S	Degree of saturation
S_a	Saturation at the residual air content
S_e	Effective degree of saturation
S_f	Terminal residual or final degree of saturation
S_o	Yield suction
S_r	Initial residual degree of saturation
SSC	Secondary scanning curve
t	Temperature (^{O}C)
T	Absolute temperature, K ($273.16+t^{O}C$)
TSC	Tertiary scanning curve
u_a	Pore-air pressure
u_{eq}	Equivalent pore pressure
u_v	Partial pressure of pore-water vapour
u_{vo}	Saturation pressure of water vapour over a flat surface of pure water at the same temperature
$\left(\frac{u_v}{u_{vo}}\right)$	Relative humidity
u_w	Pore-water pressure
$(u_a - u_w)$	Matrix suction at any point
$(u_a - u_w)_{AEV}$	Matrix suction at the AEV
w_v	Molecular mass of water vapour
w/c	Gravimetric water content (also w)
$(w/c)_L, (w/c)_P, PI$	Liquid limit, Plastic limit and plasticity index

GLOSSARY

AEV: Air-entry value

Cavitation: Rupture of a liquid may take place when suction increases, resulting in vapour/air entering within the liquid. The suction at which this occurs depends on the tensile strength of the liquid. In large volumes, water cavitates when the water pressure reaches about -100kPa (at 20°C). Water can sustain greater tension under appropriate conditions as the theoretical tensile strength of water is of the order of tens of MPa. Water under tension is in a metastable condition until nucleation occurs (the formation of vapour cavities within the liquid itself or at its boundaries). Cavitation is slowed down in the absence of cavitation nuclei (e.g. in a Berthelot tube) and experimental values as low as –17MPa have been measured.

Deformation state variable: Non-material variables required for the characterisation of the deformation conditions or deviations from an initial state.

Diffusion: The independent or random movement of ions or molecules (usually of air for partially saturated soils) to produce a more uniform (diffuse) distribution when there are concentration gradients.

Gauss point: Points at which Gaussian integration is carried out within a finite element in numerical analysis.

ICFEP: Imperial College Finite Element Program.

Osmotic suction gradient: process where ionic or molecular constituents move as a result of their kinetic activity (i.e. an osmotic gradient across a semi-impermeable membrane causes the movement of water through the membrane).

Relative humidity: Reflects the concentration of water vapour in air and is usually expressed as the ratio $\overline{u}_v / u_{v0}$. When the relative humidity is zero, the air is completely dry, and when it is unity the air cannot hold any more water vapour (with conditions of constant temperature and pressure).

Soil fabric: Refers to the arrangement of particles groups and pore spaces in a soil (Mitchell, J.K., *'Fundamental of Soil behaviour'*, 1976). Sometimes referred to soil texture.

Soil structure: Combined effect of fabric, composition and inter-particle forces. It is determined by the particle arrangement (fabric) and inter-particle forces and bonding.

Stress state variable: Non-material variables required for the characterisation of the stress condition (e.g. σ, σ')

SWRC: Soil-water retention curve.

Water vapour pressure: Pressure exerted by water vapour present in air, commonly expressed as partial pressure of water vapour in the air, $\bar{u}_v$. Air becomes saturated with water vapour when typically there is 4 - 5% by volume present, the saturated water vapour pressure is given by $\bar{u}_{v0}$.

Wilting point: It is a term originally used by soil scientists to reflect the maximum suction that plants can exert on the water phase of soil (before they start to wilt).

CHAPTER 1

INTRODUCTION TO SUCTION AND SCOPE OF THE RESEARCH

In many natural conditions the water table drops below the ground surface (e.g. by evaporation, evapo-transpiration). Above the phreatic surface, if the soil pore-water were only under the influence of gravity, the soil would be completely dry. However, physio-chemical forces act at the boundary between the soil and the water. Those forces cause the water to be drawn into the empty voids or held there without drainage following infiltration from the surface (Ridley et al., 2003). The pore-water pressure in the ground above the phreatic surface becomes negative with respect to atmospheric pressure and this negative pressure is referred to as suction. It is caused primarily by capillary action (Appendix 1) and can lead to consolidation and eventually desaturation in the soil. When a soil is not fully saturated, water can contain occluded air bubbles or have air present in continuous phases. The air phase becomes continuous when the degree of saturation (defined as the ratio of the volume of water to the volume of voids) is less than approximately 85-95%. When the degree of saturation is greater than about 95%, the air present is in the form of occluded bubbles and in many respects soil in this state still follows Terzaghi's principle of effective stress.

Desaturation of a deposit can also be produced by compaction processes. Environmental changes, such as increases in salt concentration, also produce changes in the soil pore-water pressure distribution, leading to shrinkage or swelling of the soil deposit.

A soil with an increasing negative pore-water pressure will eventually become an unsaturated soil. In general, the distinction between saturated and unsaturated soil mechanics is described by the degree of saturation (the ratio of the volume of water to the volume of voids). However, it is difficult to measure the degree of saturation of a soil directly and to use it as a key parameter in the analysis of unsaturated soil behaviour (Fredlund and Rahardjo, 1993). The state of stress in the water phase is frequently used as the primary quantity for classification purposes. The water in saturated soils is essentially incompressible while for unsaturated soils, the pore fluid becomes compressible as air bubbles appear in the water.

When analysing conditions within a soil element, a saturated soil is considered as a two-phase system, and an unsaturated soil with a continuous air-phase a four-phase system (Fredlund and Morgenstern, 1977). The four phases of an unsaturated soil are solids, water, air and an air-water interface or contractile skin (see Figure 1.1). The air-water interface is the boundary between the two homogeneous phases (water, and air), it can be quantified as an independent phase as it has different properties to those of the surrounding continuous materials. The air-water interface can be considered as a lamina or film with thickness and definite bounding surfaces.

On the other hand, from the perspective of volume-mass relations for unsaturated soils (see Figure 1.1 b), the contractile skin's volume is so small, that it is possible to consider it as negligible or to take its mass as a part of the water (the latter is adopted for a rigorous phase diagram analysis). In view of this, an unsaturated soil is considered as a three-phase system in this thesis. However, it is necessary to appreciate that the air-water interface behaves as an independent phase when considering an analysis with a multiphase system.

Fredlund and Morgenstern (1977) define an unsaturated soil as a combination of two phases that come to equilibrium under an applied stress gradient (i.e. soil particles and air-water interface) and two phases that flow under applied stress gradients (i.e. air and water).

The air-water interface (contractile skin) induces an inter-particle normal stress due to the pore-water pressure. A saturated soil usually possesses positive pore-water pressure. It can also exist at low suctions up to the point when cavitation (see Glossary) occurs (usually at about -100kPa gauge pressure) at which point it becomes desaturated. An unsaturated soil is usually characterized by negative pore-water pressure (suction) which applies a tensile pull at all air-water interfaces in the soil profile (Figure 1.1c). However, soil with occluded air bubbles within its pore fluid can also exist at low positive pressures up to the point when the air contracts sufficiently such that it dissolves (these processes are controlled by Boyle's and Henry's laws).

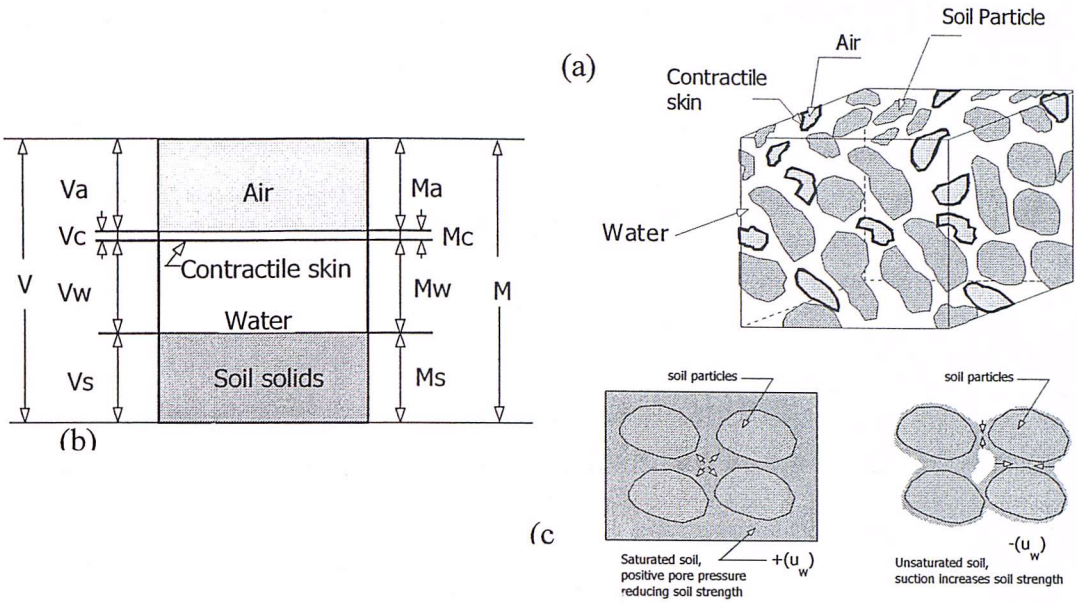

Figure 1.1 Element of unsaturated soil, (a) with a continuous air phase, (b) rigorous phase diagram, (c) effect of pore pressure on soil strength

In an unsaturated soil where air exists in continuous phases, the surface tension (see Appendix 1) on the contractile skin pulls the particles together providing additional strength. In the case of a saturated soil, the positive pore-water pressure (u_w) reduces the strength. At the air-water interface of an unsaturated soil, the pore-air pressure (u_a) is greater than the pore-water pressure (u_w). The difference $(u_a - u_w)$ between these two independent pressures is referred to as the soil matrix suction (s). Matrix suction is of particular interest because it is the stress variable which is strongly influenced by environmental changes encountered in the field.

The pore water in a soil can contain dissolved salts. The water vapour pressure (see Glossary) over a flat surface of a solvent is less than the vapour pressure over a flat surface of pure water. As the relative humidity is directly related to the water vapour pressure, this also decreases with increasing dissolved salts in the soil pore-water. Osmotic suction (π), is related to the decrease in relative humidity caused by the presence of dissolved salts in the pore-water. In reality, dissolved salts are present in both saturated and partly saturated soils, and so the effect of osmotic suction is equally significant in both saturated and unsaturated soils. The mechanical behaviour of a soil can be affected by changes in osmotic suction due to changes in salt concentration in the soil pore-water. Osmotic suction is difficult to quantify specifically by direct or indirect measurements and typically is not determined in the majority of soil mechanics applications.

Total suction is equal to the sum of the matrix and osmotic components. However in terms of their effect on the soil behaviour, osmotic and matrix suctions are not

necessarily additive. Matrix suction is defined with respect to a macro-scale element involving soil particles, soil pore-fluid and air. Osmotic suction is defined with respect to a micro-scale element relating to the chemical composition of the soil water solution (Fredlund and Morgenstern, 1977). Therefore, it is perhaps not valid to sum forces relevant to different phases; matrix and osmotic suction being associated with the contractile skin and water phases respectively.

Although methods are available for the measurement of each component of suction, few documented cases are available in which an independent measurement of matrix and osmotic suction have been performed and their sum compared with the measurement of total suction on the same sample.

However, total suction may be determined by the measurement of the vapour pressure in equilibrium with the soil water. As the vapour pressure is controlled by dissolved salts in the soil pore-fluid combined with the hydrostatic tension of the pore-water, it gives credibility to this method of determination of total suction (Krahn and Fredlund, 1972).

Environmental changes, particularly changes in applied load, produce consolidation or swelling and hence a change in the water content of a soil. Typical ranges of water content changes that occur in most geotechnical engineering applications produce changes in total suction; however, those changes are due primarily to changes in matrix suction. Nevertheless in situations where significant changes in pore fluid salt concentration occur, there will be an associated change in osmotic suction that can not be neglected.

In the following section conventional definitions of the three components of the soil suction are given.

DEFINITIONS OF SUCTION 1.1

Total suction ψ, is defined by Aitchinson (1965) and quoted by Fredlund and Rahardjo (1993), as the equivalent suction derived from the measurement of the partial pressure of the water vapour in equilibrium with the soil-water relative to the partial pressure of water vapour in equilibrium with free pure water.

The relationship between total suction and partial pressure of the pore-water vapour can be written as follows:

$$\psi = -\left(\frac{TR}{v_{w0} w_v}\right) \ln\left(\frac{u_v}{u_{vo}}\right) \qquad (1.1)$$

where:

ψ total suction (kPa)

R universal gas constant ($8.314 Jmol^{-1}K^{-1}$)

T absolute temperature, K ($273.16+t^{O}C$)

t temperature, (^{O}C)

v_{w0} inverse of the density of water (m^3/kg), (i.e. $\rho = 998$ kg/m^3 at 20°C)

w_v molecular mass of water vapour (i.e. 18.016 kg/kmol)

u_v partial pressure of pore-water vapour (kPa)

u_{vo} saturation pressure of water vapour over a flat surface of pure water at the same temperature (kPa)

$\left(\frac{u_v}{u_{vo}}\right)$ relative humidity

The above equation shows that the total suction is a function of temperature and the relative humidity above a flat surface of pure water (e.g. at a 20°C the fixed relationship between total suction in kPa and the relative humidity can be written as: $\psi = -135022 \ln\left(u_v / u_{vo}\right)$). When the relative humidity is 100% the total suction in the soil will be zero, in contrast, a relative humidity lower than that indicates suction in the soil. A relative humidity less than 100% indicates a partial pressure lower than the saturation pure water vapour pressure over a flat surface at the same temperature. A reduction in the relative humidity can be related to a curved water surface (e.g. the meniscus in a capillary tube, see Appendix 1). The relative humidity decreases as the radius of curvature of the water surfaces decreases. The radius is inversely proportional to the difference between the air and the water pressures across the surface (i.e. $u_a - u_w$), the matrix suction of a soil, this being one component of the total suction. Additionally, as discussed earlier, a decrease in relative humidity due to the presence of dissolved salts in the pore-water of a soil is related to the osmotic component of the total suction. In conclusion, the total soil suction, sometimes called the 'free energy' of the soil water, has two components: matrix suction and osmotic suction, and it can be written as follows:

$$\psi = (u_a - u_w) + \pi \qquad (1.2)$$

Where:

$(u_a - u_w)$ matrix suction

u_a pore air pressure

u_w pore water pressure

π osmotic suction

The total suction represents the combined effects of capillarity and vapour pressure reduction due to dissolved salts in a bulk solution.

Matrix suction $(u_a - u_w)$ is the capillary component of the soil suction and it is related to the energy required to move water within the soil without the water vaporising. Matrix suction is the result of two kinds of forces, adsorption and capillarity.

Adsorption describes the soil particles' propensity for attracting water. Soil particles hold water molecules tightly at their soil-water interfaces. These adsorbed water molecules in turn hold by cohesion (the attraction of molecules for each other) other water molecules further away from the solid surfaces. Together, these forces enable the soil particles to retain water and control its movement and utilization.

Aitchinson, 1965, defined matrix suction as "the equivalent suction derived from the measurement of the partial pressure of the water vapour in equilibrium with the soil water, relative to the partial pressure of the water vapour in equilibrium with a solution identical in composition with the soil water". In other words, matrix suction is the affinity that a soil has for water in the absence of any salt content gradients (Huston et al., 1993).

Matrix suction is the attraction that the water has for the soil particles. This attraction along with the surface tension of water also accounts for the capillary force. Matrix suction is governed by the size of pores in a soil in a similar manner to the capillary analogy (see Appendix 1). In other words, the smaller the void, the harder it is to remove the water from the soil.

Matrix suction is the suction component that is of main interest for understanding the engineering behaviour of unsaturated soils. It is also used for estimating the average in-situ effective stress, controlling compaction processes and assessing the stability of natural slopes (Ridley et al., 2003).

Osmotic suction π, is attributable to the presence of solutes in the soil-water. Osmotic suction is related to the decrease in relative humidity due to the presence of dissolved salts in the pore-water. It is the energy required for the water vapour to escape from the surface of a liquid. Aitchinson, 1965, defined it as "the equivalent suction derived from the measurement of the partial pressure of the water vapour in equilibrium with a solution identical in composition to the soil water, relative to the partial pressure of water vapour in equilibrium with free pure water". Osmotic suction derives from the salt content in the soil pore-water and it changes with the variation in salt content from one point to another (Huston et al. 1993).

The salt dissolved in the soil pore-water does not affect the matrix suction. However, a change in the concentration of salt in the pore-water may affect the physio-chemical forces acting at the particles' water interfaces and as a consequence can be reflected

as a change in the relationship between the soil behaviour and the suction acting in it (Burland and Ridley, 1996).

Osmotic suction is a function of the soil pore fluid chemistry. It impacts on the inter-particle stresses on a fundamentally different scale and by essentially different mechanisms than the matrix suction. On a microscopic scale, in a colloidal suspension of clays for example, the thickness of the diffuse double-layer and the degree to which ions held within those regions are restricted from moving along with the bulk solution, depend fundamentally on the salt concentration of the bulk solution. The repulsive forces between clay particles are attributed primarily to overlapping double-layers and the osmotic pressure concept.

In summary, the total suction is a measure of the combined matrix (mechanical) and osmotic (physicochemical) equilibrium state of the soil pore-water fluid.

RELEVANCE OF SOIL SUCTION AND APPLICATION TO PRACTICE 1.2

As discussed earlier in this chapter there are many situations where soils have negative pore-water pressures and are partly saturated, in fact fully saturated conditions represent one specific case. In practice soils generally do not exist in one set condition, but are in a continuous state of flux, with suction, water content and degree of saturation varying with environmental changes.

For a particular soil these changes in condition can be linked using relationships between suction (usually total suction) and either gravimetric moisture content, volumetric water content or degree of saturation. These relationships are often collectively referred to as the Soil-Water Retention Curve (SWRC), a general example is shown in Figure 1.2. It can be seen that there are two different curves, one for wetting, the other for drying, i.e. the relationship is hysteretic. The curves shown represent boundary curves derived from a soil initially formed from a slurry. The relationships for a natural soil will lie somewhere between these curves. There are in fact an infinite number of sub-curves within the outer boundary curves.

Currently, analytical frameworks for the behaviour of partly saturated soils lack a detailed implementation for this relationship. The SWRC clearly is of fundamental importance as it relates suction, which is a difficult quantity to measure, to basic quantities such as water content. Suction is important as it controls a soil's stress level which in turn is directly related to its strength and compressibility characteristics.

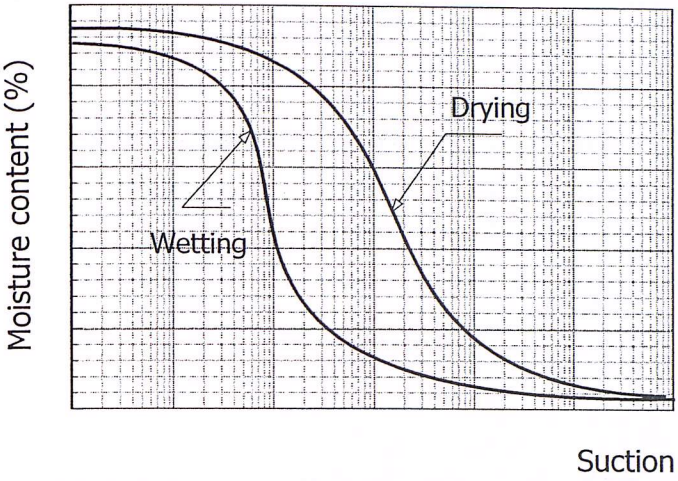

Figure 1.2 Schematic example of the hysteretic soil-water retention curve

The research described in this thesis sets out to investigate experimentally in detail the SWRC and its characteristics for a number of soils under the condition of zero total stress. It also investigates the accuracy of proposed analytical expressions for the curves with a view to implementing them in constitutive models for partly saturated soils.

SCOPE AND CONTENT OF THESIS 1.3

A brief description of partly saturated soils, definitions of suctions and an introduction to the Soil-Water Retention Curve (SWRC) are given in this chapter.

Many researchers have suggested different formulations and analytical expressions to represent the SWRC. In Chapter 2, the SWRC is characterised in detail and some of the current relationships are reviewed and compared, highlighting their advantages and shortcomings. The intention of this review is to establish which relationship is the most appropriate for the soils investigated in this research. Details of some of the formulations are given in Appendix 2.

Chapter 3 starts with a review of the equations and frameworks that currently exist for describing the mechanical behaviour for partly saturated soils. It then goes on to explain briefly how the Finite Element method is used to model partly saturated soil behaviour. Simplified constitutive models have been implemented in the Imperial College Finite Element Program (ICFEP) by others (e.g. Georgiadis, 2003 and Smith, 2003). The model implemented by Smith uses a very simplified hypothetical SWRC that does not account for the hysteretic behaviour often observed in natural soils. This is described and its shortcomings explained.

As the main emphasis of this research involves an experimental investigation of the SWRC for various soils, a key component of this work is the measurement of soil

suction. Soil suction is notoriously a very difficult quantity to measure accurately. There are a number of methods available for measuring suction directly and indirectly by relating it to other quantities such as moisture content. The various methods and those adopted in this research are described in Chapter 4.

During the course of the experimental programme, much was learnt about the filter paper technique (the most frequently used method of suction measurement in this study). In Chapter 5 the method is discussed with particular emphasis on expected accuracy (an error analysis is described) and the equilibration time allowed between measurements. Suggestions are also given for improving the technique.

In Chapter 6 the results from the experimental study are presented, described and discussed. Soils from eight locations across the globe were investigated, including residual soils from Colombia, Brazil and Hong Kong, clays from the UK and Colombia and an ash fill. Complete SWRCs were established for most of these soils and their characteristics and differences are discussed.

In Chapter 7 The SWRCs were modelled using some of the available expressions (described in Chapter 2). The findings from this study are discussed first and equation constants related to the soil characteristics. The most appropriate model is considered for future implementation in ICFEP.

Chapter 8 describes the implementation and development of the SWRC models for numerical analysis. It goes on to present the results from preliminary ICFEP runs used to simulate a simple boundary value problem.

Conclusions and recommendations for further research are given in Chapter 9.

CHAPTER 2

SOIL-WATER RETENTION CURVE

The moisture content (or water content) of a soil defines the amount of water within the pores of the soil. It is generally quantified by mass in terms of gravimetric water content, w/c, but it is sometimes represented in terms of volumetric water content, θ, or by degree of saturation, S. Additionally, when the pressure in the pore-water is negative, it is called suction and suction in the soil matrix is related to the inter-particle forces, the amount of water present in the soil pores and the pore water chemistry.

Two different forms of the relationship between moisture content and soil suction have been identified. The first form is obtained from soil specimens compacted at different densities and moisture contents, (these samples are not identical in the sense that they may have different fabrics). In addition, different methods of compaction result in different structure. The second form of the relationship between moisture content and soil suction is called the ***Soil-Water Retention Curve (SWRC).*** This curve is obtained by testing one soil specimen or several identical soil specimens. This relationship shows the progressive decrease or increase in moisture content as a single specimen (or several identical ones) dries or wets, with a corresponding increasing or decreasing suction. There is a unique relationship between the SWRC of a soil and the behaviour of a soil. In general, the SWRC defines the relationship between the volumetric moisture content in the soil and the suction (Adams, et al., 1996).

The important difference between these two relationships is that the SWRC characterizes a particular soil with a certain fabric. A variation in suction in this case is induced by wetting or drying. It is essential to recognise that there may be considerable hysteresis in the SWRC. Accordingly, if the stress history of the soil is not known, knowledge of the moisture content only (i.e. a deformation or strain state variable) may not be sufficient for determining the matrix suction. (i.e. a stress state variable) (Adams, et al., 1996). The central subject of the research described in this thesis is to study the Soil-Water Retention Curve (SWRC), its features and behaviour.

In the case of the relationship between the moisture content and the suction of a soil with the same fabric (i.e. the SWRC), it can be plotted in terms of gravimetric water

content, volumetric water content or degree of saturation against suction (usually on a logarithmic scale). It might be expected that one unique curve of each type exists for any particular soil. The three different curves (depending on the way of quantifying the moisture content) would be related and logically be similar in appearance.

Laboratory data have indicated that a change in total suction is essentially equivalent to a change in the matrix suction for many situations (Fredlund & Rahardjo, 1993). Therefore, the SWRC is usually defined in terms of the matrix suction. At high suctions (greater than about 1,500kPa) matrix suction and total suction can generally be assumed to be equivalent.

The soil-water retention curve is controlled by three important aspects of the soil state: pore size distribution, amount of moisture contained in the pores at any suction and the stress state of the soil. Additionally, as just stated, the SWRC exhibits hysteresis which is a phenomenon that affects most porous media. It is the difference observed in the SWRC depending upon whether the sample is wetting or drying.

The advantage of using the SWRC in the analysis of partly saturated soil behaviour is that in general it is straightforward and cheap to establish the moisture content of a soil and its suction. However, it is time consuming to develop the entire curves in the drying and wetting ranges of matrix suction and different types of equipment are required (e.g. pressure plates and suction probes) for measuring the entire range of suction accurately.

The moisture content–suction relationship was used originally by soil scientists for predicting the availability of water for plants. For engineering purposes, it is mainly used for deriving and linking soil behaviour such as the permeability, shear strength and volume change of a partly saturated soil. It can be used as a basic component representing the engineering behaviour of an unsaturated soil. The SWRC provides a means of relating fundamental soil properties to each other and defining the state at which engineering behaviour is assessed. This is important when modelling more than one aspect of soil behaviour in analysis (Adams, et al., 1996).

2.1 CHARACTERIZATION OF THE SOIL-WATER RETENTION CURVE

The moisture content of a soil at various matrix suctions determines the SWRC. Generally, the moisture content range in the SWRC is represented using an arithmetic scale and the SWRC is plotted on a logarithmic scale over the entire suction range.

The general shape of the SWRC is sigmoidal describing a smooth S-shape as shown by the boundary curves in Figure 2.1.

The SWRC is generally presented in terms of volumetric water content, θ. This is defined as the ratio of the volume of water to the total volume of soil. The volumetric water content can be written as follows:

$$\theta = \frac{V_w}{V} = \frac{SV_v}{V} = S\phi = \frac{(Se)}{(1+e)} \qquad (2.1)$$

where:

θ volumetric water content,
S degree of saturation,
e void ratio, and
ϕ porosity.

It can be seen that when a soil is fully saturated, the saturated volumetric water content, θ_s, is equal to the porosity of the soil.

The relationship between volumetric water content, and gravimetric water content, w/c, can be written as follows:

$$\theta = \frac{(w/c)\rho_d}{\rho_w} \qquad (2.2)$$

where:

ρ_d dry density of the soil
ρ_w density of water
w/c gravimetric water content

The volumetric water content is often normalized by using the saturated volumetric water content, θ_s. In this case the normalized volumetric water content, Θ is equivalent to the degree of saturation, S, it can be written as follows:

$$\Theta = \frac{\theta}{\theta_s} = \frac{Sn}{n} = S \qquad (2.3)$$

A change in matrix suction can produce a more significant change in the degree of saturation or moisture content than can be produced by a change in the net total stress (defined as the total stress σ minus the pore air pressure u_a, $(\sigma - u_a)$). The degree of saturation (S) and the matrix suction are commonly used to describe another general representation of the SWRC. The degree of saturation, for the analyses of unsaturated soil properties, provides better conditioned curves than the volumetric water content in some situations. However, volumetric water content can be measured with greater accuracy than the degree of saturation, as discussed in

Chapter 5, and for this reason θ is often used in preference to S. When the degree of saturation is used, it is asymptotic to a horizontal line at zero suction.

Many researchers have shown that there is a relationship between the SWRC for a particular soil and the properties of the soil in a partly saturated state. To investigate these relations the SWRC must be determined experimentally in the laboratory.

In the laboratory the SWRC can be obtained by taking a soil sample in its initial state (which might be fully or partly saturated) and gradually drying it, taking measurements of suction and moisture content during the drying process. If, from an air-dry state, the sample is subsequently wetted up the relationship between suction and moisture content will be different because of the phenomenon of hysteresis. The two curves are often termed boundary curves (see Figure 2.1). The end of the wetting curve may differ from the starting point of the drying curve because of air entrapment in the soil. Both curves have a similar form.

The hysteresis effect may be attributed to several causes: the geometric non-uniformity of the individual pores, the pore fluid contact angle, entrapped air and swelling, shrinking or ageing. Hysteresis is very important where wetting and drying cycles occur such as in many natural environments in the field. The natural SWRC relationship is contained within two boundary curves, but will probably have a unique form, particularly if small wetting and drying cycles occur. These intermediate curves are often called scanning curves (see Figure 2.1), and are likely to be representative of the real behaviour of a soil deposit (Hillel, 1998).

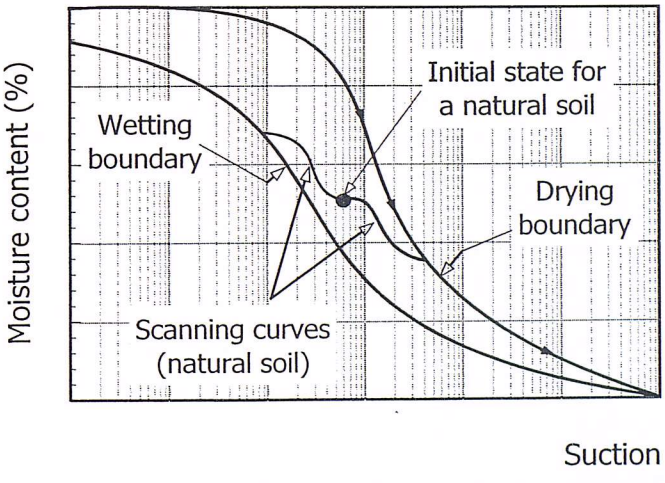

Figure 2.1 Hysteretic soil-water retention curve (drying and wetting paths of an initially partly saturated soil)

The amount of water present at relatively low values of matrix suction (0 to 100kPa) depends primarily on the capillary effect and the pore-size distribution and hence, suction is strongly influenced by the fabric of the soil. On the other hand, moisture content at the higher suction range is governed by the amount of adsorbed water

and, as a result, the suction is influenced less by density and more by the grain size and specific surface of the soil.

The shape of the soil-water retention curve is affected by the particle size distribution, pore size distribution, soil fabric, soil texture and the drying and wetting processes. Typical soil-water retention curves for sandy, silty and clayey materials with a uniform pore size distribution are shown in Figure 2.2(a). In general the shape and the range of the SWRC depend strongly on soil texture. A greater clay content induces a greater moisture retention at any particular suction and a more gradual slope of the curve. In a sandy soil, most of the pores are relatively large, and once these large pores are emptied at a given suction, only a small amount of water remains. In a clayey soil the pore size distribution is more uniform and more of the water is adsorbed, so applying increments of matrix suction causes a more gradual decrease in moisture content.

The existence of two distinct pore size distributions results in a bimodal soil water retention curve (Figure 2.2(b)). In the majority of studies, bimodal soil water retention curves have been observed for structured soils, such as aggregated loams, (Smettem and Kirby, 1990; Wilson et al., 1992; Mallants et al., 1997). Bimodal soil retention curves also have been observed for porous media that exhibit significant secondary structure, such as fractured tuff (Peters and Klavetter, 1988; Pruess et al., 1990; Wang and Narasimhan, 1985, 1990). In general, the multi-modal shape of the SWRC is due to both a secondary (structural) pore system, i.e. a macro-pore system, in addition to the primary (textural) pore system (Mallants et al., 1997).

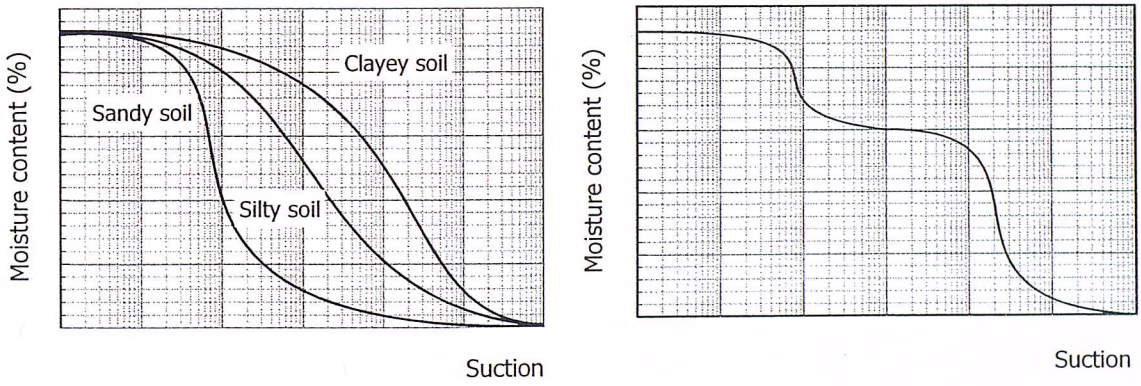

Figure 2.2 Typical soil-water retention curves (a) for sandy, silty and clayey materials (b) for a soil with two distinct pore size distributions

Soil density also affects the shape of the soil-water retention curve, particularly in the low suction range. As the dry density of the soil reduces so the slopes within the SWRC increase, evident for example, in soils compacted to different initial dry densities (see Figure 2.3).

In general, the soil structure of compacted soils influences the shape of the SWRC mainly in the low suction range. The distribution of intermediate size pores is likely to increase with soil density (as some of the originally large pores have been squeezed to an intermediate size by the compaction). As a result of increasing the density, the saturation moisture content and the initial decrease of moisture content with the application of low suction are reduced. The intra-aggregate micro-pores remain unaffected by compaction and thus the curves for the compacted and non-compacted soil tend to converge in the high suction range (Figure 2.3). In the high suction range (greater than 1,500kPa), soil water interaction (water retention) is controlled by adsorption (in the clay-size particles) rather than capillary water pressures and hence the slope of the SWRC depends more on the soil grain size distribution than on its density (the water retention becomes more dependent on texture rather than on soil structure).

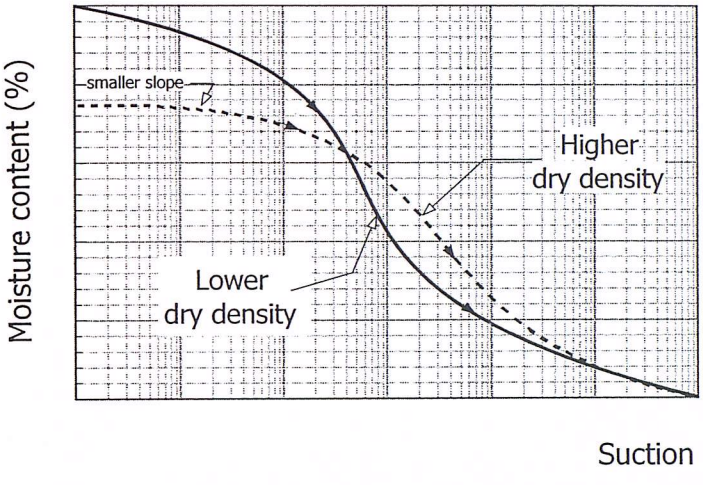

Figure 2.3 Effect of soil density on the SWRC

If two soil samples with different grain size or density are in direct physical contact, they will tend towards a state of equilibrium in which the pore water pressure would become equal in both samples. However, each sample will retain an amount of water determined by its own soil-water retention curve. Two soil layers can then be in equilibrium and yet exhibit a marked difference in water content. This can be seen in Figure 2.4 where soil A with an initial suction of 1,000kPa and moisture content of 13% is placed in contact with soil B with an initial suction of 500kPa and a water content of 10.5%. Although soil B has a smaller initial water content than soil A, water will flow from the higher to the lower energy situation (in terms of suction) because the pore water suction in soil A (drier) is higher than in soil B. The equilibrium condition will take place at an intermediate suction between the original conditions that are controlled by density, grain size, depth of interface and osmotic or thermal differences.

VARIABLES ASSOCIATED WITH THE SWRC 2.2

As a result of changes in the volume-mass properties of a partly saturated soil the coefficient of permeability can vary considerably. The change in void ratio in the soil may be small and its effect on the permeability secondary, however the effect of a change in the degree of saturation may be highly significant.

An important aspect of the SWRC is that it does not exhibit any discontinuity (singularity) as the soil desaturates. The void ratio approaches a constant value at the shrinkage limit of the soil as the moisture content approaches zero (see Figure 2.5). Even for a sandy soil, the soil suction continues to increase with drying towards zero percent moisture content.

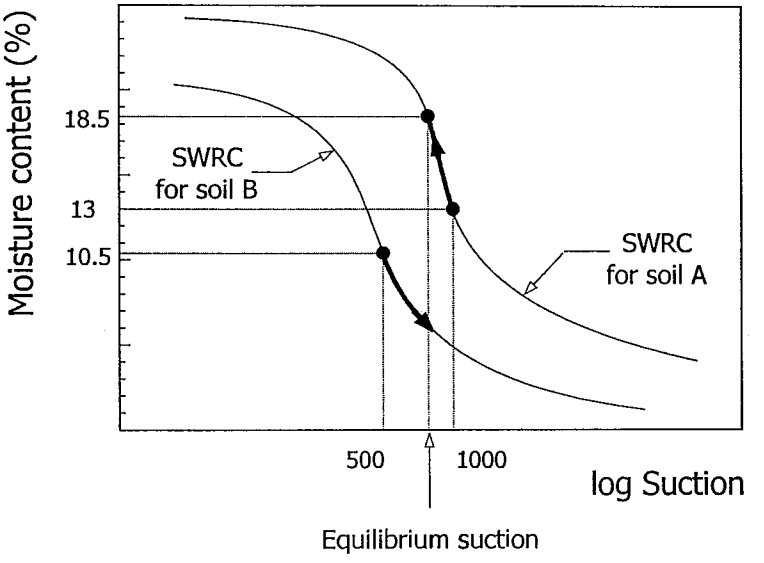

Figure 2.4 Soil-water retention curve for two soil layers in contact

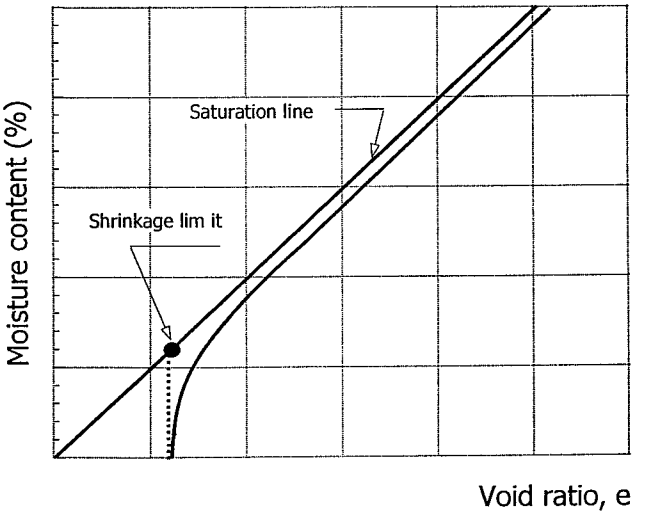

Figure 2.5 Void ratio and moisture content relationship

From the SWRC a number of parameters can be defined: the desaturation point, the graphical air-entry value (AEV) and the initial residual condition point (see Figure 2.6).

The *desaturation point* is the suction at which air starts to be present in the soil in the form of occluded bubbles (as air comes out of solution). As the degree of saturation reduces the *air-entry value* of the soil, AEV, is approached. This is defined as the suction at which air starts to enter the largest pores in the soil. It is the pressure at which the air phase breaks through into the pore structure. The AEV depends on the pore size thus the finer the particles, the smaller the pore size and the higher the AEV. It commonly occurs between degrees of saturation of 90 and 100%. In the soil-water retention curve it is defined graphically as the intersection between the straight sloping line and the line from the initial saturation (100%) at low suction values (Figure 2.6).

Although the desaturation point and the graphical AEV do not coincide, the difference between them is not significant in terms of suction value. For the purposes of this study the desaturation point is considered to be a theoretical air-entry value and the AEV is defined by the graphical air-entry value of a soil.

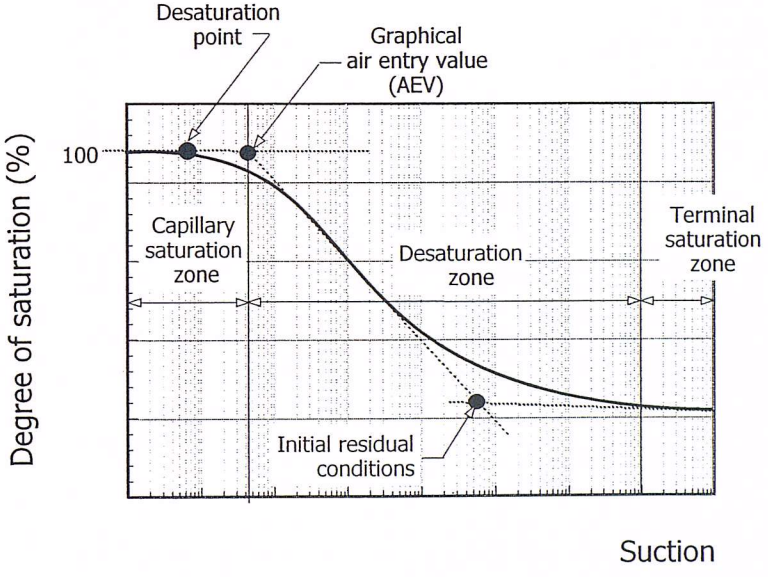

Figure 2.6 Definition of variables associated with the soil-water retention curve (Fredlund & Rahardjo, 1993)

The point of the *initial residual conditions* is defined descriptively as the moisture content beyond which large suction changes are required to remove additional water from the soil. The residual condition zone appears to have physical significance for the behaviour of an unsaturated soil. The flow of water at suctions greater than the initial residual volumetric water content appears to be primarily in the vapour phase, while flow is predominantly in the liquid phase at lower values of suction. This point occurs at relatively low suction values for gravels, sands, silts and mixtures of them (i.e. generally between 20-200kPa suction range) and it is well defined. The point of

initial residual conditions of such soils can be reasonably well predicted from the SWRC plotted on an arithmetic scale. For clays with low plasticity, the initial residual point will generally be in the range of 500 to1,500kPa. However, for intermediate to highly plastic soils, the initial residual state can be greater than 1,500kPa. In some cases, (e.g. highly plastic intact clays) it is difficult to define the initial residual point on the SWRC.

The moisture content and the suction at the initial residual conditions have been defined in many ways in the literature and there is not always agreement about the accepted use of these terms.

Some features of the SWRC are useful in the mathematical modelling of the mechanical behaviour of partly saturated soils. There are some parameters that can be identified from the matrix suction versus degree of saturation curve (see Figure 2.7). These are the degree of saturation at the residual air content S_a, the initial residual degree of saturation, S_r, the terminal residual degree of saturation S_f, the pore size distribution index, λ_p (see Figure 2.8), and the AEV of a soil.

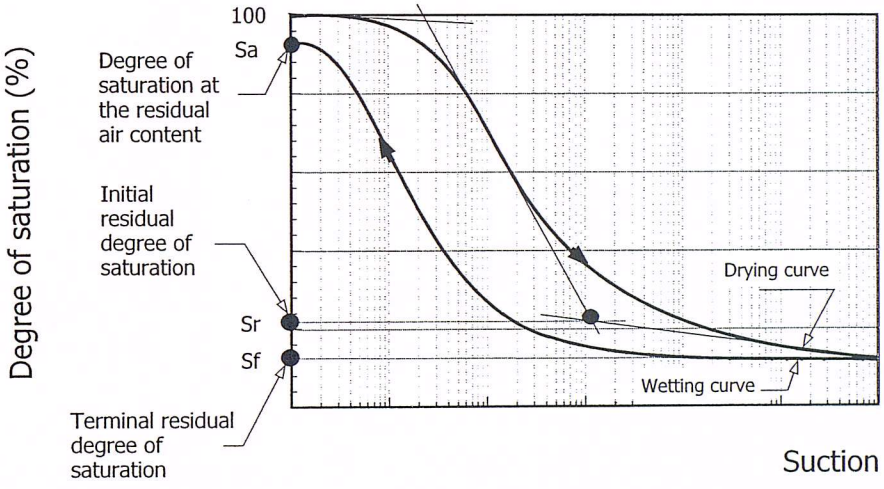

Figure 2.7 Definition of variables associated with the soil-water retention curve in terms of degree of saturation

The *degree of saturation at the residual air content,* S_a, is the maximum degree of saturation after a wetting process when the suction eventually reduces to zero (see Figure 2.7). The *initial residual degree of saturation,* S_r, is the degree of saturation at which an increase in matrix suction does not produce a significant change in the degree of saturation (Figure 2.7) and the final stage is termed the *terminal residual (or final) degree of saturation,* S_f, by which point the curve is almost flat. The pore particle size distribution index, λ_p, is defined as the negative slope of the effective

degree of saturation, S_e, versus logarithm matrix suction curve as shown in Figure 2.8 (Brooks and Corey,1964).

The effective degree of saturation, S_e, can be related in terms of the current degree of saturation, S, and the terminal residual degree of saturation, S_f, as follows:

$$S_e = \frac{S - S_f}{1 - S_f} \qquad (2.4)$$

The initial residual moisture content and its corresponding soil suction on the SWRC, have been defined historically in different ways. Originally, it was suggested that the initial residual water content related to the value at a suction of about 1,500kPa for plants, 1,500kPa corresponding roughly to the wilting point. Water in the liquid phase drains from most of the pores when the suction has attained a value of about 1,500kPa. Desaturation beyond residual conditions occurs primarily as a result of vapour movement up to the point where the soil moisture content is in equilibrium with the vapour pressure of its surroundings. Later, for modelling purposes, a graphical construction procedure was proposed. This involves first drawing a tangent through the inflection point on the drying portion of the SWRC. The SWRC in the high suction range can be approximated by another straight line. The coordinates of the initial residual moisture content are given by the intersection of these lines (see Figures 2.6 and 2.7).

A second procedure for estimating the initial residual conditions (Brooks and Corey,1964), considers the relationship of S_e versus suction. An SWRC in terms of degree of saturation is plotted and the first estimation of S_r is obtained by drawing a horizontal line passing through the point at high suction, i.e. about 1,500kPa (see Figure 2.8 (a)). Once S_f has been estimated the effective degree of saturation (S_e) is calculated and plotted on a logarithmic scale against log suction as is shown in Figure 2.8 (b). A horizontal and a sloping line can be draw through the points which have a roughly bilinear distribution. However, points at high suctions, may not always lie on the straight line produced from the first estimation of the residual degree of saturation. Therefore the point with the highest suction must be forced to lie on the straight line by estimating a new value of S_r. The second estimate of S_f is then used to recompute the values of S_e. A new graph of log suction versus log S_e is then plotted. The above procedure is then repeated until all the points on the sloping line constitute a straight line.

From Figure 2.8, the sloping line for the points having a suction value greater than the AEV can be described by the following equation:

$$S_e = \left\{ \frac{(u_a - u_w)_{AEV}}{(u_a - u_w)} \right\}^{\lambda_p} \quad \text{for } (u_a - u_w) > (u_a - u_w)_{AEV} \qquad (2.5)$$

where:

$(u_a - u_w)$ matrix suction at any point

$(u_a - u_w)_{AEV}$ matrix suction at the AEV

λ_p pore size distribution index, defined as the negative slope of the effective degree of saturation, S_e, versus matrix suction $(u_a - u_w)$.

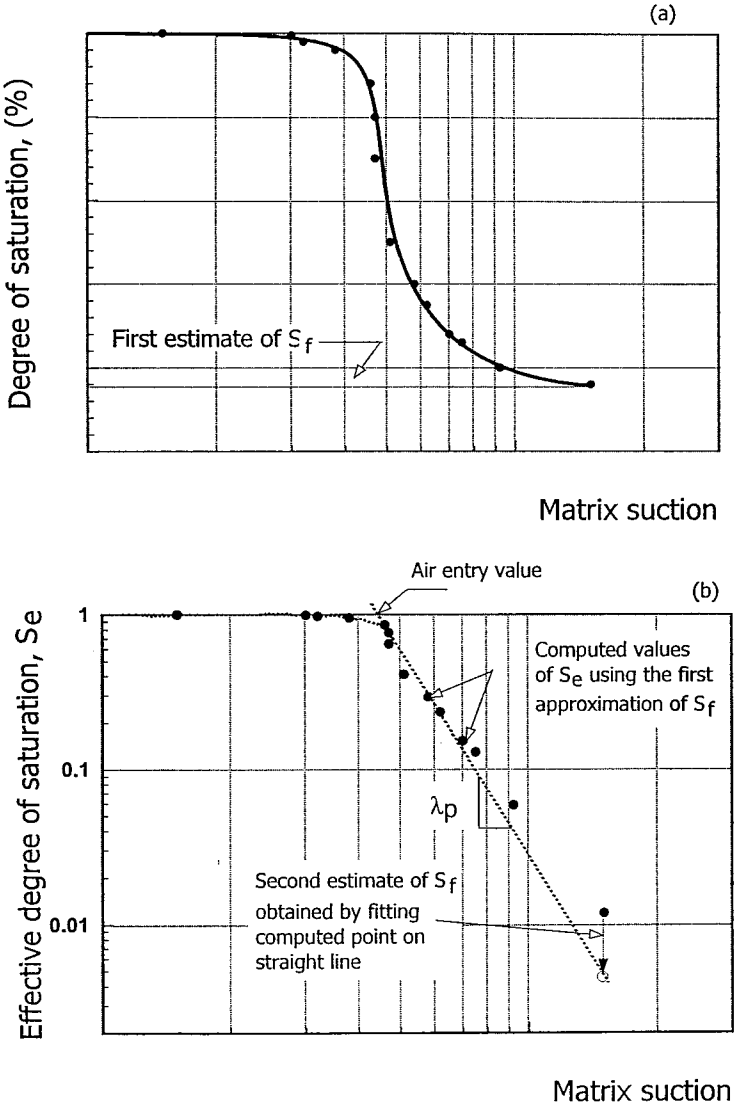

Figure 2.8 Determination of the final residual degree of saturation and pore size distribution index, (from Brooks and Corey, 1964) (a) degree of saturation-suction and (b) effective degree of saturation-suction relationship

Soils with a wide range of pore size have a small value of λ_p. The more uniform the distribution of the pore size in a soil, the larger is the value of λ_p.

The *terminal residual suction* on the SWRC appears to be a common value of total suction (matrix plus osmotic suction) where all types of soil approach zero change of moisture content. It appears to be very similar for all soil types. Therefore, this value provides a higher limit to the size of the SWRC. This means that there is a maximum total suction value corresponding to a zero relative humidity in any porous medium (Fredlund and Rahardjo, 1993). The experimental results from various types of soil have shown that the terminal residual suction value corresponds to about 10^6kPa (Croney et al., 1958; Fredlund, 1964; Vanapalli et al., 1996). The observed behaviour is also supported using thermodynamic principles (Richards, 1965). However, as engineers are concerned with the performance of geotechnical structures in the relatively low suction range (up to about 1,500kPa) the measurement of such high suction values is not of great relevance. The terminal residual suction is however important when defining the entire soil-water retention curve.

In the volumetric water content–suction relationship the variables associated with the SWRC are the volumetric water content at saturation, θ_s, volumetric water content at the residual air content, θ_a, initial residual volumetric water content, θ_r, and the terminal residual volumetric water content, θ_f, (see Figure 2.9)). Fredlund and Rahardjo (1993) proposed that the SWRC in terms of the volumetric water content could be visualized as an indication of the configuration of the water filled pores. The parameters of the SWRC in terms of volumetric water content can also be related in terms of the effective degree of saturation S_e, by using the following relation:

$$S_e = \frac{\theta - \theta_f}{\theta_s - \theta_f} \qquad (2.6)$$

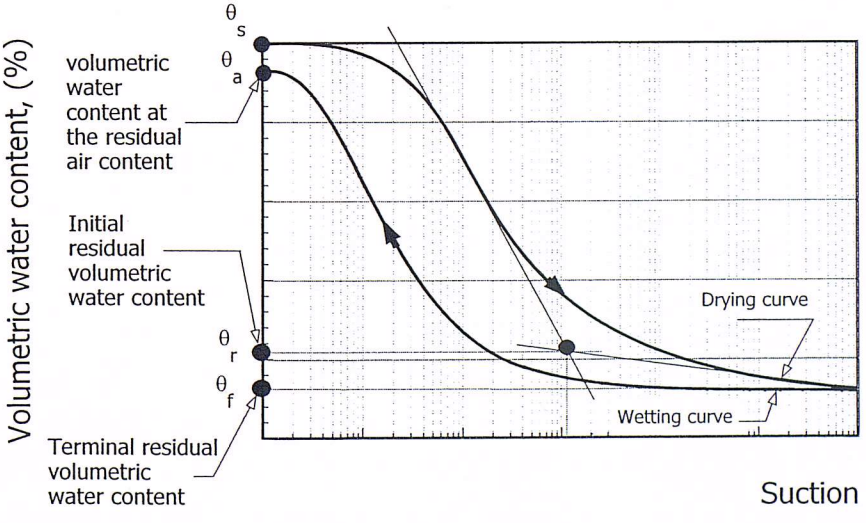

Figure 2.9 Definition of variables associated with the soil-water retention curve in terms of the volumetric water content

STAGES OF THE SOIL-WATER RETENTION CURVE 2.3

When a soil desaturates air first replaces some of the water in the largest pores. Subsequently water is forced to flow through the smaller pores with an increased tortuosity. Further increases of the matrix suction lead to further decreases in the pore volume occupied by water and reductions in the degree of saturation. The air-water interface (contractile skin) will be drawn closer to the soil particles and the coefficient of permeability with respect to the water phase decreases rapidly as the space available for water flow reduces.

The air phase of an unsaturated soil can exist in two forms. These are the continuous air phase form and the occluded air bubble form. The air phase generally becomes continuous when the degree of saturation reduces to something typically in the range between about 95% and 85% (Corey, 1957). The flow of air through an unsaturated soil commences at this point. Under natural conditions, the flow of air through a soil may be caused by factors such as variations in barometric pressure, water infiltration by rain that compresses the air in the soil pores and temperature changes. The flow of air in compacted fills may be due to applied loads. When the degree of saturation is above 90 to 95%, the air phase becomes occluded, and air flow is reduced to a diffusion process through the pore-water (Matyas, 1967).

The diffusion process occurs in response to a concentration gradient, meaning that ionic or molecular movement takes place from regions of higher concentration to regions of lower concentration. The air and water phase in a soil (i.e. soil voids) are the conducting media for the process of diffusion. The soil structure determines the path length across the sectional area that is available for diffusion. The transport of gases (i.e. O_2, CO_2), water vapour and chemicals are examples of diffusion processes in soils. There are two diffusion mechanisms common to unsaturated soil behaviour.

The first type involves the flow of air through the pore-water in a saturated or unsaturated soil (similar to the flow of air through the water in a high air-entry ceramic disk). This type of diffusion involves gases dissolving into water and subsequently coming out of solution. The second type of diffusion involves the movement of components through the water phase due to a chemical concentration gradient or an osmotic suction gradient (see Glossary).

The various stages in the SWRC provide a conceptual and physical model for understanding the behaviour of an unsaturated soil. They basically describe the relative connectivity of the air and water phases across a soil element. For a *drying* process, three identifiable main stages of desaturation along the SWRC have been defined. The stages are defined by different degrees of desaturation along the s-shaped curve and they are a representation of the state of the water related to air in

a partly saturated soil. These are named the Boundary effect stage, the Transition effect stage (which is divided into Primary and Secondary Transition portions) and the Residual effect stage of desaturation (Figures 2.10 and 2.11). These three stages are also applicable to the wetting-up branch of the SWRC and their characteristics are described in Table 2.1.

In the first stage, the Boundary effect stage, the soil is considered to be fully saturated, all the pores are filled with water (water menisci in contact with the soil particles or aggregates are continuous), and no air is present (as shown in Figure 2.11 in the cross-section of a typical element of a soil). There is no reduction of water area. The boundaries of the stage are at zero suction and the point where the soil starts to desaturate (i.e. where air starts to become present in the soil). In this stage the theory relating to saturated soil mechanics is applicable. Under these conditions the single stress state $(\sigma - u_w)$ describes the behaviour of the soil. In general as water begins evaporating or draining from a saturated soil, the outer menisci at the boundaries are pulled inwards and the suction increases. While the change in moisture content is very small, the change in pore water pressure has an important global effect on the soil mass which remains saturated away from the boundary.

The second stage, the Transition stage (Figures 2.10 and 2.11), is divided into two zones called the Primary and the Secondary transition stages of desaturation. In the transition stage the water content in the soil reduces significantly with increasing suction, the amount of water at the soil particle or aggregate contacts reduces as desaturation continues (i.e. the water menisci area in contact with the soil particles or aggregates starts reducing). Once air starts to penetrate, the soil mass becomes unsaturated. Water still exists as a continuous phase. As drying proceeds, the suction increases gradually following a quasi-linear trend with decreasing saturation. Any local change in water pressure is rapidly homogenized through the mass by pressure diffusion within the continuous water phase. The drying rate is reasonably constant in this region.

The Primary transition stage represents the zone where the air can be present as occluded bubbles after coming out of solution. The air starts to penetrate into the soil from the boundary as is shown in the cross-section shown in Figure 2.11. However, the air does not pass into the soil mass. In this stage the lower boundary is considered the desaturation point of the soil, and the point obtained from the graphical procedure for obtaining the AEV of the soil is the upper boundary (the graphical procedure was explained earlier in this chapter). An important consideration in the analysis of the behaviour of a partly saturated soil in this primary transition stage is that its behaviour in this condition can still be analysed in the same way as a saturated soil (allowing for the compressibility of the pore fluid).

Moreover, water is considered as the continuous phase rather than the air which is in the form of occluded air bubbles (see Figure 2.11).

In the Secondary transition stage (see Figures 2.10 and 2.11) dramatic changes in the behaviour of the partly saturated soil occur. The SWRC shows a marked change in its slope, eventually reaching an inflection point. Additionally the air starts to penetrate extensively into the soil. The lower boundary of the Secondary transition stage is the point called the initial residual suction of the SWRC.

From the end of the Primary transition stage to the inflection point of the SWRC, the water phase is still considered as a continuous phase and the air is still discontinuous. However, from the inflection point until the end of the secondary transition stage although the water acts as a continuous phase flowing freely, the air phase starts to be considered as continuous (see Figure 2.11).

In the Transition effect stage water and air can flow in all directions if the soil is being compressed externally. However, after the inflection point, although the water and air will still flow, as both are continuous, the air will flow more readily than the water.

In the Residual stage of saturation, large changes in suction lead to relatively small changes in moisture content. The amount of water present is small (i.e. the water menisci are small). In this stage water acts as a discontinuous phase and air is continuous. Water is considered almost immobile except for some water vapour flow. From the start of the residual stage it is considered that an external compression of the soil will only cause flow of air, additionally changes in moisture content will not lead to any changes in the volume of the soil (see Figure 2.11).

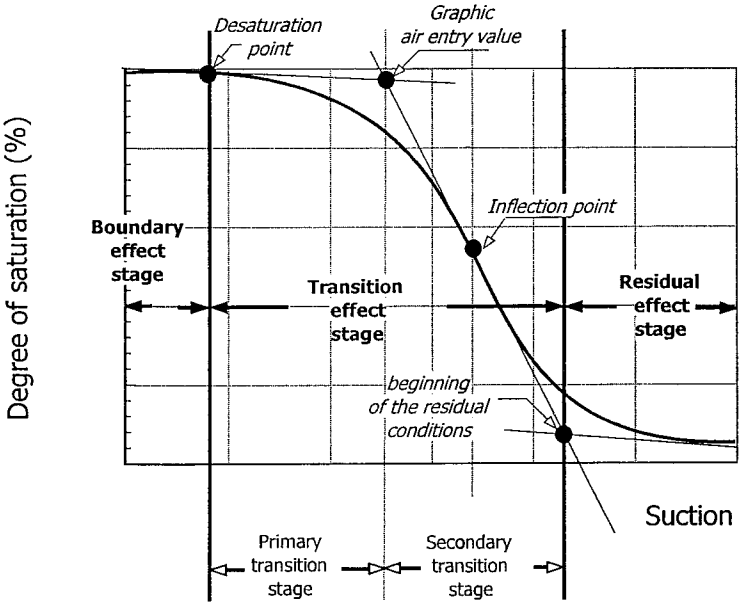

Figure 2.10 Stages of the soil-water retention curve (Fredlund et al., 1993)

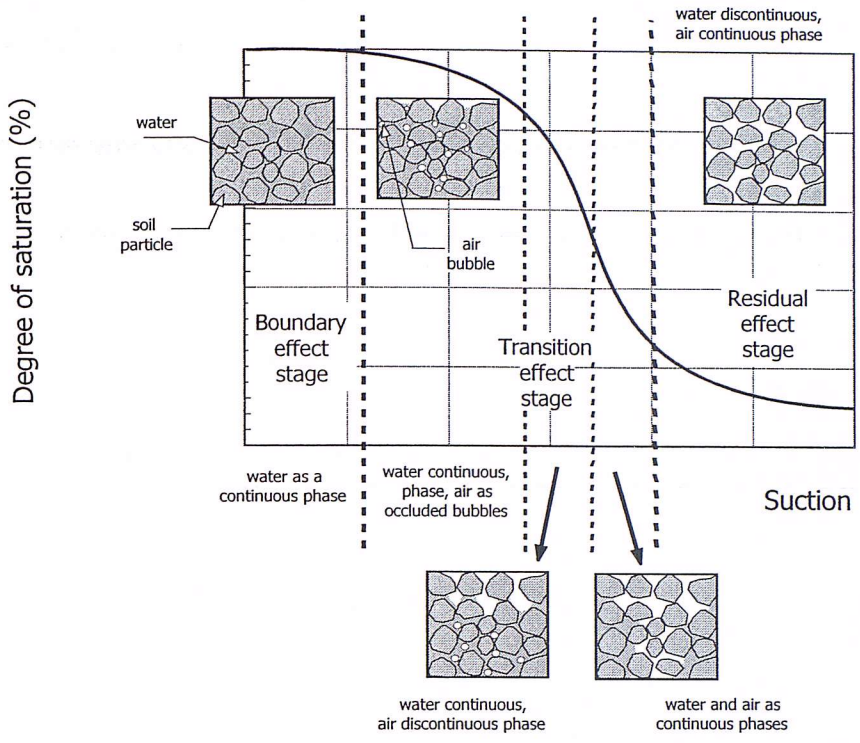

Figure 2.11 Phases of the stages of the soil-water retention curve (Fredlund et al., 1993)

When water begins to become disconnected, water rings are formed around the particle contacts and only a film may be present on particle surfaces. The radii of the menisci are small, thus the suction pressure increases significantly. Because this is only a contact-level effect, a change in suction within a meniscus is felt at other menisci through the corresponding change in vapour pressure. This is a slow homogenization process. The drying rate during this stage gradually reduces.

The definition of the stages of the SWRC is based on the hypothesis that Darcy's law is applicable and that the particles are homogeneous, rounded and incompressible. It is also assumed that the air is free to flow with a constant zero air pressure as a result (Fredlund and Rahardjo, 1993). Applying Darcy's law, water can be visualized as flowing only through the pore space filled with water. The air-filled pores are non-conductive channels to the flow of water. Therefore, the air-filled pores in a partly saturated soil can be considered as behaving similarly to the solid phase, and the soil can be treated as a saturated soil having reduced moisture content (Childs, 1969). Consequently the validity of Darcy's law can be verified in an unsaturated soil in a similar manner to its verification for a saturated soil. However, the volume of water should be constant while the hydraulic total head gradient is varied. The rate of water flow through a partly saturated soil is linearly proportional to the hydraulic head gradient, with the coefficient of permeability being a constant, similar to the situation for a saturated soil, confirming Darcy's law in partly saturated soils. However, the coefficient of permeability will differ for different volumetric water contents.

Table 2.1 Characterisation of the stages of the SWRC (Fredlund & Rahardjo, 1993)

BOUNDARY EFFECT STAGE	TRANSITION EFFECT STAGE (PRIMARY AND SECONDARY)	RESIDUAL EFFECT STAGE
Almost all the soil pores are filled with water.	The moisture content in the soil reduces significantly with increasing suction.	Large increases in suction eventually lead to relatively small changes in moisture content (degree of saturation, volumetric water content or gravimetric water content). There appears to be a fraction of "relatively immobile" water in the pores of the soil.
There is essentially no change in the degree of saturation of the soil at suctions below the air-entry value.	The soil starts significantly to desaturate. A dramatic change in partly saturated soil properties takes place.	There is no significant change in the degree of saturation; the effect of a change in the soil suction on the mechanical behaviour of a soil may become negligible as the soil approaches a very dry condition.
Θ is equal to unity and there is no change in the wetted area (equal to unity).	The wetted area reduces as desaturation continues. The wetted area decreases as a result of an increase in suction	The wetted contact area has reduced significantly. Θ is extremely small and so is the wetted area.
The coefficient of permeability, up to the air-entry value of the soil, is equal to the saturated coefficient of permeability, k_s.	The connectivity of the voids reduces with increased values of suction. Therefore, the unsaturated coefficient of permeability reduces by several orders of magnitude.	There is little or no flow through the pores.
Flow takes place through the voids in a manner similar to that for a saturated soil. Water acts as a continuous phase.	The flow of water is in the liquid phase as suction increases. As soil suction increases, flow occurs through increasingly smaller size pores.	The flow of water is primarily in the vapour phase. Water acts as a discontinuous phase rather than air which acts as a continuous phase.
Matrix suction is equivalent to net normal stress in mobilizing the shearing resistance of the soil. The shear strength contribution due to suction, represented by ϕ, is equal to the effective angle of shearing resistance ϕ', up to the air-entry value of the soil and is primarily through the wetted inter-aggregate contact area. In general, there is a linear increase of the shear strength up to the AEV.	The contribution of suction to the increase in shear strength reduces with desaturation. As a result, there is a non-linear increase in the shear strength of the soil with respect to soil suction beyond the air-entry value of the soil.	The changes in matrix suction do not significantly contribute towards an increase in the shear strength of the soil and they do not produce any significant change in the volume of the soil. The net normal stress $(\sigma - u_a)$ may become the only stress state variable controlling the behaviour for the dry soil. The shear strength may increase, decrease or remain relatively constant during further desaturation. In soil that desaturates relatively fast (i.e. sands, silts) the shear strength will decrease (there is little water left in the soil pores, so it may not transmit suction effectively to the soil particle or aggregated contact points, thus even large increases in suction will result in a significant increase in shear strength). In clays with even a high suction value there could still be considerable water in the form of adsorbed water available to transmit suction along the soil particles which contributes towards increases in the shear strength, this phenomenon can occur for a large range of suction for clays.

It is clear that the stages of desaturation can be defined for each individual non-hysteretic SWRC. However, the various literature sources agree in applying the model of the SWRC stages independently to the direction of the process that changes the value of the suction (i.e., drying, wetting). Additionally, it is clear that the effect of the hysteresis in the SWRC is significant, shifting the position of the SWRCs, and as a result the zones (i.e. the various stages) do not coincide for both the drying and wetting curves.

2.4 HYSTERESIS IN THE SOIL-WATER RETENTION CURVE

The relationship between moisture content and the suction of a soil is not unique because of the phenomenon of hysteresis. The hysteresis effect in the soil may be attributed to several factors, such as the irregular and combined sizes and shapes of soil pores, the contact angle effect may be lower during wetting than during drying and during wetting some air is entrapped which reduces the water content from the initial saturated water content. Additionally hysteretic phenomena also occur in soils as a consequence of swelling or shrinking.

Assuming that a soil is initially a particle arrangement completely free of water (i.e. neither liquid nor vapour) and is then subsequently wetted up until it has no air phase (just liquid water and its vapour), the factors that influence the SWRC in the drying and wetting processes can be described as follows.

- In a wetting process, where water is added to the soil, small pores fill first, followed by successively larger and larger pores until all pores that can be filled are filled and the matrix suction is zero. The water content and matrix suction relationship will follow the wetting curve similar to that shown in Figure 2.12. At this stage, some small pores might be isolated during wetting, so that they remain dry while larger pores are filled (Koorevaar et al., 1983). However, this would not be the case at equilibrium in the absence of air, because the vapour transfer would guarantee the wetting of all pores small enough to retain water at a particular matrix suction (Koorevaar et al., 1983).

- In a drying process, resulting from water evaporating, draining or by bringing the soil into contact with a dry porous material that draws water away from the soil system, pores will begin to empty, generally from large to small (Koorevaar et al., 1983). However, liquid water may be trapped in large pores in such a way that they will not empty in the order that they filled. Water will be held in large pores until conditions are reached where at least one interconnecting smaller pore can empty. At this time the larger pore quickly empties (Koorevaar et al., 1983). The water content and matrix suction relationship follow the drying curve in Figure 2.12.

The sudden release of a relatively large amount of water from a large pore floods surrounding pores and reduces the matrix suction in them temporarily. If matrix suctions were monitored in a small porous element having discrete differences in pore size, the matrix suction and water content relationship for drying might be saw-toothed (Koorevaar et al., 1983) as shown in Figure 2.12.

Altogether, soil pores are highly variable in size and shape and interconnect with each other in a variety of ways. Soils have large cavities but narrow points of connection to adjacent pores. Water is held most tenaciously in small pores, which fill first when water is added to the soil. But they do not always empty again during drying in the same order as they were filled (Koorevaar et al., 1983).

The pore size distribution contains pores in all sizes. As the water content and pore water pressure distributions tend to an average, the SWRC is obtained as a smooth curve. However, the water content for a given matrix suction is higher for the drying processes than for the wetting processes (as is shown by the curves in Figure 2.12). This principle is illustrated by the pore-water system in Figure 2.13(a). From the figure it can be seen that the curvature of the vapour-water interface in the small pores in two identical pore systems can be in equilibrium with each other even though their water contents are dramatically different. The matrix suction is governed by the curvature of the liquid interface, which at equilibrium would be precisely the same in the small pores connecting with the large pore in each case (Koorevaar et al., 1983).

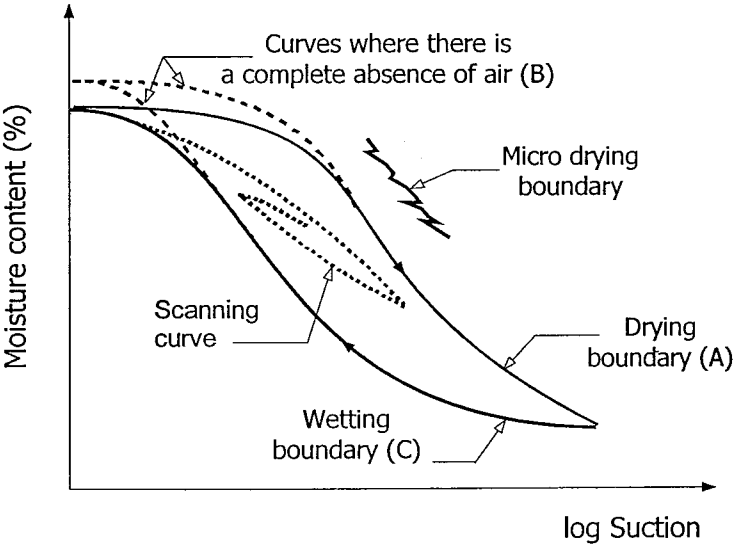

Figure 2.12 Hysteresis in the SWRC

Large pores that are interconnected by smaller pores do not make any contribution to the hysteretic behaviour of the soil. It is possible for a single pore to contain the same amount of water at two different pore-water pressures (see Figure 2.13 (b)). The diagonal cross-hatched area shows water that condenses (onto the soil

particles) from a humid environment. As condensation proceeds, water at the centre finally coalesces and a concave meniscus is formed as a consequence of surface tension forces (vertical hatching). Whereas positive pressure existed in the system before coalescence, the system suddenly has a negative pressure as a consequence of its new configuration (Koorevaar et al., 1983).

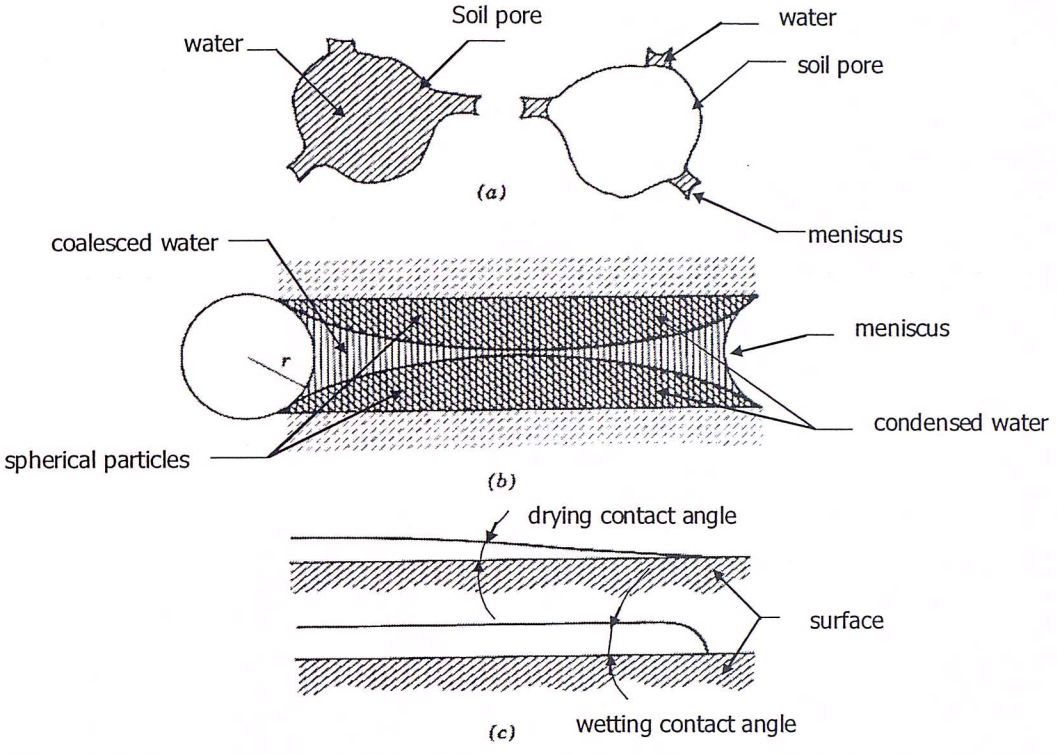

Figure 2.13 Representation of the three causes of water content - suction hysteresis (a) same pore water system in equilibrium each other with different water content, (b) cross-section of a pore (c) contact angle in two different surfaces
(Koorevaar et al., 1983)

Dependence of the moisture content-suction relationship upon wetting and drying further involves a surface wetting phenomenon. Unless particle surfaces are meticulously clean, a wetting angle exists when the surface is wetted (it will form a non-zero contact angle with water when wetted) as can be seen in Figure 2.13(c). The contact angle during wetting results in thicker films than would be present in the drying phase where water films are drawn tightly over the surface by adsorptive forces (Koorevaar et al., 1983). The contact angle of a given liquid on a given solid is generally governed by their interaction under given physical conditions. This angle may be different for the case of a liquid that is advancing over the solid surface than for the case of the same liquid receding over the surface. The phenomenon is called contact angle hysteresis. The wetted angle of pure water on clean and smooth mineral surfaces is generally zero but where the surface is rough or coated with adsorbed surfactants of a hydrophobic nature the contact angle and especially the wetting angle can be considerably greater than zero. The contact angle effect can be appreciated by considering the contact angle and the curvature radius which are greater in the case of an advancing meniscus than in the case of a receding one. A soil at a given moisture content will tend to exhibit greater suction in desertion than

in sorption. The contact angle can increase because of the surface roughness, the presence of impurities on the solid surface and the mechanism by which liquid molecules are adsorbed or desorbed when the interface is displaced.

Moreover, the presence of air in the processes (drying and wetting) can introduce additional differences between moisture content at a given matrix suction during wetting and drying. As small pores and interstices between particles fill with water, air may become entrapped in large pores. Continued water entry into such pores will cause a build up of air pressure. Since air is soluble in water, pressures in such pores may gradually be relieved, which will sometimes allow more complete pore filling. As the order of filling and access to pores will be influenced by entrapped air, the water content is permanently affected despite the fact that some air may go into solution (Koorewaar et al., 1983).

Furthermore, in the complete absence of air at low suctions, the relationship between suction and the moisture content for complete wetting and complete drying will follow approximately the dashed line loop shown in Figure 2.12. However this loop is not exactly reproducible because of the inherent characteristic that the exact order of pore filling over each cycle is not necessarily repeated.

On the other hand, when air is present in the system, curves are offset moderately toward the dry side (solid line, see Figure 2.12, curve A). If a soil is completely wetted (no air is present in the arrangement) and then is dried, the SWRC will follow the dashed-solid curve down (curve B). During the re-wetting process in the presence of air, the SWRC will follow the solid wetting curve (curve C) and it will not return to the starting point because of the presence of the entrapped air. If the process is reversed at any time during wetting or drying, intermediate or scanning curves are reproduced.

Since air is almost always present when such curves are produced experimentally, the solid curves, shown in Figure 2.12, are obtained. However, some ambiguity exists, because the starting point for many measurements is from the sample's natural state and although it might be considered to be saturated, the degree of air removal is unknown.

Hysteretic phenomena also exist in soils as a consequence of shrinking and swelling, which can affect microscopic pore size geometry as well as overall bulk density. Both factors would lead to a volumetric water content for a given suction that differs from that which would exist if the soil matrix remained fixed. Shrinking and swelling often take place slowly and usually irreversibly; this complicates the evaluation of their contribution to hysteresis (Baver et al., 1972).

Among the alternative concepts for explaining the hysteresis there is the theory of the independent domain (Poulovassilis, 1970) and the theory of the dependent domains (Mualem and Miller, 1979; Mualem, 1984). The former is based on the assumption that all pores are free to drain independently. The latter approach recognizes that only pores with access to the atmosphere can drain, and that access depends on whether the surrounding pores are water-filled or air-filled. To account for that dependence, a domain dependence factor is applied.

2.5 TERMINOLOGY USED TO DEFINE COMPONENTS OF THE SWRC

The terminology used for describing the models presented in this thesis is illustrated in Figure 2.14. The principal drying curve of the SWRC (PDC) is defined by the initial drying of a soil sample from a slurry to the point where there are no further changes in volumetric water content and the suction reaches a terminal value ψ_f. A typical PDC is shown in Figure 2.14. The principal wetting curve (PWC) is then defined by wetting the sample from the end of the PDC. The PWC is generally strongly hysteretic compared with the PDC and does not regain the same volumetric water content from which the PDC started (compare θ_a and θ_s in Figure 2.14) The PDC and PWC define boundaries within which all wetting and drying responses of the soil are expected to take place.

The main drying and wetting curves or loops (MDC and MWC) are the enclosing curves of the volumetric soil-water content versus suction graph, which are described along the paths $(\psi_u \rightarrow \psi_{tr2} \rightarrow \psi_c)$ and $(\psi_c \rightarrow \psi_{tr1} \rightarrow \psi_u)$. The main curves are different from the principal curves in that they are defined from the point where the soil is under some finite suction (stress) rather than a slurry. The MWC and PWC in many cases are almost collinear (and are shown as such in Figure 2.14). In some cases, the suction is not increased to ψ_f prior to starting the wetting curve. The resulting path lies within the MWC (or PWC) and is known as the effective wetting curve. Primary scanning curves (PSC) described by $(\psi_{tr2} \rightarrow \psi_u, \psi_{tr1} \rightarrow b \rightarrow \psi_c)$ are those that depart directly from the main curves, while the secondary scanning curves, SSC, $(\psi_{tr1} \rightarrow a \rightarrow \psi_{tr2})$ depart from the primary scanning curves. The wetting and drying behaviour of most natural soils would be expected to lie within the main curves, following either PSCs or SSCs depending on the flow conditions within the soils (climatic cycles etc).

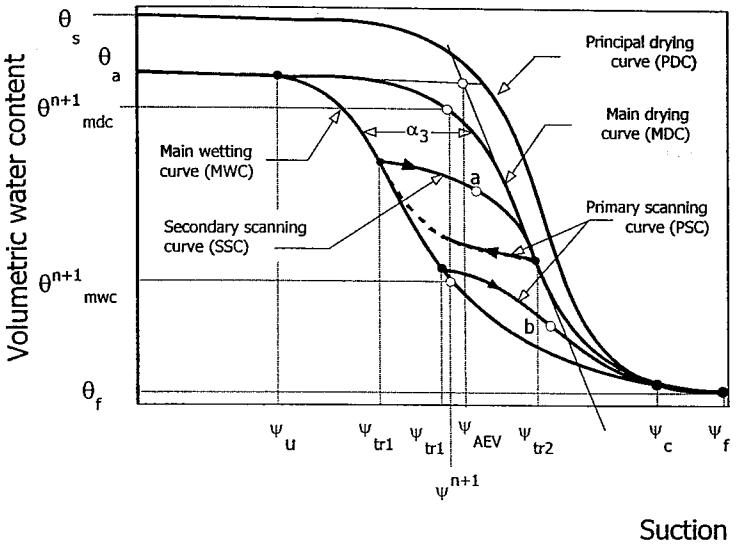

Figure 2.14. Terminology used for the hysteretic behaviour of the SWRC

where:

ψ_{tr1} transition suction pressure at which the soil changes from wetting to drying

ψ_{tr2} transition suction pressure at which the soil changes from drying to wetting

ψ_{AEV} suction at the graphic air-entry value

ψ_c suction where the hysteresis curves merge

ψ_u suction at which the main curves separate

ψ^{n+1} suction at a new point of a predicted scanning curve

α_3 maximum suction difference between the main wetting and drying curves at the same moisture content

ϕ porosity at saturated slurry state, corresponding to the volumetric water content with any randomly distributed air being dissolved

θ_f volumetric water content at the terminal residual degree of saturation

θ_s volumetric water content at saturated slurry state

θ^{n+1} volumetric water content of the new point of the predicted scanning curve

θ_{mwc} volumetric water content on the main wetting curve

θ_{mdc} volumetric water content on the main drying curve

$\theta^{n+1}{}_{mdc}$ volumetric water content at a starting point of a predicted scanning curve from a main drying curve

$\theta^{n+1}{}_{mwc}$ volumetric water content at a starting point of a predicted scanning curve from a main wetting curve.

MATHEMATICAL FORMS FOR THE SOIL-WATER RETENTION CURVE 2.6

No satisfactory theory exists for the prediction of the relationships between suction and moisture content. A large number of empirical equations have been suggested

for the soil-water retention curve but none of these equations accurately fit laboratory data over the entire soil suction range. Unfortunately, almost all the equations were suggested based on the shape of a particular curve and each equation has its own limitations.

Most of the equations describe an s-shaped form and are asymptotic to horizontal lines in both low and high suction ranges. However, some do not give a sigmoidal form. Equations exhibiting a poor fit near to the saturation point result in a discontinuity in the slope of the curve at the air-entry value, contradicting the presence of a smooth transition zone near that suction. Moreover, some equations describe a sigmoidal curve for a particular kind of soil with excellent agreement with experimental data but the equation is not applicable to other soil types.

2.6.1 MODELS PROPOSED FOR A SINGLE SOIL-WATER RETENTION CURVE

Some proposed equations for modelling of the SWRC are summarized in Table 2.2. The equations proposed to describe the relationship between moisture content and matrix suction are usually in terms of the porosity ϕ, pore size distribution index λ, volumetric moisture contents at saturation θ_s , at initial residual state θ_r and at terminal residual state θ_f. Additionally, all the equations are based on the constants α, n and m (see Table 2.2), which define the shape of the curves and are related to the air-entry value (AEV) and the initial residual moisture contents. These constants α, n and m , give a smooth, flexible, continuous and differentiable s-shaped curve between the saturated and the initial residual moisture contents.

In general, the saturated volumetric water content, θ_s, is measured whereas the terminal volumetric water content, θ_f is not always known and so the initial residual volumetric water content, θ_r, is difficult to estimate. If θ_s is treated as a known parameter, the maximum number of parameters that is suggested to define the soil-water retention equation is four. Hence, the remaining unknowns in the soil-water retention curve equations are $\theta_r, \alpha, n,$ and m.

When the terminal residual volumetric water content, θ_f, is not clearly evident or measured, it must be estimated by extrapolating measured soil-water retention data to the lower moistures contents. One possible way is to apply graphical methods using different values for θ_f, and subsequently selecting that value of θ_f which gives the best fit of the equations to the experimental data available (as described in

Section 2.2, see Figure 2.8). An alternative procedure would be to use the least squares curve-fitting technique.

Several graphical procedures for the determination of the parameters for the equations have been suggested in the literature. However, a graphical interpretation only gives approximate values for the parameters (Fredlund and Xing, 1994). To obtain a closer fit to experimental data these parameters are best obtained employing the least squares method. In general, the curve-fitting parameters should be obtained from experimental data that include measurements around the initial residual state, if data points after the initial residual point are not included; the curve starts to deviate (Fredlund and Xing, 1994). The idea is to choose the parameters such that the calculated values from the equations are as close as possible to the measured data available.

Figures 2.15, 2.16 and 2.18 show the effect of varying the parameters α, n and m applying the equation given in Table 2.2 by Van Genuchten (1980). When n and m are fixed, the parameter α, is closely related to the air-entry value (AEV). Figure 2.15 illustrates the lateral translation of the SWRC as a result of varying α with n and m fixed.

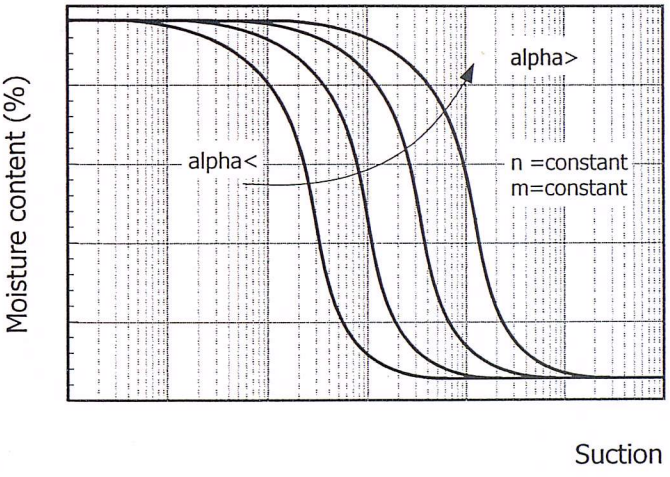

Figure 2.15 Effect of varying α parameter in the SWRC

In general, the value for the parameter α, would be higher than the ψ_{AEV}. However, for small values of m, ψ_{AEV} is sometimes adopted as an approximate value for the parameter α.

The parameter n controls the slope of the SWRC as seen in Figure 2.16 which illustrates the change in the slope of the SWRC as a result of changing the n parameter with the α and m parameters fixed. Some of the equations in Table 2.2 reach a common value for the volumetric water content at a suction corresponding to the α value (e.g. $\theta = \theta_s$ when $\alpha = \psi$). Therefore, the point $(\alpha, \theta(\alpha))$ can be used to approximate the inflection point (see Figure 2.16).

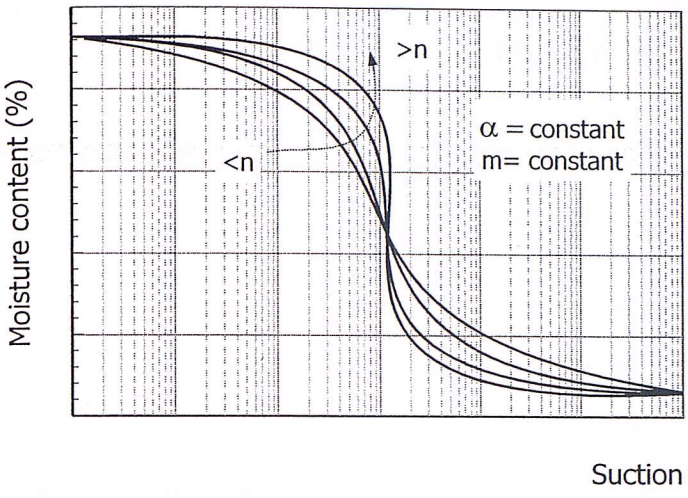

Figure 2.16 Effect of varying *n* parameter when α and *m* are fixed

Using this information a graphical estimation for the parameters α, n, m can be obtained from the SWRC. The graphical method suggested by Luckner et al. (1989) first locates the inflection point (ψ_i, θ_i) on the soil-water retention plot and draws a tangent line through this point (see Figure 2.17). Then, the three parameters α, n, m are determined as follows:

$$\alpha = \psi_i$$

$$m = 3.67 \ln\left(\frac{\theta_s}{\theta_i}\right) \qquad (2.7)$$

$$n = \frac{1.31^{m+1}}{m\theta_s} 3.72 \Delta s \psi_i$$

where,

ψ_i suction at the inflection point

θ_i volumetric water content at the inflection point

Δs slope of the tangent line

$$\Delta s = \frac{\theta_i}{\log\left(\frac{\psi_p}{\psi_i}\right)}$$

ψ_p intercept of the tangent line and the matrix suction axis.

According to Mualem (1984), if the terminal residual volumetric water content, θ_f, is unknown, the inflection point can be found using the mid-way point between the saturated water content and the initial residual volumetric water content (see Figure 2.17). It is assumed that the terminal residual water content is defined here as the moisture content for which the gradient becomes zero (excluding the region near to θ_s, which also has zero gradient). This approach is inconsistent with the general shape of the SWRC defined for some equations (especially when defining the

SWRC for fine grained soils) and probably invalidates the concept of θ_f, but from a practical point of view the assumption seems to be acceptable.

Table 2.2 Proposed equations for the SWRC (Fredlund and Xing, 1994)

YEAR	AUTHOR	EQUATION	SOIL PARAMETER
1953	Burdine	$\theta = \frac{\theta_s}{\left(1+\left(\frac{\psi}{\alpha}\right)^n\right)^m}$	α, n
1958	Gardner	$\theta = \theta_r + \frac{\theta_s - \theta_r}{1+\alpha\psi^n}$	θ_r, α, n
1964	Brooks and Corey	$\theta = \theta_r + (\theta_s - \theta_r)\left(\frac{\alpha}{\psi}\right)^n$	θ_r, α, n
1976	Mualem	$\theta_w = \frac{\theta_s}{\left(1+\left(\frac{\psi}{\alpha_m}\right)^{m_m}\right)^{m_m}}$	α, n $m = 1-\frac{1}{n}$
1980	Van Genuchten	$\theta = \theta_r + \frac{\theta_s - \theta_r}{\left(1+\left(\frac{\psi}{\alpha}\right)^n\right)^m}$	α, n, m
1983	Williams	$\theta = \left(\frac{\psi}{e^{\alpha}}\right)^{1/n}$	α, n
1984	Mc Kee and Bumb	$\theta = \theta_r + (\theta_s - \theta_r)\exp\left(\frac{\alpha-\psi}{n}\right)$	θ_r, α, n
1987	Mc Kee and Bumb	$\theta = \theta_r + \frac{(\theta_s - \theta_r)}{1+\exp\left(\frac{\psi-\alpha}{n}\right)}$	θ_r, α, n
1994	Fredlund and Xing	$\theta = \frac{\theta_s}{\ln\left(e+\left(\frac{\psi}{\alpha}\right)^n\right)^m}$	α, n, m
1994	Fredlund and Xing	$\theta = \frac{\ln\left(1+\frac{\psi}{\psi_r}\right)}{\ln\left(1+\frac{1000000}{\psi_r}\right)} \frac{\theta_s}{\left\{\ln\left[e+\left(\frac{\psi}{\alpha}\right)^n\right]\right\}^m}$	ψ_r, α, n, m
1994	Fredlund and Xing	$\theta = \theta_r + \frac{(\theta_s - \theta_r)}{\ln\left(e+\left(\frac{\psi}{\alpha}\right)^n\right)^m}$	θ_r, α, n, m

Fredlund and Xing (1994) developed a method of graphically estimating the four parameters α, n, m, θ_f, considering the initial residual water content. The procedure

involves determining the suction corresponding to the initial residual water content, ψ_r from the SWRC, by locating the point where the curve starts to drop linearly in the high suction range.

Then, locate the inflexion point (ψ_i, θ_i) on a semi log-plot and draw the tangent line through this point (see Figure 2.17). Then, the fitting parameters (α, n, m, θ_r) can be determined as follows:

$$\alpha = \psi_i$$

$$m = 3.67 \log\left(\frac{\theta_s C(\psi_i)}{\theta_i}\right) \qquad (2.8)$$

$$n = \frac{1.31^{m+1}}{mC(\psi_i)} 3.72 \Delta s^*$$

where

Δs slope of the tangent line

$$\Delta s = \frac{\theta_i}{\log\left(\frac{\psi_p}{\psi_i}\right)}$$

$$\Delta s^* = \frac{\Delta s}{\theta_s} = \frac{\psi_i}{1.31^m (\psi_i + \psi_r) \log\left[1 + \left(\frac{1000000}{\psi_r}\right)\right]}$$

$$C(\psi_i) = \frac{-\log\left(1 + \frac{\psi_i}{\psi_r}\right)}{\log\left[1 + \left(\frac{1000000}{\psi_r}\right)\right]} + 1$$

ψ_r suction corresponding to the initial residual water content, θ_r.

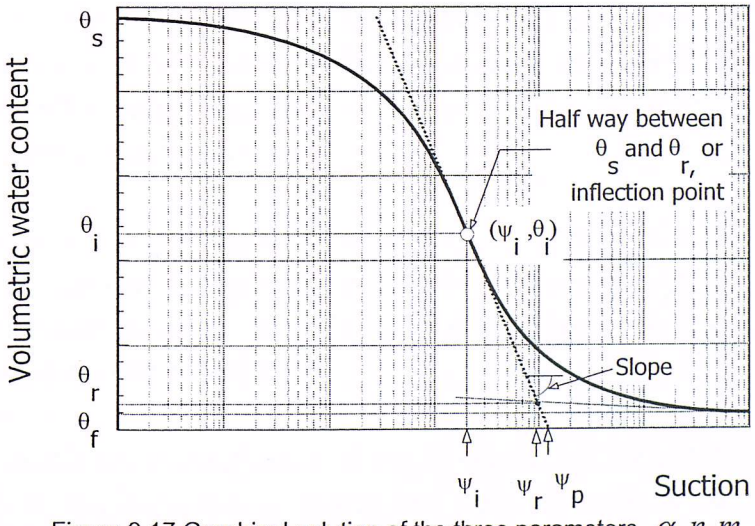

Figure 2.17 Graphical solution of the three parameters, α, n, m
(Fredlund and Xing, 1994; Mualem, 1976)

Figure 2.18 indicates that small values of *m* result in a moderate slope in the high suction range while large values of *m* produce a more pronounced corner at the air-entry value.

The terminal residual and saturated volumetric water contents are sometimes treated as two additional parameters. The five parameters $\theta_r, \theta_s, \alpha, n, m$, can then be systematically identified through a best fit analysis of experimental data.

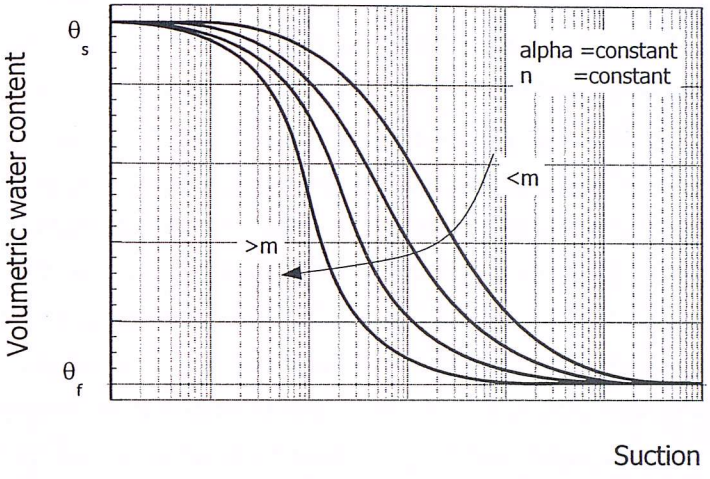

Figure 2.18 Effect of varying *m* parameter when *n* and α are fixed

In 1997, Fredlund et al. proposed a method of estimating the soil-water retention curve from the particle size distribution curve, dry density, void ratio and specific gravity of the soil. A good curve-fit of the particle-size distribution curve including the minimum particle size is essential for the prediction of a reasonable SWRC of a soil. Experimental results have indicated that if the minimum particle size is too large the deficiency of smaller particles will result in the soil drying out prematurely. On the other hand, if the minimum size is too small the excess of clay size particles will dominate the prediction. The method seems to provide improved accuracy for predicting the SWRC for sands and a reasonable accuracy for silts. The SWRC for clays, tills and loams are more difficult to predict, although the accuracy of the prediction algorithm again appears to be reasonable. Additionally, the prediction tends to be sensitive to the porosity.

In this approach, the grain-size distribution curve is divided into small groups of uniformly sized particles. A porosity and soil-water retention curve is assumed for each group of particle sizes. The incremental soil-water retention curves are then summarized to produce a final SWRC.

Initially, the model fits a modification of the Fredlund and Xing (1994) Equation (2.9) (see below) to the particle-size distribution curve (based on Wagner and Ding, 1994). Fredlund et al. (1997) modified the equation to permit the fitting of grain-size

distribution curves, allowing a continuous fit and proper definition of extremes of the curve). Secondly, the grain-size distribution curve is analyzed as an incremental series of particle sizes from the smallest to the largest in order to build up an overall soil-water retention curve. Thirdly, small increments representing uniform sized particles are transposed to obtain a SWRC for the average particle size. Finally, once the entire particle-size distribution curve is incrementally analyzed, the individual SWRCs are superimposed to give the SWRC for the entire soil.

The method assumes that a soil composed entirely of a uniform, homogeneous particle size would have a relatively unique SWRC. Using a best-fit analysis with the Fredlund and Xing (1994) equation, α, n and m constants are calculated for pure sands, silts and clays. These three parameters are associated with a dominant particle size on the grain-size curve. Additionally, the method assumes that as a soil tends towards uniformity, the n and m constants would show a trend towards a particular value. With an approximation of the particle sizes falling between pure clay, pure silt and pure sand it is possible to produce two plots one for the n and one for the m parameter which will describe the variation in the n and m constants with the particle-size distribution curve. This results in the estimation of n and m constants for any soil composed of uniform particles. After dividing up the particle-size distribution plot into small divisions of uniform soil particles, a packing porosity is estimated for each division starting at the smallest diameter size and the SWRC is estimated for each region. The incremental soil-water retention curves can then be summed starting with the smallest particle size and continuing until the volume of pore space is equal to that of the entire heterogeneous soil. The result is the theoretically predicted SWRC of a soil. The mathematical fit of the particle size distribution curve led to the development of an algorithm capable of predicting the SWRC.

$$P_P(d) = \frac{1}{\log\left[\exp(1) + \left(\frac{g_a}{d}\right)^{g_n}\right]^{g_m}} \left[1 - \left[\frac{\log\left(1 + \frac{d_r}{d}\right)}{\log\left(1 + \frac{d_r}{d_m}\right)}\right]^7\right] \qquad (2.9)$$

where,

$P_p(d)$ percent passing a particular grain-size distribution, d

g_a fitting parameter corresponding to the initial change in the slope in the particle-size distribution curve

g_n fitting parameter corresponding to the maximum slope of the particle-size distribution curve

g_m fitting parameter corresponding to the curvature of the particle-size distribution curve

d particle diameter (mm)

d_r residual particle diameter (mm)

d_m minimum particle diameter (mm)

MODELS PROPOSED FOR THE HYSTERETIC BEHAVIOUR OF THE SWRC 2.6.2

Four groups of curves can be distinguished in the SWRC. At the onset of drying from a saturated state, the main drying curve (MDC) of the SWRC is obtained. Branching from this curve is a primary scanning curve in wetting (PSC), which in turn leads to a secondary scanning curve upon drying (SSC). The primary scanning curves (PSC) can start at any point (θ_0, ψ_0) within the limits of the PDC and PWC curves.

Several models of varying complexity for describing the hysteretic behaviour of the SWRC have been presented in the literature. The models can be classified based on their parameter identification requirements and on their theoretical foundation.

The former criterion involves estimating parameters that characterise the soil, the number of these depends on factors such us the complexity of the model. Models, which describe an arbitrary curve, as a function of *n* other curves, can be referred to as an *n*-branch model. In this case a 1-branch model is referring to a model which needs only one initial curve to define the other hysteretic curves. Most of the models are empirical and so the parameters are based on experimental data.

Using this former criterion, we can also distinguish conceptual as well as empirical models. The empirical models rely on the analyses of the shape of the observed SWRC and its properties. The conceptual models found in the literature are based on the independent domain theory of capillary hysteresis (Mualem, 1976). The conceptual model assigns soil water to domains according to a distribution function $f(\psi_d, \psi_w)$ in which the subscripts stand for drying and wetting, respectively. Knowledge of this distribution function allows the determination of the moisture content from degree of saturation, volumetric water content or gravimetric water content, by integrating over the domains that are filled after any series of wetting or drying.

Detailed descriptions of the most commonly used empirically based hysteretic models are given in Appendix 2 along with their advantages and limitations (e.g. the Linear, Point and Slope methods, Parlange's model, Luckner's model). The conceptual models (e.g. Mualem method) link physical behaviour with a theoretical framework.

MODELS ADOPTED FOR VALIDATION USING THE RESEARCH TEST DATA 2.7

As described in Chapter 1, the research presented in this thesis is largely concerned with establishing the wetting-drying response of a number of soils (although strictly ash is not a soil). This has been achieved experimentally by gradually changing the water content of the materials and measuring the consequent changes in suction. Therefore the intention was to establish a SWRC for each soil so that as a minimum the PDC and PWC or MWC are defined. In many cases complex paths were followed involving primary, secondary and tertiary scanning curves.

This extensive data set provides a unique opportunity to check the effectiveness of some of the proposed formulations described in this chapter for a wide range of materials (natural clays, artificial clay, residual soil, ash). For each material, the modelling of the primary components of the SWRC can be verified, i.e. the principal and/or main drying and wetting curves. This is the first stage. Depending on the success of this, the modelling of more complex paths involving scanning curves and reversals in wetting or drying can be investigated.

It is evident that a number of the formulations presented in this chapter have many similarities (see Table 2.2) some being slight modifications of others. The initial curve fitting of the data has been done using the relationship proposed by van Genuchten (1980). This model was chosen because it was one of the first conceived for general application and while being sufficiently comprehensive to model the entire SWRC, the three parameters required to define it (α, n, m) are readily determined from the experimental data. In modelling the hysteretic response and the scanning curves the models described in Appendix 2 (primarily Luckner's model) have been applied.

The results from the curve-fitting exercises are given and discussed in Chapter 7 after the experimental data have been presented and described. One of the ultimate aims of identifying and validating the best model for simulating all aspects of the SWRC is so that it can then be incorporated into a numerical FE analysis. The intention is to be able to model the long-term behaviour of a soil, say within a slope or embankment, that is subjected to a complex series of wetting and drying cycles. Although this will be a subject of future research by others, analyses were performed as part of this research using a simplistic model in order to illustrate the impact on predicted soil response of taking the SWRC into account. Details concerning the method of numerical analysis and the model used are described next in Chapter 3.

CHAPTER 3

FINITE ELEMENT FORMULATION FOR PARTLY SATURATED SOIL BEHAVIOUR

The objective of this chapter is to summarize a set of the classical equations for unsaturated soils that are widely accepted to be a logical extension of those applied to saturated soils. Additionally the chapter will describe briefly the basis of the Finite Element theory, describing the approaches used for analysing boundary value problems in partly saturated soil mechanics that have been recently implemented in the Imperial College Finite Element Program (ICFEP).

MECHANICAL BEHAVIOUR OF A PARTLY SATURATED SOIL 3.1

If the soil particles and the pore water in a soil element are considered incompressible, the application of a stress in a drained fully saturated soil (voids completely filled with pore-water) will produce volumetric water content changes leading to a corresponding change in the volume of the voids of equal magnitude.

In a partly saturated soil, the volumetric change in the pore voids will no longer be equal to the volumetric water content change. A given change in the volume of the soil mass (for the same applied stress) would result in a change to the volume of the water within the soil of lesser magnitude, with the difference being the volume change of the air phase. The pore fluid in a partly saturated soil, is two-phase combining water and air. The air can be present in the soil's pores as occluded bubbles or as a continuous phase. When the air phase consists of occluded air bubbles, the fluid becomes significantly compressible and can flow. When the air phase is continuous, the air-water inter-phase interacts with the soil particles and has an influence on the mechanical behaviour of the soil (from meniscus forces). In a partly saturated soil, the volumetric water content is related to the matrix suction (SWRC) thus, a change in the matrix suction will result in a change in the volumetric water content and vice versa. A change in matrix suction acts like a change in the applied stress, producing changes in the soil structure leading to a variation in the volume of the voids.

Any study on partly saturated soil mechanics has to deal with the mechanical behaviour described above which leads to the inclusion of a number of additional new soil parameters This has been considered in detail by Smith (2003) and Georgiadis (2003) when modifying the Imperial College Finite Element Program.

STRESS STATE VARIABLES AND THE EFFECTIVE STRESS PRINCIPLE 3.1.1

Most proposed equations for expressing the stress state in partly saturated soils have taken the form of a single effective stress equation (see Table 3.1). The common factor to all the equations is the incorporation of a soil 'parameter' that allows the soil behaviour to be characterised in terms of the effective stress state combining together more than one stress variable (e.g. pore air or water pressure, total stress) and other associated soil properties. One difference between some of the equations and that for a fully saturated soil is that they account for variations in air pressure in the soil's pores. Accordingly, the equations lead into a constitutive relationship rather than simply a description of the stress state (Fung, 1965). The soil parameter has been shown to be practically impossible to evaluate individually and is difficult to apply to practical problems (Coleman, 1962; Jennings and Burland, 1962; Bishop and Blight, 1963; Blight, 1965; Burland, 1965). The description of the stress state should include independent stress variables, the number being dependent on the number of phases of the material as stated by Fredlund and Rahardjo in 1993 (for example, the effective stress variable for a saturated soil is independent of the physical properties of the soil). As a result of this viewpoint, there has been a tendency to study the effective stress equation, treating the stress variables independently (Aitchison, 1961; Barden et al., 1969; Matyas and Radhakrishna, 1968).

The use of the stress variables $(\sigma_1 - u_a)$, $(\sigma_3 - u_a)$ and $(u_a - u_w)$ to represent the axial, confining and pore water pressures respectively in triaxial compression tests was introduced in 1962 by Coleman. The stress variables concept was then used for formulating constitutive relations for volume changes. Later in 1963, the use of a single effective stress equation was re-evaluated by Bishop and Blight; they asserted that a change in matrix suction did not always result in the same change in effective stress. They also proposed that data from the laboratory must be plotted in terms of the independent stress variables $(\sigma - u_a)$ and $(u_a - u_w)$, which marked the beginning of the transition towards utilizing the stress variables in an independent manner. The same approach was further reinforced by Blight (1965) and Burland (1964, 1965).

The concept of linking stress state parameters with the volumetric behaviour of an unsaturated soil was introduced by Matyas and Radhakrishna (1968), with volume changes and degree of saturation being plotted versus $(\sigma - u_a)$ and $(u_a - u_w)$. Barden, Madedor and Sides (1969) also suggested analysing volume change in terms of independent stress state variables.

As an unsaturated soil can be considered as a four-phase system (Fredlund and Morgenstern, 1978) the solid phases (considered to be soil particles and the contractile skin) will reach *equilibrium* under applied stress gradients, whereas the fluid phases (i.e. water and air) will *flow* under applied stress gradients. Using multiphase continuum mechanics Fredlund and Morgenstern (1978) presented a theoretical stress analysis basis for the use of independent stress state variables. The theoretical analysis of this four-phase system provides several combinations of independent stress state variables.

Multiphase continuum mechanics considers a three–dimensional element of a size which contains a large number of particles such that it quantifies as a continuum. The equations for force equilibrium are written for each phase of the element such that each phase has an independent continuous stress field associated with each of the Cartesian coordinates and an overall or total stress field can be assumed.

The number of equations depends on the number of phases involved. Each equation is written in the form of stress matrices and relates to a specific stress state variable.

The assumptions in the stress analyses are that the solids are incompressible and the soil is chemically inert. These assumptions are comparable to those associated with the stress state description for a saturated soil (Fredlund and Rahardjo, 1993). The stress analysis shows that any two of the three possible stress variables can be used to describe the state of stress of an unsaturated soil. The possible suggested combinations are: (1) net total stress $(\sigma - u_a)$ and matrix suction $(u_a - u_w)$ (Bishop & Blight, 1963; Alonso et al., 1990; Cui et al., 1993; Wheeler & Sivakumar, 1995), (2) effective stress $(\sigma - u_w)$ and $(u_a - u_w)$, (3) $(\sigma - u_a)$ and $(\sigma - u_w)$ (Fredlund and Morgenstern, 1978). The first pair (1) is considered to have the most common application and to be the most advantageous pair since the effects of total stress changes and pore-water pressure response can be separated. However, no analysis or test has been performed to confirm which combination is most satisfactory. Recently other stress variables have been used successfully for various existing constitutive models, some examples are $\sigma - u_a + \chi(u_a - u_w)$ and $(u_a - u_w)$ given by Bolzon et al. (1996), $(\sigma - \pi_c)$ and π_c (where π_c is capillary pressure) given

by Modaressi & Abou-Bekr (1994), $(\sigma - u_{eq})$ and $(u_a - u_w - s_{AEV})$ given by Kohgo et al., 1993 where u_{eq} and s_{AEV} are the equivalent pore pressure and the matrix suction at the air entry value. Also Houlsby in 1977 presented an analysis of the work input into an unsaturated granular material and suggested that the stress variable suggested by Bishop, i.e. effective stress with $\chi = S$ along with suction controlled by the volumetric water content θ (defined in Chapter 2) to be appropriate. The stress state variable can be extended to a matrix form when multi-directional analyses are being attempted (see Equation 3.1). As a soil approaches saturation the pore air-pressure approaches the pore-water pressure. Therefore the matrix suction term goes to zero and $(\sigma - u_w)$ undergoes a smooth transition to the saturated soil stress state variable.

$$\begin{bmatrix} (\sigma_x - u_a) & \tau_{yx} & \tau_{zx} \\ \tau_{xy} & (\sigma_y - u_a) & \tau_{zy} \\ \tau_{xz} & \tau_{yz} & (\sigma_z - u_a) \end{bmatrix} \text{ and } \begin{bmatrix} (u_a - u_w) & 0 & 0 \\ 0 & (u_a - u_w) & 0 \\ 0 & 0 & (u_a - u_w) \end{bmatrix} \quad (3.1)$$

SHEAR STRENGTH 3.1.2

The shear strength of a partly saturated soil can be expressed as an extension of the Mohr-Coulomb form for a saturated soil as was shown by Bishop et al., in 1960 and Fredlund et al., in 1978 (see Table 3.2). In general, at low suction (with the soil still considered to be saturated), the shear strength is defined by the effective stress increasing linearly with suction, but once the soil becomes partly saturated (i.e. the suction exceeds its air-entry value AEV), the increment of the shear strength is smaller and non linear. However, there is a smooth transition between saturated and partly saturated soils in terms of the shear strength equation.

In the Bishop et al. (1960) equation for a completely dry soil or for a fully saturated soil the expression reduces to the fully saturated Mohr-Coulomb failure criterion (see Table 3.2). Fredlund et al. (1978) made use of $(\sigma - u_a)$ and $(u_a - u_w)$ as stress state variables (see Table 3.2). They have suggested that an unsaturated soil has the same internal angle of shearing resistance as a saturated soil, but that the cohesion increases with an increment of matrix suction. Additionally, they stated that an unsaturated soil can be considered as having two components of cohesion $c = c' + (u_a - u_w)\tan\phi^b$. The equation given by Fredlund et al., 1978 (see Table 3.2) can be visualised in a three-dimensional plot with matrix suction as the third axis (see Figure 3.1).

Table 3.1 Effective stress equations for describing the stress state in unsaturated soils

Reference	Effective stress equation	Variables
1958 Croney, Coleman and Black	$\sigma' = \sigma - \beta' u_w$	σ total normal stress u_w pore water pressure β' bonding factor = number of bonds under tension effective in contributing to soil strength
1959 Bishop	$\sigma' = \sigma - u_a + \chi(u_a - u_w)$	χ parameter related to degree of saturation, u_a air pressure
1960 Lambe	$\sigma' = \overline{\sigma} a_m + u_a a_a + u_w a_w + R - A$	$\overline{\sigma}$ inter-particle stress a_m particle contact area, a_w water phase contact area a_a area which is air-air contact R repulsive pore fluid stress due to chemistry A attractive pore fluid stress due to chemistry
1961, Aitchison	$\sigma' = \sigma + \psi p''$	ψ parameter varying from 0 to 1 p'' pore water pressure deficiency
1960, Jennings	$\sigma' = \sigma + \beta p''$	β experimental factor related to contact area
1966, Richards	$\sigma' = \sigma + u_a + \chi_m(\psi + u_a) + \chi_s(\pi + u_a)$	χ_m effective stress parameter for matrix suction ψ matrix suction (i.e. negative in terms of pressure) χ_s effective stress parameter for solute (osmotic) suction π solute (osmotic) suction

In such a plot, as the soil approaches full saturation (i.e. $S = 1$) the matrix suction becomes zero and u_a approaches u_w reducing the equation to the fully saturated Mohr-Coulomb failure criterion. However, Escario and Saez (1986) have shown that the assumption that ϕ^b is constant is not realistic and that it is equal to ϕ' at very low suctions and then decreases considerably to a constant low value at high values of suction. Moreover, Escario and Saez, suggested that at high values of suction it becomes negative, meaning that at a very high suction the apparent cohesion tends to zero. Fredlund et al. (1995) and later Vanapalli et al. (1996) and Oberg and Salfors (1997) confirmed that the term $(u_a - u_w)\tan\phi^b$ can be predicted from the

shape of the SWRC, also that at high degrees of saturation the negative pore water pressure provides a direct increase in effective stress, thus increasing the shear strength in this manner and that at a lower degree of saturation, the effect of suction on the strength is more variable, with the strength possibly reducing, and must be explicitly allowed for. They also suggested that the saturated shearing resistance ϕ' can be assumed constant at least for the practical engineering suction range of 0 to 500kPa.

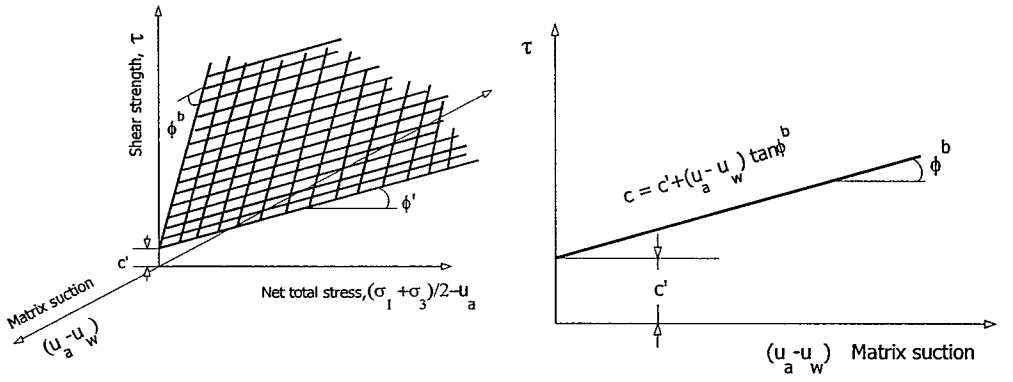

Figure 3.1 Tri-dimensional Mohr-Coulomb criterion

The critical state shear strength equation proposed by Toll in 1990 (see Table 3.2) suggests that at low degrees of saturation, suction has no effect on the soil strength where as the contribution of the net mean stress increases with increasing degree of saturation. Additionally, Toll suggested that $M_a = M_w = M_s$ for fully saturated soils.

Maksimovic (1993) proposed an hyperbolic type function to describe the non-linear failure envelope. The model is based on the maximum angle of dilatancy, the angle of friction at the highest stress level (angle of friction for no volume change) and a median angle pressure (which reflects mainly the strength or the rigidity of grains to crushing). Maksimovic´s model shows very good agreement with the results of triaxial compression tests for a wide range of confining pressures for different kinds of materials.

After some attempts at trying to predict the shear strength of an unsaturated soil using a curve fitting technique, the main conclusion from this works is that the proposed equations are valid only in a limited range of stress and suction and there is difficulty in giving a physical meaning to the parameters used. Cabarkapa (2001) suggested a model for the shear strength of an unsaturated soil using the SWRC and the shear strength parameter of the saturated soil. The model is based on the angle of friction, the angle of the highest dilatancy, the median angle pressure and the median suction pressure Carbarkapa describes a non-linear failure envelope.

Table 3.2 Shear strength equations for unsaturated soils

Reference	Shear strength equation	Variables
1960 Bishop, Alpan, Blight, Donald	$\tau = c' + (\sigma - u_a)\tan\phi' + \chi(u_a - u_w)\tan\phi'$	τ shear strength c' effective cohesion ϕ' friction angle χ is a soil parameter which varies between zero (for dry soil) and 1 (fully saturated soil).
1978 Fredlund, Morgenstern and Widger	$\tau = c' + (\sigma - u_a)\tan\phi' + (u_a - u_w)\tan\phi^b$	c' cohesion intercept when $u_a = u_w$ as evaluated in the conventional manner as for saturated soils ϕ' friction angle with respect to changes in the $(\sigma - u_a)$ stress variable, independent of suction evaluated in the conventional manner as for saturated soils ϕ^b friction angle indicating the rate of increase in shear strength relative to matrix suction, $(u_a - u_w)$, slope of the failure surface in $\tau - suction$ plane. It increases with $(u_a - u_w)$ and appears to be smaller than ϕ' in experimental data.
1996 Vanapallie Et al.	$\tau = c' + (\sigma - u_a)\tan\phi' + (u_a - u_w)\tan\phi'\left(\frac{S - S_f}{100 - S_f}\right)$	S degree of saturation S_f terminal residual degree of saturation
1988 Karube	$q_f = M(p - u_a)$ $M = M'\left(\frac{1}{\alpha}\right) + \left(-\frac{\Delta\upsilon}{\Delta\varepsilon_s}\right)_f$ and $\left(\frac{1}{\alpha}\right) = \left(1 + \frac{f(s)}{p}\right)$	$(\sigma_1 - \sigma_3)$ deviator stress at failure p total mean stress $\left(\frac{1}{3}(\sigma_1 + \sigma_2 + \sigma_3)\right)$ $\left(\Delta\upsilon/\Delta\varepsilon_s\right)_f$ dilatancy index at failure ε_s shear strain defined as $\varepsilon_s = 2(\varepsilon_1 - \varepsilon_3)/3$ M' inclination of the failure lines $f(s)$ intercept of the failure lines on the axis $(p - u_a)$
1990 Toll	$q = M_a(p - u_a) + M_w(u_a - u_w)$	q deviator stress M_a, M_w soil parameters which depend on degree of saturation, total stress and suction ratio respectively representing the contribution of the net mean stress $(p - u_a)$ and suction $(u_a - u_w)$ respectively to the shear strength

The model describes the non-linear shear strength envelope for saturated soil and the influence of the mean net stress on the SWRC and the non-constant variation of the angle of shearing resistance with matrix suction. The model showed good agreement with the experimental results of triaxial and direct shear tests on a wide range of soil types for a wide range of suction and mean net stress. As stated in Chapter 2 (Table 2.1) and as stated in Carbarkapa, 2001, in general two main portions of the failure envelope can be observed: a linear portion up the AEV (where the soil remains saturated), and a non-linear portion as the soil starts to desaturate (the non-linearity of the failure could be related to the fact that the AEV depends on the normal stress that the soil is experiencing). There is no contribution to the shear strength of the suction at the terminal residual suction (described in Chapter 2), therefore the failure envelope flattens and finally becomes horizontal, where ϕ^b attains a zero value.

3.1.3 VOLUME CHANGE BEHAVIOUR

Volume change due to changes in suction is dependent on the processes that control the moisture content of a soil and hence the suction. These processes can be drying, wetting or drying and wetting and vice versa.

In the case of ***total volume changes due to drying,*** once the soil is in a partly saturated state, the effects of suction changes are not equivalent to mean net stress changes, as illustrated in Figure 3.2. The path from A to B in Figure 3.2(a) shows the initial stage of drying from zero suction, where the soil remains fully saturated. While the soil is saturated (up to B), the total volume change is equal to the pore-water volume change, additionally the increase of suction is equivalent to an increase of isotropic total stress. Once desaturation has occurred (point B at the desaturation suction value of AEV) the reduction in the total volume is smaller than the pore *water* volume reduction (Toll's model, 1995). In Figure 3.2(b), the *total* volume changes are expressed in terms of voids ratio, e (volume of voids / volume of solids), and the *water* volume changes in terms of an equivalent void ratio, e_w (volume of water / volume of solids). In this figure, the line from A to B is equivalent to the fully saturated virgin compression line (VCL) and it is followed by both the void ratio line and the equivalent void ratio line, indicating that the total volume changes are equal to the water volume changes. After desaturation has occurred (point B at AEV), both the void ratio and the equivalent void ratio lines deviate from the VCL, the void ratio decreases at a more gradual rate and the equivalent void ratio (expressing changes in water volume) decreases sharply. The behaviour of e described continues until point C (Shrinkage limit) from where very small changes in

e can occur. e_w continues decreasing until point D where the degree of saturation cannot vary significantly with any further reduction in matrix suction.

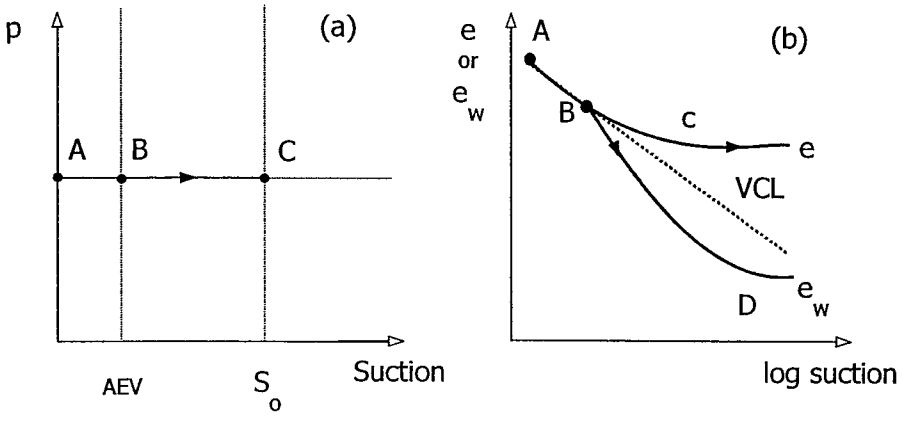

Figure 3.2(a) Drying path from zero suction under constant total mean stress (b) Virgin compression line for a saturated soil and deviations as soil becomes partly saturated

Normally it is accepted that for low plasticity soils, volumetric changes during drying beyond desaturation are small and reversible, however, plastic deformations may occur at high values of suction. Alonso et al., (1990) suggested that the yield suction, S_o , (point C in Figure 3.2(a) beyond which the soil is elasto-plastic) is independent of the confining stress (p) and equal to the maximum previously achieved value of suction. Wheeler and Karube (1996) proposed that yielding due to drying is only possible for partly saturated soils containing saturated clay packets. However, Chen et al., (1999), performed drying tests on compacted low plasticity loess, which exhibited a distinct yield value of suction, and it was shown that the value of the yield suction depends not only on the drying and wetting history but also on the initial soil density. For high plasticity expansive soils, the volumetric deformations due to increasing suction (beyond point B in Figure 3.2(b)) can be large and irreversible.

When considering ***total volume changes due to wetting,*** a partly saturated soil may either collapse or expand upon wetting, depending on whether the confining stress is sufficiently high or low respectively (Alonso et al., 1987). Also a soil may experience a reversal in volumetric behaviour during wetting (initial expansion followed by collapse). In general, if the stress state is not high enough to cause collapse upon wetting, the swelling experienced by a low plasticity non-expansive soil will be small and reversible. On the other hand, high plasticity expansive clays can experience large irreversible volumetric strains from uptake of water. If the stress state of a soil is such that collapse occurs upon wetting, the volumetric deformations depend on the confining stress at which wetting takes place.

A partly saturated soil can also experience ***water volume changes due to drying-wetting.*** For typical stress ranges relevant to engineering practice, total volume changes for fully saturated soils are equal to the water volume changes since both water and solid phases are nearly incompressible and the volume changes are caused by inflow or outflow of water. Due to the presence of air in a partly saturated soil, the water volume changes are no longer equivalent to the overall volume change. As a result, the overall and the water volume changes due to changes of stress and suction need to be considered independently in order to understand the behaviour of a partly saturated soil.

Frequently, water volume changes caused by drying and wetting are studied in unconfined conditions and are expressed in the form of relations between moisture content (i.e., volumetric water content, degree of saturation or gravimetric water content) and suction, i.e. soil-water retention curve (SWRC). It was explained in Chapter 2 that the hysteretic behaviour observed in the SWRC means that the soil can be in a very different state for the same value of suction and thus have different properties depending on its drying and wetting history. This is influenced by various factors such as pore-fluid composition, pore size distribution and contact angles.

Another aspect to consider for a partly saturated soil is the **volume *change due to changes in confining stress.*** Changes in confining stress (i.e. applied total stress on the boundary of the soil) on a partly saturated soil lead to changes in the soil suction, resulting in a volumetric response that can increase the isotropic yield stress, and change the soil compressibility.

The *increase of the yield stress* with suction has been reported by many authors (Duddley, 1970; Maatouk et al., 1995; Cui and Delage, 1996; Rampino et al., 1999). Figure 3.3(a) shows the behaviour of compacted soil samples of speswhite Kaolin. The samples were initially under zero mean net stress and at the same suction (point A). The suction then reduced as an increment of mean net stress was applied (to point B or B_o). Equalization of pore pressure after wetting with increasing amounts of water resulted in the samples reaching points C_3 to C_0, respectively. They were then consolidated under those constant suction values (by increasing p). The increase of the yield stress with suction is clear for samples consolidated from points C_1, C_2 and C_3, as can be seen from Figure 3.3(b) where the yield points observed during the consolidation stage are shown. On the other hand, as seen in the same plot, as yield had already occurred during wetting, samples consolidated from a fully saturated stage C_0 deviate slightly from the observed trend, indicating that the fully saturated yield stress was even smaller.

Additionally, experimental data indicate that the elastic (pre-yield) compressibility coefficient, κ, may decrease slightly with suction instead of being independent as is

normally assumed (see Figure 3.3 (c)). Rampino et al., (2000) in tests performed on partly saturated samples of compacted kaolin have shown that κ, decreases only slightly with suction, while the elasto-plastic (post-yield) compressibility coefficient λ, is affected to a greater degree by suction. From the same tests, the compressibility coefficient λ, appears to be lower (i.e. the soil is less compressible for a given stress increment) for a sample with higher suction. Nevertheless, other studies have found different effects of suction on λ, as was shown by Maatouk et al. (1995) where only a slight decrease of λ with suction was indicated, while Wheeler and Sivakumar (1995) reported an increase (see Figure 3.3 d and e). It is therefore evident that the compressibility behaviour of partly saturated soils is not at all clearly defined.

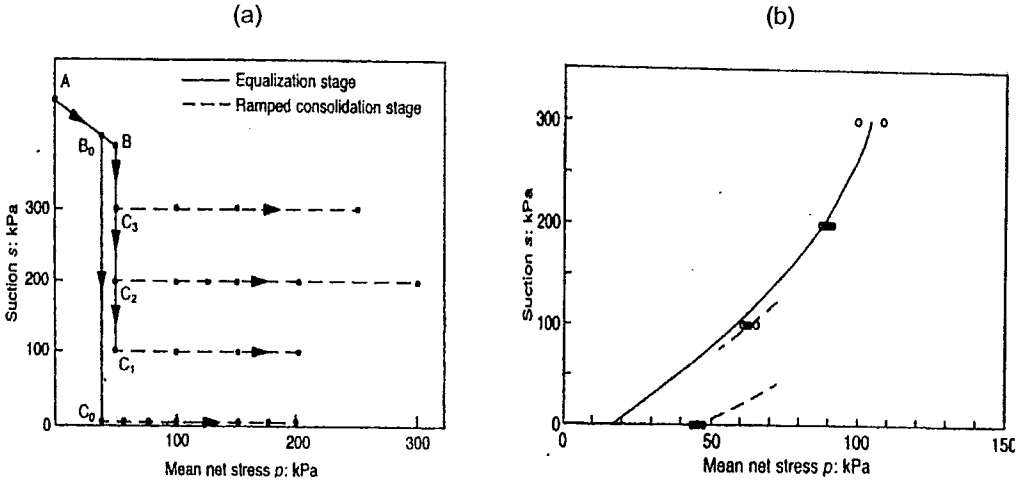

Figure 3.3 (a) stress path and (b) yield points for compacted Kaolin (after Wheeler & Sivakumar (1995)); note that p in these figures relates to mean net stress.

The value of λ, and its dependency on suction measured in the laboratory tests probably depends on the range of the mean net stress at which the tests were carried out. The increase of λ in some test results from Wheeler & Sivakumar 1995, with suction presumably implies that the stress range investigated by them was above the value of p corresponding to the maximum collapse for the particular soil.

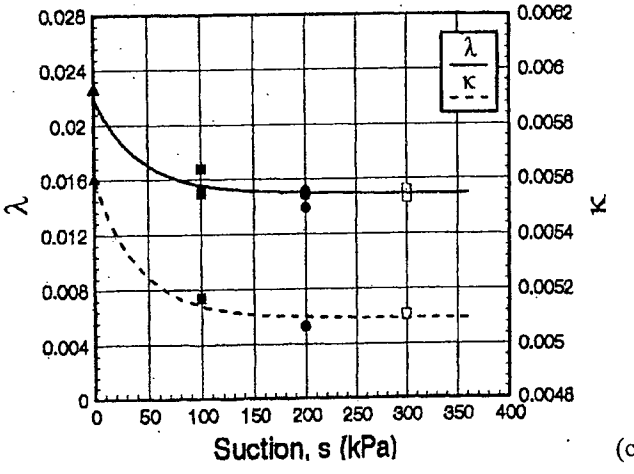

Figure 3.3 (c) Variation of κ and λ with suction (after Rampino et al., (2000)

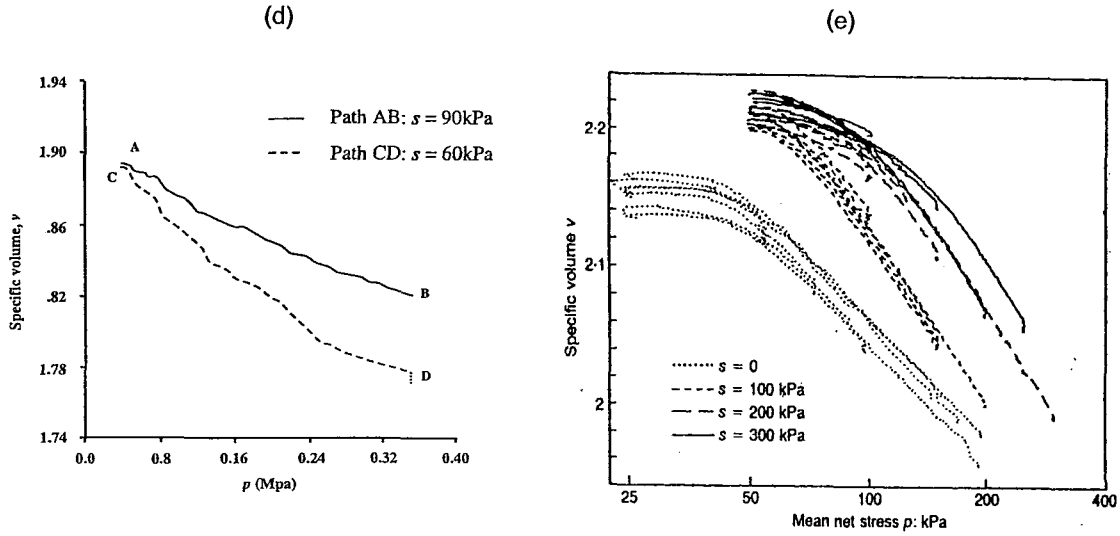

Figure 3.3 Changes in specific volume versus mean net stress during isotropic compression at constant suction (d) after Alonso et al., (1990) (e) after Wheeler & Sivakumar (1995); note that *p* in these figures relates to mean net stress

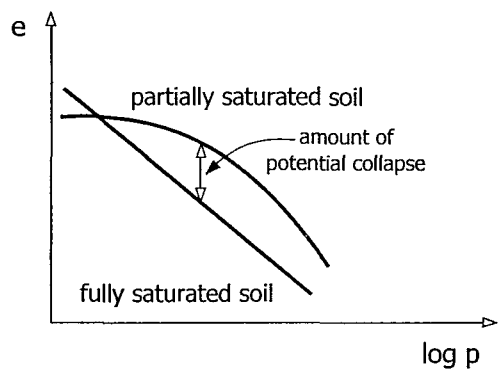

Figure 3.4 Isotropic compression lines for samples with different initial values of suction; note that *p* in this figure relates to mean net stress

The amount of potential collapse due to wetting initially increases with the confining stress, reaches a maximum value and then decreases. The amount of collapse represents the difference between the partly saturated and fully saturated isotropic compression lines (Figure 3.4).

Volume change due to changes in both confining stress and suction is also significant in the behaviour of a partly saturated soil. Many researchers have described the response in terms of net stress and suction related to void ratio (Bishop and Blight, 1963) or to degree of saturation (Matyas and Radhakrishna, 1968) as it can be seen in Figures 3.5 (a) and (b). Most of these researchers proposed analytical expressions for the state surfaces relating void ratio, degree of saturation or water content to the net stress and suction. An example of these is the analytical expression given by Fredlund (1976) in terms of the final and initial stress state, compressive index and water content with respect to total stress and suction. Lloret and Alonso (1985) also suggested a different set of analytical expressions for

a void ratio state surface for a limited range of total external stress and for a larger range of total external stress and for the degree of saturation state surface.

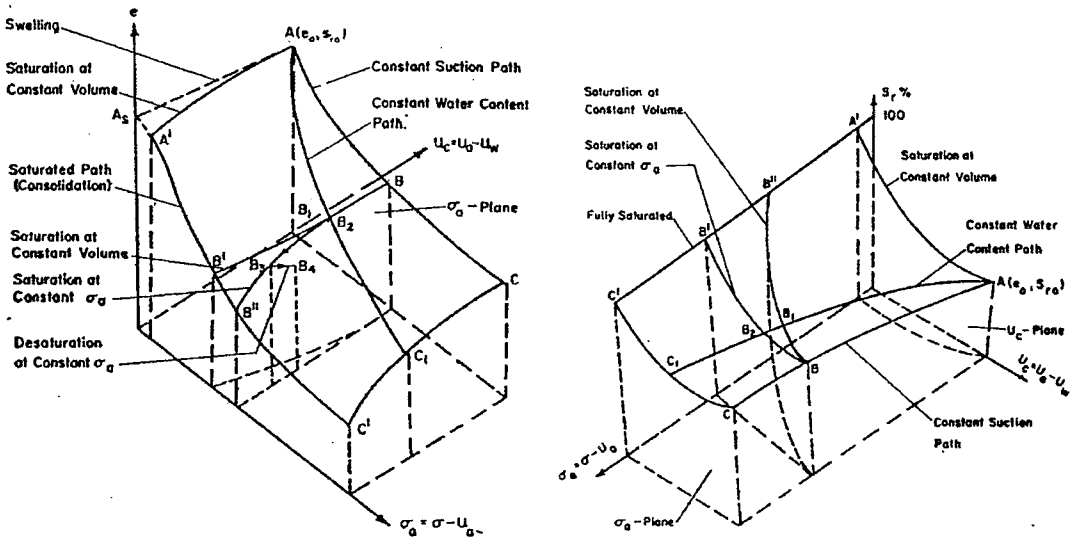

Figure 3.5 (a) State surface for void ratio (b) state surface for degree of saturation after (Matyas and Radhakrishna, 1968)

FLOW LAWS AND SEEPAGE 3.1.4

Childs and Collis in 1950 and Freeze and Cherry in 1979 proposed using Darcy's law to describe the flow of water through an unsaturated soil. Flow of water using Darcy's law states:

$$v_w = -k_w \frac{\partial h_w}{\partial y} \qquad (3.2)$$

where:

v_w velocity of the water flow

k_w coefficient of permeability with respect to the water phase, for unsaturated soil

h_w total head in the water phase

y coordinate direction of flow

However, the coefficient of permeability is strongly controlled by the negative pore-water pressure head and so consequently it should be written as a function of this quantity. The most common form for the variation of permeability with negative pore-water pressure head is the one described by Gardner (1958):

$$k_w = \frac{k_s}{1 + a\left(\frac{u_a - u_w}{\rho_w g}\right)^n} \qquad (3.3)$$

where:

$\left(\frac{u_a - u_w}{\rho_w g}\right)$ negative pore pressure head

k_s saturated coefficient of permeability

ρ_w density of water

g gravitational acceleration

a, n dimensionless material constants

Equation 3.3 is most useful for sands and silts, more research must be done in clay soils which tend to crack as suction increases.

The flow velocity of air through an unsaturated soil may be required in the analysis of certain problems. The flow of air though a partly saturated soil commences at the point when the air phase becomes continuous, at higher degrees of saturation flow of air can only take place as a diffusion process (Fredlund and Rehardjo, 1993). Darcy's and Fick's laws have been applied by researchers to model the flow of air through porous media. The flow velocity of air, v_a, is often described using a modified version of Fick's law for the diffusion of gases through liquids (Fredlund and Rahardjo, 1993).

$$\lambda_a = -D\frac{\partial u_a}{\partial y} \qquad (3.4)$$

where:

λ_a mass rate of air flow

D transmission constant of proportionality for the air phase

The steady state seepage equation for the water phase in an unsaturated soil becomes an expansion of the Laplace equation when it includes the variation of the permeability with negative head (Equation 3.5). Equation 3.5 is a non-linear partial differential equation where the second and fourth terms account for the variation of the permeability with respect to space while the fifth term is referred to as a gravity term. As the soil approaches saturation the special variations of the permeability go to zero, resulting in a smooth transition to the saturated soil case.

$$k_w\frac{\partial^2 h}{\partial x^2} + \frac{\partial k_w}{\partial x}\frac{\partial h}{\partial x} + k_w\frac{\partial^2 h}{\partial y^2} + \frac{\partial k_w}{\partial y}\frac{\partial h}{\partial y} + \frac{\partial k_w}{\partial y} = 0 \qquad (3.5)$$

FINITE ELEMENT ANALYSIS 3.2

ICFEP ANALYSIS FOR PARTLY SATURATED CONDITIONS 3.2.1

The fully coupled constitutive relationship for finite element analysis is a combination of the constitutive relation for the *soil structure* and that for the *water phase*. The

Imperial College Finite Element Program (ICFEP) has been modified by researchers at Imperial College (ICFEP version 9.0) to permit the modelling of coupled behaviour for unsaturated soils as well as fully saturated situations. In respect of the constitutive relation for soil structure, modifications were made to include two new soil parameters. The first, *H*, is the elastic modulus for the soil structure with respect to the matrix suction affecting the deformation of the soil structure that occurs when suction changes. The second, *R*, governs the change in the water storage within the soil due to a change in suction, it is the gradient of the SWRC.

Equation 3.6 represents the governing model that was implemented in ICFEP to enable the analysis of partly saturated soils. As for the case of saturated soils, the ICFEP adaptation for partly saturated soils was based on the constitutive relationship for the *soil structure* and for the *water phase* developed by Potts and Zdravkovic (1999) for saturated soils (see also Smith, 2003, Georgiadis, 2003 for detailed explanations).

$$\begin{bmatrix} [K_G] & [L_d] \\ \Omega[L_G]^T & -\beta\Delta t[\Phi_G]-\omega[M_N] \end{bmatrix} \begin{Bmatrix} \{\Delta_d\}_{nG} \\ \{\Delta_{pf}\}_{nG} \end{Bmatrix} = \begin{Bmatrix} \left([n_G]+Q+[\phi_G]\{pf\}_{nG}\right)\Delta t \\ \{\Delta R_G\} \end{Bmatrix}_1 \tag{3.6}$$

where:

$[K_G]$ global stiffness matrix,

$$[K_G]=\sum_{i=1}^{N}\left(\int[B]^T[D'][B]dVol\right)_i$$

$[B]$ strain matrix

$[D']$ effective stress constitutive matrix

$[L_G]$ off-diagonal (cross-coupling) sub-matrix

$$[L_G]=\sum_{i=1}^{N}\left(_{vol}\int\{m\}[B]^T[N_p]dVol\right)_i$$

$$\{m\}^T=(111000)$$

$[N_p]$ matrix of pore fluid pressure interpolation functions

Ω governs directly the water flow resulting from a change in the soil volume (see Smith, 2003 for further details).

$$[L_d]=\sum_{i=1}^{N}\left(_{vol}\int[D']\{m_H\}[B]^T[N_p]dVol\right)_i$$

$\{m_H\}^T$ equal to (1/H 1/H 1/H 0 0 0)

β time-stepping factor reflecting the variation of pore water pressure with time

Δt time increment

$[\phi_G]$ permeability sub-matrix

$$\omega = \frac{1}{R} - \frac{3\Omega}{H}$$

R modulus relating a change in volumetric water content to change in matrix suction $(u_a - u_w)$

H elastic modulus of the soil structure with respect to $(u_a - u_w)$

$[M_N]$ mass matrix, where $[M_N] = \langle N \rangle \langle N \rangle^T$ with $\langle N \rangle$ being the row vector of shape functions

$\{\Delta_d\}_{nG}$ vector of global nodal displacements for the entire FE mesh

$\{\Delta R_G\}$ vector of global nodal forces

$\{\Delta_{pf}\}_{nG}$ vector of global pore fluid pressures

$$[n_G] = \sum_{i=1}^{N} \left(\int_{vol} [E]^T [k] \{i_G\} \partial Vol \right)_i$$

$[E]$ matrix containing the pore fluid pressure interpolation functions

$[k]$ permeability matrix

$\{i_G\}$ vector defining the direction of gravity

Q flow due to sources/sinks

Initially, Smith (2003) supported the modification to ICFEP based on the fact that in unsaturated soils the pore-water pressure has to be related to the displacements (suction changes may result in changes to the overall soil structure). Smith (2003) proposed an indirect link to the suction and displacement relationship (there is not a direct link between them, suctions and displacements are unknown variables calculated within the FE analysis). The link was made through the top right-hand side (the cross-coupling matrix) of the governing equation (Equation 3.6), as follows:

$$\begin{bmatrix} - & X \\ - & - \end{bmatrix} \begin{bmatrix} D \\ \hline u_w \end{bmatrix} = \begin{bmatrix} R \\ \hline - \end{bmatrix} \qquad (3.7)$$

In the Equation 3.6 representation of the cross-coupling term *X*, the unsaturated equation was modified from its saturated form (see Smith, 2003), and generates the reactions $\{\Delta R_G\}$ necessary to produce the actual deformations $\{\Delta d\}_{nG}$ induced by changes in suction (pore pressures, u_w).

Additionally, in an unsaturated soil the volume of voids is the sum of the volume of water plus the volume of air within the element. In the case where the soil is compressed the volume of voids will reduce and changes will occur with flow of both air and water. However, the proportion of water and air flow is unknown.

Equation 3.6 describes the relationship between water flow and soil deformations through the lower left-hand side of the governing equation as follows:

$$\begin{bmatrix} - & - \\ \Omega & - \end{bmatrix}\begin{bmatrix} D \\ - \end{bmatrix} = \begin{bmatrix} - \\ F \end{bmatrix} \qquad (3.8)$$

According to Smith the water flow lies somewhere between the total deformations (all water flow/no air flow) and zero (all air flow/no water flow) as the total air and water flow equals the volumetric deformations in unsaturated soils. ICFEP models the water flow through the inclusion of the parameter Ω (Ω is explained in more detail later in this chapter) in the lower left-hand side of Equation 3.6.

On the other hand, changes in matrix suction induce changes in volumetric water content. Thus in addition to the flow generated due to the relationship between suction and water content, there may also be flow generated due to the changes in the volume of the element of soil.

In unsaturated soils the suction-induced flows must be generated in the lower right-hand side of Equation 3.6 since this is where flow and pore pressures interact, as is shown in Equation 3.9, where ω incorporates the matrix suction functions and given flow components generated by changes in matrix suction.

$$\begin{bmatrix} - & - \\ - & (X - \omega) \end{bmatrix}\begin{bmatrix} - \\ \mu_w \end{bmatrix} = \begin{bmatrix} - \\ F \end{bmatrix} \qquad (3.9)$$

The implementation of partly saturated soil behaviour into ICFEP in this manner is consistent with the conceptual and physical model given for the stages of the SWRC (see Chapter 2).

ICFEP MODEL FOR PARTLY SATURATED SOIL ANALYSIS 3.2.2

The non-linear constitutive model applied to the numerical analysis performed in this research project to describe the behaviour of unsaturated soils was developed by Smith (2003). The model implemented (denoted model 82 in the ICFEP manual) allows a soil to be modelled in accordance with three-dimensional Mohr-Coulomb theoretical behaviour. The model developed by Smith is based on ICFEP-model 16 with the inclusion of the *H* parameter (elastic modulus of the soil structure with respect to matrix suction $(u_a - u_w)$).

For saturated soils, ICFEP-model 16 enables the soil behaviour to be analysed using effective stress in accordance with the standard Mohr-Coulomb failure criterion giving the soil's yield surface the shape of a hexagonal cone in principal effective stress space $\sigma_a', \sigma_b', \sigma_c'$ (Potts & Zdravkovic, 1999) as shown in Figure 3.6.

$$\tau_f = c' + \sigma'_{nf} \tan \phi' \qquad (3.10)$$

where:

τ_f	shear stress at failure (on the failure plane)
c'	effective cohesion
σ_{nf}'	effective normal stress (on the failure plane) at failure
ϕ'	effective angle of shearing resistance

In partly saturated analysis, ICFEP-model 82 implies that when the magnitude of suction exceeds the AEV, ICFEP switches to operating in total stress. This means that σ_{nf}' is automatically changed to σ_{nf}. This is consistent with Fredlund et al., (1978) as presented in Table 3.2. However as noted by Smith, ICFEP-model 82 makes no allowance for the ϕ^b term given by Fredlund et al. Essentially, the term $(u_a - u_w)\tan\phi^b$ (from the equation given by Fredlund et al. in Table 3.2), is assumed to be equal to zero.

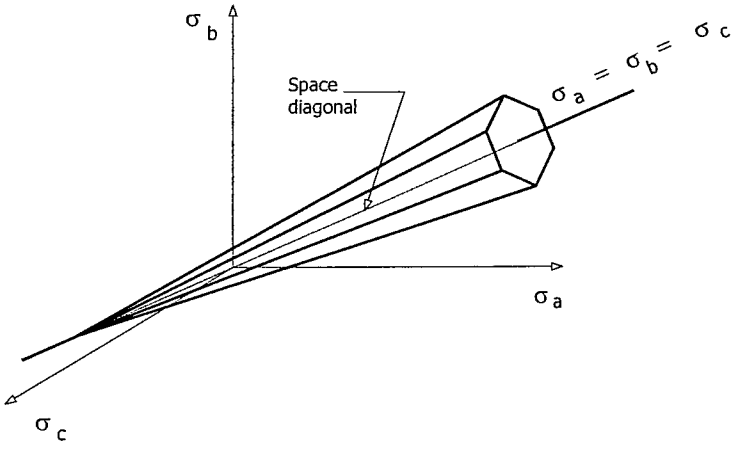

Figure 3.6 Mohr-Coulomb yield surface in principal stress space (after Potts and Zdravkovic, 1999)

H is assumed to be a function of matrix suction (Wong et al., 1998), it relates a change in matrix suction to the resulting change in soil structure. Smith (2003) reports that Biot (1941), who described the consolidation of a partly saturated soil sample with occluded air bubbles, stated that "the coefficient $1/H$ is a measure of the compressibility of the soil for a change in water pressure". H under the situation of an isotropic stress state is a parameter, which relates stress with volumetric water content change, and it may also affect the relationship between the soil structure deformation and the volumetric water content (see Smith, Chapter 5).

H was implemented in ICFEP as a simple tri-linear curve (see Figure 3.7). The function is linear because of the lack of data available, however the simplicity of the general variation of *H* appears to be consistent with the limited experimental data currently available (Wong et al., 1998 reported in Smith 2003).

Figure 3.7 shows the relationship between matrix suction and *H* in ICFEP-model 82. In the figure, no value is given for *H* at suctions with magnitude less than the soil's AEV (air-entry value) since in this range the soil is assumed to behave as a saturated soil. Beyond this value, *H* varies piece-wise linearly and is specified by three values with their corresponding matrix suctions. Afterwards, *H* becomes constant (the idea of *H* becoming constant at higher suctions is a convenient assumption for dealing with this suction range which is unlikely to be measured in most practical field-based problems (Smith, 2003)). The use of three points to define *H* has a theoretical justification in some respect according to Toll's theoretical model (1995). The zones described by the points mark the different behaviours of the soil coinciding with the stages of the SWRC.

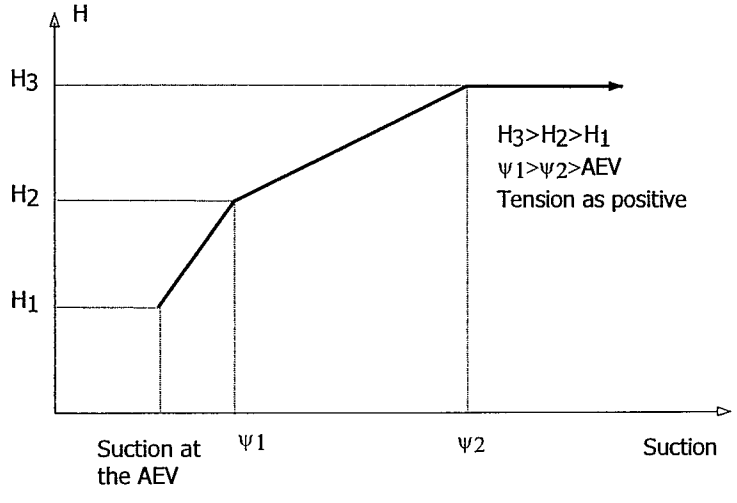

Figure 3.7 Variation of *H* parameter proposed in ICFEP-model 82 (Smith, 2003)

ICFEP-model 82 is not perfect for modelling unsaturated soil behaviour, however it was intended to simulate the basic response of such soils. The data required for ICFEP-model 82 (see Appendix A3 which includes relevant pages from the ICFEP user's manual for Model 82) are the same as required for ICFEP-model 16: the cohesion, c'; the angle of shearing resistance, ϕ' ; the angle of dilation, υ , (governing the plastic volumetric strains) and the parameters defining *H*. It is also necessary that the SWRC and the Ω parameter are specified. These are input using a Soil-Water Retention Curve formulation, the implementation of a simplified model of which was part of this research (the experimental data and its simulation with hysteretic models will allow more realistic analyses to be performed in the future).

It is important to note that at pore-water pressures lower than the AEV the soil is saturated or tension saturated, so ICFEP treats the soil as saturated. Accordingly, when H is not required ICFEP-model 82 reverts to ICFEP-model 16. Thus the advantage of ICFEP-model 82 is that it enables the study of the behaviour of an element of soil that may change from being saturated to unsaturated or vice versa.

The parameter omega, Ω (see Equation 3.6), was defined in ICFEP by Smith (2003) to model the fact that in a partly saturated soil the total air and water flow correspond to the volumetric deformations (water flow lies somewhere between the total deformation - all water flow/no air flow - and zero – all air flow/no water flow). Ω represents the volume of water that flows for a given change in the volume of voids of the soil. Ω is equal to 1 when the soil is fully saturated and once the water phase becomes discontinuous it reduces to zero. The definition of Ω in ICFEP is a simple linear variation because of the lack of experimental data to indicate how Ω varies between a saturated state and a state with a very low degree of saturation.

Thus for the SWRC conceptual model implemented in ICFEP, if the pore water pressure is equal to or greater than the AEV, $\Omega = 1$, and once the water phase becomes discontinuous (at a suction value specified by the user), Ω reduces to zero. Also, it is important to note that while H increases with an increase in matrix suction, Ω decreases.

As stated earlier, the implementation of partly saturated soil behaviour into ICFEP is consistent with the conceptual model given by the description of the stages of the SWRC (see Chapter 2). Additionally, the modification of ICFEP is in accordance with the conceptual definition of the new parameters implemented (i.e. Ω, H). For instance, in the initial part of the secondary transition stage of desaturation, where both air and water flow, if the soil is influenced by an external compression, the Ω parameter will be less than unity but greater than zero. On the other hand, in the final part of the same stage, Ω will still be greater than zero, although it will progressively tend towards zero. According to the characterization of the residual stage where compression of a soil will cause only air flow, Ω will be equal to zero.

ICFEP SWRC MODEL FOR PARTLY SATURATED SOIL ANALYSIS 3.2.3

In ICFEP two SWRCs were implemented for use in unsaturated soil analysis. The first one was developed by Smith (2003) and the other was implemented as a part of the research described in this thesis.

The SWRC was intentionally implemented in terms of degree of saturation rather than in terms of volumetric water content as commonly adopted in the literature (see Smith 2003). Smith stated that this is useful as the degree of saturation is always 100% when the soil is fully saturated whereas the volumetric water content at full saturation depends on porosity. In ICFEP the soil is assumed to be fully saturated if the pore water pressure is greater than the AEV.

Smith (2003) stated that the decision is also supported by the fact that the SWRC in terms of degree of saturation and volumetric water content must be related and be similar in form. However, it is important to remember that there is no unique SWRC for a given soil, it is more correct to represent a SWRS (soil-water retention surface) which can be plotted in terms of degree of saturation or volumetric water content as is shown in Figure 3.5. The advantage of implementing an SWRC independently of the applied stress in ICFEP is that the model is more practical since the parameters are limited but available. In the case where a stress-dependent SWRC is needed for an analysis in ICFEP, it can be simulated by representing the soil within the analysis as a series of layers each with its own SWRC (Smith 2003).

ICFEP SWRC model 1 does not exist as an SWRC formulation. The first curve developed, ICFEP SWRC model 2 was a temporary model and has a simple four-part piece-wise linear form curve (Figure 3.8). The model enables the gradient of the curve to be defined, but it was clearly very simplified and Smith (2003) found that the points at which the slopes in the curve change could induce numerical convergence problems during analysis. The ICFEP user's manual for ICFEP SWRC model 2 is presented in Appendix 3.

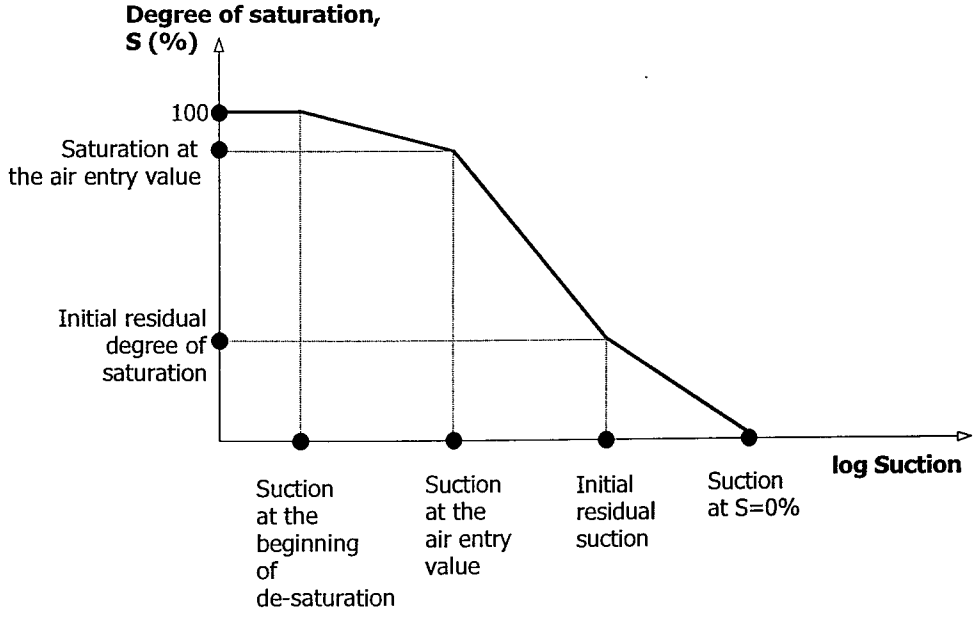

Figure 3.8 ICFEP SWRC model 2, simple, non-hysteretic.

In the case of the simplified SWRC model 2, it was suggested that in ICFEP a reasonable estimation for the suction at which Ω becomes zero to be input as an independent variable. Additionally, Ω will be equal to 1.0 at the AEV. Between these two suction conditions a linear variation is assumed. However, the real variation of the parameter Ω must be a subject of further research in partly saturated soil mechanics.

ICFEP SWRC model 3 was implemented as a first step to introducing the hysteretic nature of the SWRC (Figure 3.9 and Appendix 3.3). This model 3 is based on the van Genuchten equation (1980) which is described in Chapter 2. In this stress-independent model, the minimum possible value of the degree of saturation has to be greater than 0% for modelling a residual degree of saturation (Figure 3.9).

Van Genuchten (1980) developed a relatively simple equation for the SWRC (see Table 2.2). The resulting expression for the SWRC contains five independent parameters which may be obtained by fitting the proposed SWRC model to experimental data. The equation provides a reasonably accurate description of the SWRC. Van Genuchten derived the SWRC equation from knowledge of the normalised (i.e. dimensionless) volumetric water content, Θ (described in Chapter 2):

$$\Theta = \frac{\theta - \theta_f}{\theta_s - \theta_f} \qquad (3.11)$$

where:

θ current volumetric water content

θ_r residual volumetric water content

θ_s saturated volumetric water content

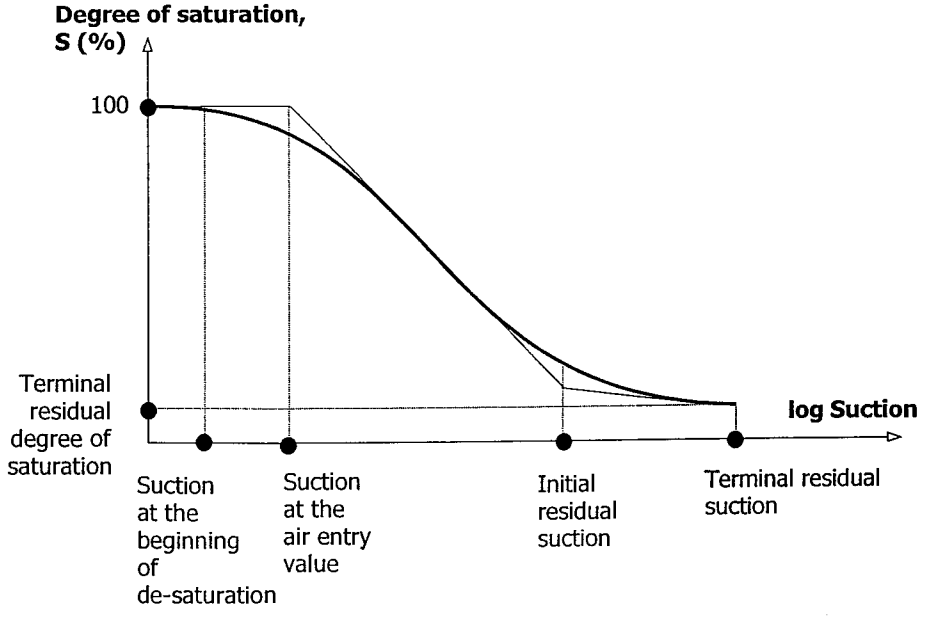

Figure 3.9 ICFEP SWRC model 3, simple, non-hysteretic, non-linear

In order to relate the normalised water content with the pressure head, van Genuchten developed the following equation:

$$\Theta = \left[\frac{1}{1 + \left(\frac{h}{\alpha} \right)^{n}} \right]^{m} \quad (3.12)$$

where

α, n, m experimentally determined constants

h pressure head (assumed to be positive).

The SWRC as a function of the pressure head and water content (see Equation 3.13) is obtained from Equations 3.11 and 3.12, additionally, the SWRC as a function of the suction at the desaturation point and terminal degree of saturation is shown in Equation 3.14:

$$\theta = \theta_r + \frac{(\theta_s - \theta_r)}{\left[1 + \left(\frac{h}{\alpha} \right)^{n} \right]^{m}} \quad \text{(3.13) in terms of volumetric water content or}$$

$$S = \left[\frac{1}{1.0 + [\frac{(\psi - \psi_{des})}{\alpha}]^{n}} \right]^{m} * (1 - S_f) + S_f \quad \text{(3.14) in terms of degree of saturation}$$

where:

ψ Suction at saturation S

ψ_{des} Suction at desaturation point

S_f Terminal residual degree of saturation

Equation 3.13 contains five independent variables $\theta_r, \theta_s, \alpha, n$ and m which have to be estimated from the experimentally determined soil water retention data. Of these five parameters, m can be obtained assuming $m = 1 - 1/n$ as suggested by Mualem (1976a) and θ_s is easily obtained experimentally. Additionally θ_r may be measured experimentally. Unfortunately, because of the time involved in obtaining a complete loop in the SWRC it is not always measured routinely. It is usually obtained by extrapolating the available experimental data of the SWRC towards lower volumetric water contents. The θ_r component of the van Genuchten equation is the volumetric

water content for which the gradient $\partial\theta/\partial h$ becomes zero (excluding the region near θ_s which also has a zero gradient). From a practical point of view it is probably sufficient to define θ_r as the volumetric water content at some large negative value of the pressure head (e.g. at the permanent wilting point).

Assuming for the moment that θ_r is a well defined parameter and that the parameters θ_s and θ_r can be estimated with sufficient accuracy, then the constants α and n can be obtained as explained in Chapter 2.

The implemented Equation 3.14 in ICFEP also contains five independent parameters, $\psi_{des}, S_f, \alpha, n$ and m, however once the volumetric water contents related in Equation 3.13 have been obtained, the parameters ψ_{des} and S_f are easy to determined. The parameters α, n and m in Equation 3.14 are the same parameters as those described for analysing Equation 3.13.

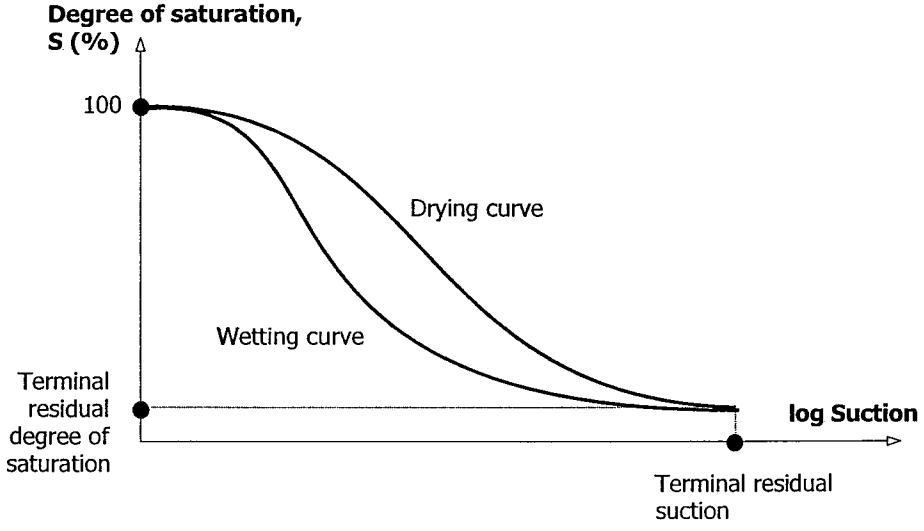

Figure 3.10 ICFEP SWRC model 4, simple, hysteretic, non-linear

The point denoted 'initial residual suction' represents the point at which the void ratio becomes constant, beyond this point changes in volumetric water content are due to changes in degree of saturation only.

ICFEP SWRC model 3 for describing the soil behaviour matches with the conceptual model given for the SWRC stages (see Chapter 2, and Smith, 2003).

ICFEP SWRC model 4 was implemented as a simple hysteretic SWRC introducing the hysteretic nature of the SWRC (Figure 3.10 and the relevant pages from ICFEP user's manual in Appendix 3.4) considering a loop, which closes at 100% of degree

of saturation. This model 4 is based on ICFEP SWRC model 3. The implemented equations are as follows (Equation 3.15 and 3.16):

For wetting curve:
$$S = \left[\frac{1}{1.0 + \left[\frac{(\psi - \psi_{des})}{\alpha_w} \right]^{n_w}} \right]^{m_w} * (1 - S_f) + S_f \qquad (3.15)$$

For drying curve:
$$S = \left[\frac{1}{1.0 + \left[\frac{(\psi - \psi_{des})}{\alpha_d} \right]^{n_d}} \right]^{m_d} * (1 - S_f) + S_f \qquad (3.16)$$

where the subscripts d and w define the parameters describing the curve for drying and wetting respectively.

The analysis of the experimental data (Chapter 6 and 7) allows the SWRC for each of the soils investigated to be accurately defined (within the limitations of using the van Genuchten formulation). It will then be possible to implement a representative theoretical model of the SWRC in a FE analysis of a boundary value problem using ICFEP. This is also a topic for future research as described in Chapter 9.

CHAPTER 4

LABORATORY INVESTIGATION OF THE SOIL-WATER RETENTION CURVE

As discussed in Chapter 2 the SWRC can be represented using different quantities, e.g. gravimetric or volumetric water content or degree of saturation which are always plotted against log suction. This chapter is concerned with the measurement of soil matrix suction, it being straightforward to measure the other quantities. The measurement of suction has presented a considerable challenge historically. Its accurate determination is important as suction has a profound influence on the behaviour of partly saturated soils.

Suction measurement devices can be divided into two categories, those that measure suction directly and those that measure suction indirectly. Direct methods measure pore-water pressure. Indirect methods measure other parameters such as relative humidity, resistivity, conductivity or moisture content which are converted to suction through known relationships or by experimental calibration.

The ***matrix suction*** is the difference between the pore-air pressure and the negative pore-water pressure in a soil. The most common devices, which directly measure negative pore water pressures are tensiometers apparatus that rely on the axis-translation principle. The most common method of measuring matrix suction indirectly is the calibrated filter paper technique. The axis-translation principle and the calibrated filter paper technique will be explained in detail in this chapter.

Total suction measurements represent the reduction in the chemical potential of a liquid solvent because of capillary pressure and the presence of the solute. Total suction can be determined indirectly by either measuring the vapour pressure of the soil water or the relative humidity of the air around in the soil (see Glossary). Total suction measurements are of particular importance in high suction ranges where matrix suction measurements are difficult to obtain. As in the case of matrix suction measurements, the calibrated filter paper technique may be used to measure total suction. Psychrometers are also used for measuring total suction.

Osmotic suction can only be measured indirectly and the measurements are not as reliable as those of total and matrix suction. Osmotic suction was not measured independently in this research.

A summary of devices commonly used for measuring total, matrix, and osmotic suctions is given in Table 4.1. The techniques used in this research for measuring matrix suction are described in this chapter.

Table 4.1 Common suction measurement devices

SUCTION COMPONENT MEASURED	INDIRECT METHOD	DIRECT METHOD
TOTAL	**Psychrometers** (subdivided into two groups thermistor / transistor--thermocouple). Range measured: 100 - 8,000kPa. Parameter measured: Humidity. **Calibrated filter papers - no direct contact.** Range measured: up to 30,000kPa. Parameter measured: moisture content of filter paper.	
MATRIX	**Calibrated filter papers - direct contact.** Range measured: up to 30,000kPa. Parameter measured: moisture content of filter paper. **Thermal conductivity sensors.** Range measured: 0 – 400kPa.	**Standard tensiometers.** Range measured: 0 - 90kPa **Axis-translation apparatus (Pressure plates).** Range measured: 0 up to 10,000kPa **Imperial College suction probe.** Range measured: 0 – 1,500 kPa
OSMOTIC	**Pore fluid squeeze.** Range measured: Entire range.	

4.1 INDIRECT MEASUREMENT OF MATRIX SUCTION USING THE FILTER PAPER TECHNIQUE

If an absorbent material is placed in contact with a soil, moisture will be transferred until both materials have a common attraction for the available moisture. After reaching equilibrium the stress state in the water in both materials will be the same (see Figure 2.4 for an analogous case). If one of the materials is very homogeneous, it is possible to relate its water content to an equivalent suction, and therefore establish the suction in the soil. This is the principle that is used in the filter paper technique for suction measurement.

The filter paper method can be used to measure soil suctions up to 30,000kPa. The method can be used to measure either the total or the matrix suction of a soil. This technique can be performed in the laboratory with disturbed and undisturbed soil samples.

The filter paper method relies on equilibrium conditions being reached. This equilibrium can be obtained by either liquid or vapour moisture exchange between the soil and the filter paper. When a dry filter paper is placed in direct contact with a soil sample, it is assumed that the water flows from the soil to the paper until equilibrium is achieved. Additionally, when a dry filter paper is placed such that it does not make direct contact, a vapour flow of moisture from the soil to the filter paper will take place until equilibrium is achieved (see Figure 4.1). Having established equilibrium conditions, after a fixed time period, the water content of the filter paper is measured (Fredlund and Rajardjo, 1993).

At equilibrium the stress state of the water in the filter paper corresponds to the matrix suction of the soil when the paper is placed in contact with the water in the soil and the total suction of the soil if the paper is not in direct contact with the surface of the soil sample.

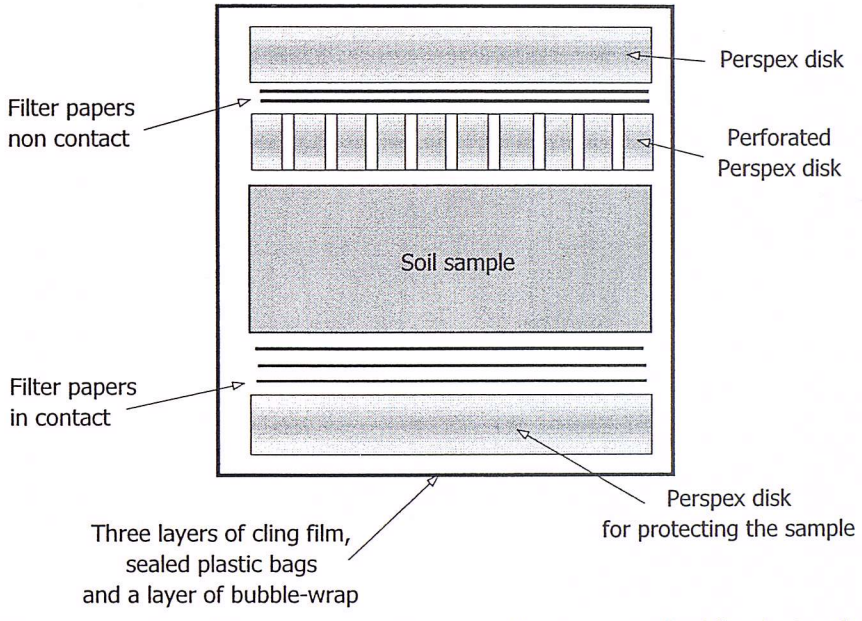

Figure 4.1 Arrangement used to measure suction using filter paper method (contact and non-contact method)

MEASUREMENT TECHNIQUE 4.1.1

The filter paper must be of the ash-free quantitative Type II as specified by ASTM standard specification E832. Whatman No. 42 and Schleicher and Schuell No. 589 White Ribbon are two commonly used brands of filter paper. Filter papers from the same brand are considered to be "identical" in the sense that all filter paper disks have the same calibration curve. In this research project Whatman No. 42 filter paper was used for the suction measurements.

The contact procedure involves placing one filter paper in perfect contact with the surface of the soil sample. However, for this arrangement, it is also possible to use

three filter papers instead of one (see comments in Chapter 5). The centre filter paper is used for the suction measurement, while the other filter papers protect the centre paper from contamination by the soil (Figure 4.1). The indirect contact procedure involves placing one (or two) dry filter paper on a perforated Perspex disk that is seated on top of the soil sample.

A standard procedure for measuring matrix suction has been developed over many years at Imperial College and was adopted in this research for performing the drying path measurements. It has been found to give excellent repeatability. First, two initially air-dry filter papers (70mm diameter) are placed in perfect contact either side of a disk-shaped soil sample usually of 100mm diameter. Both flat surfaces of the soil sample must be trimmed smooth and be free of irregularities. Each filter paper is held in place with a solid Perspex disk (approximately 100mm diameter and 25mm thick). The soil specimen (with Perspex disks) is then covered with three layers of cling film, minimizing any air trapped inside the wrapped sample and sealed with sticky tape (Figure 4.1). The sample is then placed in three sealed plastic bags and 'bubble-wrap' is placed around the sample for protection.

The soil sample (with filter papers) is stored for seven days in an insulated box in a temperature-controlled environment. This procedure allows the filter papers to absorb water from the soil specimen until suction equilibrium is reached. Changes in the ambient temperature could affect the filter paper results; therefore temperature variations during equilibration should be minimized.

At the end of the equilibrium period, the cling film is carefully cut from the sample, the soil sample unwrapped, and the top Perspex disk removed. The filter paper from beneath the disk is placed inside a small plastic bag which is then sealed and weighed immediately. The same procedure is repeated for the second filter paper at the base of the sample. The filter paper within the plastic bag should be weighed immediately using a balance capable of measuring to 0.0001g. It is important to emphasize that minimizing the period for transferring the paper to the plastic bag and weighing them both will minimize errors due to water loss or gain in the filter paper.

The practice of using a small re-sealable plastic bag for weighing each filter paper is intended to minimize errors due to changes in the moisture content of the filter paper during the weighing process. Prior to measuring the water content of the filter papers, the empty plastic bags for holding each filter paper are also weighed to the nearest 0.0001g. Tweezers must be used at all times for handling the plastic bags as well as the filter papers.

Finally, the filter papers are removed from the plastic bags and placed in an oven at a temperature of 110 ±5°C for a minimum of 2 hours. In the meantime, separate dry, clean filter papers are placed in the empty plastic bags to absorb any excess of moisture. Having dried all the water from within the plastic bags using these filter papers, the plastic bags are re-weighed and the dry filter papers from the oven are placed back inside the same plastic bags that they were removed from, and sealed. The bags plus the dry filter papers are then weighed again to determine the dry mass of the filter papers. The difference between the dry mass and wet mass of the filter papers is used to determine the equilibrium water content of the filter papers. The water content of the filter papers is calculated and the corresponding suction is estimated using the relationships described in Table 4.2.

In the case of the wetting processes, an initially wet filter paper is placed in contact with the sample. It is important to emphasize that the same small amount of water must be added to the filter paper at each end of the sample at each wetting stage of the test in order to obtain a similar reduction of suction. The filter paper is wetted by submerging it in distilled water. It is advisable to allow the filter paper to absorb the water completely before placing the paper on the sample.

Table 4.2 Filter paper calibrations for Whatman 42 paper

REFERENCE	CALIBRATION	WATER CONTENT (in the filter paper) w/c , (%)	$\log_{10}$ (suction) (kPa)
Chandler, Crilly and Montgomery-Smith (1992)	for an initially dry filter paper	<47 >47	4.842 - 0.0622 * (ω/c) 6.050 - 2.48* log10(ω/c)
Dineen (1997)	for an initially wet filter paper.	<15.5 15.5<(ω/c)<57.2 >57.2	4.842 - 0.0622 * (ω/c) 4.573 - 0.0449 * (ω/c) 2.094 – 0.0158 * (ω/c)

CALIBRATION 4.1.2

Several relationships between the filter paper water content and suction have been developed for various types of filter paper. Most calibration curves appear to have been established using initially air-dry filter papers. There is a degree of hysteresis in the water content versus suction relationship for a filter paper between wetting and drying. It is therefore necessary to establish independent calibration curves using initially wet filter papers.

The relationship between suction and filter paper water content is bi-linear (see Table 4.2), with the change in gradient occurring at a water content of about 47% for

Whatman No. 42 paper when each initially air-dry filter paper is left to equilibrate with the soil for at least 7 days before measuring its water content (Chandler, Crilly and Montgomery-Smith, 1992). The same change in linearity occurs at about 15.5% for Whatman No. 42 paper when the filter paper is initially wet (Ridley, 1993 and Dineen, 1997).

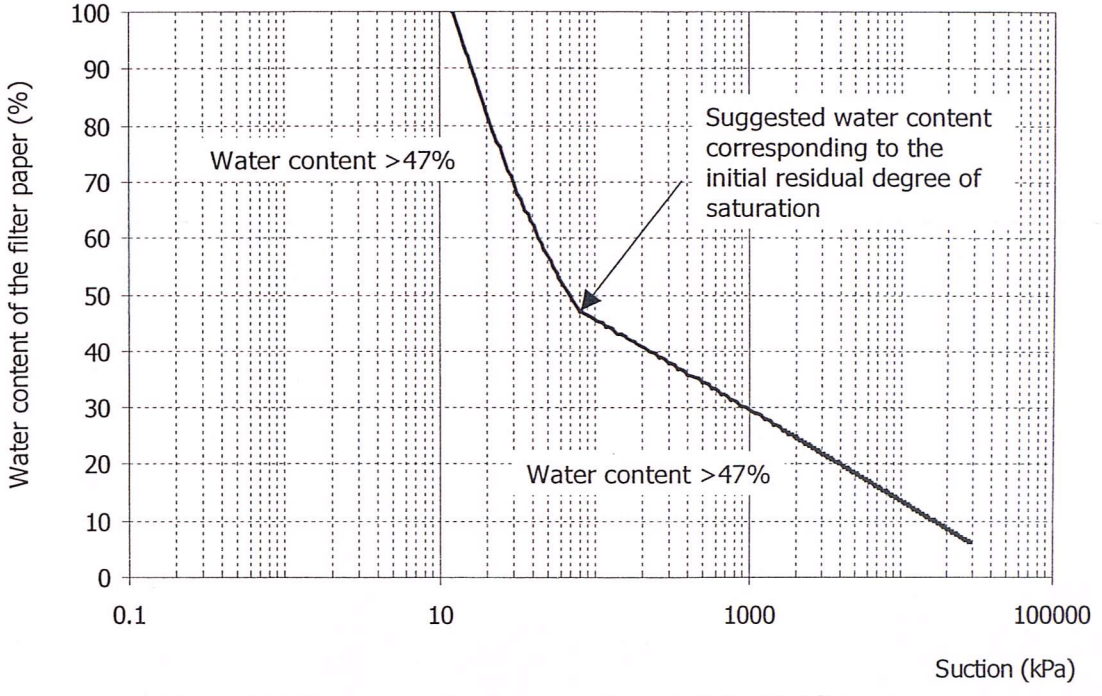

Figure 4.2 Filter paper calibration curve for an initially dried filter paper

In this research, the calibrations presented by Chandler, et al. (1992) and Dineen (1997) were used for calculating the matrix suction from initially dry and initially wet filter papers respectively. The calibrations utilized are presented in Table 4.2 where w/c is the water content of the filter paper (in percent). The equilibrium suctions in the tests performed are obtained from the calibration curves (Table 4.2) by using the measured equilibrium water content of the filter paper. The equilibrium suctions calculated from the calibrations are assumed to be equal to the suction in the soil specimen.

As for most porous media, the filter paper also exhibits an inflection point in the suction versus moisture content relationship. It is shown with the calibration curve for Whatman No 42 paper for an initially filter paper (see Figure 4.2). The Figure suggests a SWRC in the same manner as for soils, with a marked inflection point at about 47% of water content. Following the discussion in Chapter 2, the change in the gradient probably corresponds to the water content representing the initial residual conditions in the SWRC of the filter paper. The inflection point would correspond to the initial residual degree of saturation in a plot of suction versus degree of saturation.

REPEATABILITY OF FILTER PAPER MEASUREMENTS 4.1.3

The filter paper technique is highly user-dependent. The technique appears to produce a large scatter of data depending on the exact method used and the care in measurements. According to Ridley (1993), the scatter in the results is larger in the low suction range (up to 500kPa) than in the high suction range. The Building Research Establishment (BRE, 1993, reported in Ridley, 1993) suggests that the measurements fall within a range that is typically $\pm 25\%$ of the mean. However it seems that a good and consistent technique can produce a better accuracy than this. With care it is possible to achieve an accuracy of ±10%.

After the sample has been wrapped, changes in the ambient temperature can lead to condensation or evaporation during the equilibration period which will interfere with the process of the moisture transfer. When condensation occurs the measured suction will be too low while evaporation will cause suction measurements to be too high. Therefore when it has not been possible to maintain control of the temperature throughout the 7-day storage period, the suction measurements may not be reliable or representative.

Another potential cause of error in filter paper measurements is when small pieces of the soil specimen stick to the side of the filter paper that was making contact with the soil sample. It is advisable to remove these particles but care must be taken to make sure that the filter paper does not dry as they are removed. Therefore this operation must be performed in a period of only a few seconds. When small particles do remain attached to the filter paper, sealed inside the bag, the measurement should be viewed with caution and perhaps discarded.

Good contact between the soil sample and the filter paper is vital for accurate matrix suction measurements. The transfer of water will occur partly through the vapour phase in places where the soil and the filter paper do not make good contact. This results in an increase in the time required to reach equilibrium (Ridley et al., 2003).

Finally, Ridley and Edenmosun (1999) showed that with Whatman No. 42 filter papers, the equilibrium water content is significantly influenced by the presence of salt in the soil. Their results indicate that the equilibrium water content of the filter paper reduces when there is salt present in the soil sample. Therefore, the suction in salty soils may be overestimated when the calibration given by Chandler et al., (1992) is used.

Following the extensive series of measurements that were made using the filter paper technique during the course of this research, aspects of the method were appraised more carefully. A discussion of these aspects is given in Chapter 5.

DIRECT MEASUREMENT OF MATRIX SUCTION USING AXIS-TRANSLATION TECHNIQUE 4.2

The method of axis-translation is a technique used in testing partly saturated soil samples to avoid the need to measure pore water pressures less than absolute zero (-100kPa below atmospheric pressure).

When the air pressure around a soil sample is atmospheric, its matrix suction value is numerically equal to the negative pore water pressure. As the soil suction approaches 100kPa, cavitation can potentially start to take place in the water of a measuring system, e.g. a pressure transducer or manometer. Air starts coming out of solution and it is not possible to sustain or measure higher suctions (for a detailed discussion on cavitation, see Marinho, 1994). The axis-translation technique involves translating the origin of reference for the pore-water pressure from standard atmospheric conditions to an elevated air pressure applied around the sample (Hilf, 1956). Consequently the problem of cavitation is overcome if the water pressure in the measuring system does not become highly negative.

The experimental procedure involves placing the sample within a chamber in which the surrounding air pressure can be increased. The pore air pressure in the sample then becomes equal to the externally applied air pressure and the pore water pressure also undergoes the same pressure change (Hilf, 1956). The crucial factor is that the matrix suction (i.e. the difference between the pore air pressure and the pore water pressure) of the soil remains constant regardless of the translation of both the pore air and pore water pressures. The primary advantage is that the pore water pressure is referenced to an elevated air pressure such that it is raised to a positive value that can be measured reliably with standard pressure transducers.

The primary drawback of the axis-translation technique is that the air in the sample has to be in a continuous form to ensure that it is uniformly controlled by the applied outer chamber pressure. This means that technique is suitable for testing soils that are at a stage where they have a degree of saturation less than about 90%

The use of the axis-translation technique requires the control of the pore air pressure and the control or measurement of the pore-water pressure. A ceramic disk or a cellulose membrane is generally used as an interface between the unsaturated soil sample and the pore water pressure measuring system. Water in the disk or membrane acts as a link between the pore water in the soil specimen and the water in the measuring system. Continuity between the water in the soil and the water in the disk or membrane is necessary in order to establish the matrix suction correctly. At the same time, air should not pass through the interface into the measuring system. This can be achieved by using a high air-entry ceramic material. Reliable measurements are possible as long as the sample matrix suction does not

exceed the air-entry value of the ceramic material (Fredlund and Rahardjo, 1993). Once the air-entry value of the ceramic is exceeded, the presence of air in the measuring system causes erroneous measurements of the pore-water pressure.

The pressure plate and pressure membrane apparatus use the axis-translation concept in order to control the matrix suction value. A description of these apparatus and the techniques used with them is given in the following sections.

PRESSURE PLATE APPARATUS 4.2.1

The pressure plate apparatus relies on the axis-translation technique. In the research described in this thesis, pressure plates were used to measure directly matrix suction up to 1,500kPa within soil samples.

The pressure plate apparatus consists of a high air-entry ceramic disk contained in an air pressure chamber. In the base of the chamber there is a small water reservoir, immediately beneath the disk, which should always be filled with water and vented to atmospheric pressure during a test. The ceramic disk should be fully saturated and in contact with the water in the water reservoir. A schematic diagram of the pressure plate apparatus is shown in Figure 4.3.

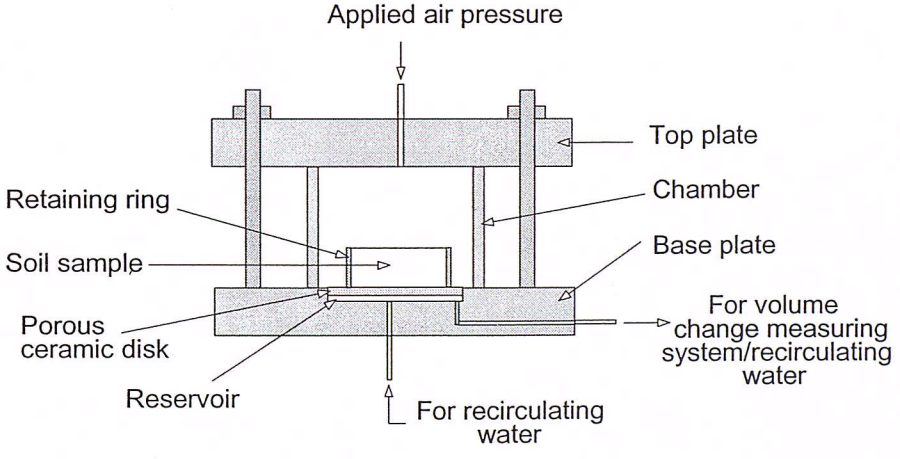

Figure 4.3 Typical pressure plate apparatus

The ceramic disk is generally made from sintered kaolin. The air-entry value of such a ceramic material is a measure of its maximum pore sizes. It is equivalent to the pressure at which air can be forced through the ceramic material when it is fully saturated and is also equivalent to the matrix suction that can be sustained before air starts entering its pores. Care needs to be taken in fully saturating the ceramic material with water, especially when it is initially dry. Once the disk is saturated it acts as a membrane between air and water such that free air cannot pass through the disk. In this research 50kPa, 100kPa, 200kPa and 1,500kPa air-entry value ceramic disks were used for measuring matrix suction in soil specimens.

The saturation procedure used for the pressure plate chamber involved applying air pressure to the pressure plate chamber which was filled of de-aired water with an initially dry ceramic disk inside. The maximum air pressure applied was always higher than the AEV of the porous material. This saturation procedure was performed before each test.

Pressure plate measurement technique 4.2.1.1

The test procedure used in this project, involved inserting a soil specimen into a 38mm retaining ring. The soil sample is then placed on top of the saturated ceramic disk. Finally, after placing and tightening the surrounding chamber, the air pressure is raised to the desired matrix suction. The maximum air pressure (matrix suction) which can be applied to the soil sample in a test, is controlled by the air-entry value of the ceramic disk and the maximum pressure limit of the chamber.

During drying processes, the matrix suction in the sample increases and as a consequence some pore water is transferred from the soil to the water reservoir through the disk and into the measuring system. During wetting processes, the matrix suction in the sample decreases and the water in the measuring system is absorbed by the soil sample.

The water content of the sample at each equilibrium condition was calculated from measurements of water volume change and after oven-drying the soil sample at the end of each test. After equilibrium at each change in the applied pressure, the samples were always removed and weighed. If a drying followed by a wetting process was planned, the water content at the initial equilibrium condition for the wetting stage had to be stable. Stable equilibrium was defined as when there was no change in the pore water volume measuring system for at least three hours. Only at this point was the wetting process commenced.

The pressure plate apparatus can be used with a number of different arrangements to provide a more accurate volumetric measurement of water flow in or out of the soil sample (see Figures 4.4, 4.5 and 4.6). The ancillary components used in this research were selected depending on the pore-water pressure range that was to be measured.

In general the accessory most commonly used with a pressure plate is a bubble trap for collecting air bubbles in the water volume measuring system (see Figure 4.4). The bubble trap is used in conjunction with a small-diameter burette connected for storing water flowing out from the sample or as a reservoir for supplying water to the sample in wetting processes. This arrangement was used in the early stages of this research for soils with a suction range between 50 and 1,500kPa.

A different system for extracting air bubbles from the water volume measuring system was developed during this research for samples subjected to a drying process at very low values of suction (up to 14kPa) as shown in Figure 4.5 (the necessity for measuring accurately such very low suctions is explained in Chapter 5). Low air pressure from a pressure controller is fed through a solenoid valve with a restricted outlet flow. This air at low pressure goes first into an additional pressure chamber with a connected pressure transducer and then into the pressure plate apparatus.

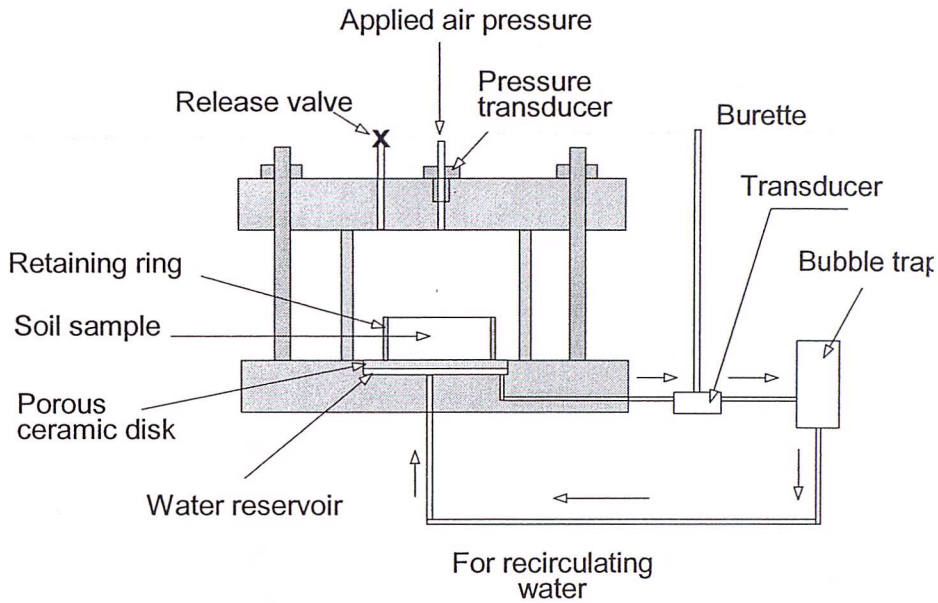

Figure 4.4 Pressure plate apparatus connected with bubble trap and burette

The purpose of the additional chamber is to increase the overall capacity of the low-pressure reservoir that is necessary for accurately controlling the pressure within the pressure plate. The desired effect is achieved by measuring the pressure in the additional chamber (with the pressure transducer) and using a computer control program to open the solenoid valve for a short time. The pressure is read by the computer and if the pressure is still too low the valve is opened once again and the process repeated until the desired pressure is reached.

As water is displaced from the sample it is measured as it enters a small burette with an internal diameter of 5mm using a very sensitive low-range pressure transducer mounted at its base. The transducer is calibrated to give a reading in cubic centimetres (cc) or millilitres (ml) of water flowing in or out of the sample. Additionally the same transducer is calibrated to show the pressure in kPa generated by the height of the water in the column and this should be taken into account when determining the pore water pressure in the sample.

The drying or wetting processes are considered to be complete when a steady state is maintained in the burette for three hours.

For measuring suctions from 14kPa to 1,500kPa, a peristaltic pump was used to re-circulate water in the reservoir beneath the ceramic disk so as to facilitate removal of air-bubbles (see Figure 4.6). The peristaltic pumps used have a flow rate of about 0.1ml/s when energized with12volts. Tubing of 2.5mm internal diameter was used to connect the peristaltic pump to the water reservoir and to a beaker (500ml). The beaker was filled with distilled water and silicone oil (200/1,000cS) placed on its surface, and the silicone oil was also covered with a dish glass. The silicone oil and the glass dish were used to prevent evaporation. Additionally, the beaker acts as a reservoir for transferring water to or from the sample as required. The beaker with water and silicone oil allows air bubbles to escape from the pore water or from the water pressure measuring system as the peristaltic pump circulates water.

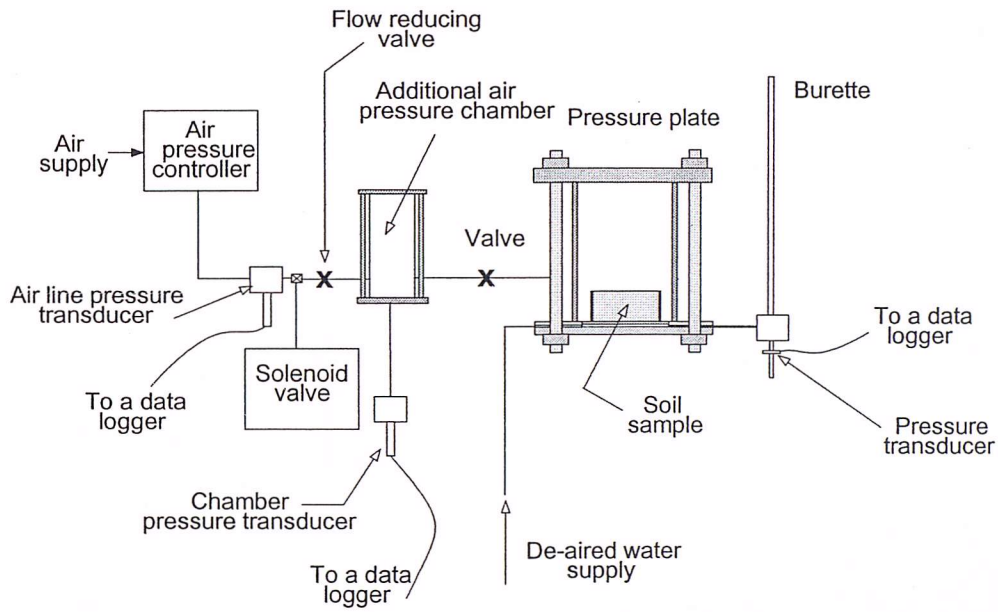

Figure 4.5 Pressure plate apparatus arrangement for measuring matrix suction up to 14kPa

The beaker is placed on a weighing balance, which has a resolution of 0.01g. Measurements from the balance allow the volumetric water change in the soil sample to be determined (these are logged automatically by the computer). When water stops flowing out of or into the soil sample for three consecutive hours (with the balance reading stable) an equilibrium condition is then considered to have been reached.

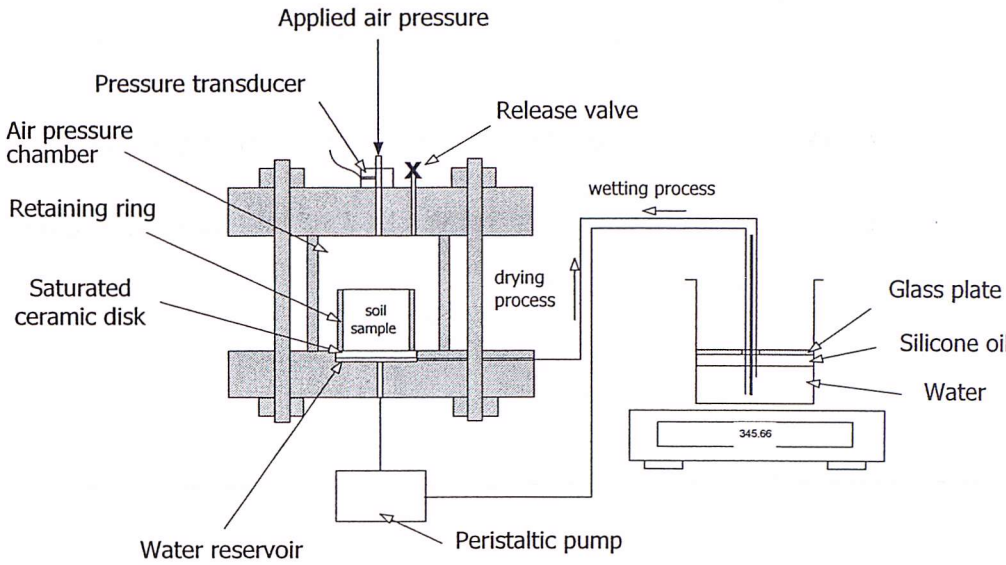

Figure 4.6 Pressure plate apparatus for measuring suctions up to 1,500kPa

The tubes going into the water in the beaker are held in place so that they do not apply any load on the beaker or the balance.

PRESSURE MEMBRANE EXTRACTOR 4.2.2

The pressure membrane extractor controls the matrix suction directly using the principles of the axis-translation technique. It works in a similar way to the pressure plate except that the ceramic material is replaced with a cellulose membrane. The pressure membrane was used in this research for measuring high range matrix suctions, between 1,500 and 10,000kPa by applying compressed air from a gas bottle. The equipment was purchased from Soilmoisture Equipment Corporation of Santa Barbara, California.

The pressure membrane extractor that was used consists of a cellulose membrane disk (30cm diameter), extractor cylinder with an inlet pressure valve, top and bottom plates, screen drain plate with outflow tube and clamping bolts and nuts (see Figure 4.7).

The cellulose membrane discs used in this research were Model No 1041D12 supplied by Soilmoisture Equipment Corporation. The cellulose membrane material allows water to flow through its pores, but not air, thereby keeping constant air pressure levels inside the chamber. The membrane is made from regenerated cellulose material with an average pore diameter of 2.4 nanometres. The air-entry value for this cellulose material is 10,000kPa.

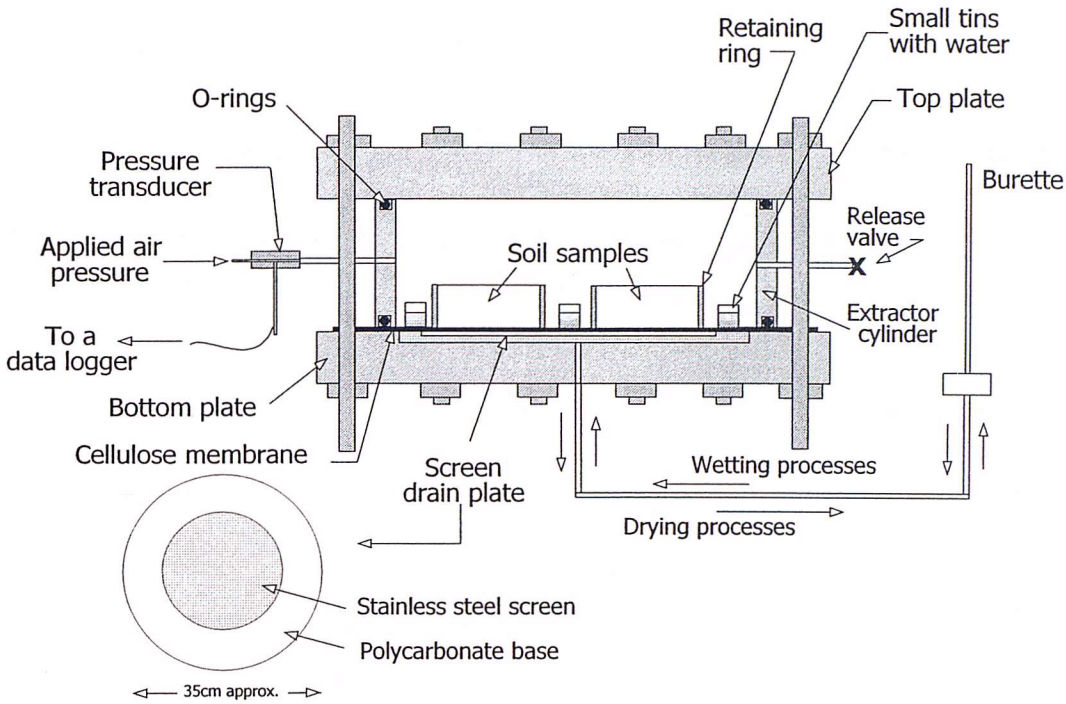

Figure 4.7 Pressure membrane apparatus for measuring suction up to 10,000kPa

As a consequence of the manufacturing processes, the cellulose membranes are usually supplied folded in half, and are stiff in a dry condition. It is therefore necessary before using each cellulose membrane disk to submerge it in water to soak. In this research the membranes were prepared for achieving saturation by immersing them in distilled water in their folded state for one day, then unfolding them and leaving them for a further two days until they were fully saturated and flexible.

The extractor cylinder (30cm diameter) is a steel ring that forms the working chamber of the pressure membrane extractor. The extractor cylinder has a groove in both its top and bottom end faces to hold two o-ring seals in place. The o-rings provide an airtight seal between the top plate, the extractor cylinder and screen drain plate. The inlet pressure valve is mounted on the side of the extractor cylinder for connection to the gas bottle and the pressure regulator.

The bottom plate forms the lower boundary of the extractor and has a small hole at the centre for the screen drain plate's outflow port.

The screen drain plate consists of a stainless steel mesh installed in a polycarbonate base. It provides the support surface for the cellulose membrane and channels moisture out of the extractor through its outflow port in the centre of the plate and the attached outflow tube. The small outflow port contains an o-ring that provides a seal for the outflow tube.

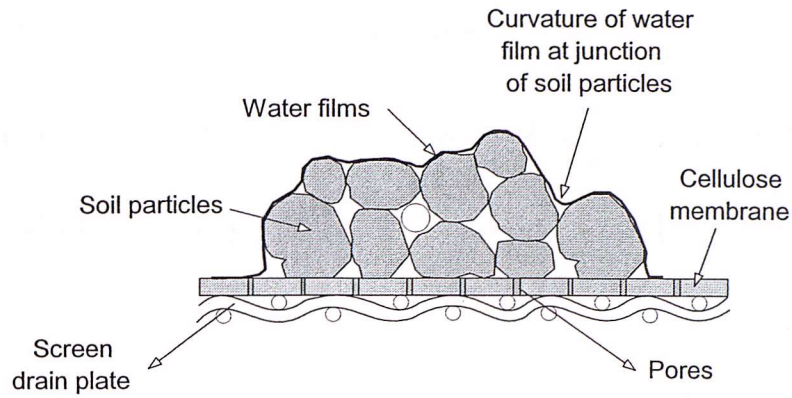

Figure 4.8 Water films surrounding soil particles in the pressure membrane extractor

For the initial setting-up stage of the test, a pressure regulator is used to maintain a slightly higher pressure behind the screen plate than inside the chamber in order to keep the soil specimen in contact with the cellulose membrane during the test.

The pressure membrane extractor is assembled as follows (see Figure 4.7). First, the screen drain plate is seated on the bottom plate and the cellulose membrane is placed on the top of the screen drain plate. Then an o-ring seal is put onto the membrane disk. The extractor cylinder is located on top of this o-ring (with the o-ring fitting into a groove in the base of the cylinder). Finally, after placing the soil sample inside the pressure membrane extractor, the top plate is positioned on the extractor cylinder and tightened down with bolts and nuts.

Additional accessories incorporated as a part of the pressure membrane apparatus used in this research were an air bubble trap and a small-diameter burette. The air bubble trap was used for collecting air bubbles in the water volume measuring system and was also useful for checking for any leaks in the cellulose membrane. As was described for the pressure plates, the burette (10mm internal diameter) is connected for storing the water coming from the sample or as a reservoir for supplying water to the sample in the wetting processes (see Figure 4.7). A change in the volume of water in the burette during a test indicates water volume change in the soil specimen.

Pressure membrane extractor measurement technique 4.2.2.1

The pressure membrane extractor is able to extract moisture from a soil sample because of the microscopic pores in the wetted cellulose membrane at its base (see Figure 4.8). When the pressure inside the extractor chamber is increased above the pressure behind the screen plate (atmospheric pressure), the higher pressure forces excess water through the microscopic pores of the cellulose membrane and out of

the extractor through the outflow port. The high-pressure air will not flow through the pores of the cellulose membrane since they are filled with water.

The surface tension of the water in the pores of the membrane at the air-water interface support the air pressure, much the same as a flexible rubber diaphragm. When the air pressure inside the extractor is increased, the radius of curvature of these interface menisci decreases (Figure 4.9). Water films will not break and allow air to pass through, even at the maximum extractor pressure because of the small pore diameters (2.4 nanometres). There is an exact relationship between the magnitude of air pressure in the extractor and the radius of curvature of the air-water interface of the water in the pores of the cellulose membrane (see Appendix 1 for relationships between meniscus radius and pressure).

When soil samples are placed on the top of the cellulose membrane in the pressure extractor, the air pressure is raised above atmospheric pressure (i.e. the pressure that the outflow tube is vented to) and water will flow from around each of the soil particles and out through the pores of the cellulose membrane. At any given air pressure inside the extractor, water will flow until the curvature of the water film menisci between each of the soil particles is the same as that in the pores of the cellulose membrane and corresponds to the curvature associated with that pressure (Figures 4.8 and 4.9).

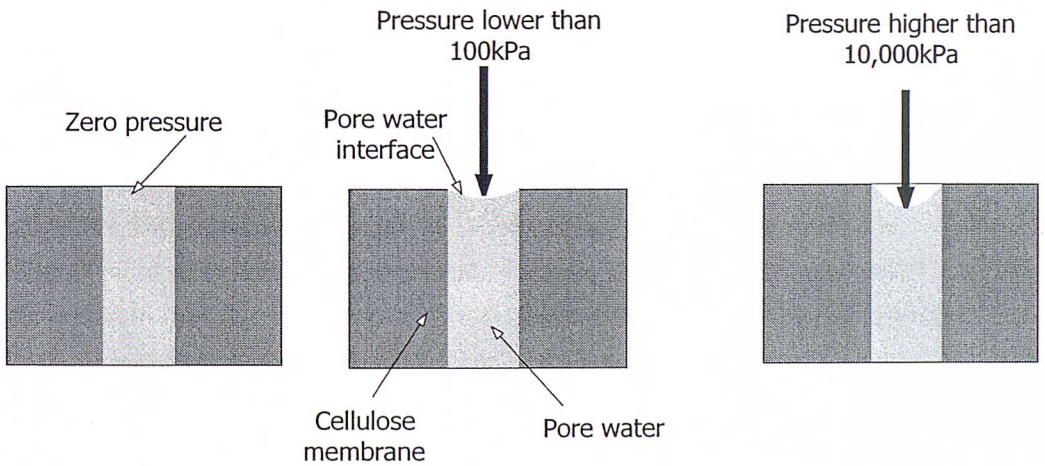

Figure 4.9 Water menisci under air pressure

After increasing the air pressure slowly to the desired air pressure in the pressure membrane extractor, water will flow immediately from the extractor into the burette attached to the outflow tube. After a few hours the rate of outflow of water from the soil samples will fall off markedly. The effect explained above is also seen when a test in the pressure plate apparatus is undertaken.

Prior to running a test using the pressure membrane extractor, disturbed samples were prepared by passing the soil through a 2mm sieve to remove the larger particle sizes and to reduce all aggregates less than 2mm. Undisturbed and disturbed soil

samples were tested In retaining rings (38mm diameter) and their top and bottom ends were prepared with flat surfaces on which to lay the cellulose membrane. Detailed procedures for preparing and testing soil samples in the pressure membrane are given in the ASTM Standard specification, designations D421-85, D422-63 and D3152-72. During this project two soil samples were tested at the same time in the pressure membrane apparatus.

Sample preparation involves installing the soil specimens into the retaining ring by either compaction, tamping disturbed soil or trimming intact samples. The ring is then placed on top of the saturated cellulose membrane. Once the airtight chamber is pressurized to the desired matrix suction, an equilibrium condition is considered to have been reached when there are no noticeable changes in the level of the water in the burette over two days. The applied air pressure (matrix suction) should not exceed the air-entry value of the membrane. Additionally, the membrane and the strength of the chamber govern the maximum air pressure (matrix suction), that can be applied to the soil sample.

During a test, small amounts of air pass through the cellulose membrane. This is caused by air that dissolves in the water under the air pressure in the chamber and then comes out of solution when the water flows from the pressure extractor at normal atmospheric pressure.

When equilibrium is reached the air pressure in the pressure extractor is released, so the extractor can be opened. In a single drying process at the end of each test the samples must be removed as soon as possible after releasing the pressure in the chamber in order to avoid changes in their moisture content. Therefore, the water drainage system is also completely detached from the pressure membrane extractor immediately after releasing the pressure. The cellulose membranes are discarded after each test.

In the case of either drying or wetting processes, once equilibrium has been reached, and the air pressure released, the top plate is carefully removed, paying attention to avoid moving the cylinder extractor. The samples are weighed within their retaining rings. The samples are returned to the pressure extractor membrane ensuring firm contact between the soil surface and the cellulose membrane. The extractor is then closed and the air pressure raised or lowered to the next level of air pressure so the soil samples can come to equilibrium with the new air pressure value. The Author considers that it is necessary to wet carefully the cellulose membrane with drops of water or using a spray, and to wet the outside of the chamber where the membrane protrudes and around the rings of the soil samples. However, the amount of water added should be minimized to avoid changing the

moisture of the soil samples. By wetting the membrane at this stage, micro-cracks and fissures in the membrane will be avoided when the chamber is tightened down.

Repeatability of pressure membrane measurements 4.2.2.2

Tests that rely on the axis-translation technique involve movement of water from the sample to the measurement system or vice versa depending on the value of the air pressure applied to the chamber and the pore water pressure in the sample. A small error will be caused by this movement of water in a single determination of the matrix suction using the axis-translation technique. Flow from the measurement system into the soil sample will cause an under-prediction of the suction and flow in the opposite direction will cause an over-prediction. This effect can be minimized by reducing the volume of water in the reservoir or by increasing the size of the sample (Ridley and Burland, 1993).

However, it is advisable to keep sample heights small in order to keep the time to reach equilibrium reasonable as the time required to reach equilibrium varies with the square of the sample height (e.g. a soil sample 2cm high will take four times as long to reach equilibrium as a sample 1cm high). Additionally, when running tests on tall soil samples or certain types of soils (e.g. clays), where reaching equilibrium requires many days, bacteria may attack the cellulose membrane causing air leaks and potential sample contamination. In cases where bacterial activity is relevant, the cellulose membrane needs to be soaked in an antibiotic (e.g. ampicillin) anhydrous solution (1gr/lt) prior to use.

The Author considers it advisable to use an antibiotic solution as a standard practice because of the extremely long equilibrium times resulting from the very small pore size of the cellulose membrane. The flow rate through the membrane is very low even at pressure differentials across the membrane of 10,000kPa. Most of the soil samples tested needed more than one day to approach hydraulic equilibrium (frequently much more than one day).

In order for moisture to be extracted from the soil samples it is essential that the sample be in perfect contact with the cellulose membrane in the pressure extractor. It is therefore advisable to prepare the sample sitting on top of the cellulose membrane in order to 'connect' the water films in the sample with those in the cellulose membrane. This procedure ensures the maximum rate of water flow from the sample during the extraction process and good accuracy in the results.

The accuracy of the equilibrium values obtained from the soil samples tested in the pressure membrane extractor will be no more accurate than the regulation of the air pressure supplied to the pressure plate. In this research project the pressure control

manifold used a regulator, designed to control the pressure in the gas bottle up to 42,000kPa (± 1,000kPa) and the pressure in the pressure membrane extractor up to 16,000kPa (± 250kPa).

Tiny cracks in the cellulose material may cause air to leak during a test and consequently produce erroneous results. Care should be taken when handling the screen drain plate to prevent damage or breakage of the fine wires in the mesh which could perforate the cellulose membrane material. Also the cellulose material should be handled carefully while it is in a dry condition to avoid sharp bends or wrinkles.

4.3 DIRECT MEASUREMENT OF MATRIX SUCTION USING TENSIOMETER DEVICES

4.3.1 IMPERIAL COLLEGE SUCTION PROBE

Ridley and Burland (1993) introduced a new tensiometer with an extended range. The device comprised a stainless steel body, a pressure transducer and a 1,500kPa air-entry value porous stone. Ridley and Burland (1995) presented a modified version of the tensiometer which they named Imperial College suction probe (see Figure 4.10). It comprises a miniature tensiometer constructed of stainless steel with a pressure transducer, a 1,500kPa air-entry porous stone, a diaphragm and a miniature strain gauge rosette (see Figure 4.10). The IC suction probe can be used for measuring negative pressures up to about 1,500kPa. It should be noted that the probe cannot measure osmotic suction.

The IC suction probe measures suction through the porous ceramic disk, which transmits the soil suction from the soil to a water reservoir once the suction probe is in perfect contact with the soil sample. The reservoir is between the porous stone and the diaphragm (see Figure 4.10). The water reservoir contains a very small quantity of de-aired water (about 3 mm^3).

4.3.1.1 Saturation procedures for the IC suction probe

During the saturation process, a dry suction probe is first placed in a vacuum chamber for a period of about 30 minutes (see Figure 4.11). The aim of this step is to evacuate air present in the porous stone and in the reservoir behind the stone. Secondly, the suction probe under vacuum is wetted by submerging it under water in the vacuum chamber. The vacuum is maintained for another 30 minutes and then the pressure is increased to atmospheric level (Figure 4.11 shows a general scheme of the procedure).

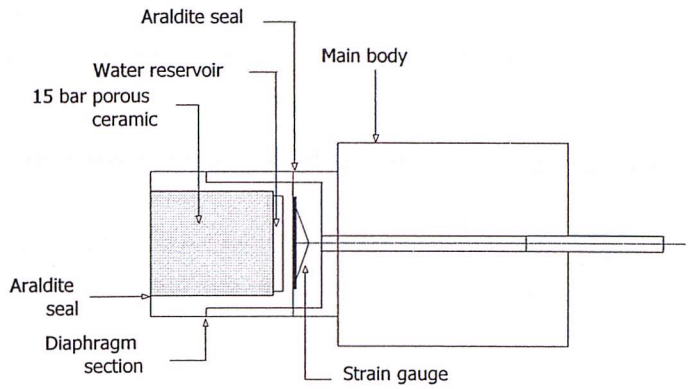

Figure 4.10 Imperial College suction probe

Finally, the suction probe is placed into a pressure manifold with a positive water pressure of 4,000kPa, which is applied with a hand pump. The IC suction probes used in this study were left for a minimum of 7 days under this pressure. If air enters into the probe during use, it will need a minimum of 2 days under positive water pressure for re-saturation. Longer periods under pressure are required for re-saturation if the porous tip has dried out completely.

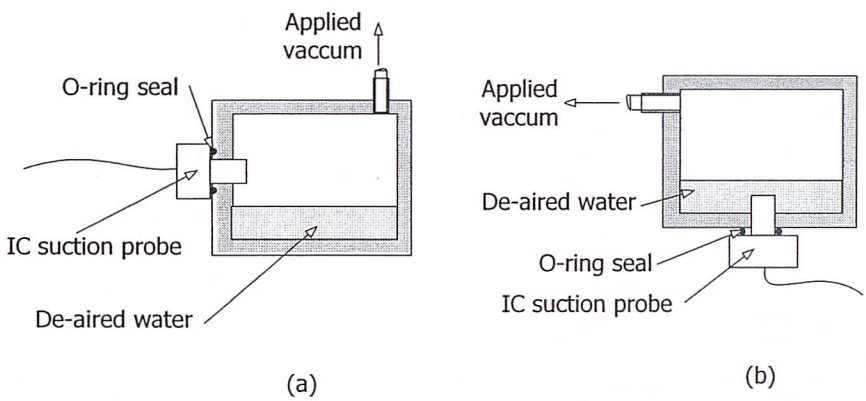

Figure 4.11 Pre-saturation processes for the Imperial College Suction probe:
(a) vacuum is applied to the chamber (b) the chamber is rotated to allow water to fill the porous stone and the reservoir

Calibration of IC suction probe 4.3.1.2

After the saturation process, each probe is calibrated by the application of positive pressures. The response of the diaphragm is checked to ensure that the hysteresis loop during loading and unloading is not significant. The suction probe is then ready to be used. When measuring negative pore water pressures the positive calibration is extrapolated into the negative range. Ridley and Burland (1993) showed that this extrapolation is valid.

Measurement with IC suction probe 4.3.1.3

The Imperial College approach involves measuring the soil suction using a suction probe mounted in a platen, as shown in Figure. 4.12. The soil sample is placed on

the platen covering the face of the suction probe. To restrict evaporation of water from the soil sample, it is covered with layers of cling film and a cover.

The contact between the porous stone and surface of the soil sample strongly controls the reliability of the measurements. Contact should be perfectly complete over the entire area of the porous stone.

Each suction measurement with a suction probe necessitates reaching an equilibrium condition. Equilibrium will be reached within a time period that depends on the nature of the soil and the suction being measured. Additionally, the equilibrium time depends on the amount of excess moisture on the surface of the porous stone prior to placing the soil sample in contact with the suction probe and the ability to achieve a good contact between the soil sample and the porous stone.

If there is an excess of moisture on the surface of the porous stone prior to placing the sample in contact with the suction probe, the suction measurement will indicate a lower value than the actual soil suction. However, equilibrium at the correct current suction will be established a few hours later.

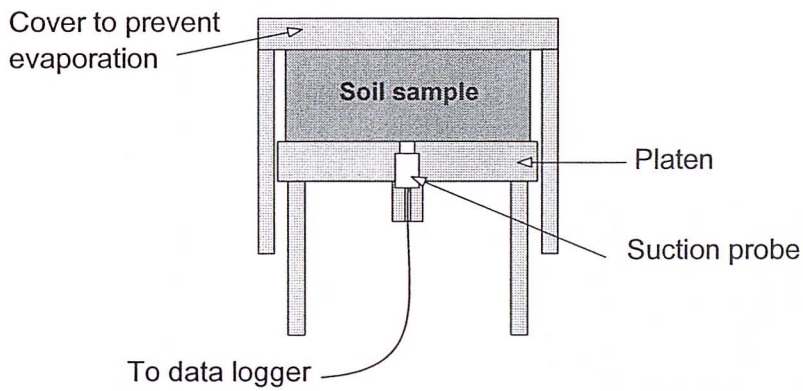

Figure 4.12 Platen used to make suction measurements in the laboratory with suction probes

At equilibrium the suction probe reading will remain stable; this reading is assumed to be the matrix suction in the soil sample. If the contact between the soil sample and the porous stone is not perfect, the latter will dry out and the measurement will not reach equilibrium. In this case, the suction measurements will keep increasing until air enters the probe and the measurement breaks down. Figure 4.13 shows two suction probe readings reaching the equilibrium suction. In these particular cases the suction probes was in contact with reconstituted Kaolin soil samples.

When the material is granular, as was the case for some of the materials tested in this research project, it is difficult to get a perfect contact between the suction probe and the soil sample. Additionally, non-homogeneities in the micro-fabric of a sample increase the difficulty in getting perfect contact between the suction probe and the soil sample.

To improve the contact between the porous stone of the suction probe and the soil sample surface, the common practice at Imperial College is to use a small amount of wet Kaolin paste (about 1mm thick) smeared on the probe (see Figure 4.14). The Kaolin paste used in this research was hydrated with distilled water for at least three weeks and stored for further use.

Ridley et al. (2003) also suggest that it is good practice to leave the surface of the suction probe slightly moist, or to cover it with a small amount of soil paste formed by wetting up some of the material being tested. Apparently, with this practice the measurement will then approach 90% of the soil suction quite rapidly, but may take a few hours to reach full equilibrium.

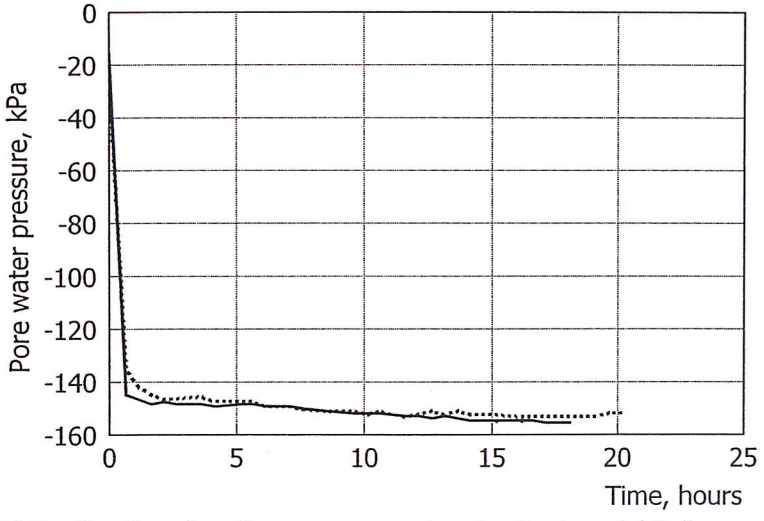

Figure 4.13 Equilibration of suction measurements using the Imperial College suction probe

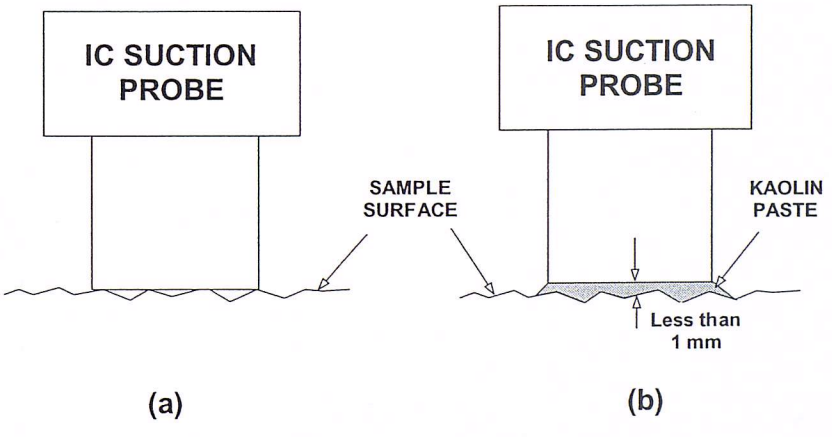

Figure 4.14 Improving the contact between the porous stone and granular soils
(a) poor contact (b) full contact with Kaolin paste

Repeatability of IC suction probe measurements 4.3.1.4

To obtain accurate and stable measurements of matrix suction using IC suction probes it is essential to achieve good contact between the porous stone and the

water in the soil. In the case of poor contact between the soil water and the porous stone the suction measurement may appear, at first sight, to be approaching an equilibrium state, but may then begin to increase again and fail to reach equilibrium. Equilibrium in matrix suction measurements on fully saturated soil samples should normally be reached very quickly, i.e. in no more than two to three hours. However, partially saturated soil samples may take several hours or even days to achieve full equilibrium. Ridley et al. (2003) suggest that patience and care are required to obtain accurate measurements. Alternatively, as just described, the experience at Imperial College indicates that in fact a small amount of Kaolin paste improves the contact between the surfaces (Figure 4.14 (b)), giving reasonably repeatable results.

The repeatability and stability of the measurements made with the IC suction probe were checked, by placing the suction probe on a reconstituted Kaolin sample prior to performing a test on the actual sample. Two probes were placed on the sample. Figure 4.13 shows a set of measurements made with two new suction probes. The repeatability of the measured suction is acceptable and the difference could be due to non-homogeneity of the water content within the sample.

Figure 4.15 shows comparisons between the suction measurements made on a reconstituted Kaolin sample with Whatman No. 42 filter papers and the Imperial College suction probe. The results are the average of two filter paper measurements and two suction probe measurements on a single specimen that was allowed to dry between measurements. The agreement between the two methods can be seen to be good over the range of suctions measured in this research and illustrates the accuracy that can be achieved with the filter paper method by adopting the testing procedure described earlier.

Most of the apparatus and techniques described in this chapter have been used to measure suctions of soils over their wetting and drying ranges to enable their soil-water retention curves to be established. The results from these measurements and their analysis are presented and discussed in Chapters 6 and 7 respectively.

It should be noted that most of the suction measurements made in this research to define the SWRCs of the various soils were performed using the filter paper method. In this technique the sample is under zero total stress, while measurements using the pressure plate apparatus have a steadily increasing total stress applied to it. Recent studies (Vanapalli et al., 1999; Ng and Pang, 2000) have shown that the applied stress level acting on the samples does influence the shape of the SWRC. Ng and Pang (2000), investigating natural and compacted samples of a volcanic soil, found that during drying the samples subjected to higher applied stresses possessed larger air-entry values and the rate of desaturation reduced. On wetting, the degree of hysteresis reduced for the samples at higher stress levels. It was

noted that these effects were more significant for natural intact samples compared with those that had been compacted.

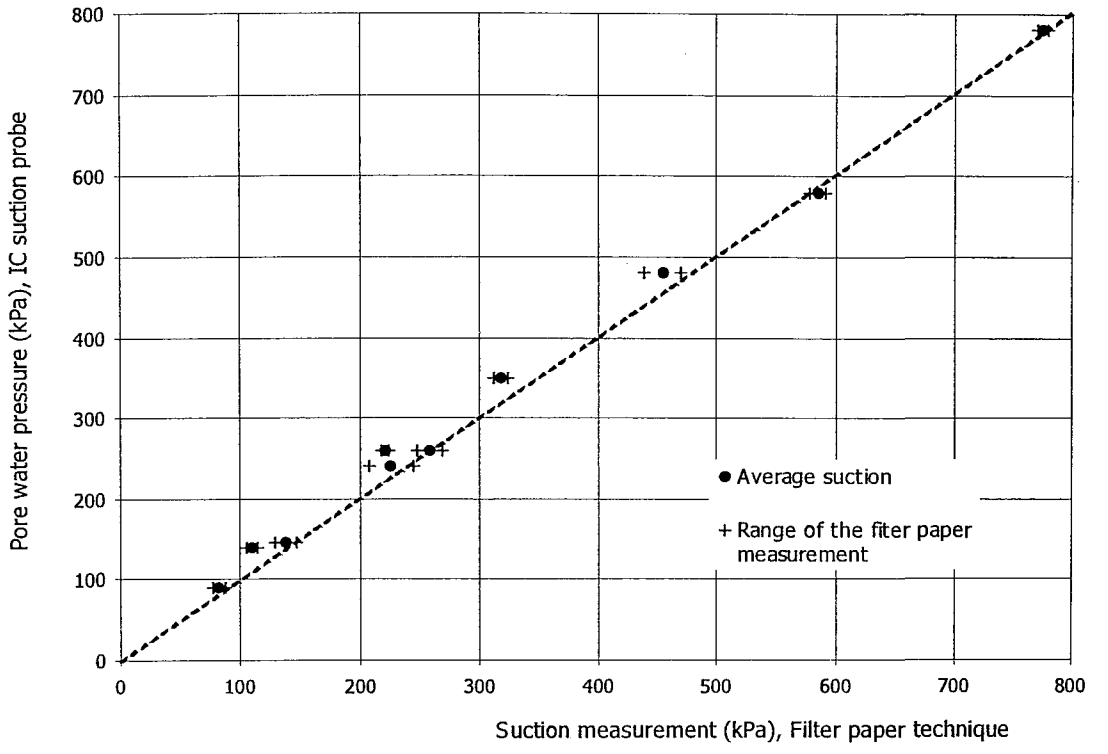

Figure 4.15 Comparison between suction measurements with filter paper and IC suction probe

It was necessary during the course of the research described in this thesis to use different methods of suction measurement as described earlier. No attempt has been made to correct for the fact that in some cases the samples were subjected to applied total stresses greater than zero. This would not have been realistic given the scarcity of experimental data available and the uncertainty of exactly how the level of applied stress affects the SWRC. However, the experimental data and SWRCs presented in Chapter 6 generally exhibit curves without sudden jumps between the ranges of data measured using the different techniques; there is usually a smooth transition. The other point is that the experimental data available (e.g. Ng and Pang) indicate that the most severe hysteresis occurs at zero applied total stress and so the SWRCs presented here should represent an extreme case.

CHAPTER 5

ASSESSMENT OF THE FILTER PAPER TECHNIQUE

Numerous measurements were made during the course of the experimental study to establish the various components of the SWRC. The method used for measuring suction (indirectly) for the majority of cases was the filter paper technique. Prior to presenting the experimental data in Chapter 6, it is appropriate to consider various aspects of the filter paper technique and also to estimate the likely range of experimental errors. This chapter is divided into three sections. First, error ranges are considered, which are important when assessing the scatter of data in the SWRCs. The filter paper technique involves gradually drying or wetting a disk of soil and usually a period of one week is allowed between each stage of drying or wetting up. The second section investigates whether this equilibrium period is appropriate. A simplistic parametric study has been performed based on saturated soil mechanics but with modified parameters to account for desaturation. The assumptions involved are discussed. The final section explains and describes some suggested modifications to the technique to improve the accuracy of suction measurements. These ideas are based on the experience gained over the three-year period during which thousands of suction measurements were made.

INVESTIGATING POTENTIAL ERRORS IN EXPERIMENTAL MEASUREMENTS 5.1

A basic error analysis has been performed in order to have an idea of the influence of measuring error on the calculated quantities necessary for constructing the SWRC. Suction is the parameter common to all the representations of the SWRC and measurements of suction using the filter paper technique has been investigated, this being the method used most frequently. The effect of measurement error on the determination of gravimetric and volumetric water content, void ratio and degree of saturation is also considered.

As described earlier, the SWRC is mapped out by drying or wetting a disk of soil, taking measurements of:

(I) suction, indirectly using the filter paper method which involves weighing filter papers wet and dry to determine their water content;

(II) sample volume, directly by measuring the sample diameter and height at a number of positions and taking an average; H

(III) sample mass, directly with a weighing scale.

The following quantities are therefore measured for each stage of drying or wetting the sample.

m_{wfp} mass of wet filter paper

m_{dfp} mass of dry filter paper

giving $m_w = m_{wfp} - m_{dfp}$ which equals the mass of water in the filter paper

and $(\omega/c)_{fp} = \dfrac{m_w}{m_{dfp}}$ which equals the gravimetric water content of the filter paper

D diameter of the soil disk

H height (thickness) of the soil disk

giving $V_T = \dfrac{1}{4}\pi D^2 H$ which equals the total volume of the sample

M_T total mass of the sample (soil disk).

Table 5.1 summarises the measurements made, the measuring systems used, their resolution and their estimated accuracy. The estimated accuracy is to a degree subjective but based on the experience gained during the three-year period of measurements.

Table 5.1 Summary of quantities measured, the measuring systems and their resolution and estimated accuracy for the determination of the SWRC using the filter paper technique.

QUANTITY	MEASURING SYSTEM	RESOLUTION OF SYSTEM	ESTIMATED ACCURACY
m_{wfp}	Salorius research R200D weighing scale	$0.0001g$	$\pm 0.0005g$
m_{dfp}	Salorius research R200D weighing scale	$0.0001g$	$\pm 0.0005g$
M_T	Oertling 1500D weighing scale	$0.01g$	$\pm 0.02g$
D	Vernier calliper	$0.01mm$	$\pm 0.025mm$
H	Vernier calliper	$0.01mm$	$\pm 0.025mm$

The main purpose of investigating the potential range of measuring errors is to assess to what degree it might influence the scatter of data on the SWRCs formulated for the various soils investigated. As will be seen when the data are presented (Chapter 6), most of the curves exhibit very little scatter. The approach adopted follows roughly guidelines given by Barry (1978). Clearly a very rigorous statistical analysis can be undertaken for any experimental data set, but this is considered to be outside the scope of the study and not necessary given the quality of most of the data.

The approach taken has been to calculate the upper and lower limits of ranges of values for the parameters used for expressing the SWRC, namely: suction; volumetric water content; degree of saturation and void ratio. This has being done by using typical measured values of the quantities given in Table 5.1 and applying the upper and lower limits of the estimated accuracy. The typical values are assumed to be representative of a nominal true value. The required parameters are then calculated using appropriate relationships that express them as a function of the measured quantity. The procedure is best explained by example, the basic calculations for each parameter are given in the following sections.

Suction. Three sets of typical values within the high, medium and low suction ranges were investigated. It was assumed that the mass of the dried filter paper would remain essentially constant $(m_{fp} = 0.36g)$. For high suction measurements a typical value of $(m_w = 0.04g)$ As (m_w) is determined from two measurements, i.e. of m_{wfp} and m_{dfp}, the range of accuracy has been increased two fold when it is applied to m_w to give an extreme value (as though the worst error margin occurred in both measurements). Calculating m_{wfp} at two extremes (given as (a) and (b) in the following).

(a) (b)

$$(\omega/c)_{fp} = \frac{0.04 - 2*0.0005}{0.36 + 0.0005} = 0.10818g \qquad (\omega/c)_{fp} = \frac{0.04 + 2*0.0005}{0.36 - 0.0005} = 0.11404g$$

The expression for determining suction for $(\omega/c)_{fp} \leq 47\%$ is given in Table 4.2:

$$\psi = 10^{(4.842 - 0.0622(\omega/c)_{fp})} \qquad \text{with } (\omega/c)_{fp} \text{ In \%.}$$

(a) $\psi = 14{,}761kPa$ (b) $\psi = 13{,}571kPa$

Therefore the difference in extremes $\Delta\psi = 1{,}190kPa$ i.e.. $\pm 595kPa$.

Performing a similar exercise for the mid-suction range with typical $(m_w = 0.10g)$ gives an error range of. $\pm 59kPa$. An alternative expression is used for low suctions (with $(\omega/c)_{fp} \geq 47\%$), taking typical. $(m_w = 0.18g)$

(a) (b)

$$(\omega/c)_{fp} = \frac{0.18+2*0.0005}{0.36-0.0005} = 0.50347g \qquad (\omega/c)_{fp} = \frac{0.18-2*0.0005}{0.36+0.0005} = 0.49653g$$

$$\psi = 10^{(6.050-2.48\log(\omega/c)_{fp})}$$

(a) $\psi = 69{,}8kPa$ (b) $\psi = 67{,}5kPa$

Therefore the difference in extremes $\Delta\psi = 2{,}3kPa$ i.e.. $\pm 1.1kPa$.

Volume and mass. In investigating the range of error measurement of volume the smallest size soil sample disk diameter is considered, combined with the thinnest size sample, i.e. $D = 50mm$ and $H = 10mm$.

(a)

$$V_T = \frac{1}{4}\pi(50-0.025)^2 * (10-0.025) = 19{,}566.2mm^3$$

(b)

$$V_T = \frac{1}{4}\pi(50+0.025)^2 * (10+0.025) = 19{,}703.7mm^3$$

In considering errors in the measurement of mass, again the estimated accuracy range will have greatest influence on the smallest sample size. Assuming a value of $\gamma = 18kN/m^3$ for soil and the sample dimensions given above, a typical sample mass can be taken as $M_T = 35.343g$. Therefore the extreme values of mass measured might be:

(a) (b)

$$M_T = 35.343 - 0.02 = 35.323g \qquad M_T = 35.343 + 0.02 = 35.363g$$

Gravimetric and volumetric water content. The effect of the extremes of ranges of M_T and V_T on the gravimetric and volumetric water content, ω/c and θ respectively, can now be investigated.

$$\omega/c = \frac{M_T - M_S}{M_S}$$

A value of $M_s = 25.723g$ is used in the following calculations. This is a representative value for the sample dimensions being used (and in the calculation of $\omega/c, M_s$ remains a constant value throughout). Occasionally small particles from the samples were dislodged during handling. Although these were collected and weighed using the more accurate weighing scale, they are not taken into account in these error calculations because their mass was always smaller than the estimated accuracy of the coarser weighing scale.

(a) $$\omega/c = \frac{35.323 - 25.723}{25.723} = 37.321\%$$

(b) $$\omega/c = \frac{35.363 - 25.723}{25.723} = 37.476\%$$

Therefore the difference in extremes $\Delta\omega = 0.155\%$ i.e. $\pm 0.075\%$.

Investigating the effect of differences in M_T and V_T on the determinations of volumetric water content θ, is first approached by considering possible ranges of the volume of water, V_w, present in the sample.

$$V_w = \frac{M_T - M_s}{\rho_w}$$

(a) $$V_w = \frac{35.323 - 25.723}{0.001} = 9{,}600mm^3$$

(b) $$V_w = \frac{35.363 - 25.723}{0.001} = 9{,}640mm^3$$

with $\rho_w = 1{,}000kg/m^3 = 0.001gr/mm^3$.

Combining the extremes of ranges ((a) and (b)) for V_w and V_T to establish the maximum error range in determining the volumetric water content.

$$\theta = \frac{V_w}{V_T}$$

(a) $\theta = \frac{9600}{19{,}703} = 0.4872$ (b) $\theta = \frac{9640}{19{,}566} = 0.4927$

Therefore the difference in extremes $\Delta\theta = 0.55\%$ i.e. $\pm 0.28\%$.

Void ratio. The influence of the error range of M_T and V_T on void ratio, e is considered as follows.

$$e = \frac{V_v}{V_s} = \frac{V_T - V_s}{V_s} = \frac{V_T - M_s/G_s\rho_\omega}{M_s/G_s\rho_\omega}$$

G_s is taken to be 2.65.

(a)

$$e = \frac{19{,}566.3 - 25.723/0.00265}{25.723/0.00265} = 1.0157$$

(b)

$$e = \frac{19{,}703.7 - 25.723/0.00265}{25.723/0.00265} = 1.0299$$

Therefore the difference in extremes $\Delta e = 0.0142$ i.e. ± 0.0071.

Degree of saturation. A similar exercise can be carried out for the degree of saturation, S

$$S = \frac{V_w}{V_v}$$

(a)

$$S = \frac{9{,}600}{19{,}703.7 - \left(25.723/0.00265\right)} = 0.9603$$

(b)

$$S = \frac{9{,}640}{19{,}566.3 - \left(25.723/0.00265\right)} = 0.9777$$

taking the smallest divided by the largest values for (a) and vice versa for (b)
Therefore the difference in extremes $\Delta S = 1.74\%$ i.e. $\pm 0.87\%$.

The preceding calculations have not followed a rigorous statistical analysis but they provide realistic ranges of error that might be expected in taking the various measurements to generate the SWRCs for the different samples. This allows the curves to be assessed taking account of whether scatter results from measuring errors or sample response. There are other potential causes of scatter, for instance the effect of the time allowed for equilibration of moisture content within the filter papers and the influence of sample thickness. These are discussed in the next section.

A summary of the potential error ranges that might be expected in the determination of the various quantities used to express the SWRC is given in Table 5.2. As the calculations given are based on typical values from measurements made during the course of the research, values given to define the ranges have generally been rounded up.

It should be noted that it has been necessary to consider the full range of appropriate values of suction because of the nature of the expression used to determine it. This is evident from the markedly different error ranges given in the table. Although the 'appropriate values' given for $\omega/c, \theta, e$ and S might seem very

specific, the range of error is not sensitive to these values and the rounding-up will ensure that they are relevant for most measured values encountered.

Table 5.2 Estimated error ranges for parameters used to express the SWRC.

PARAMETER	APPROXIMATE VALUE (where appropriate)	ESTIMATED ERROR RANGE (maximum)
Suction, ψ	high ($14{,}000kPa$) mid ($1{,}300kPa$) low ($70kPa$)	$\pm 600kPa$ $\pm 60kPa$ $\pm 1kPa$
Gravimetric water content, ω / c	mid to high (37%)	$\pm 0.1\%$
Volumetric water content, θ	mid to high (48%)	$\pm 0.3\%$
Void ratio, e	mid to high (1.02)	± 0.01
Degree of saturation, S	mid to high (97%)	$\pm 1\%$

5.2 ASSESSMENT OF EQUILIBRATION TIMES NECESSARY IN FILTER PAPER MEASUREMENTS

In performing filter paper tests, disks of soil are progressively either dried out or wetted up. The former is usually achieved by placing a new dry filter paper in contact with the sample at the start of the equilibrium period. This period is usually taken to be one week, judged to be sufficiently long for suction in the filter paper to come into equilibrium with that in the sample. The water content of the filter paper is then determined from which the suction in the sample can be calculated through known relationships (see Table 2.2). A similar procedure is followed for wetting except that small amounts of water are added to the sample (or to the filter paper). During the course of the measurements and the analysis of the data presented in this thesis it has been observed that leaving the sample for more than one week appears sometimes to lead to a greater scatter of data.

There are a number of factors that might cause this. It is possible that, although the sample is well wrapped up during the one-week equilibration periods, some evaporation from the wrapping might have occurred. Occasionally it was noticed that some of the pore water had condensed on the inside surface of the wrapping, especially during hot weather. These two causes cannot be easily controlled.

Another possible factor is the length of time allowed for equilibration to take place. It was therefore decided to perform a parametric study to investigate the period of dissipation allowed during each stage of drying or wetting. Clearly, there are limitations to such a parametric study as the assessment of these periods is not straightforward because of the changing degree of partial saturation as the soil dries or wets. Much of the theory required for an accurate assessment is complex and its development is still in its infancy. This is particularly the case at high levels of suction when water flow occurs primarily by water vapour transfer (i.e. in the residual effect stage, see Figures 2.10 and 2.11). However, a simplified analysis has been undertaken, making a number of assumptions that are discussed in the following paragraphs.

The approach taken has been to use Terzaghi's basic equation of one-dimensional consolidation, taking into account the fact that permeability reduces dramatically with increasing suction and decreasing degree of saturation. Although one of the assumptions of Terzaghi's theory is that the soil is fully saturated, Childs (1969) reports that water can be visualised as flowing only through the pore space filled with water. Therefore, the air-filled pores in an unsaturated soil can be considered as behaving similarly to the solid phase and the soil can be treated as a saturated soil having a reduced water content. The magnitude of the coefficient of permeability will reduce as the water content of a saturated soil decreases (which also contravenes Terzaghi's theory where it is assumed that the permeability remains constant: this is discussed shortly).

Terzaghi's consolidation theory can be expressed in a number of ways. In this study, the form expressing consolidation in terms of the average degree of consolidation, *U*, (which in this exercise can be considered as the degree of dissipation or equilibration) has been used. The equation is given as follows:

$$U = 1 - \sum_{m=0}^{m=\infty} \frac{2}{M^2} e^{-M^2 T_v} \qquad (5.1)$$

where $M = \frac{\pi}{2}(2m+1)$ and $T_v = \frac{c_v t}{d^2}$ with c_v being the coefficient of consolidation, t the time and d the length of the drainage path (half the sample disc thickness).

In using this theory it is assumed that the majority of flow through the sample is one-dimensional. Filter papers are placed at the flat ends of the soil disc and held in contact with the soil by Perspex discs. Flow would therefore be expected to be primarily one-dimensional. The *M* factor in the equation is related to the initial distribution of excess pore pressure. In many applications, the distribution is taken to be linear with depth (or flow direction) although accounting for other variations such as increasing or decreasing triangular distributions does not have a significant

influence on the above equation which is often presented in terms of T_v plotted against U. In the filter paper test, the agent causing the change in pore water pressure, in this case suction, is the filter paper itself. Considering the case where a sample is being dried, dry filter papers are placed close to or in contact with the end faces of the disc of soil. The suction immediately adjacent to the paper will increase as the dry paper draws water from the soil to try to come to equilibrium with the soil suction. This process is the same as that described in Figure 2.4 of Chapter 2 where conditions for two samples with different grain or pore size distributions, initially at different suctions, are brought into contact with one another. As the suction immediately adjacent to the paper increases this causes an imbalance of suction within the sample disc and further equilibration starts taking place. Effectively there is a front of changing suction that moves in towards the mid-height of the disc (assuming there are filter papers at both ends). It is likely that this front oscillates to and from the mid-plane of the disc until equilibration is reached. Given the uncertainty of the initial distribution and the approximate nature of this parametric study, it was decided to assume a linear distribution with M expressed as given above.

In Terzaghi's consolidation theory, the soil characteristics within the general equation are represented by the coefficient of consolidation, c_v , contained within the dimensionless time factor, T_v . c_v is a function of the ratio of permeability, k_s (for saturated soil) to the coefficient of volume change, m_v:

$$c_v = \frac{k_s}{m_v \gamma_w} \qquad (5.2)$$

As a soil consolidates (or in the case of the filter paper test, as the suction within it increases) its permeability will decrease, as discussed above, and its compressibility will also reduce. Another of the assumptions of Terzaghi's consolidation theory is that k_s and m_v remain constant during consolidation. It can be seen that although this is not the case, the fact that both change in the same sense implies that the effect on c_v might not be significant, particularly at lower suction values (and prior to the shrinkage limit being reached). This assumption is now investigated further by assessing likely changes in permeability as the suction increases in the soil. It should be noted that it is the overall compressibility of the sample that is being considered, induced by changing suction. This includes the compressibility of the skeleton and the pore fluid, although the latter is probably not so significant for the filter paper test where is no externally applied total stress. It is the presence of air bubbles impeding flow through the liquid phase that affects the permeability and hence c_v as discussed below.

There are several relationships available (Fredlund and Rahardjo, 1993) for expressing the change in permeability associated with the water phase, k_w , with matrix suction and the saturated degree of permeability, k_s. k_w essentially represents the permeability in the partly saturated state. The expression given by Gardner (1958) has been adopted for this parametric study.

$$k_w = \frac{k_s}{1 + a\left\{\frac{(u_a - u_w)}{\rho_w g}\right\}^n} \qquad (5.3)$$

where n and a represent the slope of the function and its 'breaking point' respectively. In practice these would be determined experimentally. For the purpose of this parametric study, values from experimental tests quoted by Fredlund and Rahardjo (1993) have been used as a starting point and the effect of varying them has been investigated, the intention being to cover a wide range of soil types. Values of a ~ 0.1 and n ~ 3 are given for tests performed on colluvium and decomposed granite from Hong Kong (this material has similarities to two of those tested in this study). The ranges investigated here were for a = 0.01, 0.1, 1 and 10 and n= 1, 2, 3 and 5. The form of the Gardner equation is such that the ratio of k_w/k_s can be investigated while varying a and n. In Figure 5.1 the ratio of k_w/k_s is plotted against matrix suction, both on a logarithmic scale. Also marked on the figure is the maximum value of matrix suction that can be measured reliably using the filter paper technique (i.e. $30{,}000kPa$).

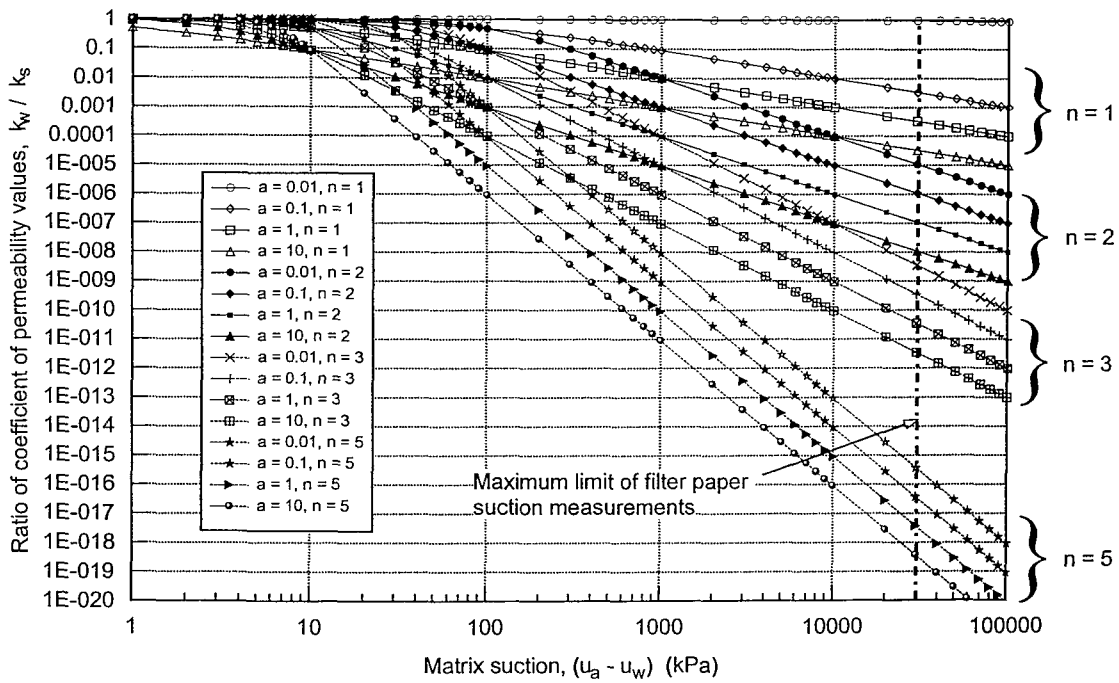

Figure 5.1 Ratio of coefficients of permeability k_w/k_s determined using Gardner's equation

The nature of the Gardner equation is evident from Figure 5.1. The a-value largely controls the effect of suction on permeability at low suction values. At higher values the influence of suction is more marked and changes in permeability are almost directly related to the n-value. It can be seen that once the lines become linear, a change of one logarithmic cycle of suction causes n cycles of change in permeability (with respect to the saturated permeability k_s). It is evident that the larger the n-value, the greater the change in permeability. At n = 5 this has a very dramatic effect.

A selected range of a and n values are represented in Figure 5.2 which shows the permeability associated with the water phase, k_w, plotted against matrix suction for a saturated permeability, k_s = 10^{-7}m/sec. In this figure the influence of the a-value can be seen more clearly. The reduction in permeability becomes greater as a increases, although this is largely a result of the shape of the curve in the low suction region.

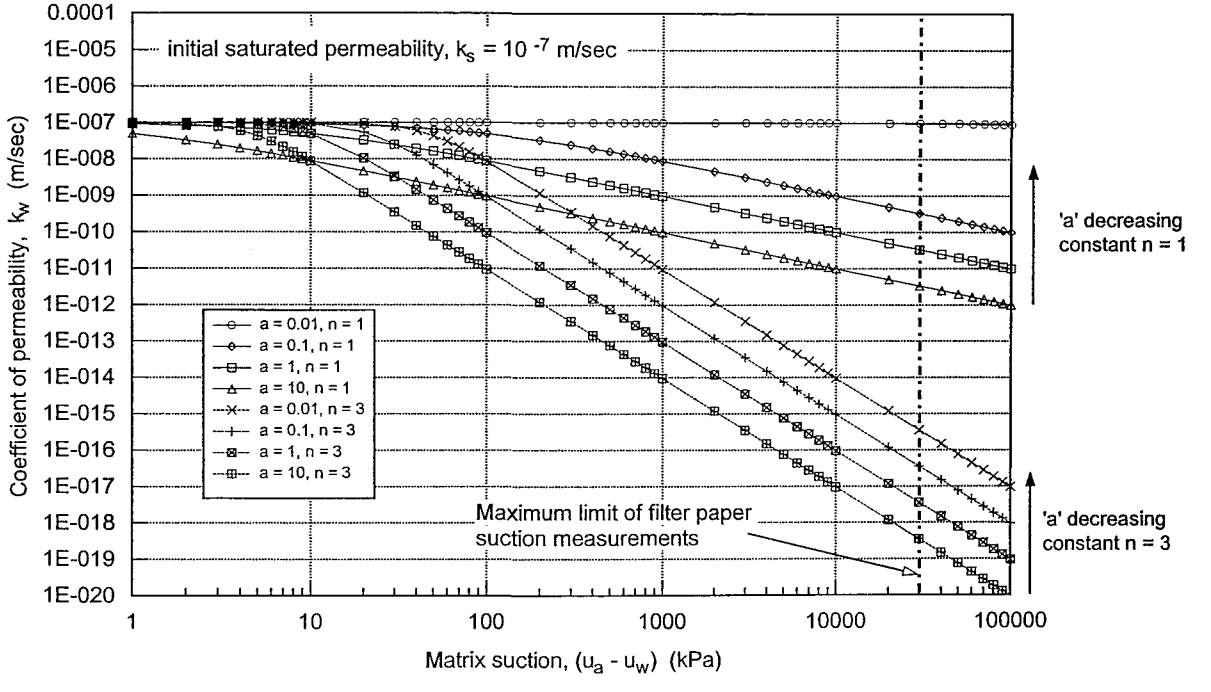

Figure 5.2 Coefficients of permeability with respect to water phase k_w for k_s = 10^{-7} m/sec (determined using Gardner's equation)

A value of n = 3 was chosen in Figure 5.2 as this corresponds to the decomposed granite material from Hong Kong (with a = 0.1). This is a reasonably coarse material for which the order of magnitude of k_s was reported to be about 10^{-5}m/sec. It can be deduced that n increases as the coarseness of the material increases. Soils with a low initial permeability, such as clays, would remain saturated for

greater suction values and their change in volumetric water content or void ratio would be smaller and hence their permeability would be less affected by changing suction. These trends in behaviour are also evident from the SWRC profiles (comparisons between fine and coarse grained soils are shown in Figure 2.2). In practice the lines for n = 5 at high suction values are probably unrealistic as the soil would desaturate rapidly at low suction values and reach the residual effect stage where water flow does not take place through the water phase but only via transfer by water vapour. It is assumed that the behaviour illustrated by the lines for n = 1, 2 and 3 in Figures 5.1 and 5.2 are representative for most of the soils investigated in this study.

Having assessed the possible range of changes in permeability that might be expected as a result of increasing suction and decreasing degree of saturation, the possible influence on c_v values is now discussed.

It is assumed that typical values of c_v for clays usually lie in a range of about 0.5 to $5 m^2/year$. If it is assumed that n = 1 is appropriate for clay soils, then changes in permeability over two log cycles of suction would also result in a reduction in permeability (i.e. from k_s to k_w) of two orders of magnitude. Therefore, if m_v remained constant, the range of c_v given above would decrease to 0.005 to $0.05 m^2/year$ (considering Equation 5.2). However, as discussed earlier, c_v and m_v tend to change in the same sense and hence to some degree compensate for each other, resulting in a much smaller influence on c_v. A reasonable value of c_v to investigate for clays as a result of suction increasing to the limiting value of $30{,}000 kPa$ might therefore be taken as $0.01 m^2/year$, which is within the modified range, towards its lower limit.

In the case of coarser materials, consolidation takes place much more quickly and a lower limit value of c_v might be $25 m^2/year$. For this case a much greater reduction in permeability is likely to occur, e.g. six orders of magnitude for two log cycles of suction. Additionally the compressibility of coarse-grained soils is less likely to reduce as much as the case with fine-grained soils. A value of $c_v = 0.00025 m^2/year$ has been selected as appropriate for a coarse-grained soil as it approaches the limiting value of $30{,}000 kPa$. This takes into account the six orders of magnitude decrease in permeability while assuming that the compensating effect of the compressibility changes will increase this by one order of magnitude.

A range of c_v values from 0.0001 to $1m^2/year$ has therefore been considered using Terzaghi's theory of one-dimensional consolidation (Equation 5.1) for saturated soils to investigate the times required for dissipation within the filter paper samples to take place. This range covers the lower extremes of values for the partly saturated fine and coarse soils and extends to a realistic fully saturated value for a clay. The analysis has been performed for two values of sample thickness as the drainage path length clearly influences the time of dissipation (i.e. the *d* term in Equation 5.1). The results are shown in Figure 5.3. It should be noted that the modified ranges of c_v values discussed above are extreme values relevant to the very high suction range at the limit of the filter paper technique.

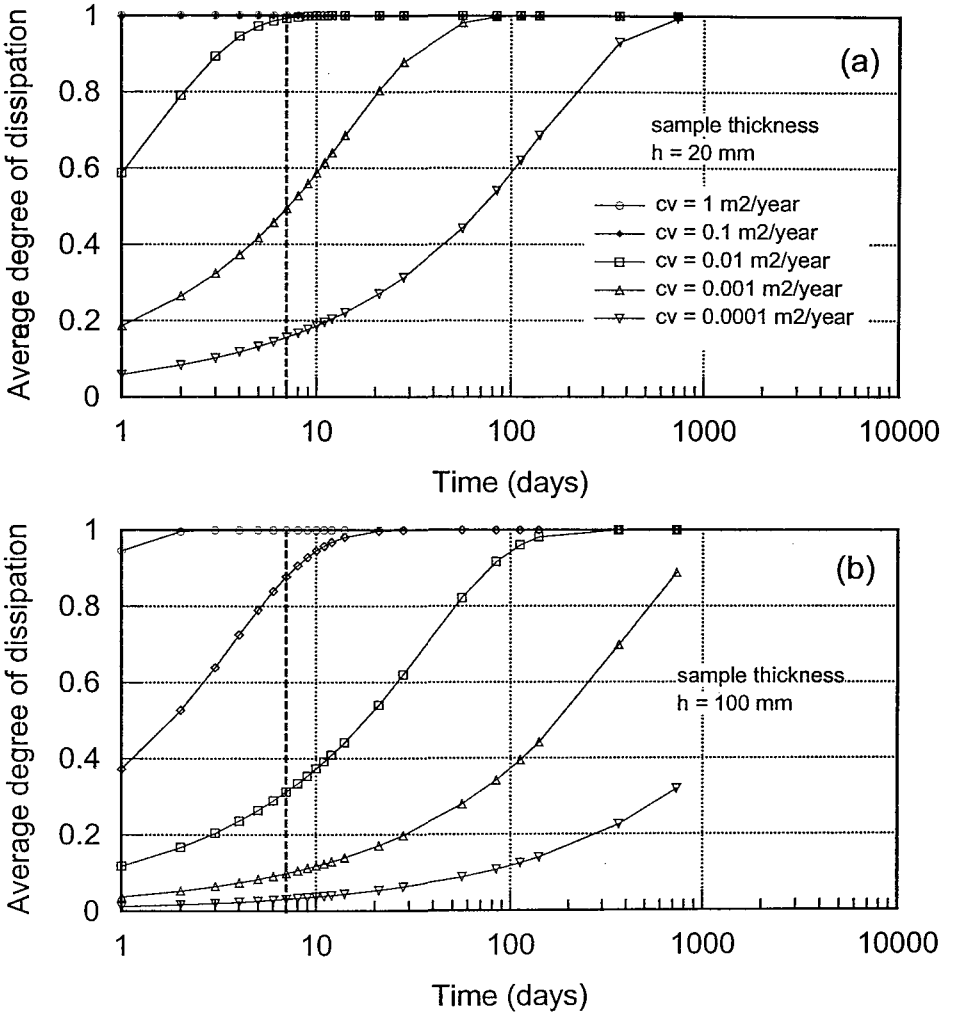

Figure 5.3 Dissipation times for different c_v values calculated for samples of thickness (a) 20mm and (b) 100mm (determined using Terzaghi's theory of one-dimensional consolidation).

The curves shown in Figure 5.3a, for the $20mm$ thick sample disc, indicate that for c_v values greater than $0.01m^2/year$ dissipation will be complete well within the 7-day period allowed regardless of the suction value. The curves for lower c_v values

imply that much longer periods might be necessary for measurements at the very high suction range. However, at these very high suctions the slope of the SWRC is almost flat and so changes in suction are very sensitive to small changes in volumetric water content. Waiting for long equilibration periods might therefore have an adverse effect because of loss of water through evaporation.

It might also be argued that for soils at low suctions and with higher c_v values, the period allowed for equilibration might be reduced. For the $20mm$ thick sample, the analysis indicates that equilibration occurs almost immediately for soils with c_v greater than $0.1m^2/year$. This could offer considerable time savings in measurements during the initial stages of drying from the initial state. However, given the approximate nature of this parametric analysis, a more rigorous analysis ought to be made or an experimental study undertaken to investigate this possibility further.

As would be expected, the results for a thicker $100mm$ sample indicate that much longer equilibration periods are necessary. They indicate that even the samples with a c_v value of $0.1m^2/year$ require more than the 7-day period usually allowed (in practice the filter paper might have almost come to equilibrium but the oscillating front of suction discussed earlier might not have fully stabilised). It would therefore seem advisable to avoid having a sample thickness greater than about 20mm for filter paper measurements. Additionally, thicker samples are more prone to moisture loss through their sides.

In conclusion, the approximate parametric study performed indicates that for most soils and for most of the suction range investigated with the filter paper technique, the 7-day period allowed for equilibration should be adequate. In theory longer periods might be required for measurements at the high suction end of the range, but in practice this might have adverse effects through unwanted evaporation. At low suction values and for soil samples with a c_v value greater than $0.1m^2/year$, it might be possible to reduce the 7-day period. The thickness of soil samples should be kept to about $20mm$ maximum where possible. This parametric study, although intended as a means of investigating the equilibration period for filter paper measurements, also gives insight into the expected behaviour of the soil discs during the drying and wetting processes in terms of their consolidation characteristics. The nature of the experimental techniques used in the research discussed in this thesis generally did not allow this aspect of the soil behaviour to be investigated.

SUGGESTED IMPROVEMENTS IN MEASURING SUCTION USING THE FILTER PAPER TECHNIQUE 5.3

Following the previous sections and the experience gained during this research, a number of improvements are suggested to increase the accuracy of suction measurements.

In preparing the reconstituted clay samples from slurry, the samples should be mixed at $1.5(\omega/c)_L$ to avoid any residual fabric (Burland, 1990). Consolidation was generally performed within a standard oedometer apparatus and generally there were no problems with samples formed in this manner. In the case of granular materials much greater care is required in preparing reconstituted samples. In this study samples were prepared such that they have constant values of initial void ratio and bulk unit weight to ensure that a unique SWRC was followed. Particular care is needed to avoid segregation of different particle sizes.

In trimming the sample disks (where appropriate, i.e. trimming is not necessary for those samples formed in the oedometer) the thickness should not be greater than about $20mm$. This is to avoid excessive equilibration times, as discussed in the previous sections (see Figure 5.3). With thicker samples there is also a greater possibility of evaporation from the sample sides.

The diameter of the disk ideally should be the same as that of the filter paper. In order to improve the accuracy of the volume measurements, the diameter should not be too small. It is important to achieve accurate volume measurements as these are used in determining the omega parameter, Ω, required for numerical analysis (see Chapter 3). Also, the filter paper should cover the entire flat surface of the sample disk to achieve conditions of uniform moisture content in the sample (especially in wetting processes).

It is considered that it is better to place three filter papers at each end of the sample disk rather than just one. The water content of the central filter paper is then used for determining suction; the reason for this is that sometimes small soil particles adhere to the paper adjacent to the sample. However, Marinho (1994) reports that although the papers come to equilibration in terms of suction, they have different water contents and thus the expression generally used for determining suction might not be appropriate.

In some cases it may be possible to reduce the seven-day equilibrium period that is usually allowed. This is primarily for cases where the samples are at low suctions and that have coefficient of consolidation values greater than about $0.1m^2/year$.

However, a methodology needs to be established so that suitable suction ranges can be identified and suitable equilibration times chosen.

When the samples are stored, the ambient temperature and conditions (e.g. humidity) should be kept constant.

In wetting up the sample the amount of water added to the filter paper should not be too small, otherwise evaporation can occur resulting in only small changes in suction which tends to increase the scatter of data.

In this chapter various aspects of the filter paper technique have been critically assessed and some suggestions are given about improving measurements. Perhaps the main drawback is the time required to generate an SWRC. However, as indicated above, potentially the seven-day period can be reduced for significant portions of the curve.

In conclusion, it is important to note that the filter paper technique is considered to be the most reliable method of determining soil suction. It has been well-proven with many years of experience (particularly for clays) and it is also very cheap. The data from thousands of measurements of suctions on various soil/material types are presented in the next chapter, in which the success and versatility of the technique can be judged.

CHAPTER 6

EXPERIMENTAL SOIL-WATER RETENTION CURVES

In this chapter the materials investigated in this study are described and the basic data are presented and discussed. The origin of the materials is given, followed by their characterization in terms of particle size distribution, Atterberg limits and specific gravity. The SWRCs for each material are expressed using degree of saturation, volumetric water content and void ratio. Trends in the responses are discussed for each material individually and then summarized collectively.

Eight different soil types were investigated as part of the research described in this thesis and their SWRCs determined. A wide range of soil types was used in order to study the different characteristics of the SWRC. These soils were from various origins, some being natural samples and others artificial materials. Reconstituted samples were prepared from some of the soils using a slurry with a water content of $1.5(\omega/c)_L$ of the soil. Brief details of the origin of each are now given.

The most comprehensive tests were performed on *Speswhite Kaolin*, which is an artificial clay supplied by the English China Clay Company. This material was supplied in dried powder form and so it was necessary to form a slurry and to allow the clay to hydrate prior to consolidation (a minimum period of one month was usually allowed).

Natural samples of *Weald Clay* were obtained from the site of a new Gatwick Airport spur in Sussex. The soil was air-dried and ground prior to mixing into a slurry and reconstituting.

Clay samples were provided by the National University of Colombia from the campus at *Bogota*. These samples were taken in Shelby tubes near the ground surface. There were two intact samples and a further two were reconstituted.

Residual soil, derived from Granodiorite, from *Rio de Janeiro*, Brazil was obtained from a pit at a depth of about 3m. One intact sample and two reconstituted samples were tested.

Residual soil, also derived from Granodiorite, was obtained from a landslide at Mariquita, central *Colombia*. Two intact samples were trimmed from a block sample and two more were reconstituted.

Residual soil from Hong Kong derived from decomposed Granite was also tested. A block sample was obtained from a slope in King's Park as part of a slope stability investigation. When the block was unwrapped in the laboratory the soil was found to be in a very dry state and very coarse. Samples were formed by compacting the material. Reconstituted samples were prepared but were thought to not be very homogeneous because of the granular nature of the material. Consequently only the data from the compacted samples are presented here.

Compacted clay samples from a London Underground embankment were supplied and tested (referred to as *Embankment Clay*). The exact origin of those samples is unknown but the soil has been classified as described in the next sections.

Ash material produced as a by-product from coal-powered power stations was tested. This material is commonly used for maintaining the level and repairing railway embankments in the UK, and was supplied by London Underground Limited.

MATERIAL CHARACTERISATION 6.1

MOISTURE CONTENT 6.1.1

The moisture content of the soils tested was determined according to the British Standards (BS 1377: Part 2:1990:3.2) and the results are shown in Table 6.1. In many tropical soils, in addition to free water, some water exists as water of crystallization within the structure of the minerals, it may be partly removed at temperatures between 105 °C and 110 °C (Quarterly Journal of Engineering Geology, 1993). To check for the presence of this type of soil water, comparative tests were performed with duplicate residual soil samples. Measurements of the dry mass after drying the soil at a temperature of between 105°C and 110°C and also at a temperature not exceeding 60°C were made. The results did not show a significant difference in any residual soil sample tested and so it has been assumed that there was no structural water present.

PARTICLE SIZE DISTRIBUTION 6.1.2

Two methods were used to obtain the particle size distribution of the soils tested, the wet sieving (BS1377: Part 2:1990:9.2) and the hydrometer method (BS 1377: Part 2:1990:9.5) for granular soil and for the fine material respectively. The particle

size distributions of the materials are shown in Figures 6.1 and 6.2 and the data are also given in Table 6.2.

Table 6.1 Initial moisture contents

SOIL TYPE	SOIL SAMPLE ORIGIN	INITIAL MOISTURE CONTENT (%)
CLAY	Weald (UK) UN-Bogotá (Colombia) Embankment Clay fill (UK)	23.6 40.2 34.6
RESIDUAL SOIL	Rio de Janeiro (Brazil) K17 Residual soil (Colombia) King's Park (Hong Kong)	28.3 48.5 6.3
ASH	Power station (UK)	17.9

Results from several tests on ash have been provided by Mott MacDonald and are also given by MacNought (1998). The former tested material from a variety of sources, some from embankments, some direct from suppliers. MacNought tested samples from power stations and blast furnaces. From these tests, the ash used in this research could be described as a well graded sandy gravel. Generally, the larger ash particles are described as weak, with visible pores on the surface (varying in size from less than 1mm to 5mm). The smaller particles usually are more solid and stronger and they have a texture similar to coal. In shape they are predominantly planar and sub-angular.

Table 6.2 Data obtained from particle size distribution analyses

TYPE OF SOIL	CLAYEY SOIL SAMPLES			RESIDUAL SOIL SAMPLES			ARTIFICIAL SOIL
SOIL SAMPLE	Weald	UN-Bogotá	Embankment Clay fill	Rio de Janeiro (Brazil)	K17 (Colombia)	King's Park (Hong Kong)	Ash*
SIZE	PERCENTAGE PASSING (%)						
GRAVEL	4.2**	----	------	2.7**	-----	33	60
SAND	9.3	5	13	24	7	49	35
SILT	42.5	36	31	14.9	24	14	5
CLAY	44	59	56	58.5	69	4	------

*from MacNought (1998)

**mainly quartz particles

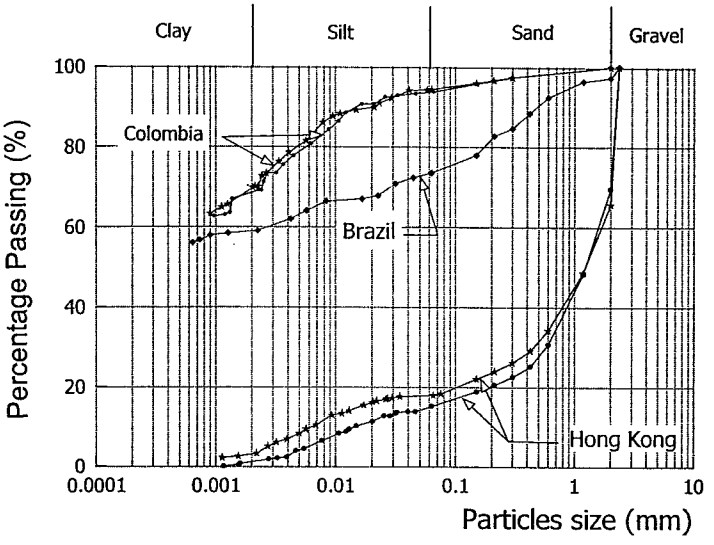

Figure 6.1 Particle size distribution for the residual soils tested.

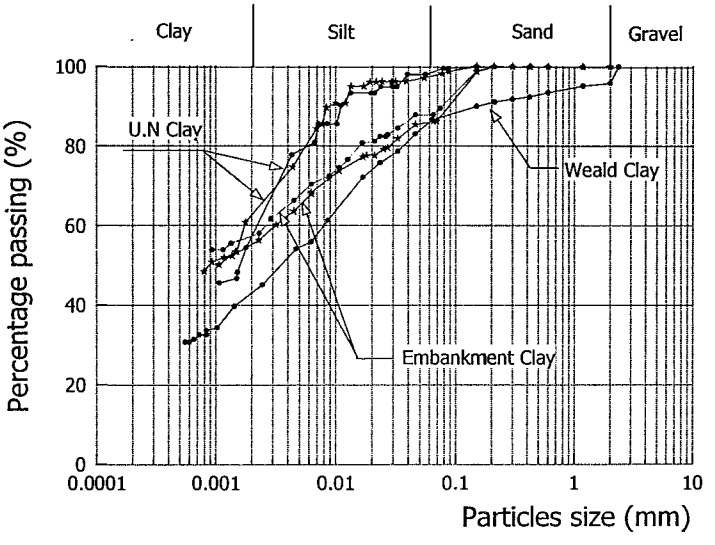

Figure 6.2 Particle size distributions of clayey materials tested.

SPECIFIC GRAVITY 6.1.3

The specific gravity of the soil particles was determined using the method given by BS 1377: Part 2:1990:8.3. The tests were performed using three different samples for each soil, the values reported in Table 6.3 are average values taking into account the maximum difference between single measurements as specified by the standard.

The values determined for the Ash material had a wide scatter, varying from 1.4 to 1.85. Previous research has indicated that the specific gravity of ash appears to vary with the size. London Underground Limited (LUL) tested ash from one of their embankments on the Roding Valley to Chigwell section of the Central Line. Ash

from this site is typical of the ash used in many of the LUL embankments in London. LUL suggested an empirical relationship to estimate the specific gravity of the ash. The relationship is as follows:

$$G_s = -0.0806 * \ln(D) + 1.9075 \qquad (6.1)$$

where:

G_s specific gravity

D average particle diameter (mm)

Fundamentally, the specific gravity would not be expected to be a function of particles size. However, the ash is a product of combustion and so has many particles with vesicular structure. The expression is probably not entirely reliable due to the small number of tests, additionally it is unclear whether it refers to discrete particles that contain precluded voids or to the material making up those particles. The former is more likely and the apparent variation with particle size is perhaps a reflection of the difficulty in grinding the material down to a small enough size to remove completely all the air voids. If the equation referred to the solid material in the particles, no variation in G_s would be expected, assuming that the mix of the chemicals making up the matrix of each particle is reasonably consistent (McNought, 1998). In view of these observations the maximum value of $G_s = 1.85$ was used in the calculation of void ratio for the Ash material.

Table 6.3 Values of specific gravity

SOIL	SOIL SAMPLE	SPECIFIC GRAVITY
CLAY	Kaolin Weald (UK) Bogotá (Colombia) Embankment Clay fill (UK)	2.61 2.76 2.76 2.78
RESIDUAL SOIL	Rio de Janeiro, Brazil K17, Colombia King's Park, Hong Kong	2.77 2.76 2.76
ASH	Power station (UK)	Variable (1.85 adopted)

ATTERBERG LIMITS 6.1.4

The Atterberg limits were determined for samples that were fully remoulded from the natural soil (i.e. without drying). The liquid limit was established using the cone penetration method (BS 1377: Part 2:1990:4:3) and the plastic limit was performed

according to BS 1377: Part 2 1990:5.3. The Atterberg Limits for each soil tested are shown in Table 6.4.

Table 6.4 Results from the Atterberg limit tests

TYPE SOIL	CLAYEY SOILS				RESIDUAL SOILS			ARTIFI-CIAL
SAMPLE	Weald	UN-Bogotá	Embankment	Kaolin*	Rio de Janeiro	K17 Colom-bia	King's Park	Ash
LIQUID LIMIT (%)	45	75	48	66	90	98	Non plastic	Non plastic
PLASTIC LIMIT (%)	25	45	27	32	47	37	Non plastic	Non plastic
PLASTICITY INDEX (%)	20	30	21	34	43	61	——	——
ACTIVITY	0.46	0.51	0.38	0.45	0.62	0.68	——	——

It has been shown that for some soils the hydration time has an influence on the measured value of the liquid limit, especially with residual soils (Quarterly Journal of Engineering Geology, 1993). Therefore, this test was performed after different periods of hydration for the residual soil sample from Brazil which was tested after one, five and eight days of hydration. As can be seen from Table 6.5 and Figure 6.3 there was a slight increase in the liquid limit with the hydration time while according to the plastic limit data, this particular soil is not sensitive to the hydration time.

Table 6.5 Variation of the Atterberg Limits with the hydration time from the residual soil from Brazil

Test	Rio de Janeiro soil sample (Brazil)		
Hydration time (days)	1	5	8
Liquid limit (%)	90	95	98
Plastic limit (%)	47	47	47
Plastic index (%)	43	48	51

The sensitivity of mixing time on some of the clayey samples was verified by using a range of mixing times prior to the Atterberg tests of between 10 and 30 minutes, however, the results did not show any substantial differences.

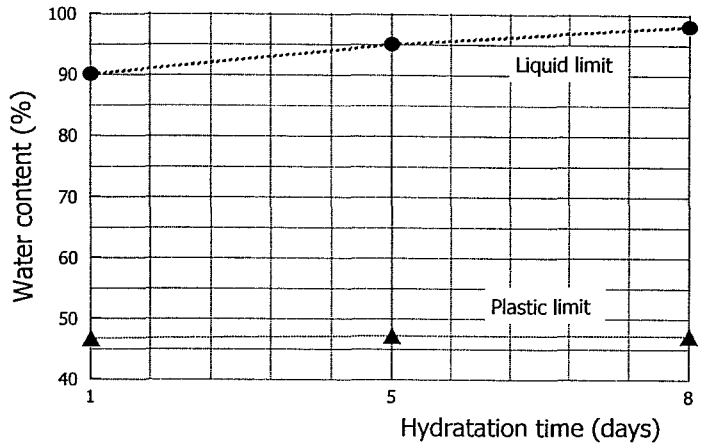

Figure 6.3 Effect of the hydration time

Figures 6.4 and 6.5 show the results of the Atterberg tests plotted on a Casagrande Plasticity Chart for the clayey fraction of the residual and clayey soils respectively. Liquid and plastic limits relating to residual soils are as equally useful as for sedimentary soils for the identification and classification of soils. However, the conventional categories defined by the A-Line may need some modification when describing residual soils. Sridharan et al., (1986) (quoted in the Quarterly Journal of Engineering Geology, 1993) suggested classifying residual soils by means of a plasticity chart incorporating a plot of activity (PI/Clay fraction). For this purpose the clay fraction should be expressed as a percentage of the particles <425 μm (Figure 6.4). It can be seen from Figure 6.4 that the fines of the soil from Brazil are clays of extremely high plasticity, and they are localised close to and below to the A-Line. In the data referred to as Daylac, 1994 (quoted in Rodriguez, 1998) will be discussed later in Chapter 8, the samples come from the same location as the residual soil from Brazil. The fines of the Colombian residual soil are also classified as clays of extremely high plasticity and they are localised close to and above the A-Line as can be seen from the same graph.

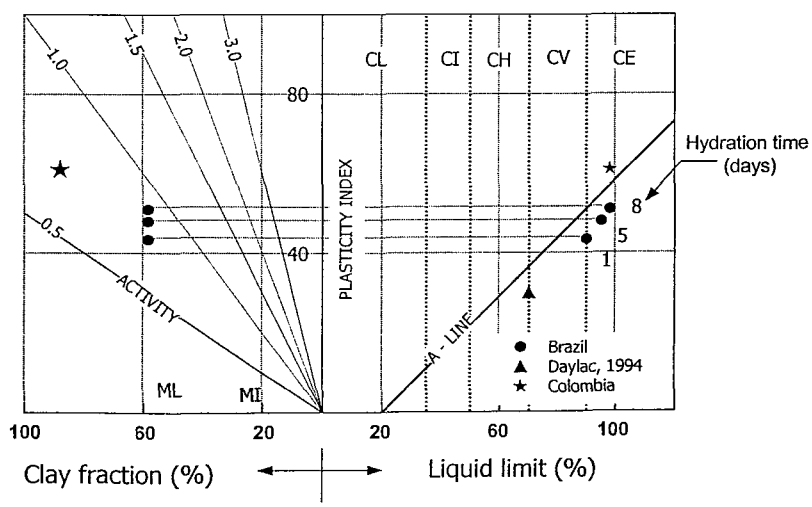

Figure 6.4 Classification by plasticity and clay fraction of the residual soil samples

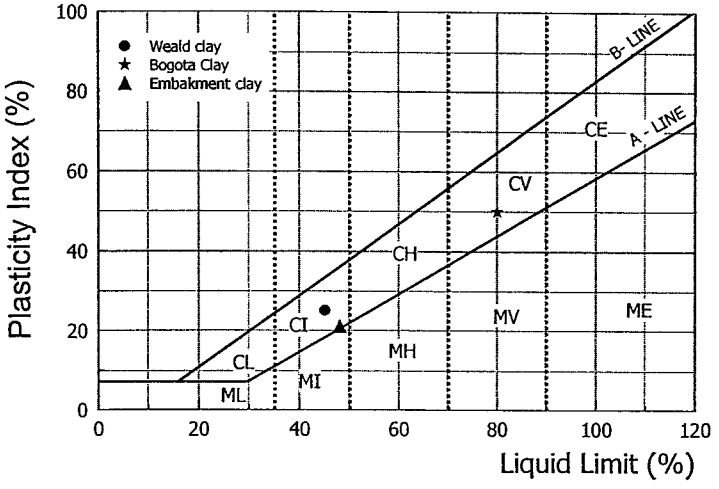

Figure 6.5 Classification of the fine particles from the clayey soils

As shown in Figure 6.5, the fine particles of the Weald Clay are mainly of medium plasticity. The fine particles from the Colombian samples are located above the A-Line but with a greater liquid limit than the Weald Clay, classifying them as fines of very high plasticity.

The activity of the soil is defined by the ratio of the plasticity index to the percentage of the clay size particles in the soil (Skempton,1953, quoted in Craig, 1992). It was calculated for each soil sample tested and the results are reported in Table 6.4.

6.2 LABORATORY MEASUREMENT OF THE SOIL-WATER RETENTION CURVE

The Kaolin slurry was reconstituted in a large consolidometer to a vertical effective stress of 250kPa. Four disks of Kaolin were trimmed from the cake formed in this way. Reconstituted samples of the residual soil from Brazil and Weald Clay were also prepared from slurry and consolidated one-dimensionally in a standard oedometer to maximum vertical stresses of 200, 1000 and 1500kPa. The samples were then unloaded and removed from the oedometer. The compression curves of the reconstituted samples for the residual soil from Brazil and Weald Clay are presented in Figures 6.6 and 6.7 respectively. The sample disks obtained from the oedometer tests were removed from their confining rings and dried and wetted, measuring matrix suction, in order to obtain the SWRC for each. The experimental determination of the SWRC for the samples investigated in this research was based on suction measurements using the filter paper technique, the axis-translation technique and the IC suction probe. The techniques involved are described in Chapter 4.

The SWRCs for the intact material were obtained by taking the samples in their initial states and gradually drying them, measuring suction and moisture content during the drying process. In addition, some samples were subsequently wetted, from a particular dry state. The filter paper method was used for making suction measurements during both drying and wetting. In the drying process, dry filter papers were placed on the flat surface of the soil sample disks, which were sealed and stored for seven days to allow the sample and filter paper to come to suction equilibrium (this seven-day period is discussed in Chapters 4 and 5). In the wetting-up procedure, wet filter papers were placed in contact with the sample. The filter paper method was used to find the SWRC in the whole range, i.e. from zero to very high suctions (30,000kPa). Residual soil samples and clayey samples were tested with the filter paper in contact. Regarding the SWRC determined using pressure plates or the IC suction probe, the experimental determination depended on the value of suction to be measured. The techniques used were complementary depending on the pressure to be measured as explained in Chapter 4. The IC suction probe was used to measure suction up to about 1,400kPa, and the different arrangements of pressure plates were used for controlling suctions in the range from 1,500 to 10,000kPa.

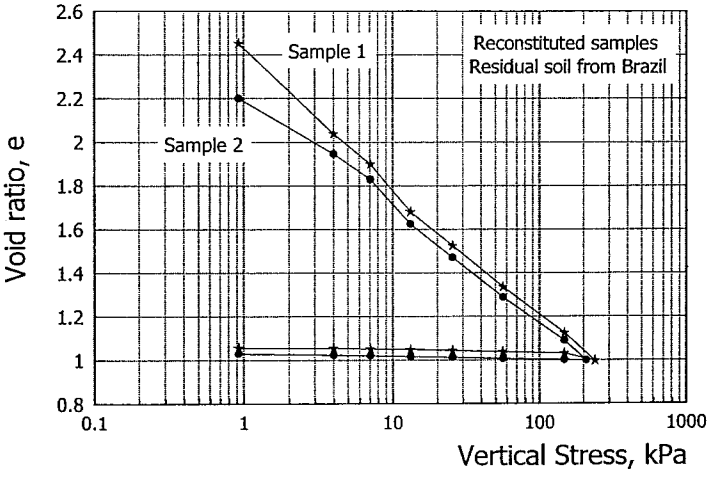

Figure 6.6 Normal consolidation and unloading curves for reconstituted Brazilian Residual soil.

6.3 SWRC FOR KAOLIN

Four individual samples of Kaolin were tested using the filter paper technique to establish various characteristics of the SWRC. All the experimental data are included in the following figures. The data are presented as matrix suction measurements against (a) degree of saturation (b) volumetric water content and (c) void ratio. Schematic diagrams showing the approximate paths followed in generating the SWRCs are shown in part (d) of the figures.

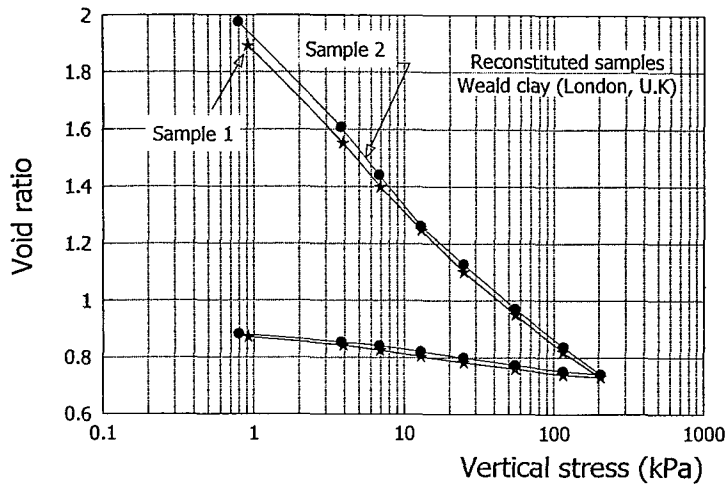

Figure 6.7 Normal consolidation and unloading curves for reconstituted Weald Clay from Gatwick.

Each data point represents an average measurement from the filter papers in contact with the top and the base of each sample. A more detailed analysis of the data is given in the next chapter, when selected data are used that are considered to be representative of the overall sample behaviour. Typically the time interval between each pair of data points was one week. Therefore it is evident that each one of these curves took many months of measurements (sometimes years).

In determining fundamental characteristics such as the AEV, S_f, S_r and S_a an average value based on all four samples has been calculated. In all the plots shown in the following figures, the limits (usually the start) of each stage are marked with an arrow and a number which allows the sequence of stages to be followed.

Sample kA. The first sample was used to establish the principal drying and wetting curves (PDC and PWC) for Speswhite Kaolin as shown in Figure 6.8. It can be seen that the PDC is well defined by the data with little scatter.

In determining the PWC (from point 2(A)), during the course of wetting the sample particular care was taken to try to define the most curved part of the PWC and to establish the beginning of the residual stage of the SWRC. It is for this reason that there are many measurements in this region (from 8,000 to 1,000kPa of suction). Only very small amounts of water were added at each decrement of suction in order to achieve this. Knowing how much water to add was to a large extent a matter of trial and error. In hindsight the quantities of water added were perhaps too small which has resulted in a slight scatter of the data, although the data are within the error band determined in Chapter 5. The scatter probably results from the fact that very small cycles of drying and wetting were induced by not adding sufficient water at each decrement and the effects of evaporation.

It can be seen (Figures 6.8(a) and (b)) that the data do not conform to the smooth convex curve that is usually expected for this region of the PWC. There is a small inward curvature with an inflexion point as the suctions approach 1,000kPa. This is perhaps because during the drying stage the sample was not dried to a sufficiently high suction so that on wetting the soil followed the PWC. Instead the data appear to have the form of a primary scanning curve, starting at a very high suction. However it should be noted that reliable measurements using the filter paper technique can not be made for suctions greater than about 30,000kPa (Marinho, 1994) and so the soil was not dried beyond this value. By the time the suction had reduced to about 1,000kPa the curve appears to have rejoined the expected path of the PWC.

A similar procedure, of adding only small amounts of water at each stage, was followed to define the upper part of the PWC and the residual air content. Following the earlier experience discussed above, it was realized that larger amounts of water were required, so less measurements were taken. Although the scatter appears worse for this part of the curve, this results from the fact that the suctions are very low and hence the error is potentially more significant (as discussed in Chapter 5).

The suction measurements below 10kPa were made using the modified pressure plate apparatus described in Section 4.2.1.1 of Chapter 4. It should be noted that at this low suction the soil is very sensitive to small changes of water content and some clearly erroneous data have been omitted.

Curves representing the PDC and PWC have been drawn by eye through the data. These curves are also included (using broken lines) in later data plots to facilitate comparison.

Void ratio is plotted against suction in Figure 6.8(c). It can be seen that the form of the data is very similar to that that would be expected for an oedometer test data with initial drying stage looking similar to a normal compression line and then the wetting stage being similar to a swelling line.

The scatter of data in the three graphs (Figures 6.8a, b and c), as mentioned above, is generally within the limits estimated from the analysis in Chapter 5 (Table 5.2). The accuracy of the suction measurements generally seems better than was estimated, while the scatter of the data in terms of degree of saturation, volumetric water content and void ratio is quite close to the values estimated, i.e. $\pm 1\%$, $\pm 0.3\%$ and ± 0.01 respectively. It should be noted that these observations are made by roughly banding the data ranges, rather than by a rigorous statistical analysis.

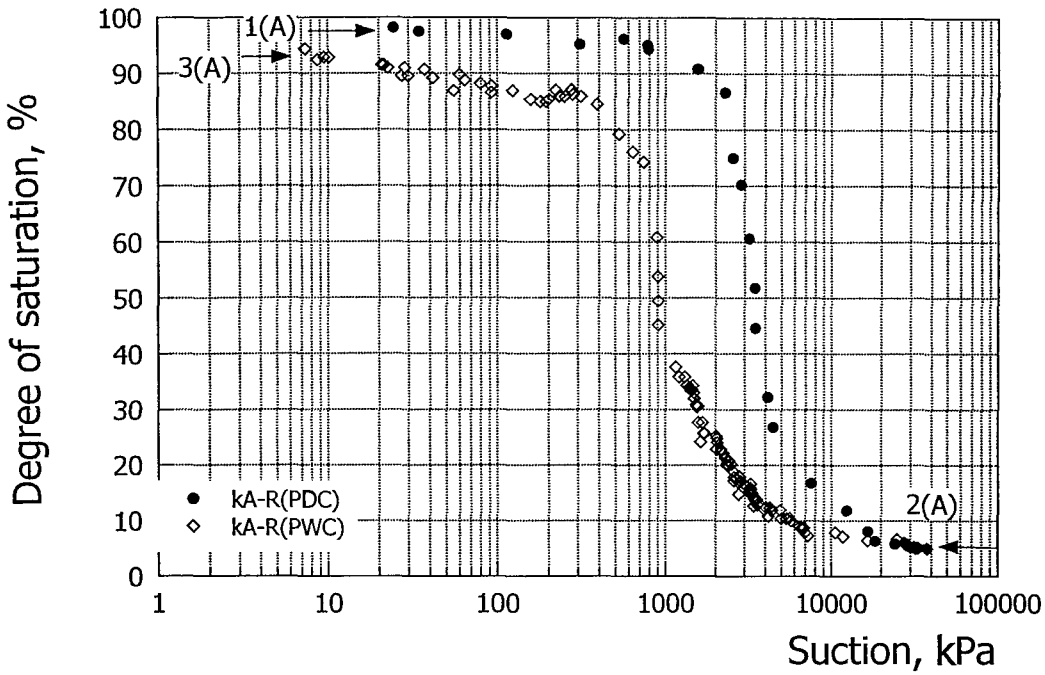

Figure 6.8(a) SWRC for Kaolin kA sample in terms of suction versus degree of saturation

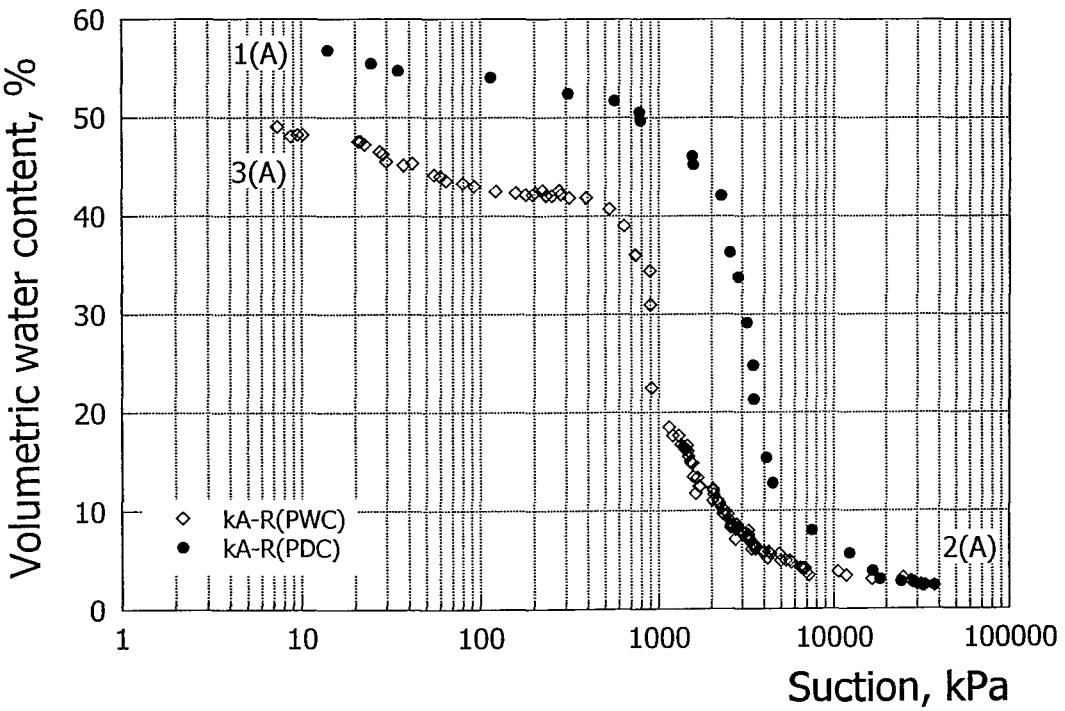

Figure 6.8(b) SWRC for Kaolin kA sample in terms of suction versus volumetric water content

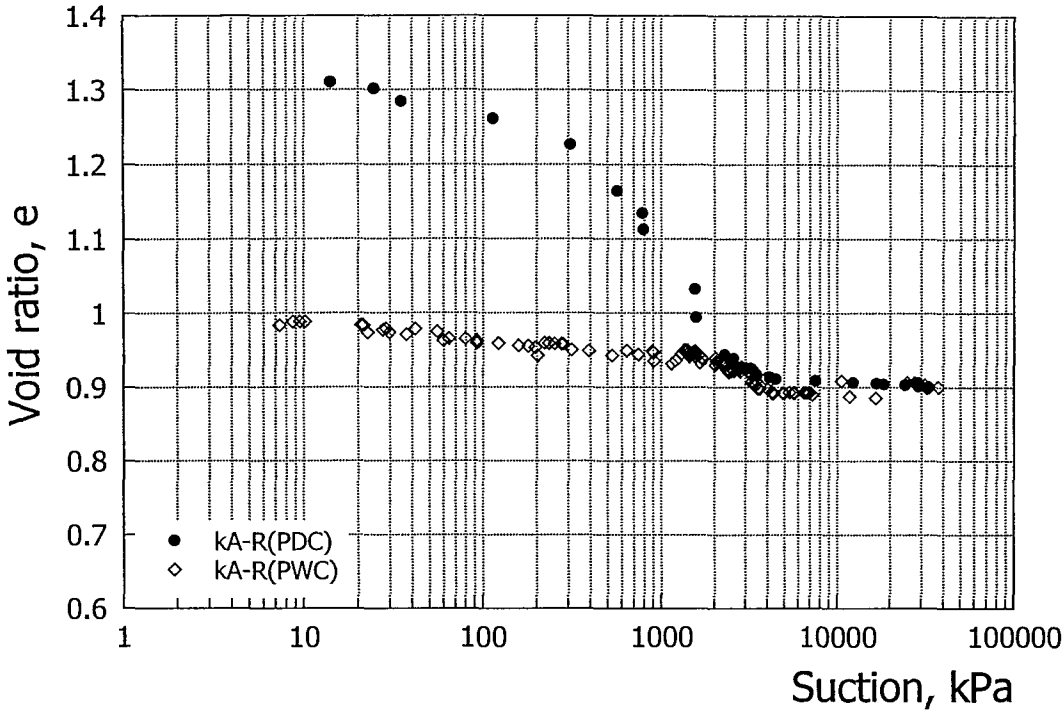

Figure 6.8(c) SWRC for Kaolin kA sample in terms of suction versus void ratio

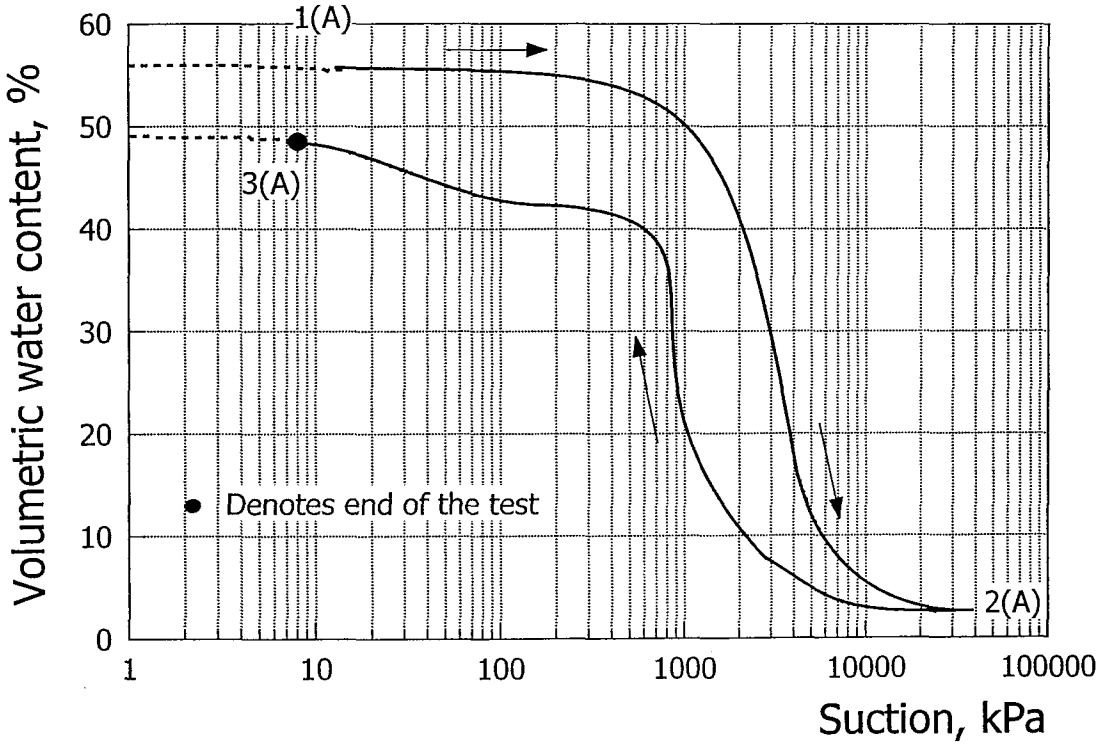

Figure 6.8(d) Schematic diagram showing approximate paths followed in generating the SWRC for Kaolin sample kA

Sample kB. There are four stages to this test (see Figure 6.9). Initially the sample was dried (from point 1(B)) such that it followed the PDC. However the drying was stopped at a degree of saturation just below 60% on the steep region of the curve (point 2(B)). It can be seen that the PDC for this sample was slightly lower than that

for sample kA, a possible reason for this is that the void ratio for this sample was slightly lower than that of the other samples (by about 0.05, see Figure 6.9(c)).

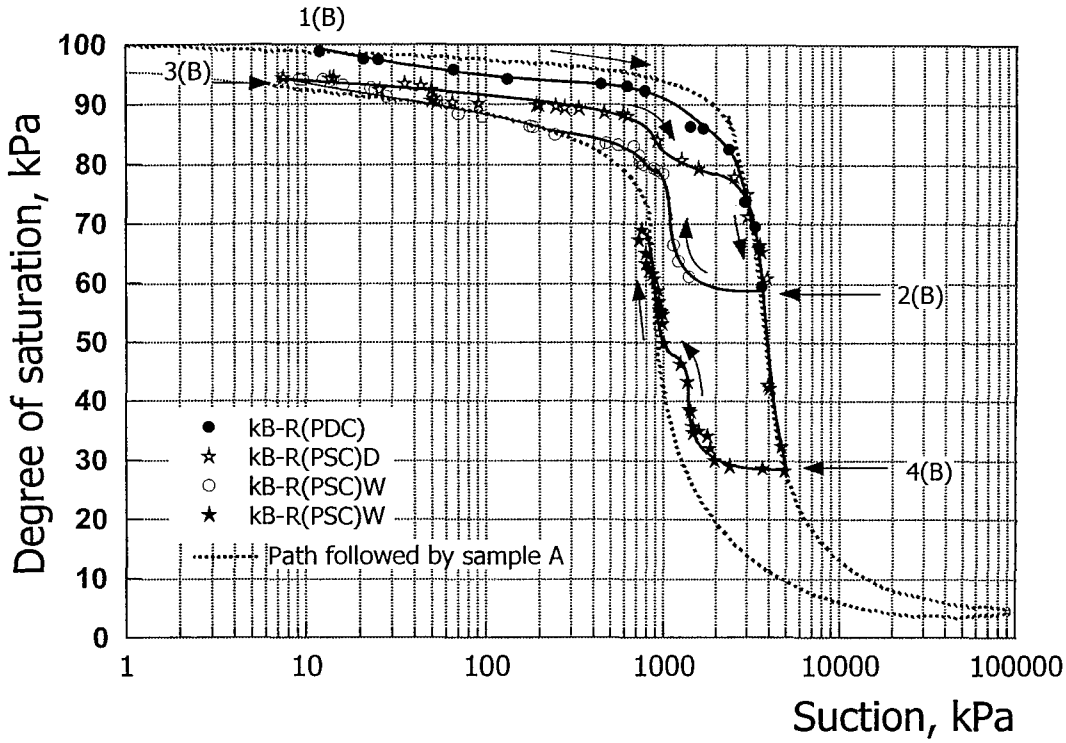

Figure 6.9(a).SWRC for Kaolin kB sample in terms of suction versus degree of saturation

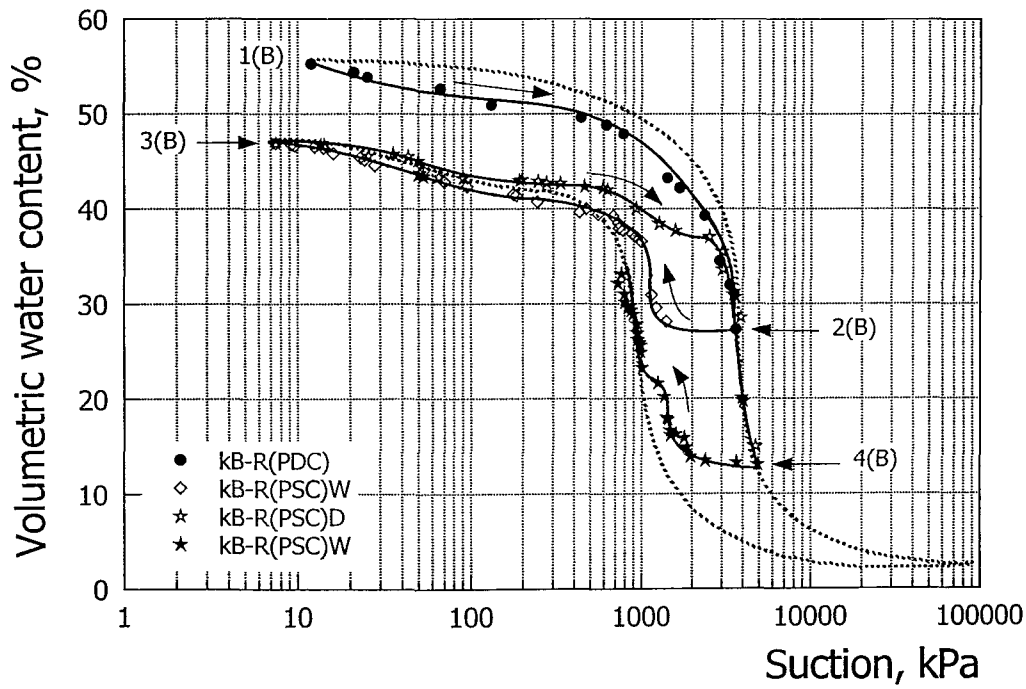

Figure 6.9(b) SWRC for Kaolin kB sample in terms of suction versus volumetric water content

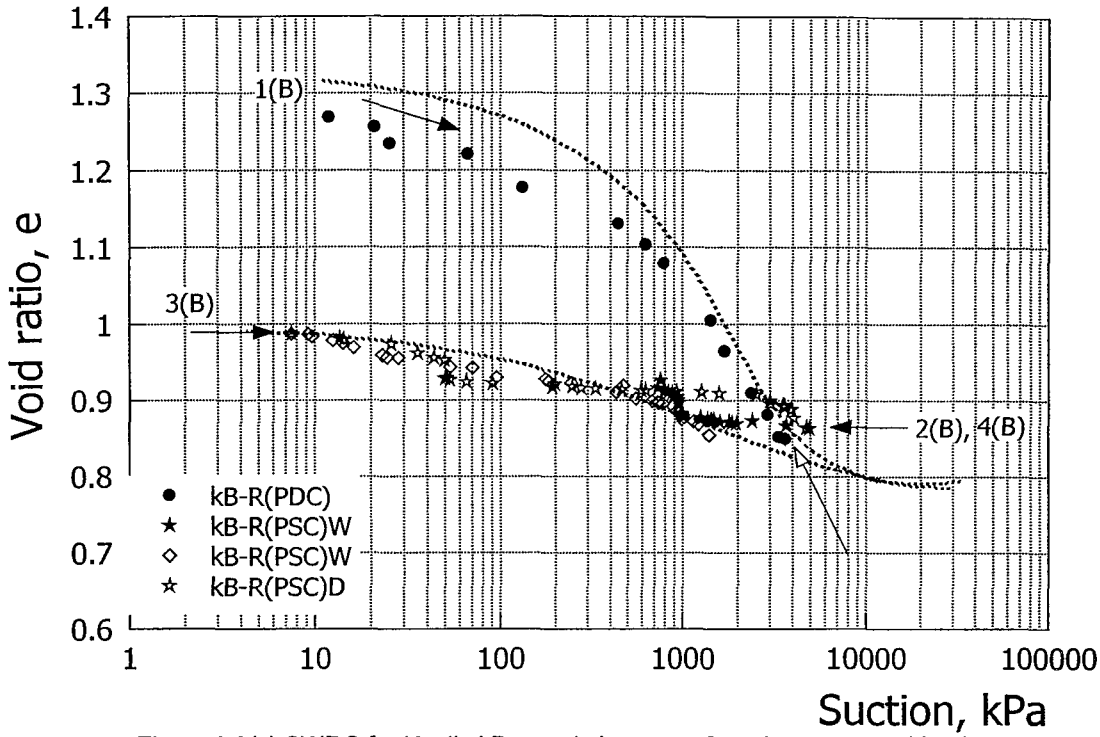

Figure 6.9(c) SWRC for Kaolin kB sample in terms of suction versus void ratio

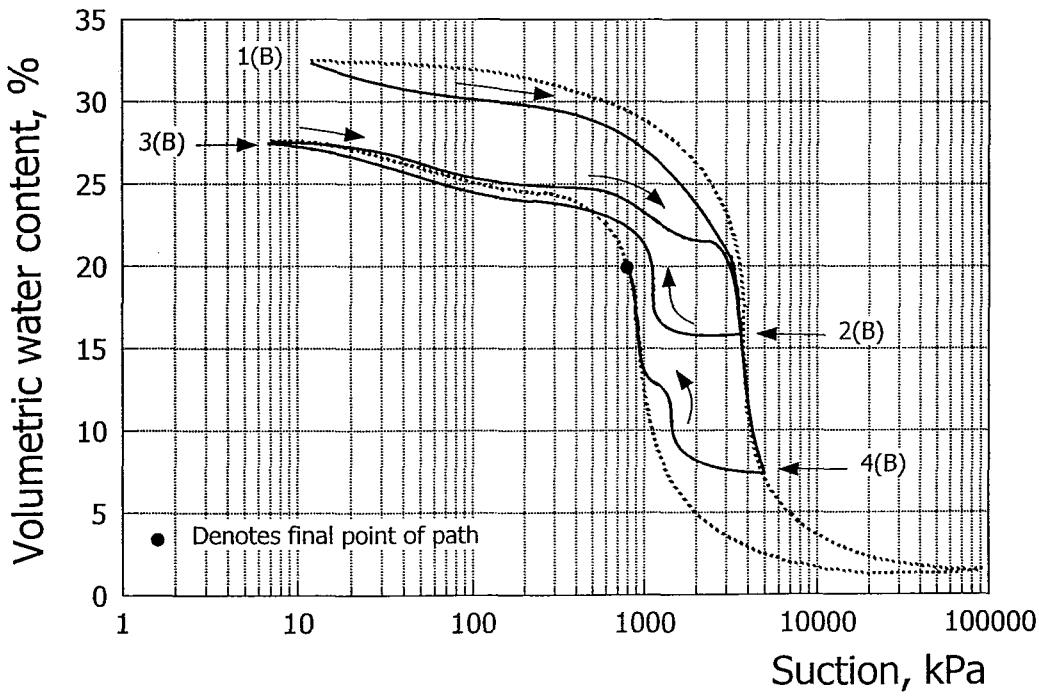

Figure 6.9(d) Schematic diagram showing approximate paths followed in generating the SWRC for Kaolin sample kB

The sample was then wetted (from point 2(B)) to generate a primary scanning curve (PSC). Wetting was continued to very low suction values of less than 10kPa. The sample response during the initial wetting follows the characteristic form expected of a primary scanning curve, with double curvature and an inflection point. The data in the later stages of wetting, i.e. from a suction of about 400kPa, compare well with the PWC determined from sample kA.

A second drying stage was then started from point 3(B) which shows a similar form to the PDC from the first stage of the test up to a suction of about 700kPa. At this point the curvature changes, again with an inflection point, similar to the shape observed from the previous primary scanning curve. By a suction of about 3,000kPa the data points once again rejoin the PDC. Drying continued to a suction of about 5,000kPa and the degree of saturation of about 28%. The sample was then wetted again from point 4(B). Once more the form of the curve is characteristic of that expected of the primary scanning curve. The test was terminated at a suction of about 700kPa (because of time constraints, the test having run for three years).

It is interesting to note that the three primary scanning curves whether wetting or drying all exhibit the common feature of double curvature with an inflexion point but to different degrees, depending on the degree of saturation. They are all within the PWC defined for sample kA. The three primary scanning curves are also consistent with that observed on the initial wetting of sample kA. In all cases the inflection point lies somewhere in the suction range of 800 to 2,000kPa.

In Figure 6.9(c) the suction is plotted against void ratio. As pointed out early the points representing the drying cycle resemble the normal consolidation line, which in this cases lies slightly below that of sample kA. The unload/reload loops are almost co-linear as the suction values at which they start are very similar, the start points being on the steep part of the PDC.

Sample kC. There are five stages to this test (see Figure 6.10). As for samples kA and kB the sample was initially dried to generate the PDC (from point 1(C)). The PDC for this sample is very similar to that of sample kA, the void ratios being almost the same. From a suction of about 30,000kPa the sample was wetted resulting in a primary scanning curve similar to that observed for sample kA, but slightly more exaggerated perhaps because the PDC did not extend as far as that for kA (i.e. 30,000kPa compared with 40,000kPa for kA). The data rejoined the suggested PWC at a suction of between 1,000 and 2,000kPa. Wetting was continued to a degree of saturation of just over 60% and at a suction of about 800kPa from which point the sample was dried again (from point 3(C)) to generate a primary scanning curve. The curve has the characteristic expected shape. Drying was stopped at the point where the PDC was almost intercepted and then wetting recommenced from point 4(C). This time wetting was not continued to the PWC but it was stopped at about the inflection point where the curvature was about to change. Another drying cycle was then started from point 5(C) in order to generate a secondary scanning curve. The secondary scanning curve was continued until it intercepted the PDC at which time the test was terminated.

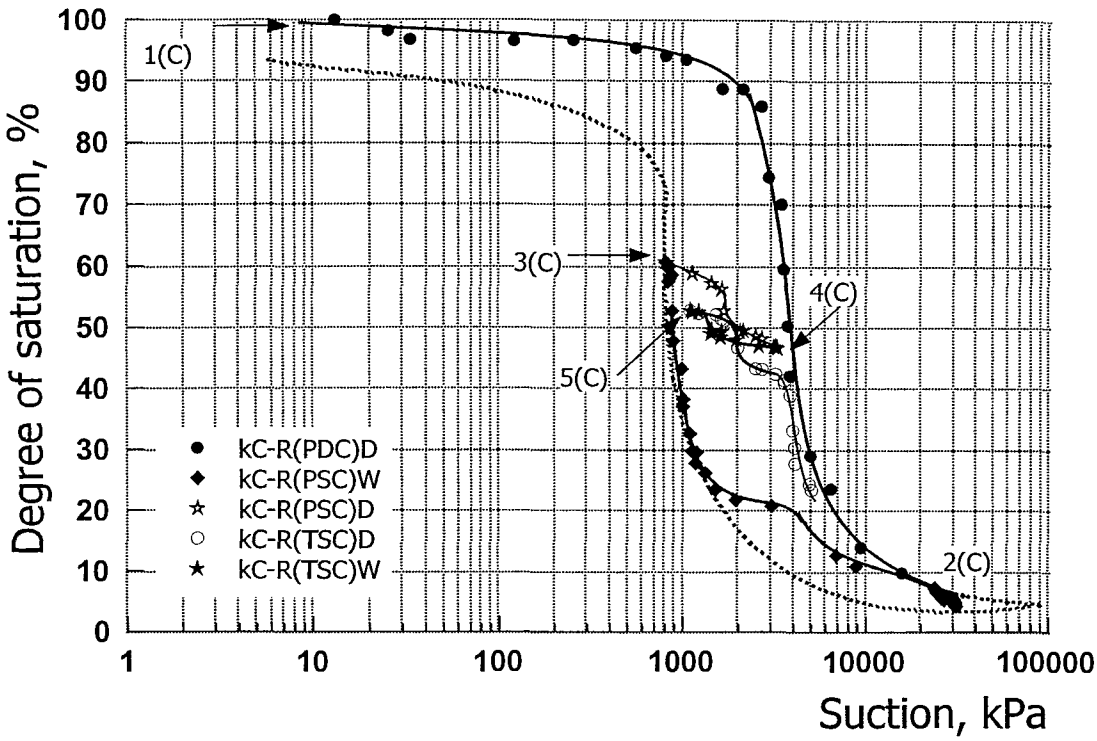

Figure 6.10(a) SWRC for Kaolin kC sample in terms of suction versus degree of saturation

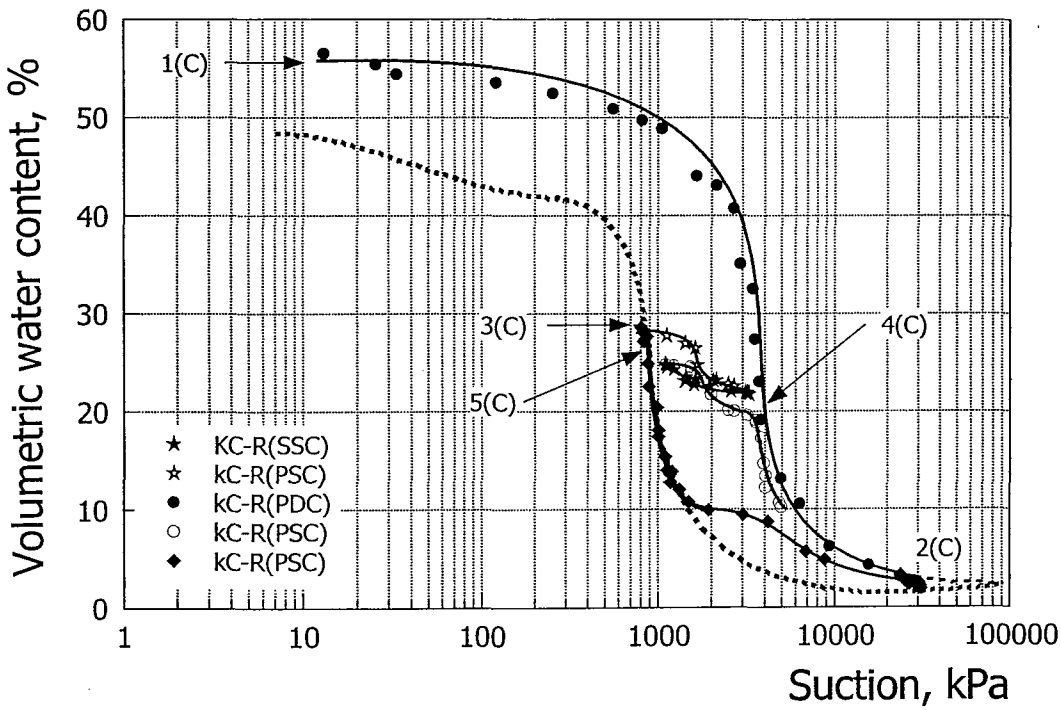

Figure 6.10(b) SWRC for Kaolin kC sample in terms of suction versus volumetric water content

As with samples kA and kB the scanning curves, including the secondary one, have the same form with double curvature.

The data in terms of suction versus void ratio is shown in Figure 6.10(c). Similar comments can be made to those from sample kB.

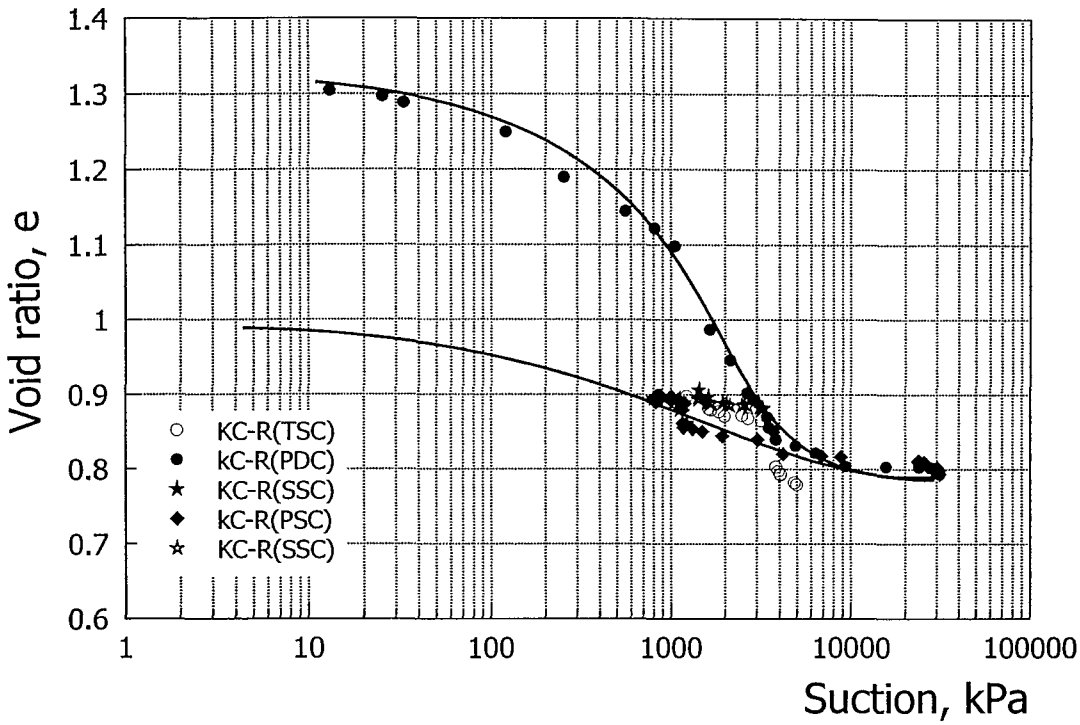

Figure 6.10(c) SWRC for Kaolin kC sample in terms of suction versus void ratio

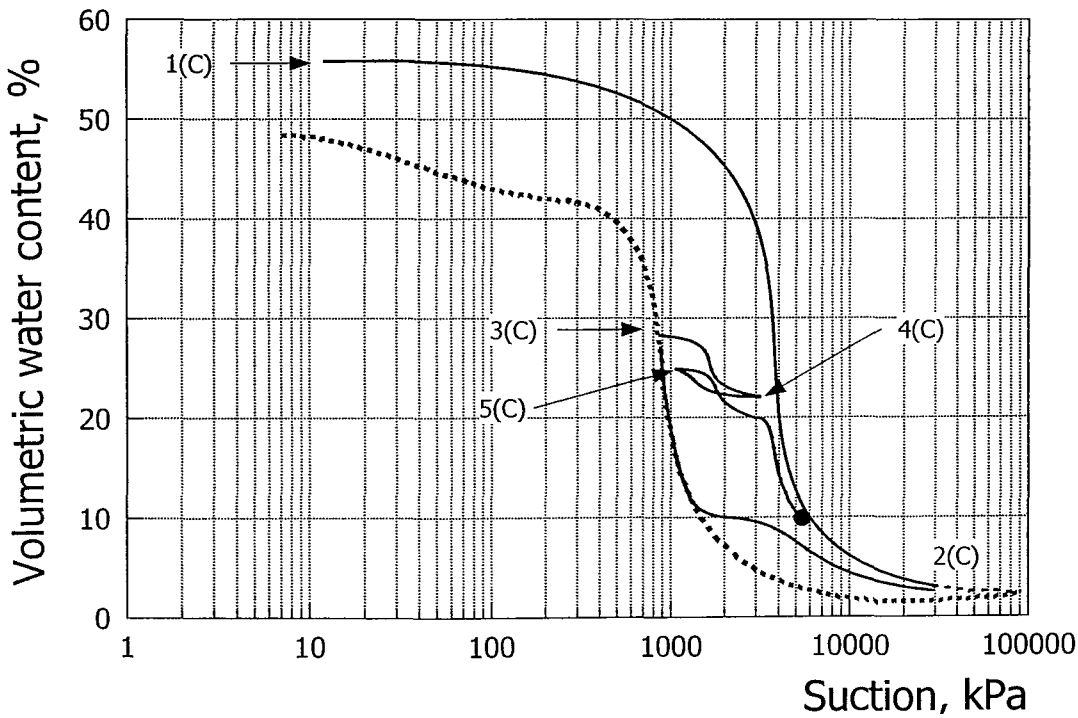

Figure 6.10(d) Schematic diagram showing approximate paths followed in generating the SWRC for Kaolin sample kC

Sample kD. Figure 6.11 shows the five stages imposed on sample kD starting from point 1(D), which were similar to those in the tests on samples kB and kC. The PDC was stopped at a lower suction of about 13,000kPa prior to wetting (from point

2(D)). Three primary scanning curves were then generated, two drying and one wetting. The form of these curves and the initial wetting curve from point 2(D) are all consistent with those observed for the other three samples. Again the inflection points are generally in the same range of suction between 800 and 2,000kPa. Similar comments made for sample kB and kC relating to the plot of void ratio against suction apply for this sample (see Figure 6.11(c)).

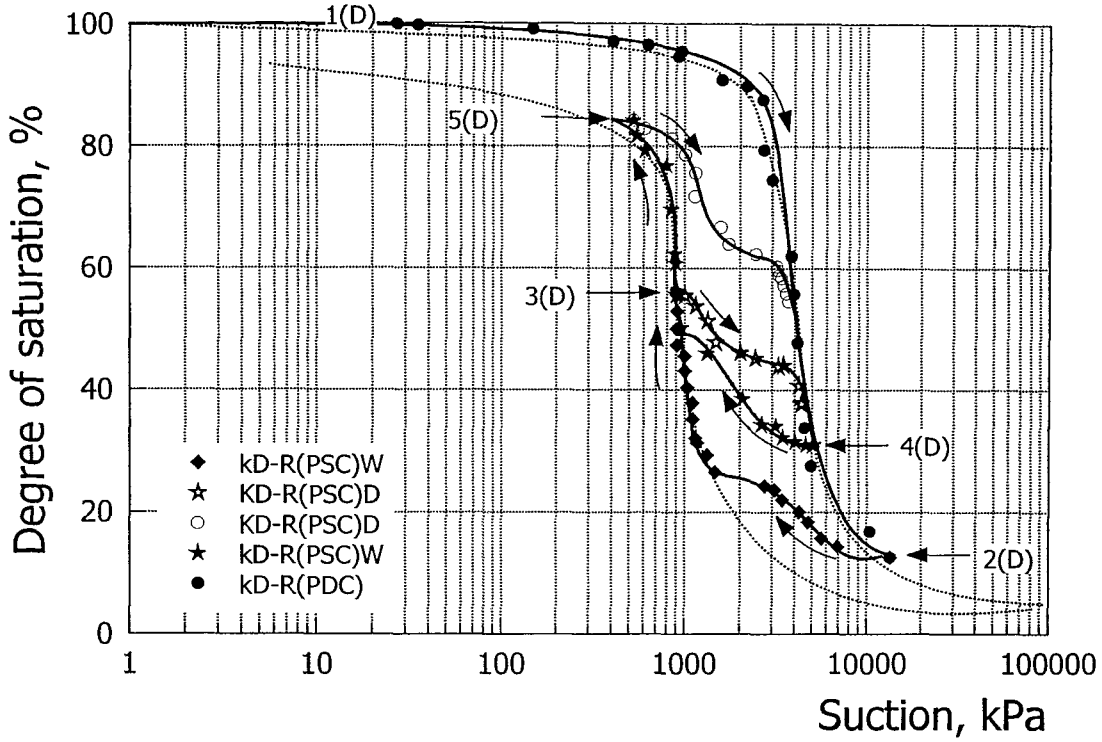

Figure 6.11(a) SWRC for Kaolin kD sample in terms of suction versus degree of saturation

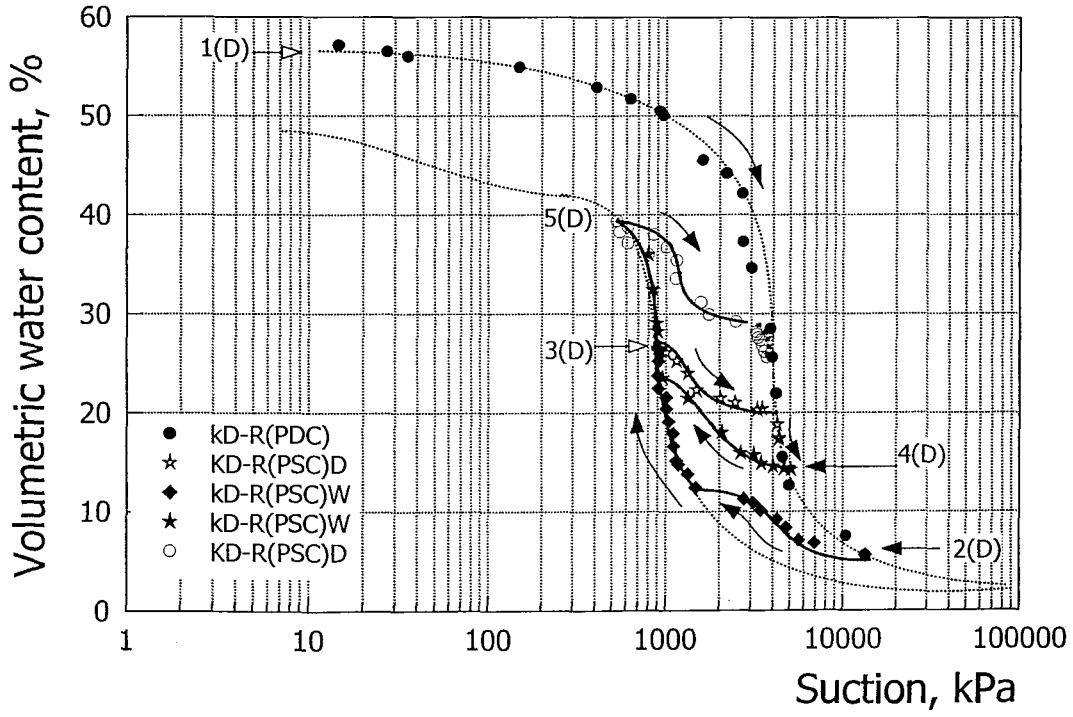

Figure 6.11(b) SWRC for Kaolin kD sample in terms of suction versus volumetric water content

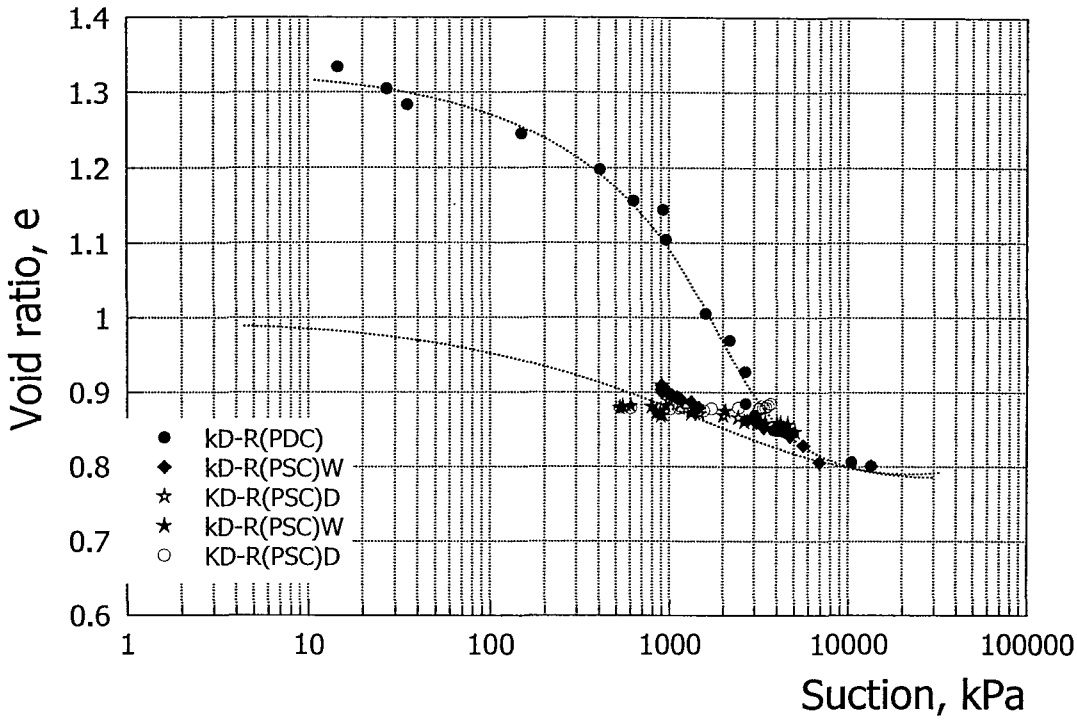

Figure 6.11(c) SWRC for Kaolin kD sample in terms of suction versus void ratio.

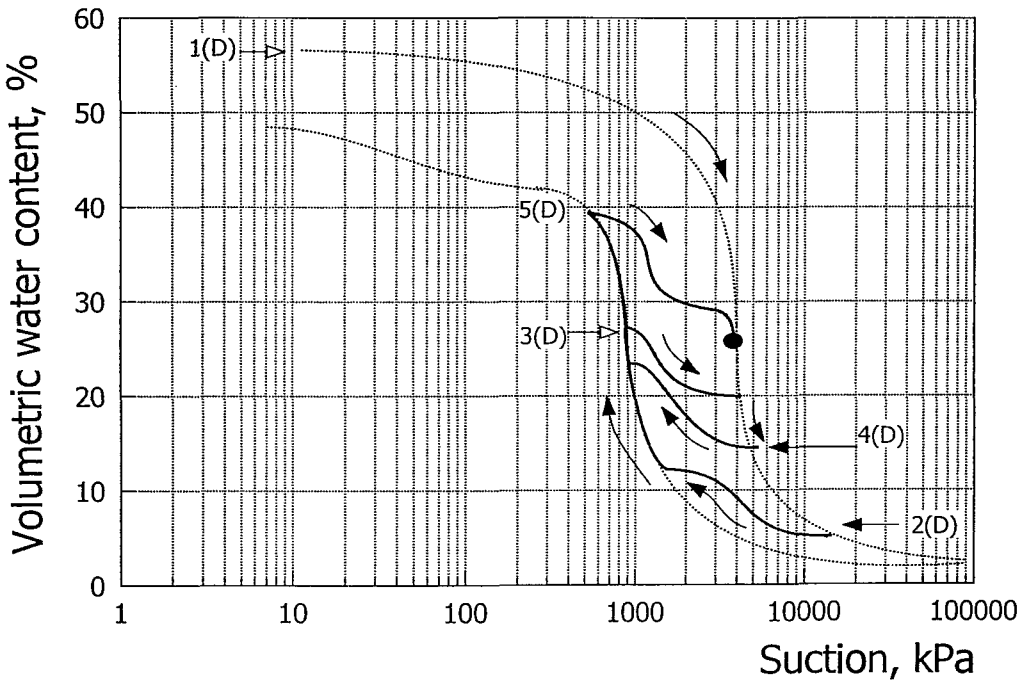

Figure 6.11(d) Schematic diagram showing approximate paths followed in generating the SWRC for Kaolin sample kD.

Similar comments made relating to the scatter of the data for sample kA, can equally be made for samples kB, kC and kD, with their ranges of scatter being better than estimated in the case of suction measurements and similar in terms of degree of saturation, volumetric water content and void ratio.

SWRC FOR WEALD CLAY 6.4

The Weald Clay is a much sandier material than the Kaolin just discussed, having about 15% sand content and a plasticity index of about 20%. Two samples of the Weald Clay obtained from Gatwick were air dried, ground and mixed into slurry at a water content of $1.5(\omega/c)_L$ Two specimens of the slurry were then consolidated in a standard oedometer of 100mm diameter to provide one dimensional reconstituted samples. Both of these samples were then allowed to dry in stages and tested using the filter paper technique to establish various characteristics of the SWRC

Sample A. The results from the different stages of drying and wetting are shown in Figure 6.12. The initial drying (from point 1(A,B)) defines the PDC and there is little scatter of the data. Drying was continued to a suction of just over 30,000kPa. The sample was then wetted to a suction of about 700kPa, defining the first half of the PWC. However, it should be noticed that there is some considerable scatter during the initial stages of wetting, greater than estimated from the analysis described in Chapter 5. This is thought to be a consequence of the very small quantities of water added at each stage, as discussed for the Kaolin samples. A primary scanning curve was generated by drying again from point 3(A), which has a standard form with double curvature and inflection point. The scanning curve approaches the PDC at a suction of about 7,000kPa. Normally the PSC would be expected to join the MDC, which lies inside the PDC, but for these data it seems to join the PDC. This implies that the PDC and the MDC are almost coincident. Drying was continued to a suction of just over 10,000kPa after which wetting recommenced from point 4(A). The resulting primary scanning curves again have the same form with the double curvature and inflection point and join the PWC at about 2,500kPa. The test was concluded at this point.

Sample B. This sample was used just to define the PDC and the PWC as shown in Figure 6.12 (the data for samples A and B are plotted on the same graph). There are two regions where there is considerable scatter. At the end of the measurements on the PDC the suctions are very high, being in excess of 20,000kPa, and so suction measurements are less reliable. Measurements on the PWC where the curve starts to flatten also exhibit scatter. This is because only very small amounts of water were added to define the curvature in this region as small changes in water content have a significant influence on values of suction. The PDC and the PWC are very similar for both samples A and B. This is perhaps a reflection of the fact that they both have very similar initial void ratios.

Comparing the SWRC for the Weald Clay with those for Kaolin, several marked differences can be observed. The AEV for the Weald Clay is about 1,000kPa compared with 2,000kPa for Kaolin. The main part of the SWRC beyond the AEV is

very steep for the Kaolin samples and changes much more gradually for the Weald Clay. Towards the end of the PDC the Kaolin seems to approach a constant degree of saturation while the Weald Clay still seems to be decreasing. These differences possibly arise because of the different characteristics of the two clays, the Weald Clay being much sandier than the Kaolin with a correspondingly lower plasticity index.

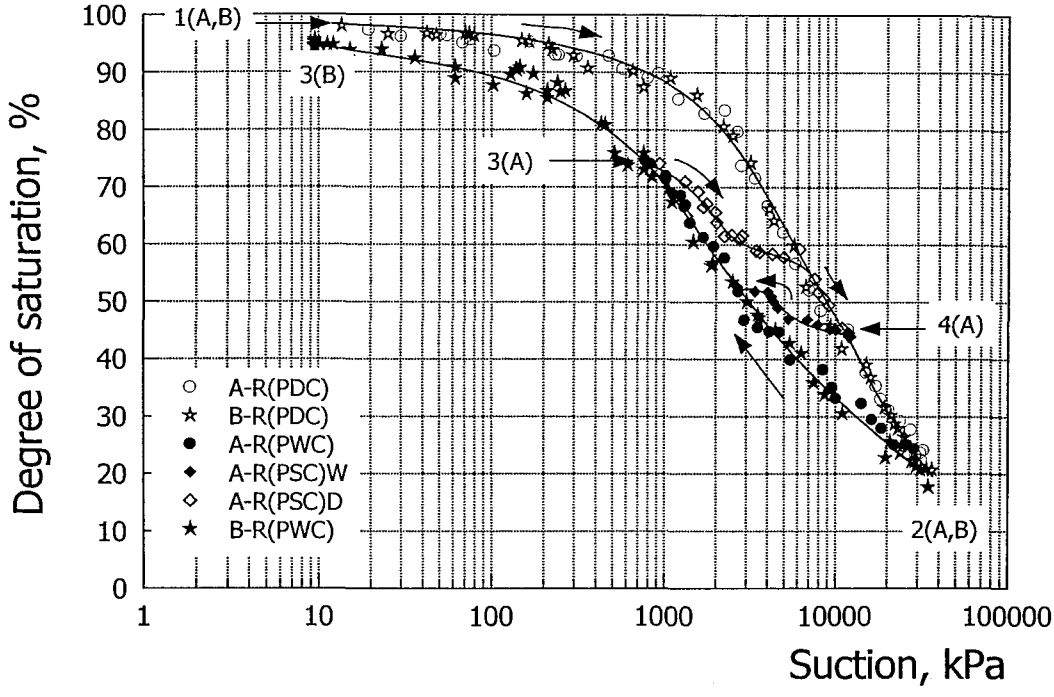

Figure 6.12(a) SWRC for Weald Clay samples A and B in terms of suction versus degree of saturation.

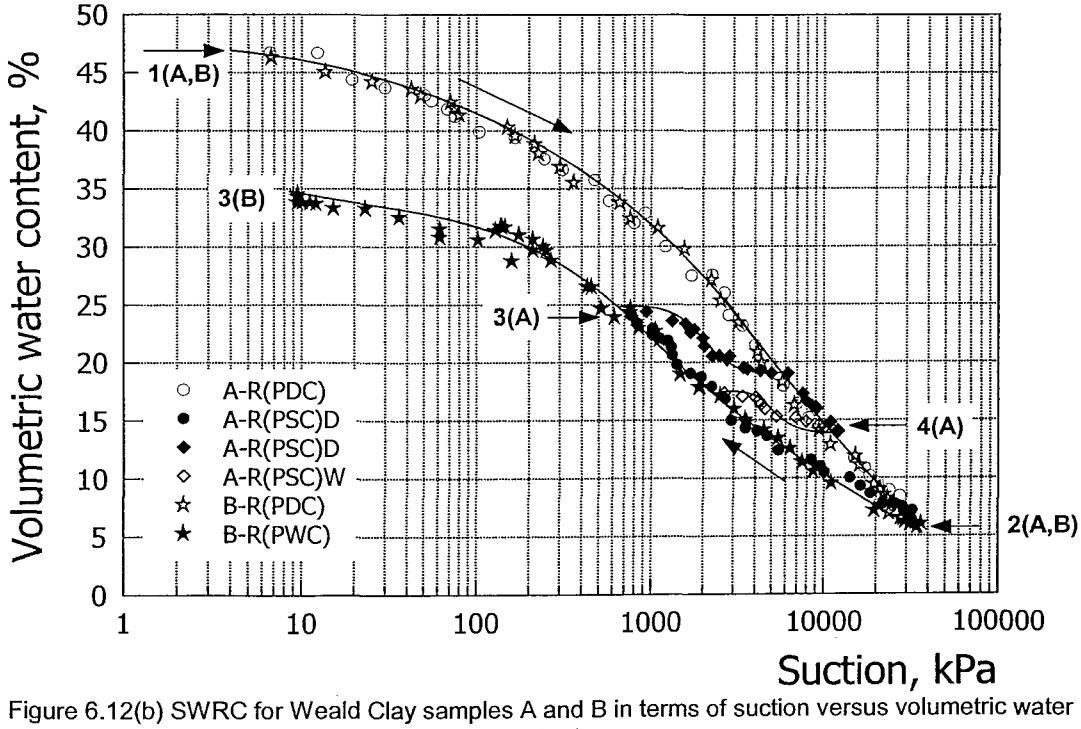

Figure 6.12(b) SWRC for Weald Clay samples A and B in terms of suction versus volumetric water content.

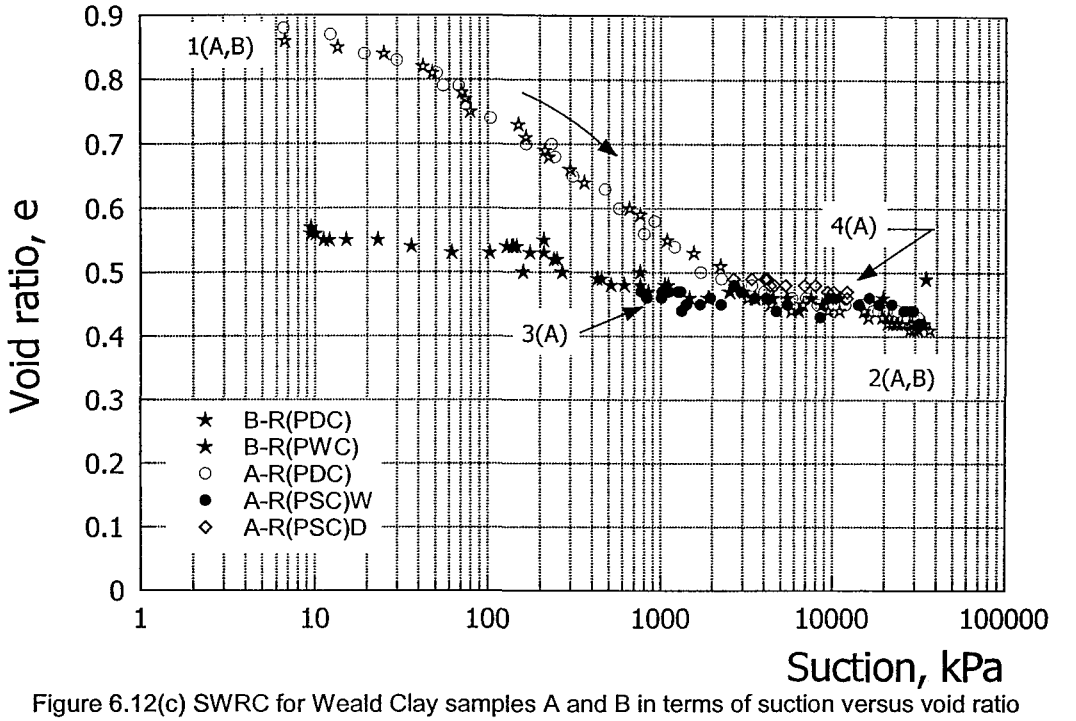

Figure 6.12(c) SWRC for Weald Clay samples A and B in terms of suction versus void ratio

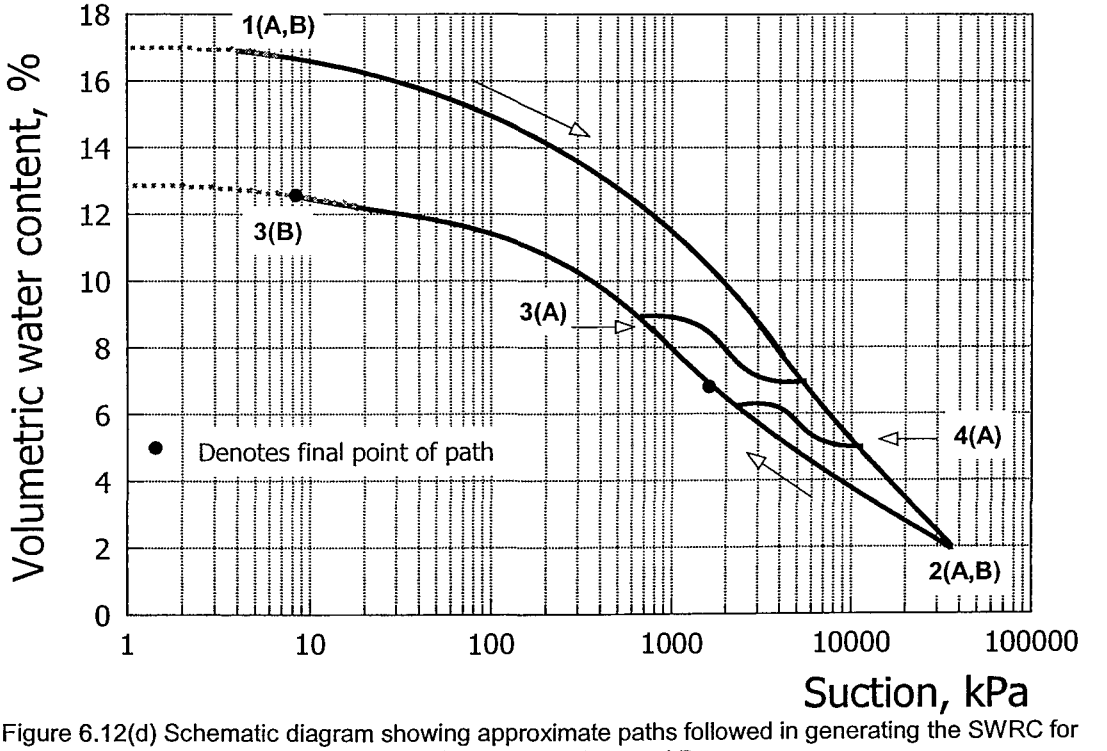

Figure 6.12(d) Schematic diagram showing approximate paths followed in generating the SWRC for Weald Clay sample A and B

This clay has similar plastic and liquid limit values to the Kaolin, but clearly in this case it is a natural soil. Four samples of UN-Bogota clay were tested, two reconstituted and two intact, using the filter paper technique for measuring the relationship between suction and moisture content (SWRC). All four samples were dried to determined the PDC and MDCs as shown in Figure 6.13. In this figure the 'I' stands for intact and 'R' for reconstituted samples. It can be seen that the reconstituted soil samples remained fully saturated to quite high suctions, i.e. about 500kPa. The data for the two samples are shown together (i.e. R(A,B)) and can be seen to follow very similar paths. Once the samples start desaturating at about 1,000kPa, desaturation occurs rapidly, evident from the steep PDC. This response is very similar to what was observed for the reconstituted Kaolin samples. From a maximum suction of about 30,000kPa one of the samples was then wetted up to establish the PWC. It can be seen (Figure 6.13(a)) that the slope of the PWC is much shallower than was observed for the Kaolin, i.e. the SWRC is much more hysteretic. At the end of the wetting cycles the degree of saturation was about 90%. As has been observed for the other samples, the volumetric water content and void ratio do not return to their initial values.

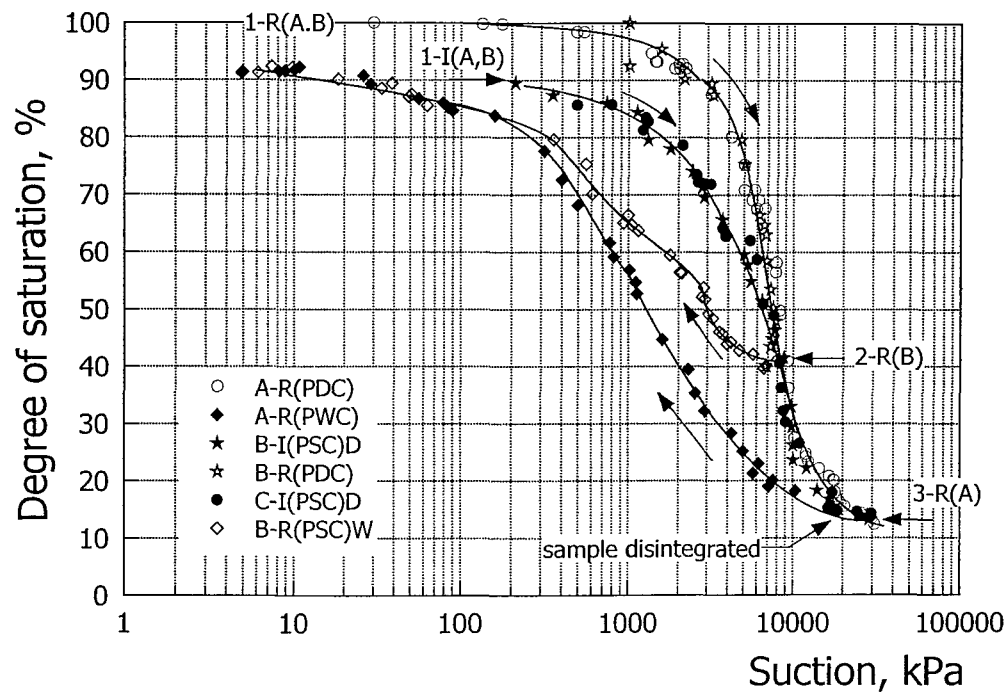

Figure 6.13(a) SWRC for UN-Bogotá Clay samples in terms of suction versus degree of saturation

The other reconstituted sample was dried to a suction of about 10,000kPa and a degree of saturation of about 40%, at which point it was wetted up to generate a primary scanning curve. There is some scatter in the data for this PSC, but it can be seen that it joins the PWC defined by the other reconstituted sample. It can be observed that there seems to be little change in degree of saturation for suctions

below about 80kPa (except for a couple of seemingly erroneous points). However a definite trend can be seen in terms of the change of volumetric water content in this low suction range (Figure 6.13(b)). This is almost certainly a reflection of the different measuring accuracies for these two quantities, as was discussed in Chapter 5 (Table 5.2).

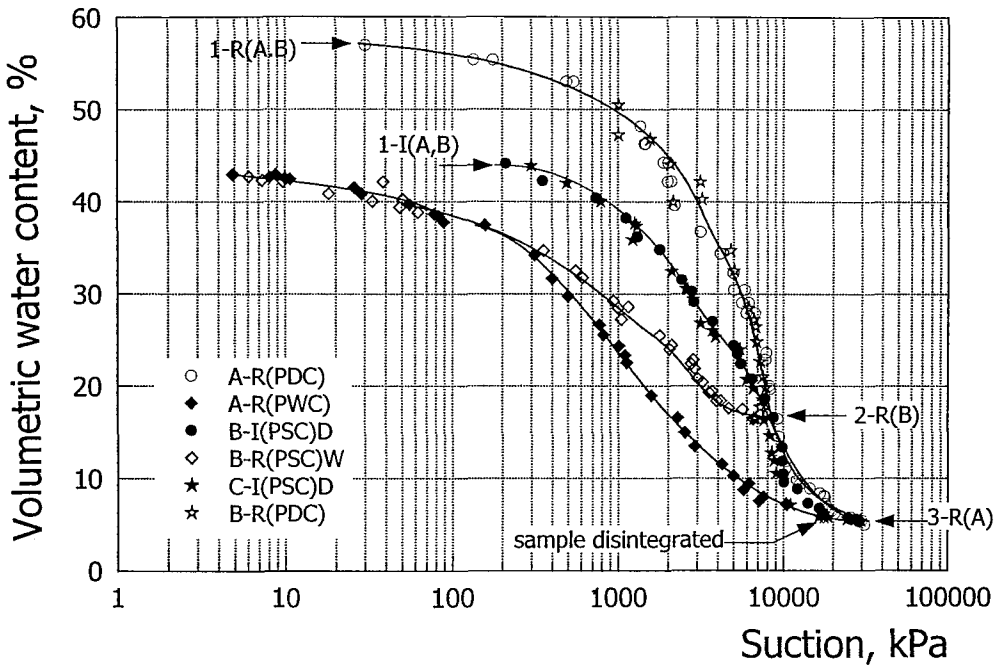

Figure 6.13(b) SWRC for UN-Bogotá Clay samples in terms of suction versus volumetric water content

The two intact samples were dried from their initial state. It can be seen that they were in a partly saturated state with an initial degree of saturation of just below 90% with suction values of about 300kPa. During drying the samples initially exhibited a shallower slope than the reconstituted samples but soon converge to similar values. It should be noted that one of the intact samples started to crack at a degree of saturation of about 70%. This sample was dried to a suction of about 30,000kPa at which point the degree of saturation was just under 15%. It was wetted up but unfortunately the sample disintegrated soon after three stages (i.e. three data points on the plot) of wetting and so the test on this sample had to be terminated. The drying process of the other sample was terminated at the end of the PDC.

In conclusion, the drying curves for the UN-Bogotá clay are similar to those of Kaolin, which might be expected given that they have similar Atterberg limits. However the wetting curves are shallower, producing greater hysteresis, possibly reflecting the increased activity of the UN-Bogotá clay. The void ratio of the reconstituted UN-Bogotá clay is significantly greater than that of Kaolin.

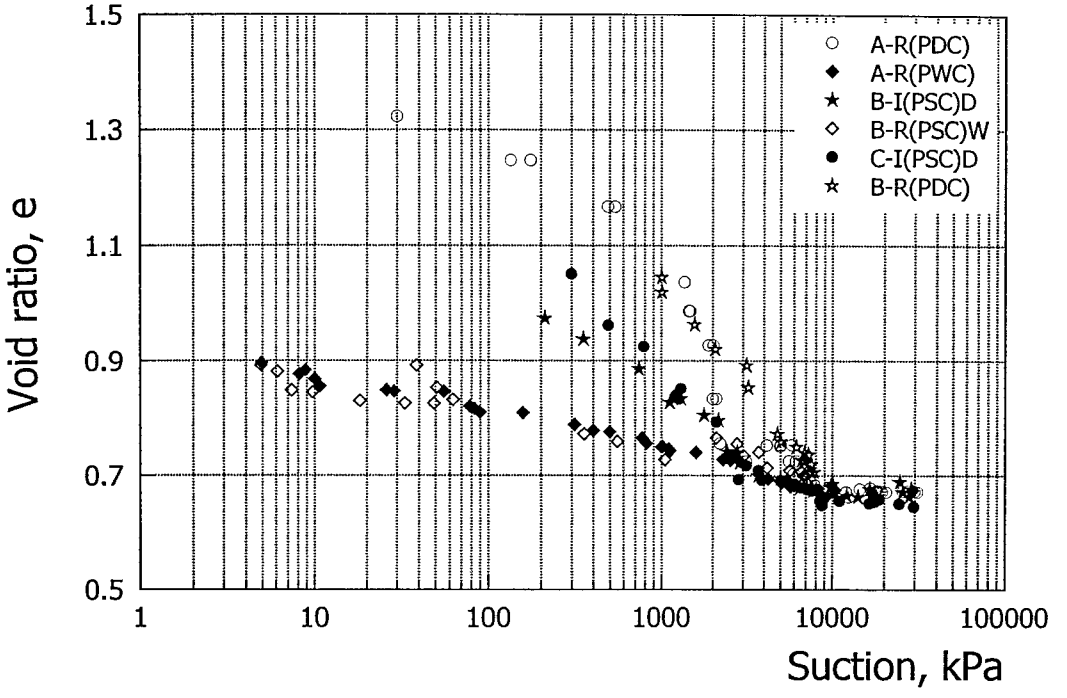

Figure 6.13(c) SWRC for UN-Bogotá Clay samples in terms of suction versus void ratio

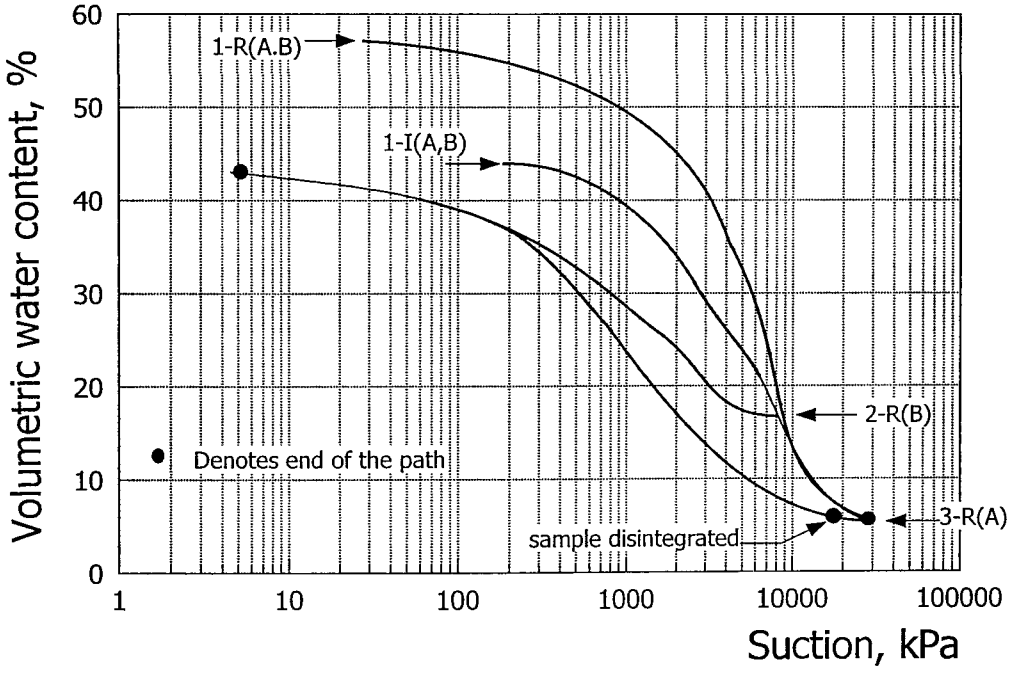

Figure 6.13(d) Schematic diagram showing approximate paths followed in generating the SWRC for UN-Bogotá Clay samples

6.7 SWRC FOR THE RESIDUAL SOIL FROM BRAZIL

Two intact samples and two reconstituted samples of the residual soil from Rio de Janeiro, Brazil were tested. Considering the plasticity of the material, the features of

these particular SWRCs were found using the filter paper technique for the four samples. The Atterberg limits for this material indicate that it is significantly more plastic than the Kaolin and with a much higher activity (0.62 compared with 0.45). The reconstituted samples were initially both dried. The first, R(A), was dried to a suction of just over about 30,000kPa, defining the PDC. It was then wetted up to define the PWC (Figure 6.14(a) and (d)). The data for the PDC are well conditioned, while the data for the PWC exhibit some scatter in terms of degree of saturation (Figure 6.14(a)), perhaps slightly more than the ±1% estimated in Table 5.2. However, as observed for previous samples the PWC is well defined in terms of volumetric water content, the PWC was continued to very low suction values (i.e. about 5kPa). The slope of the PWC is again quite shallow compared with the Kaolin curves and it is even shallower than the PWC for the UN-Bogotá clay. The resulting greater hysteresis is perhaps caused by the increased activity (0.62 compared with 0.51). It was then dried again to define the MDC. The MDC can be seen to fall below the PDC and drying was continued to a suction of about 30,000kPa without the MDC joining the PDC. The test was terminated at this point.

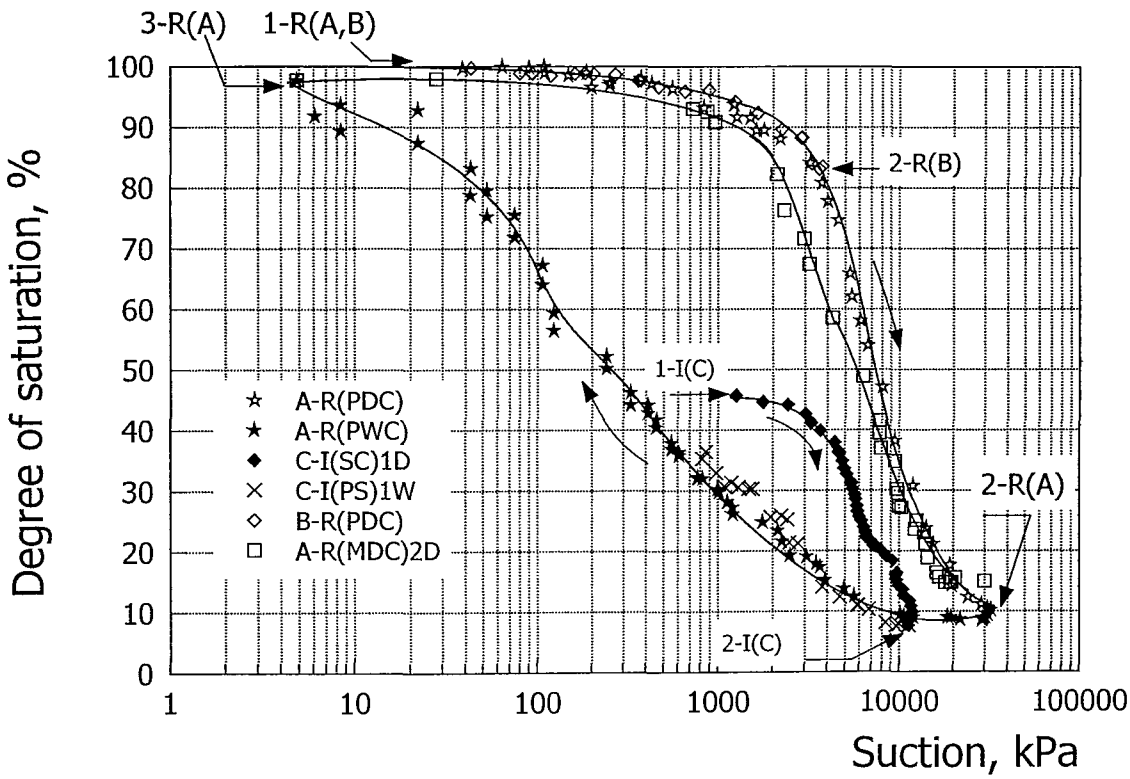

Figure 6.14(a) SWRC for the residual soil from Brazil for the reconstituted soil samples (A and B) and intact sample (C) in terms of suction versus degree of saturation.

After the initial drying, the second reconstituted sample, R(B), was wetted from a suction of almost 4,000kPa to form a PSC in wetting, which was continued to a low suction value by which time it had joined the PWC (defined by the first sample) as shown in Figure 6.14(b) and (f). Drying then recommenced, forming another PSC. It can be seen that there are large increments of suction for small changes in degree

of saturation or volumetric water content in the initial stages of drying, i.e. the line is almost horizontal (Figure 6.14(b) and (f) respectively). The data then rejoin the MDC defined by the first sample, particularly in terms of volumetric water content where the PDC, MDC and this PSC in drying are almost collinear. It appears that the PSC in terms of degree of saturation lies above the MDC (see Figure 6.14(e)). This again almost certainly results from the reduced accuracy of measurements of this quantity.

The first intact sample I(C) started at a low degree of saturation of about 46% with a suction of just over a 1,000kPa (see Figure 6.14(a) and (d)). It should be noted that this sample contained many micro-fissures and roots in its initial state. This value falls roughly midway between the PDC and PWC defined by the reconstituted samples. From here it was dried to a suction of just under 10,000kPa at which point the sample cracked in two pieces (along one of the original micro-cracks which had progressively opened). The curve up to this point had a form similar to that observed for other scanning curves and it was heading towards the MDC. The sample was re-trimmed and, perhaps as a consequence, from this time it did not increase significantly in suction despite the reducing degree of saturation and volumetric water content. The sample was then wetted up and essentially followed the PWC. The test was terminated at a suction of about 800kPa. It was necessarily to re-trim the sample on at least one occasion because of further cracking. This probably explains the slightly irregular form of the curve.

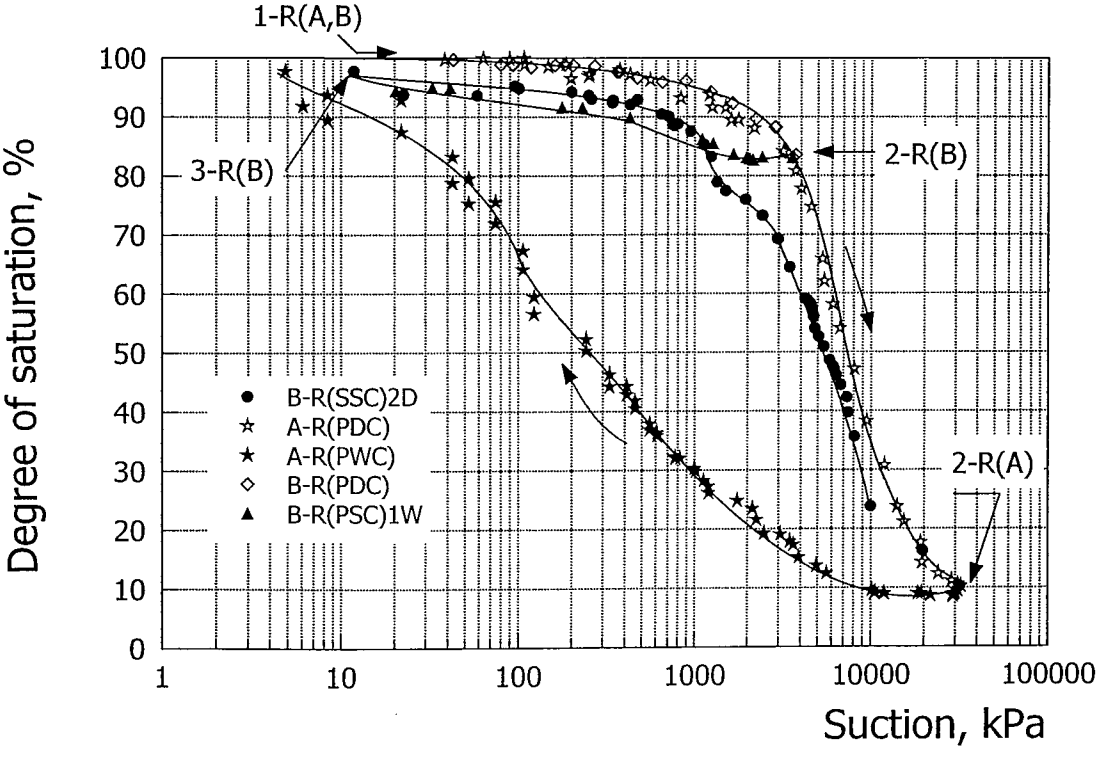

Figure 6.14(b) SWRC for the residual soil from Brazil for the reconstituted soil samples (A and B) in terms of suction versus degree of saturation

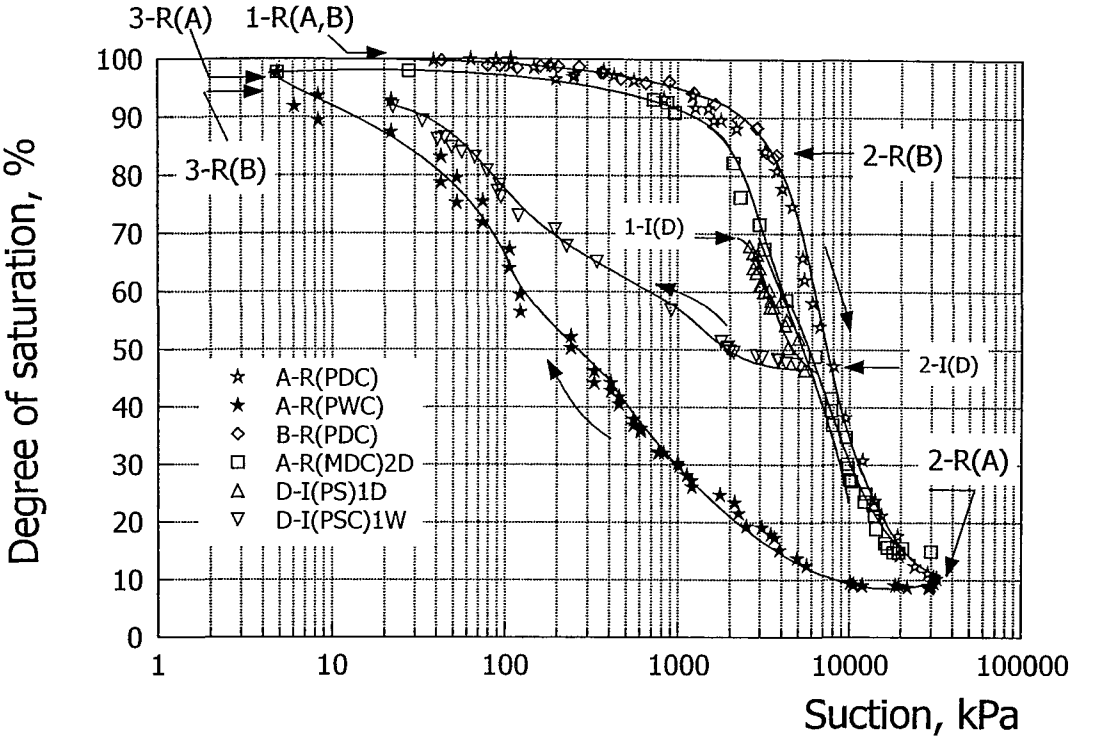

Figure 6.14(c) SWRC for the residual soil from Brazil for the reconstituted soil samples (A and B) and the intact sample (D) in terms of suction versus degree of saturation.

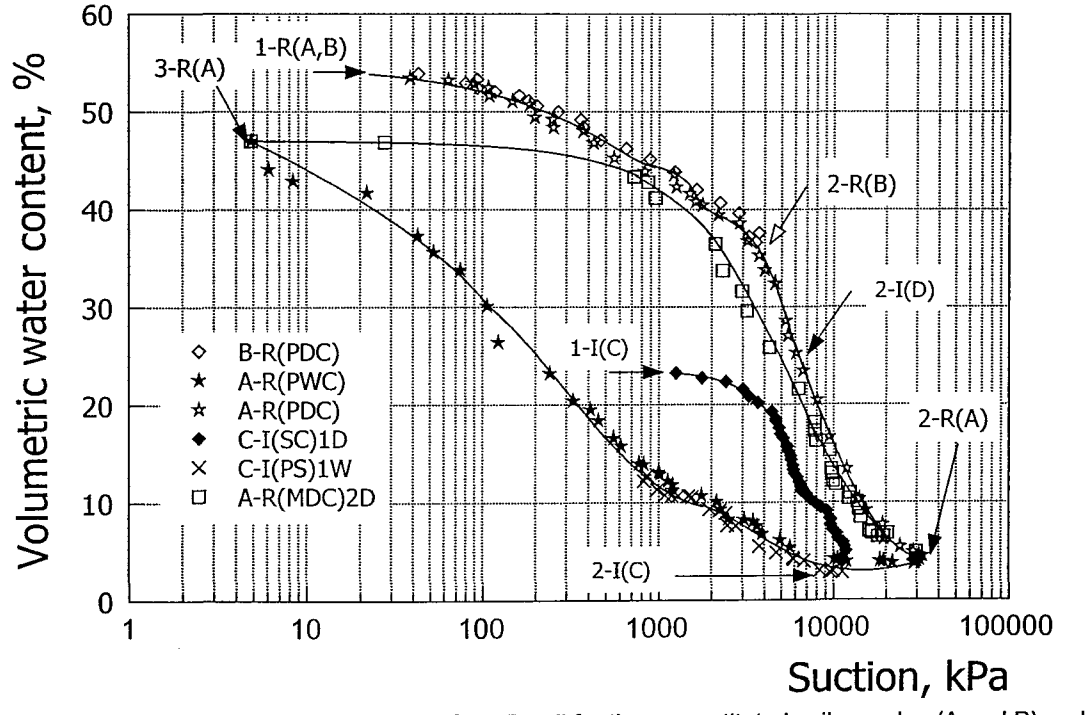

Figure 6.14(d) SWRC for the residual soil from Brazil for the reconstituted soil samples (A and B) and the intact sample (C) in terms of suction volumetric water content

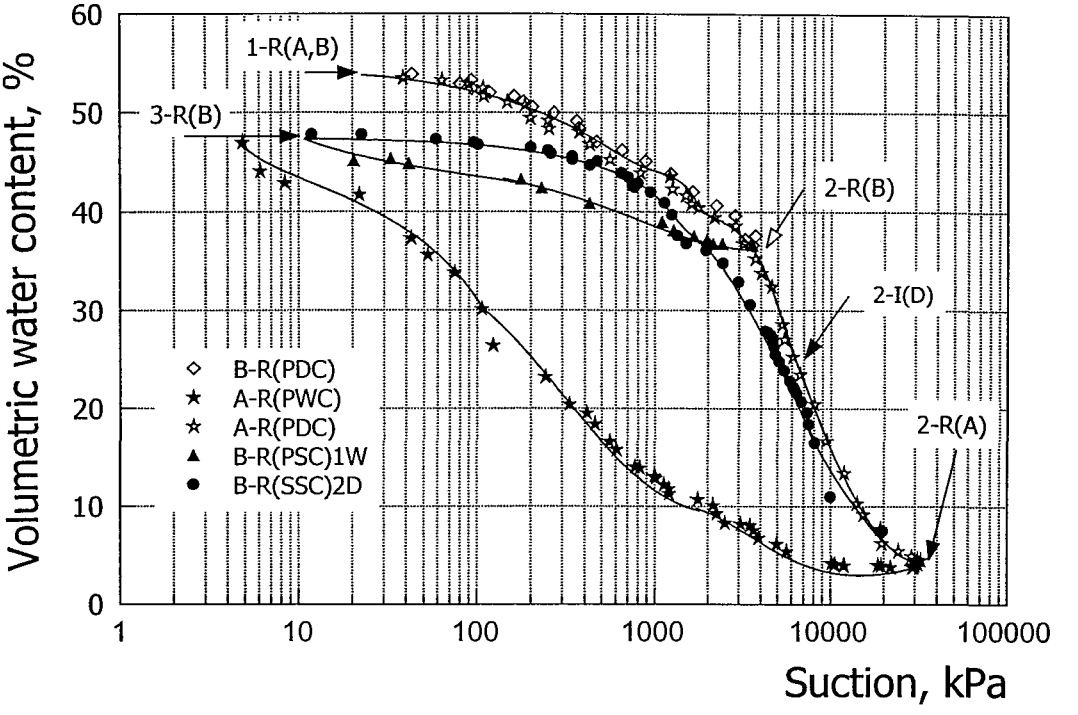

Figure 6.14(e) SWRC for the residual soil from Brazil for the reconstituted soil samples (A and B) in terms of suction volumetric water content

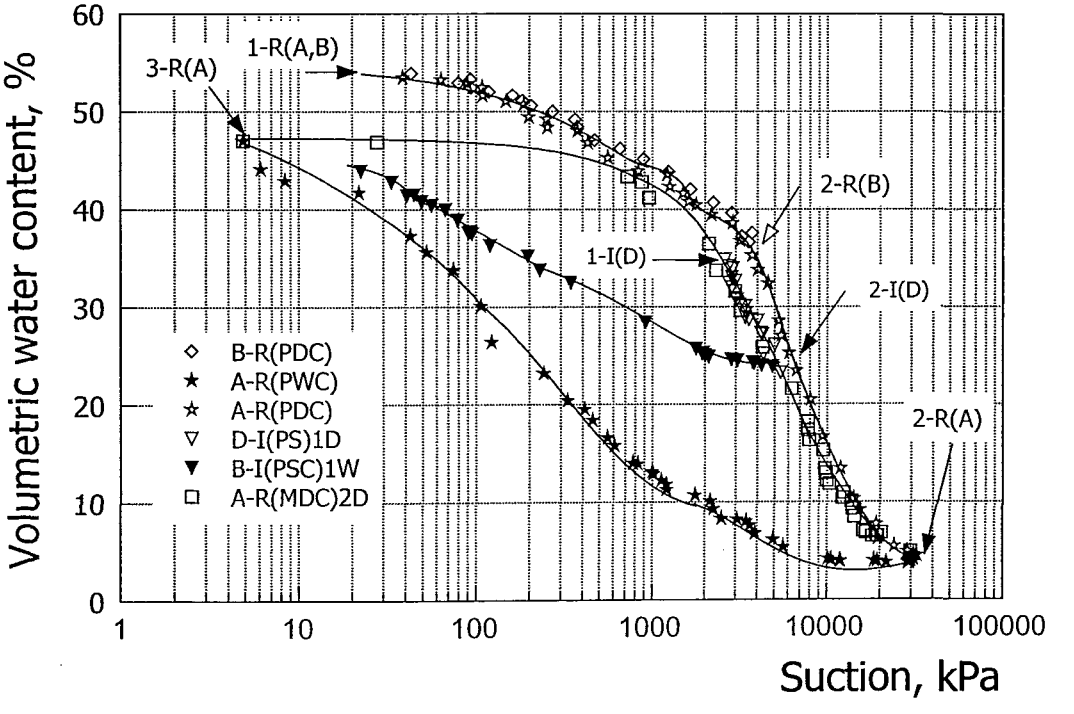

Figure 6.14(f) SWRC for the residual soil from Brazil for the reconstituted soil samples (A and B) and the intact sample (D) in terms of suction volumetric water content

A second intact sample I(D) had a higher degree of saturation, just under 70% and was also dried and followed the MDC (see Figure 6.14 (c) and (g)). It was then wetted from a suction of just over 5,000kPa to a value of about 20kPa, defining a

primary scanning curve. The form of this curve exhibits double curvature and the point of inflection and heads towards the PWC at low suction values (see Figure 6.14(g), in terms of volumetric water content).

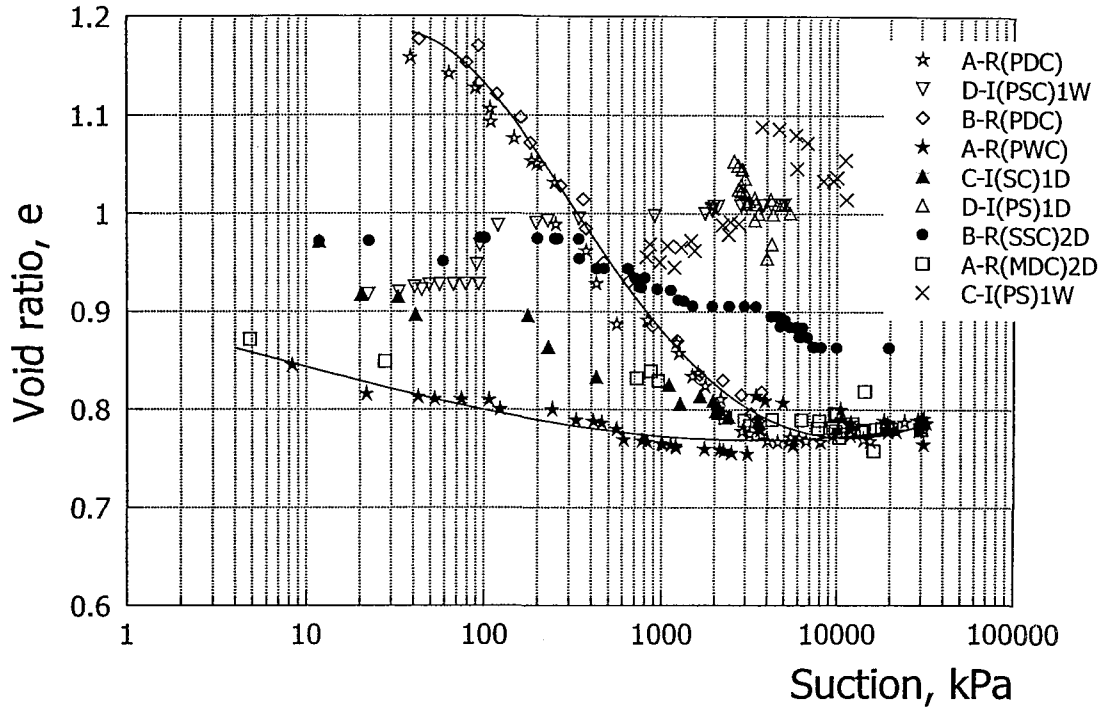

Figure 6.14(g) SWRC for the residual soil from Brazil for the reconstituted soil samples (A and B) and for the intact samples (C and D) in terms of suction void ratio

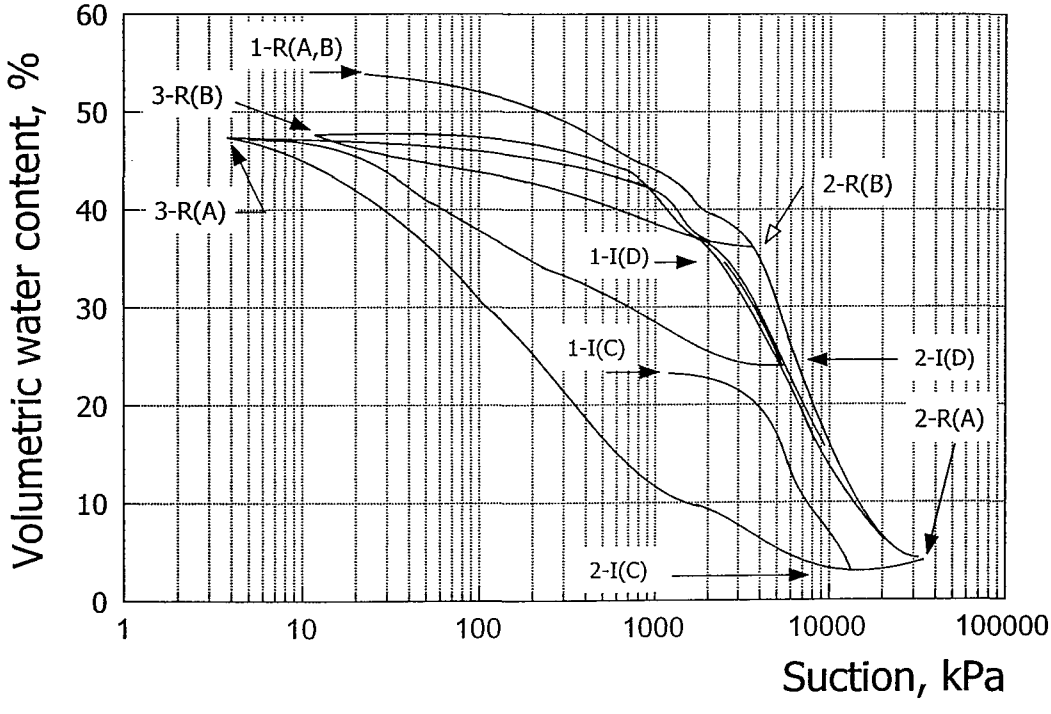

Figure 6.14(h) Schematic diagram showing approximate paths followed in generating the SWRC for the residual soil from Brazil samples

The data from the reconstituted samples in terms of void ratio are shown in Figure 6.14(g). They are well conditioned and show much greater changes in void ratio for drying than wetting as has been observed for other samples which follow a similar trend to the results from an oedometer test. The reason for the jump in data at a low suction range of the PWC is not clear.

In conclusion, the response of this residual soil from Brazil, which has similar values of void ratio but is more plastic in terms of Atterberg limits, is comparable to that of the UN-Bogotá clay except that it exhibits greater hysteresis probably because of its increased activity.

6.8 SWRC FOR THE RESIDUAL SOIL FROM COLOMBIA

This material has the highest Atterberg limits (in terms of liquid limit and plastic limit) and activity of all the samples tested. It is also evident that the material has a very high clay content from the particle size distribution curve (Figure 6.1) and from the very high initial void ratios shown in Figure 6.15(c). The SWRCs of the residual soil from Colombia were obtained using the filter paper technique for the reconstituted and for the intact soil samples. Two reconstituted and two intact samples were progressively dried. The PDC for the reconstituted samples (Figure 6.15(a)) is very shallow in terms of degree of saturation and at the limiting value of suction measurements (30,000kPa) its value was still above 50%. Because of the inability to measure higher suctions it was not possible to define most of the PDC. One of the reconstituted samples was wetted from this final suction value but this path only represents an effective wetting curve.

The intact samples were dried from degrees of saturation of about 75 and 85%. As drying proceeded, the resulting curves appear to join the limited extent of the PDC defined by the reconstituted samples, indicating that they reached the MDC.

Although it was not possible to define the full PDC, in view of the high activity and plasticity of the clay, it is expected that the terminal suction value would perhaps be well in excess of 100,000kPa and that greater hysteresis would be exhibited than was seen for the residual soil from Brazil.

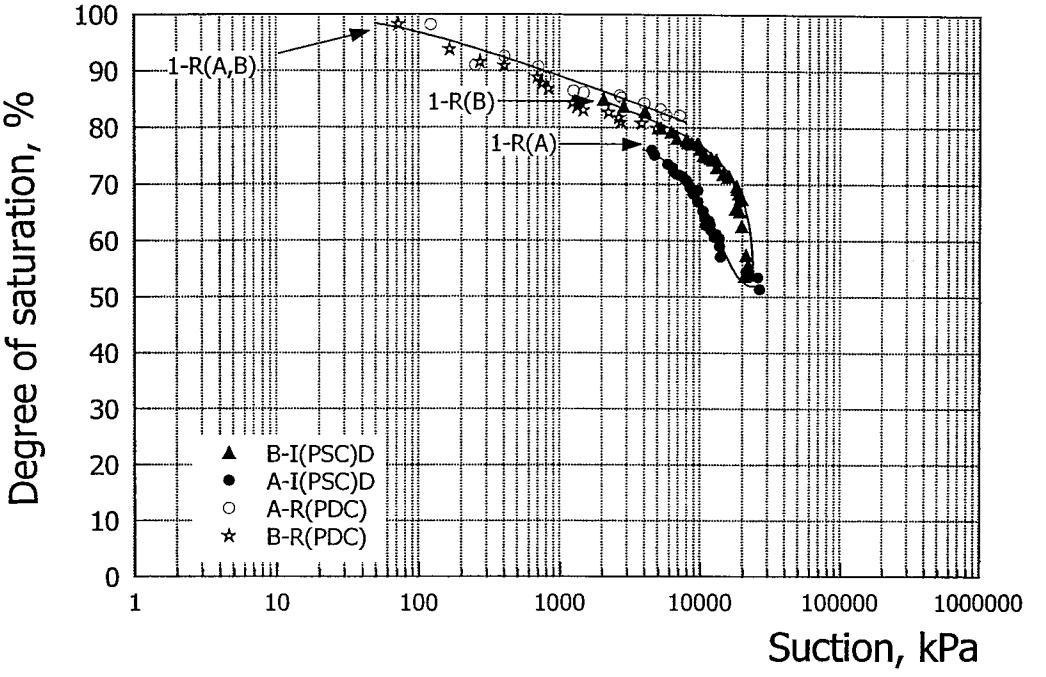

Figure 6.15(a) SWRC for the residual soil from Colombia in terms of suction versus degree of saturation

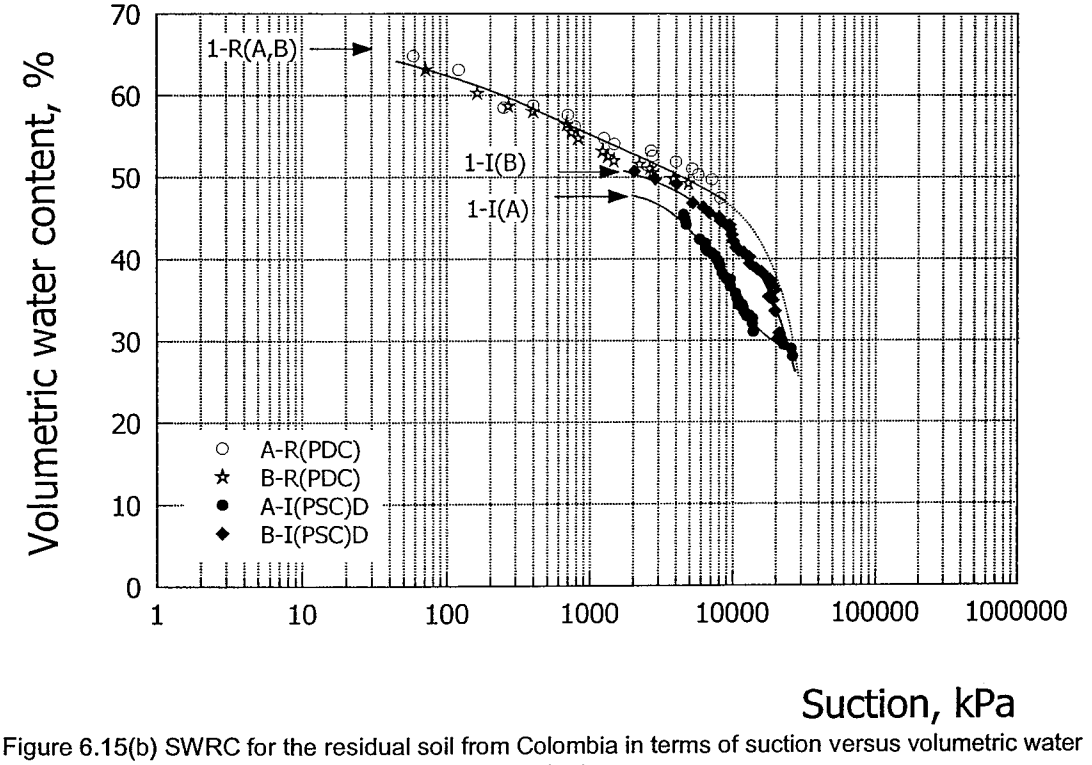

Figure 6.15(b) SWRC for the residual soil from Colombia in terms of suction versus volumetric water content

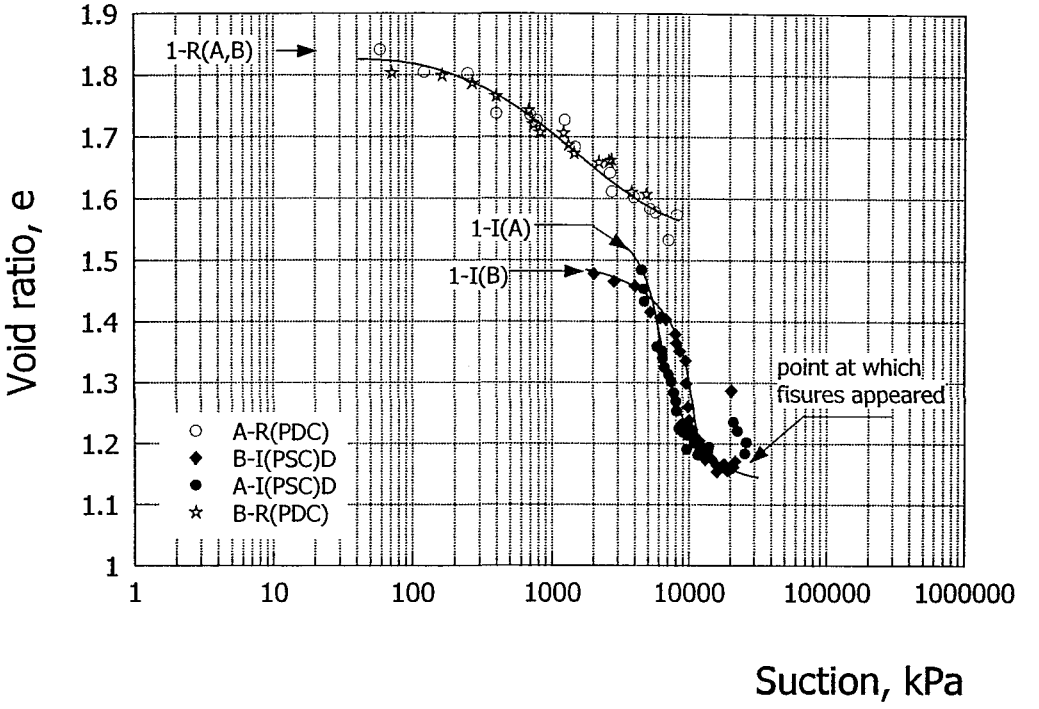

Figure 6.15(c) SWRC for the residual soil from Colombia in terms of suction versus void ratio

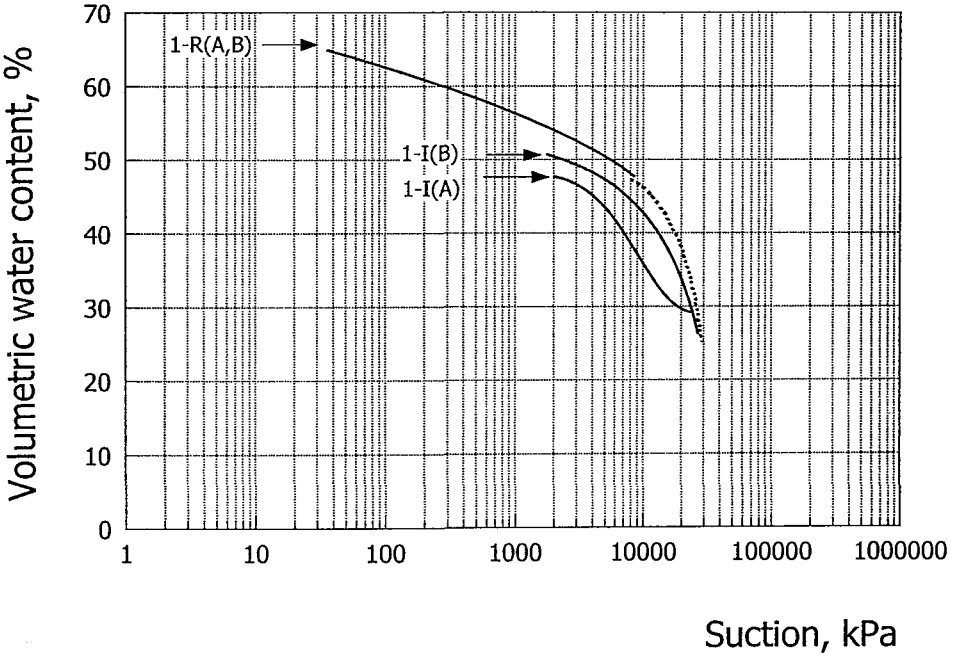

Figure 6.15(d) Schematic diagram showing approximate paths followed in generating the SWRC for the residual soil from Colombia samples

This material is essentially a silty sand (see Figure 6.1) with a very weak degree of bonding. As mentioned earlier the soil was very disturbed at the outset, probably as a consequence of its granular nature. It was therefore not possible to trim intact samples (it was difficult to form smooth surfaces and samples that were prepared disintegrated after a short time). Reconstituted samples were prepared but again because of the granular nature of the material it was not possible to achieve homogeneous samples. The data obtained from these samples are not presented because the trends in data were thought to not be representative of the true sample behaviour.

The most reliable data were obtained from compacted samples. Two specimens were prepared just wet of optimum, resulting in an initial degree of saturation of about 85%. The filter paper technique was used to obtain this particular SWRC, considering the smooth and clayey surface on each side of the compacted samples. The samples were progressively dried and are thought to follow either the PDC or MDC. There is remarkable consistency between the data from the two samples, which are shown in Figure 6.16. The curves appear to exhibit a bimodal distribution, the reason for this is not clear but it is possibly associated with the granular nature of the material. There is a negligible variation in void ratio with suction (see Figure 6.16(c)) again probably because of the soil's granular nature.

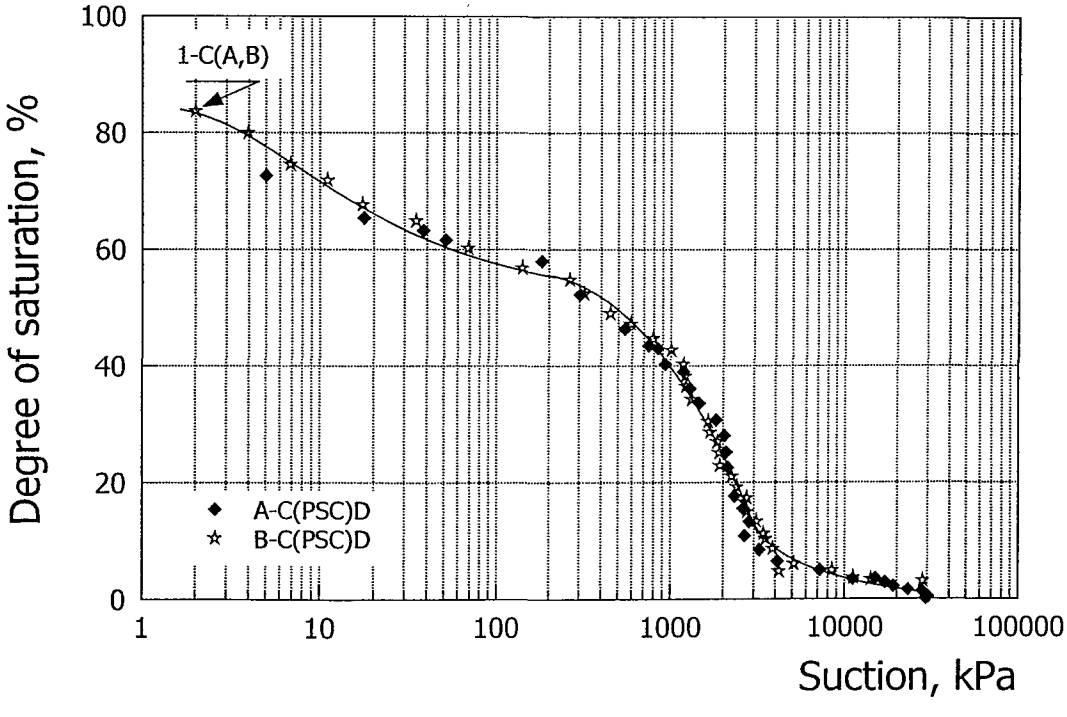

Figure 6.16(a) SWRC for the residual soil from Hong Kong in terms of suction versus degree of saturation

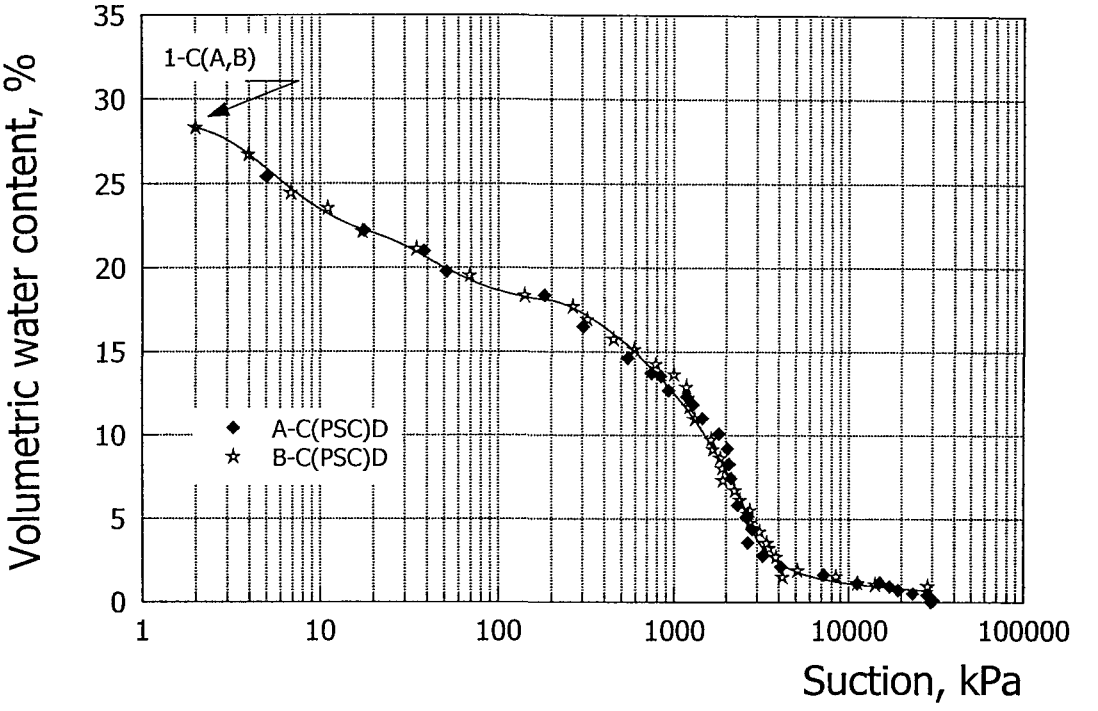

Figure 6.16(b) SWRC for the residual soil from Hong Kong in terms of suction versus volumetric water content

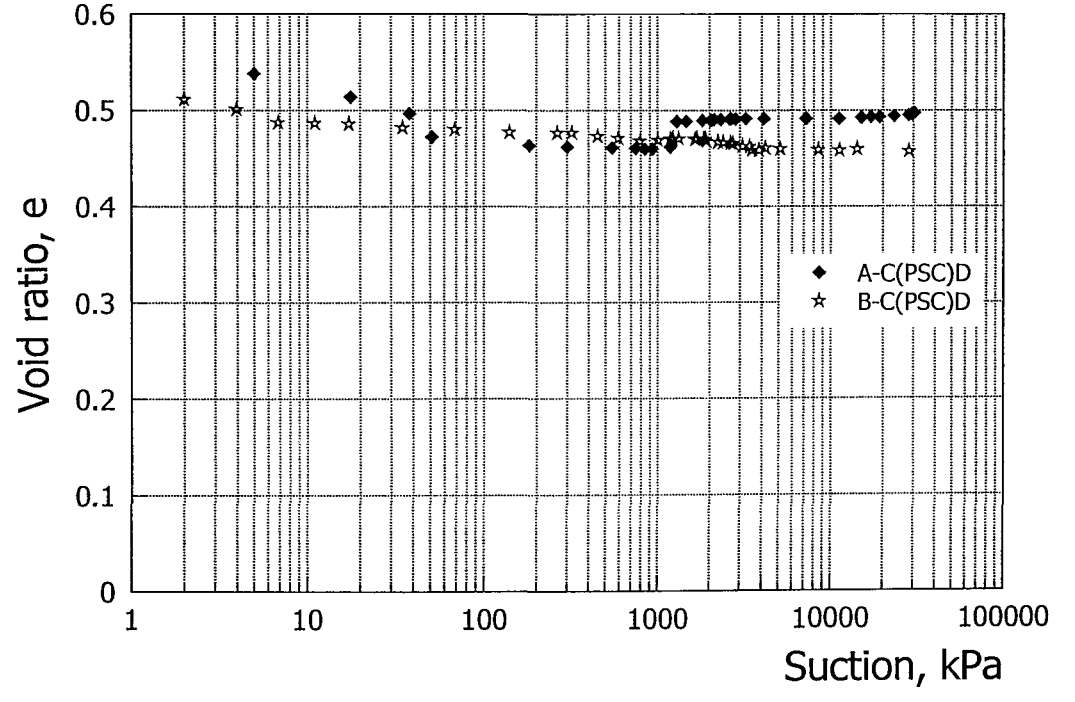

Figure 6.16(c) SWRC for the residual soil from Hong Kong in terms of suction versus void ratio

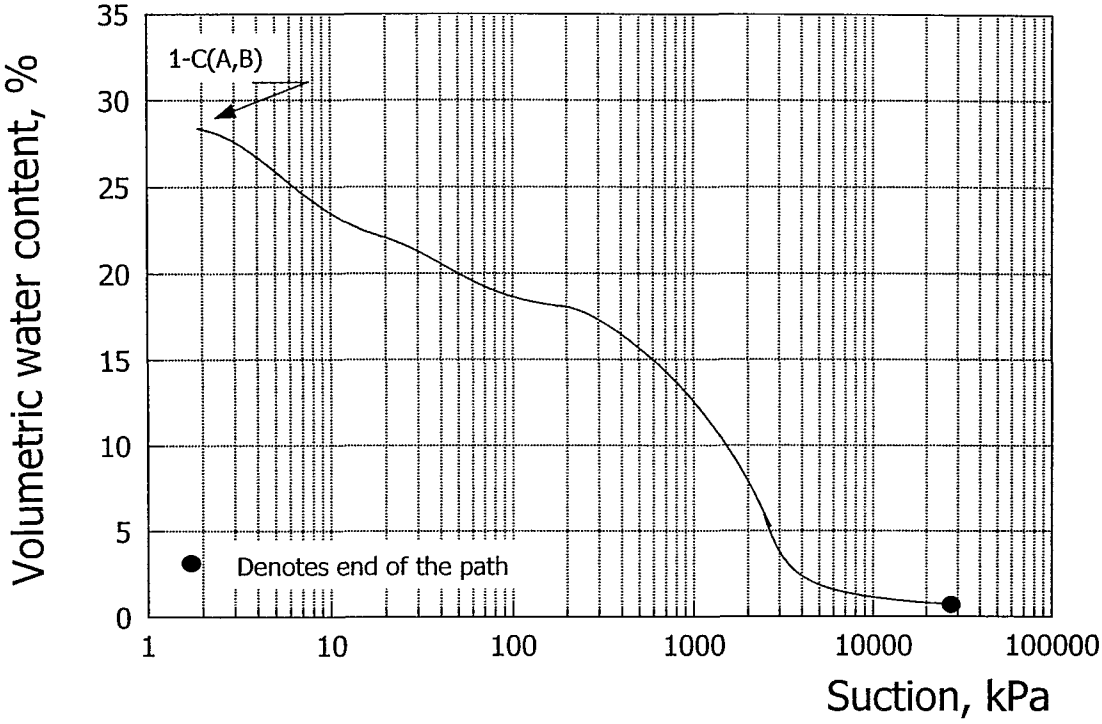

Figure 6.16(d) Schematic diagram showing approximate paths followed in generating the SWRC for the residual soil from Hong Kong samples

SWRC FOR EMBANKMENT CLAY 6.10

As mentioned earlier although the exact origin of this compacted clay is not known the soil has been characterized by the Atterberg limits and particle size distribution curve. Its Atterberg limits are very similar to those of the Weald Clay, it is likely that it is London Clay fill. Although it has higher clay content than the Weald Clay its activity is slightly lower (0.38 compared with 0.46). Two reconstituted samples were prepared from the compacted material supplied and two intact compacted samples were tested. All of the samples were dried from their initial state and tested using the filter paper technique for obtaining the characteristics of the SWRC. The reconstituted samples, formed from slurry, remained fully saturated to quite high suction values, of the order of 1,000kPa. The two samples produced very similar PDCs (see Figure 6.17) as was the case with the UN-Bogotá Clay. It was not possible to develop the full SWRC because the maximum suction that could be measured was reached at values of degree of saturation of about 35% and 40% for samples R(B) and R(A) respectively. From this point one of the samples (sample A) was wetted forming at effective wetting curve which was extended back to a suction of about 25kPa. It is interesting to note that although this material in many respects is similar to the Weald Clay it exhibits much greater hysteresis.

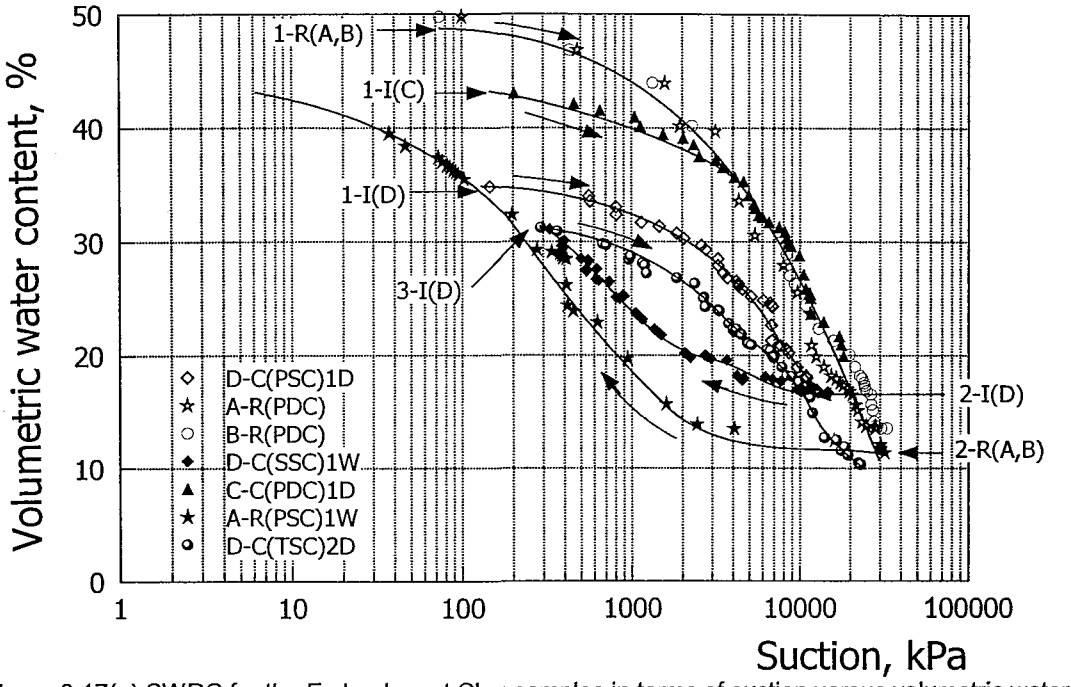

Figure 6.17(a) SWRC for the Embankment Clay samples in terms of suction versus volumetric water content

The two intact samples trimmed from the block sample were found to have quite different initial degrees of saturation with values of 88 and 74%. The sample with the higher degree of saturation soon converged to the PDC determined from the reconstituted sample. Drying was continued to a suction of about 20,000kPa. The second sample at the lower degree of saturation did not converge to the PDC, although there is a sharp downward change in gradient at about 7,000kPa. This curve almost certainly represents a primary scanning curve (it is also very likely that the path followed by the other compacted sample was also a PSC). From the end of drying the sample was wetted up, forming a secondary scanning curve (SSC). This curve almost converges onto the scanning curve generated from the reconstituted sample. It was then allowed to dry again. This curve is considered to be a tertiary scanning curve. Drying continued to a suction in excess of 20,000kPa and almost rejoined the end of the PDC formed from the reconstituted samples.

The void ratios of all four samples are remarkably similar (see Figure 6.17(c)) and again have similar initial values to those of the Weald Clay samples.

It can be noted that the scatter of data in the previous three samples (residual soils from Colombia and Hong Kong and the Embankment Clay) is generally within the estimated ranges determined in Chapter 5. Sometimes it is much smaller with the data are generally very well conditioned, allowing clearly behavioural trends to be identified.

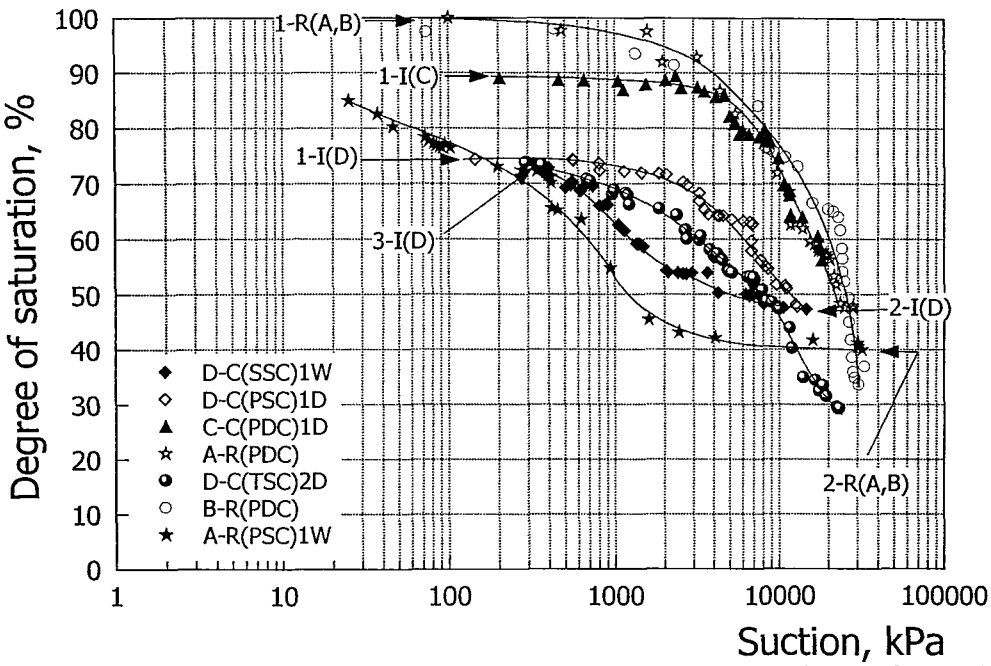

Figure 6.17(b) SWRC for the Embankment Clay in terms of suction versus degree of saturation

SWRC FOR ASH 6.11

The ash material was supplied as a disturbed bulk sample. As part of the sample preparation the material was carefully sieved and stored under water and allowed to hydrate for three months. In order to generate the SWRC for this material it was necessary to prepare individual samples for each different suction measurement. Care was taken to ensure that each of these individual samples was compatible, with similar values of initial void ratio and bulk unit weight. Because of the granular nature of this material the samples were tested using the pressure plate apparatus for the drying curve (recalling that the maximum suction that can be measured in this apparatus is 1,500kPa and the minimum is 0.1kPa) and the pressure membrane, which measures up to 10,000kPa. For wetting it was necessary to use the pressure membrane apparatus so that a much higher suction could be imposed (10,000kPa) to make sure that the terminal residual water content was reached and so wetting from this point would give data on the PWC. However, the accuracy of pressure control with the pressure membrane apparatus is much coarser than the pressure plate apparatus (being about 250kPa) and so it is not possible to determine suction accurately below about 1,000kPa. For this reason when wetting samples to lower suction values, it was necessary to transfer the ash sample from the pressure membrane apparatus to the pressure plate apparatus. Some disturbance of the sample would inevitably have occurred during this operation, evident from the slight scatter of the data shown in Figure 7.8. It was not possible to achieve accurate measurements below suctions of about 20kPa.

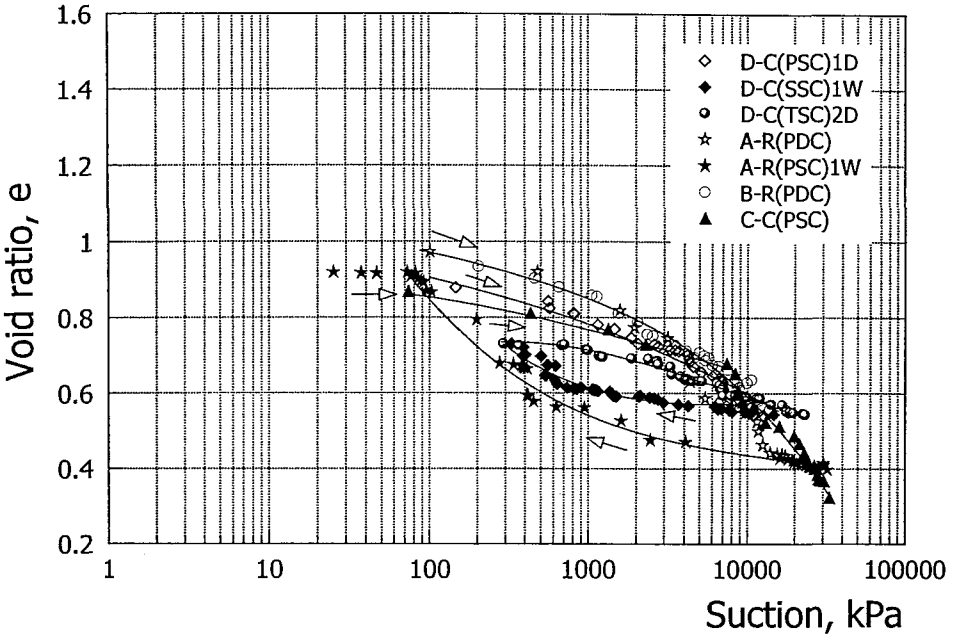

Figure 6.17(c) SWRC for the Embankment Clay in terms of suction versus void ratio

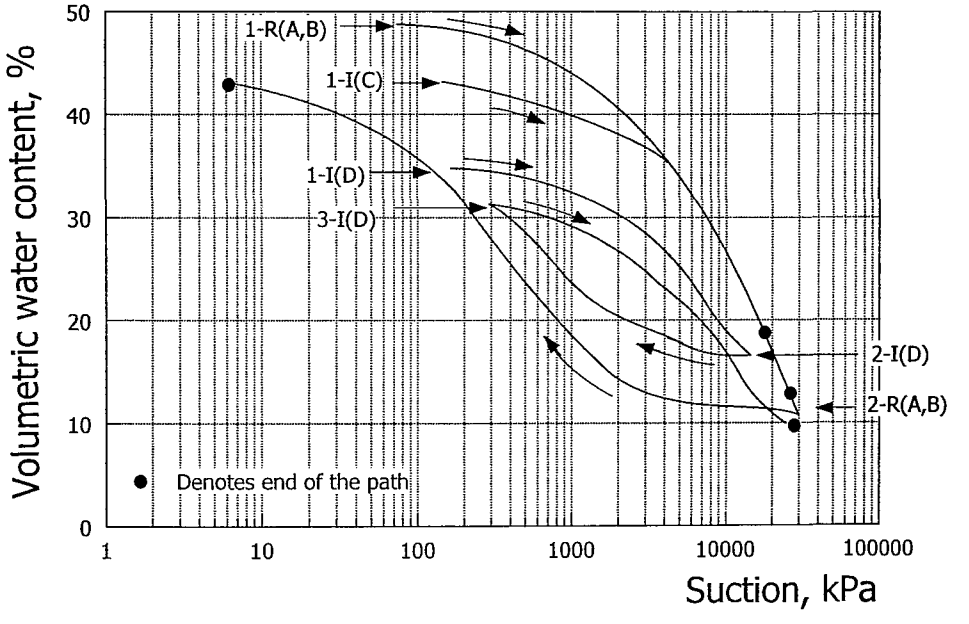

Figure 6.17(d) Schematic diagram showing approximate paths followed in generating the SWRC for the Embankment Clay samples

The principal drying curve generated for the Ash is shown in Figures 6.18. The data can be seen to be very well-conditioned for most of the curve which gives confidence in the method of sample preparation and suction measurement. Each point on the curve generally represents an average of three readings.

In order to generate the principal wetting curves each individual sample was initially dried until a suction of about 10,000kPa was reached. The sample was then wetted up by a predetermined amount to give approximately the value of suction required. The PWC thus generated, given this procedure, is remarkably well conditioned. The

points of the PWC are only slightly below those of the PDC, i.e. there is very little hysteresis. This corroborates the trend observed with the other samples that generally the hysteresis increases with increasing clay content and activity. It is worth noting, as has been observed before, that the hysteresis is more clearly evident in the plot of volumetric water content (Figure 6.18(b)) than that given in terms of degree of saturation, because of the increased accuracy in measuring the former quantity.

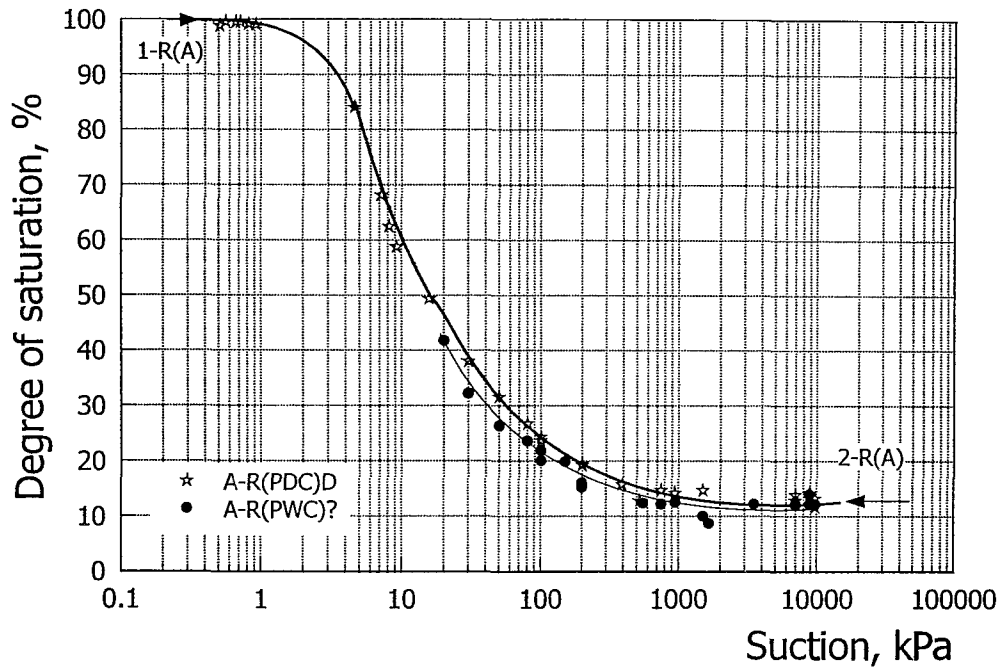

Figure 6.18(a) SWRC for the Ash material in terms of suction versus degree of saturation

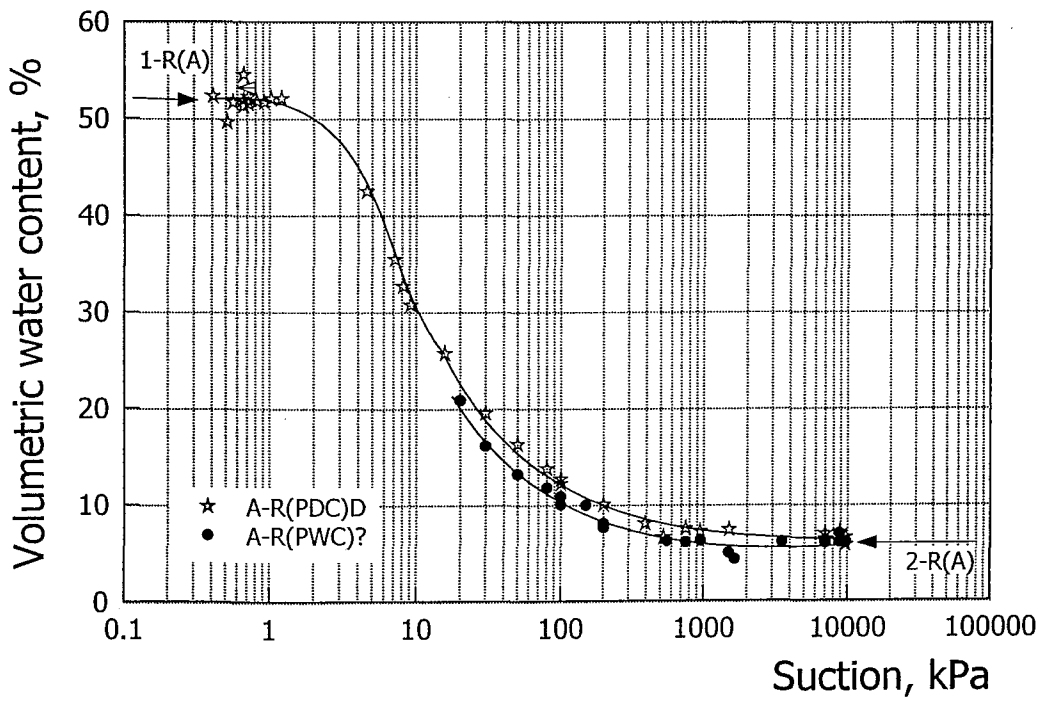

Figure 6.18(b) SWRC for the Ash material in terms of suction versus volumetric water content

The void ratios obtained for the Ash material are presented in Figure 6.18(c). It can be seen that the material exhibited almost no change in void ratio during the wetting process.

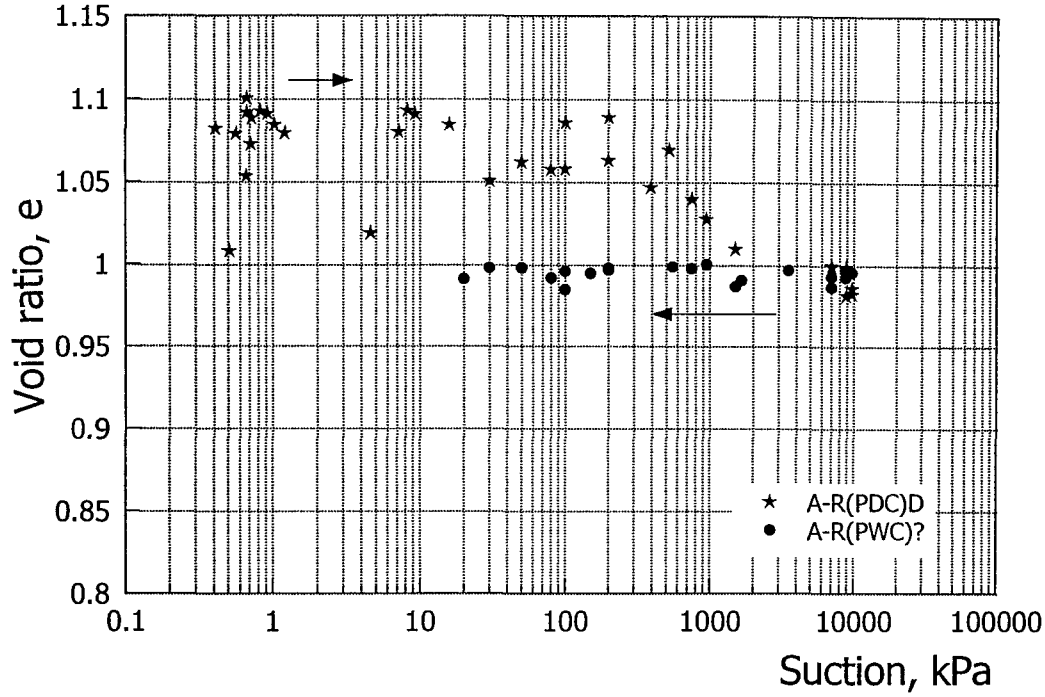

Figure 6.18(c) SWRC for the Ash material in terms of suction versus void ratio

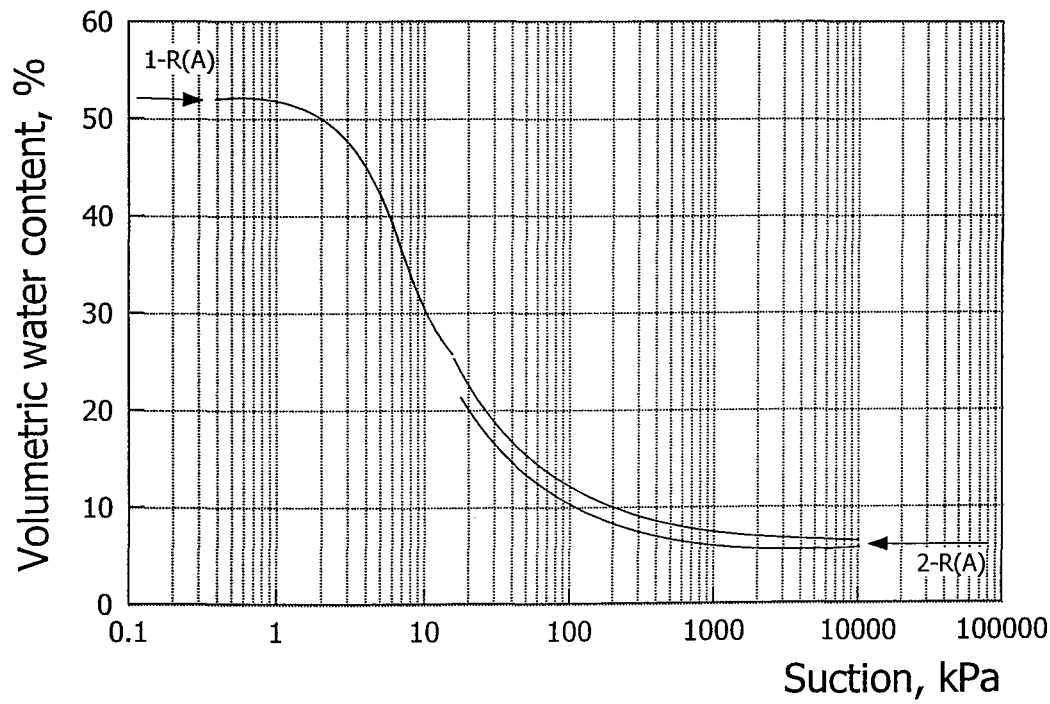

Figure 6.18(d) Schematic diagram showing approximate paths followed in generating the SWRC for the Ash material

SUMMARY OF THE GENERAL TRENDS IN BEHAVIOUR OF THE SWRC 6.12

A number of features have been observed in describing the behaviour of the SWRCs of these various soil types. It has been observed that:

1. The slope of the PDC increases with increasing clay content and activity.
2. The degree of hysteresis also increases with increasing clay content and activity.
3. For the granular ash material there was essentially no hysteresis.
4. Generally samples with high clay content have greater initial void ratios.
5. As would be expected the starting point of the intact samples always lies between the PDC and the PWC and their subsequent paths are represented by scanning curves which do not cross these boundaries.
6. The PWC and MWC are generally coincident.
7. In cases where the clay content is very high (UN-Bogotá clay and Embankment Clay fill) it was not possible to develop the full SWRC because of the limitation of the filter paper technique (i.e. 30,000kPa).

Two additional comments relating to the data are as follows.

8. It is important to remark that it is not possible to compare the data obtained using the different methods for measuring suction (i.e. filter paper technique and axis translation technique) because these methods were used to measure different ranges of suction or because the characteristics of the soils tested made it impossible to use both techniques on the same soil.
9. The scatter of the experimental data was generally within the error ranges estimated in Chapter 5 (Table 5.2). Often it was much better than estimated, especially in terms of suction.

In the next chapter the data are analyzed in more detail and some of the models described in Appendix 2 are applied, to test their ability for describing the various components of the SWRC (i.e. PDC, PWC, MDC, MWC and various PSC in drying and wetting processes).

Additionally the influence of the SWRC is illustrated by means of numerical analyses that were performed using the Finite Element method (following the description given in Chapter 3 with a simplistic model for the SWRC).

CHAPTER 7

VALIDATION AND IMPLEMENTATION OF RETENTION CURVE MODELS FOR NUMERICAL ANALYSIS

In the previous chapter the data representing the SWRCs were presented. The next stage of the research was to investigate the effectiveness of some of the models proposed for representing the SWRC by comparing the curves generated with the experimental data.

As described in Chapter 2 the van Genuchten equation is used to obtain parameters that describe the general form of the various components of the SWRC (i.e. it can model the PDC, PWC or scanning curves). These parameters can then be input into the hysteretic models, which also require values representing the volumetric water content at specific points of the SWRC. This exercise was performed for five of the eight soil types investigated to see how well the formulations fit the data.

Following from this the variation of the basic parameters α, n and m with soil characteristics such as the Atterberg limits and activity is investigated. The intention is to see whether it is possible to recommend the basic parameters for a soil in order to generate its SWRC without having to embark on a lengthy experimental programme.

Having investigated and to some degree validated the models, the implementation of such a model in a numerical analysis is described in Chapter 8 using a case study based on the work of Rodriguez, 1998. This illustrates the need to incorporate the SWRC and in particular the hysteretic response of the soil when modelling soil behaviour.

IMPLEMENTING THE VAN GENUCHTEN EQUATION 7.1

Van Genuchten's equation is as follows:

$$\theta = \theta_f + \frac{\theta_s - \theta_f}{\left(1 + \left(\frac{\psi}{\alpha}\right)^n\right)^m} \quad (7.1)$$

In Chapter 2 it was explained that the value of the α parameter translates the SWRC left or right (see Figure 2.15), increasing α moves the curve to a higher suction

range. The n parameter controls the slope of the SWRC (see Figure 2.16) with the slope becoming steeper as n increases. The m parameter varies with α and n. It can be observed that small values of m result in a moderate slope in the high suction range while large values of m produce a sharp corner at the AEV.

The approach taken when modelling the data representing a certain path of the SWRC, e.g. the PDC, is now described. Initially, by examining the data, estimates are made of the saturated and terminal residual values of volumetric water content. This can be done with reasonable confidence by looking at the form of the curve being modelled. The remaining unknowns are the α, n and m parameters. As a first estimate an optimum selection of these parameters was achieved using a least squares formulation. For any selection of α, n and m values the residuals for each data point can be determined and summed, this value provides a measure of the correctness of the curve fit. The smaller the value, the better the fit. This process was carried out using an Excel spreadsheet solver which performed the operation. The shape of the resulting curve generated was then compared with the data. Because in many cases there are different concentrations of data points for specific ranges of the curve, the combination of values determined for the minimum sum of the residuals might not necessarily provide the best-fit curve. The reasons for the different concentrations are discussed in Chapter 5, for example where a certain part of the curve was changing rapidly and wetting was performed in very small steps. It was therefore often found that it was necessary to then vary the parameters manually. This was done, bearing in mind the influence that each parameter has on the shape and position of the curve, until a best fit was achieved.

This procedure was performed for the data representing the PDC and PWC (or the MWC in cases where it was not possible to reach the terminal residual volumetric water content), which was obtained from the reconstituted samples formed from slurry. Therefore two sets of α, n and m parameters are obtained from the curve fitting, one for drying and one for wetting. In some instances it was not possible to generate the experimental data for the PDC and/or the PWC. However, it has often been observed that the main drying or wetting curves and also primary scanning curves join the PDC or PWC after some degree of drying or wetting. The curve fitting was therefore adjusted in such a way that the PDC or PWC generated from the van Genuchten equation passed through these specific regions of the experimental data. This operation is best explained by example and will be discussed where appropriate in the following sections where the data and best fit curves for the different soil types are presented.

Once the best van Genuchten curve had been selected for the drying stage, the AEV and the initial residual volumetric water content were determined using the

procedures described in Section 2.2 of Chapter 2 (see Figure 2.6). At the same time the desaturation point suction values were selected based on the basic data presented in Chapter 6 in terms of degree of saturation versus suction plots.

These values, along with the two sets of α, n and m values are summarised in Table 7.1 for each of the samples.

Kaolin. The PDC and PWC experimental data were obtained from sample kA. These are presented in Figure 7.1 along with the best fit van Genuchten curve. It can be seen that the *drying* curve fits all the experimental data reasonably well except for a couple of localised regions towards the upper and lower ends of the steeply sloping part of the curve. The equation does not produce such a good fit for the wetting data. The fit is good for the high suction values but from about the position of the inflection point of the curve there are significant deviations, with the curve under-estimating the volumetric water contents initially and then over-estimating them at low suctions (i.e. below about $200kPa$).

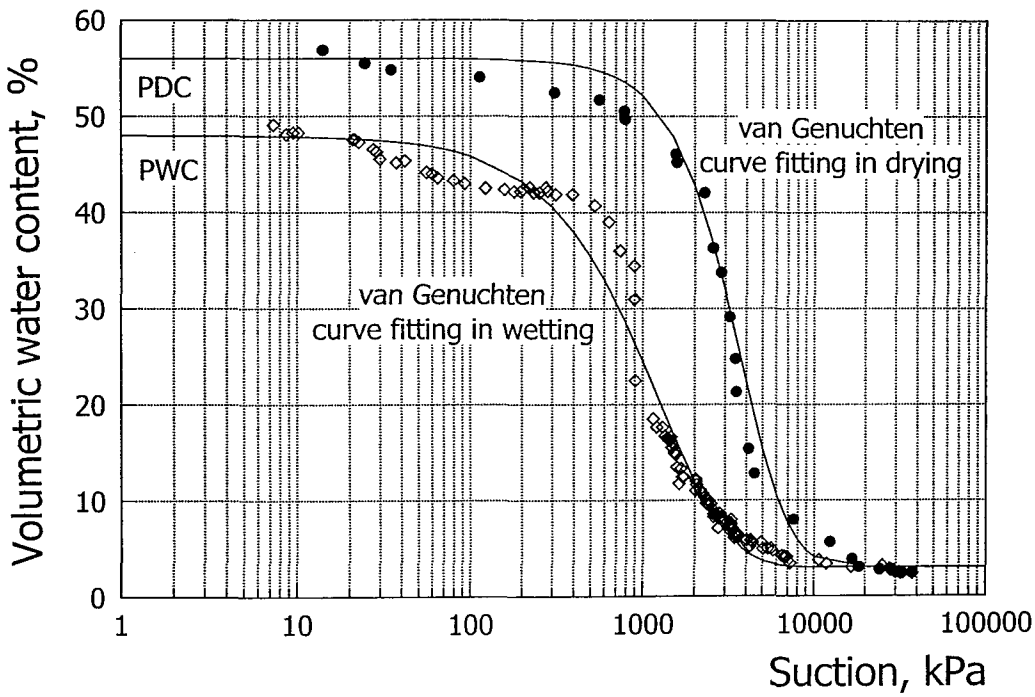

Figure 7.1 van Genuchten curve-fitting for sample kA data

Weald Clay. It can be seen from Figure 7.2 that both the drying and wetting experimental data are very well modelled by the van Genuchten equation over the entire suction range.

UN-Bogotá Clay. Once again the experimental data from the reconstituted samples are very well matched by the equation in both drying and wetting except for a small

region of the drying curve at suctions above about $10{,}000kPa$ where the experimental data form a slightly steeper curve (see Figure 7.3).

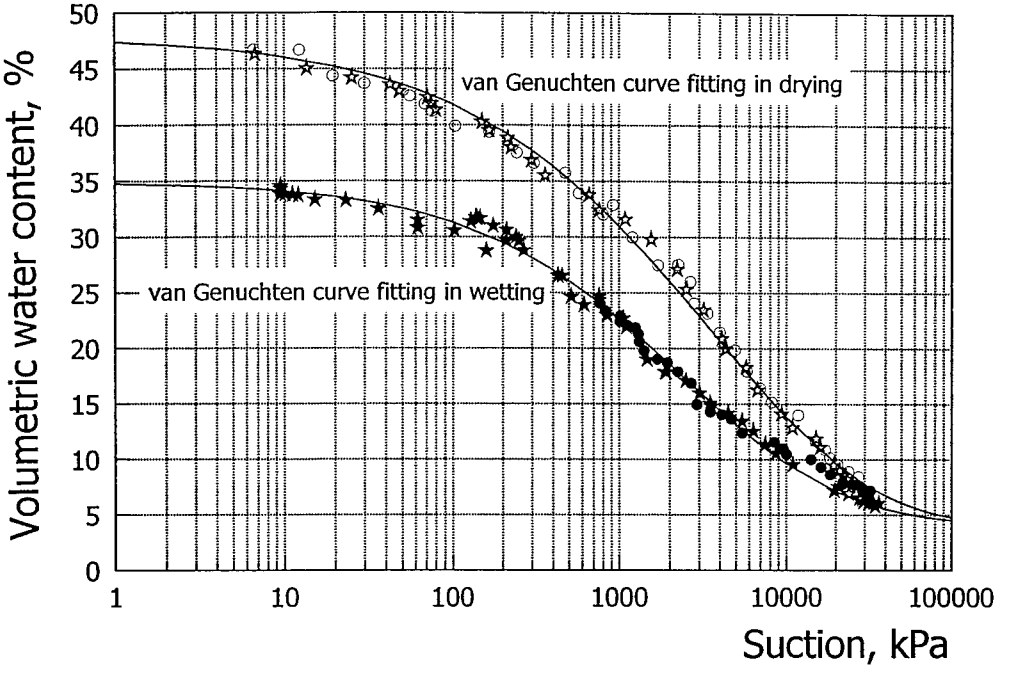

Figure 7.2 van Genuchten curve-fitting for the Weald Clay data

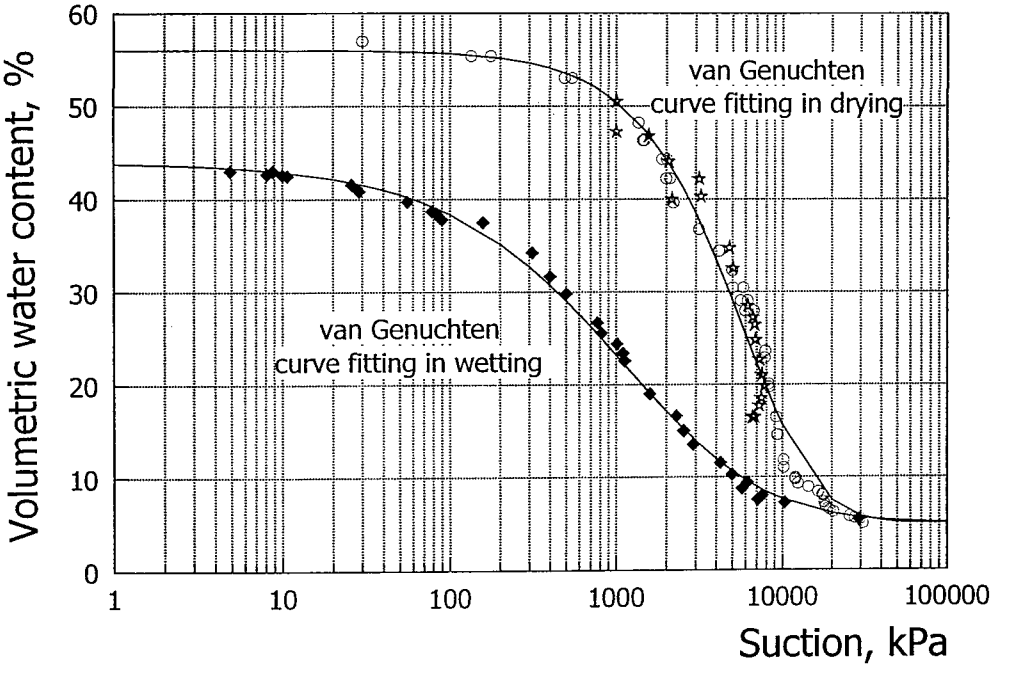

Figure 7.3 van Genuchten curve-fitting for the UN-Bogotá Clay data

Residual soil from Brazil. The data from the two reconstituted samples are well represented by the equation in both drying and wetting paths (note that one sample was dried for only part of the PDC, see Figure 7.4).

Residual soil from Colombia. Only a limited amount of the PDC is represented by the experimental data available for this material as the limit of the filter paper

technique was reached at a moderately high volumetric water content (e.g. about 30%). It was therefore difficult to estimate a value of the final volumetric water content. A value of θ_f of 5%) was chosen (see Figure 7.5). The equation fits most of the limited range of the experimental data from the drying of the reconstituted samples well (the data from both samples are reasonably consistent).

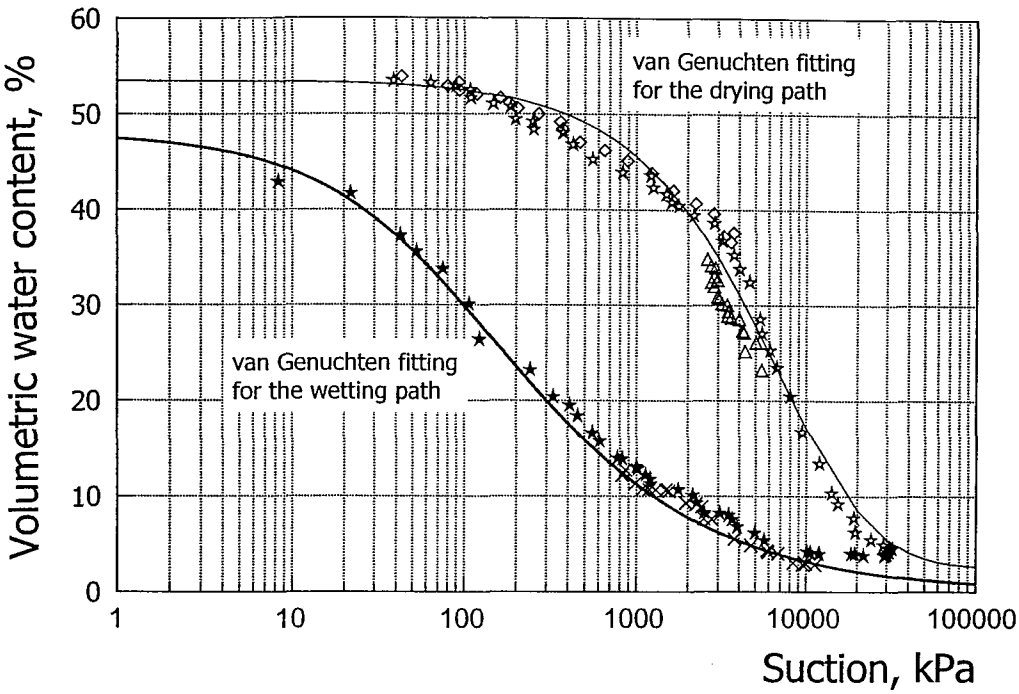

Figure 7.4 van Genuchten curve-fitting for the residual soil from Brazil data

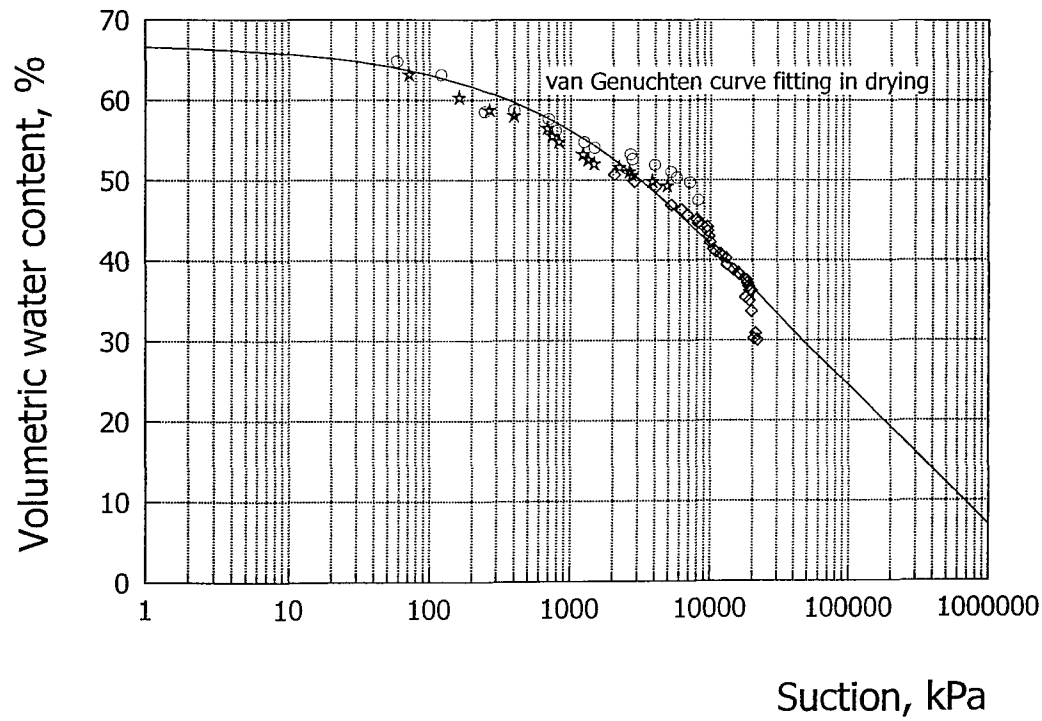

Figure 7.5 van Genuchten curve-fitting for the residual soil from Colombia data

Residual soil from Hong Kong. As explained in Chapter 6, the drying data from two samples compacted just wet of optimum exhibited a bimodal SWRC. This bimodal form has been modelled with the van Genuchten equation by considering the two parts of the SWRC individually with two curves joined by a common point (at volumetric water content of 18%) allowing them to be spliced together. The resulting curve is shown in Figure 7.6 which can be seen to fit the data very well (i.e. demonstrating that the van Genuchten equation can also be used effectively to model bimodal SWRCs). As experimental data are only available for drying and as this was carried out on compacted samples, the resulting curves are not PDCs but probably scanning curves. The two sets of values of α, n and m for the Hong Kong data are given in Table 7.2 but are not discussed further as this is special case (i.e. comparisons are not made with soil characteristics such as plasticity index).

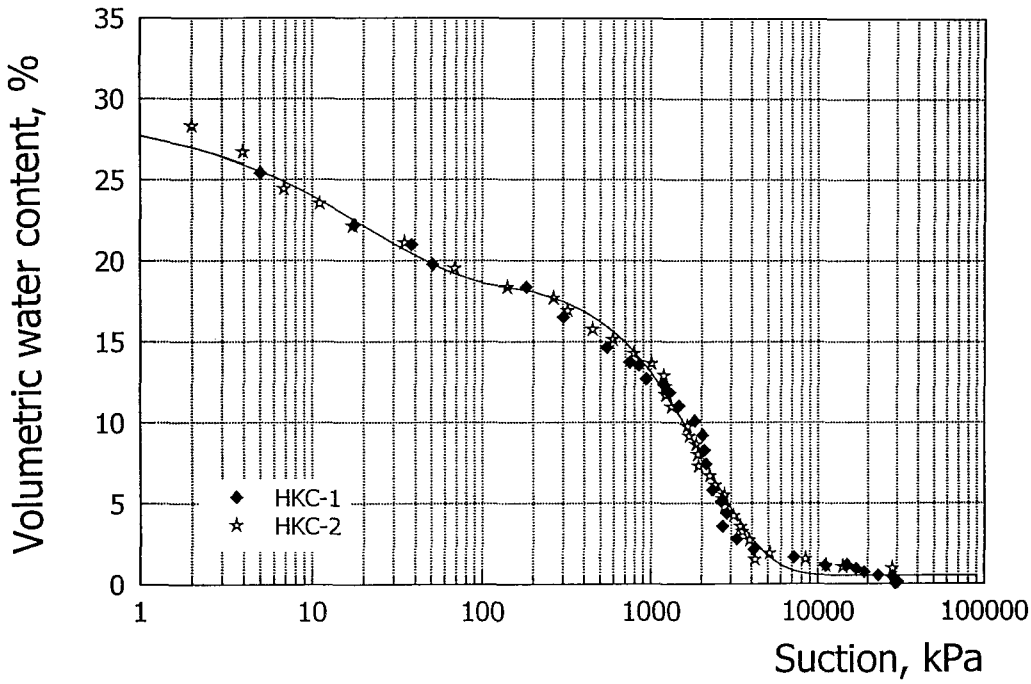

Figure 7.6 van Genuchten curve-fitting for the residual soil from Hong Kong data

Embankment Clay. The two reconstituted samples were dried to form the PDC and follow very similar paths. As for the case with the residual soil from Colombia it was not possible to define the entire PDC, although in this case a much lower volumetric water content was reached at the limiting suction value (e.g. about 10 to 15%). Again it was necessary to estimate a terminal residual volumetric water content and the value of 4% was chosen. With this terminal residual value the curve produced by the equation fits the experimental drying data well (see Figure 7.7). The PWC generated also fits most of the data very well, except those data generated during the initial stages of wetting (these data are not shown on Figure 7.7 for clarity, but can be seen in Figure 6.17(b)). This is realistic as the initial part of the wetting curve constitutes a primary scanning curve in wetting which then joins the PWC. Also included in Figure 7.7 are part of the data from one of the trimmed compacted

samples during the later stages of drying (solid triangle symbols). The data presented are those that have converged towards the PDC and joined it. These are also well represented by the curve given by the same equation (again all the raw data can be found in Figure 6.17(b)).

Table 7.1 Summary of parameters for characterising the SWRC

Parameter / material	Kaolin	Weald Clay	UN-Bogotá Clay	Residual soil from Brazil	Residual soil from Colombia	Embank-ment Clay	Ash
α_d (kPa)	7,092	111,111	18,868	35,336	31,341	70,922	3.5
n_d	1.966	0.462	1.214	0.922	0.499	0.725	2.647
m_d	3.575	4.475	4.126	4.581	1.208	3.565	0.220
α_w (kPa)	9,259	10,218	14,208	95	----	6,357	5
n_w	1.191	0.659	0.664	0.884	----	0.581	1.563
m_w	10.822	2.377	4.856	0.661	----	3.191	0.515
θ_s	0.56	0.49	0.56	0.54	0.67	0.50	0.52
θ_a	0.48	0.35	0.45	0.48	0.4*	0.45	0.50
θ_f	0.03	0.01	0.05	0.02	0.07	0.04	0.06
θ_r	0.08	Lower than 0.1	0.14	0.03	----	---	0.12
ψ_r (suction at θ_r (kPa)	6,000	Higher than 10,000	12,000	18,000	----	---	55
ψ_{AEV} (kPa)	2,000	1,000	4,000	2,200	10,000	3,000	2.5
Desaturation point (kPa)	30	10	200	110	100	250	1.0

*assumed

Ash. The experimental data, from the drying and wetting of the Ash material, exhibit only very small hysteresis. Nonetheless the van Genuchten equation has been applied to both the drying and wetting experimental data rather than taking an average (see Figure 7.8). The data are well conditioned and the curves fit them well. Note that it was not possible to obtain wetting data at suctions less than $20kPa$ for the reasons explained in Section 6.11.

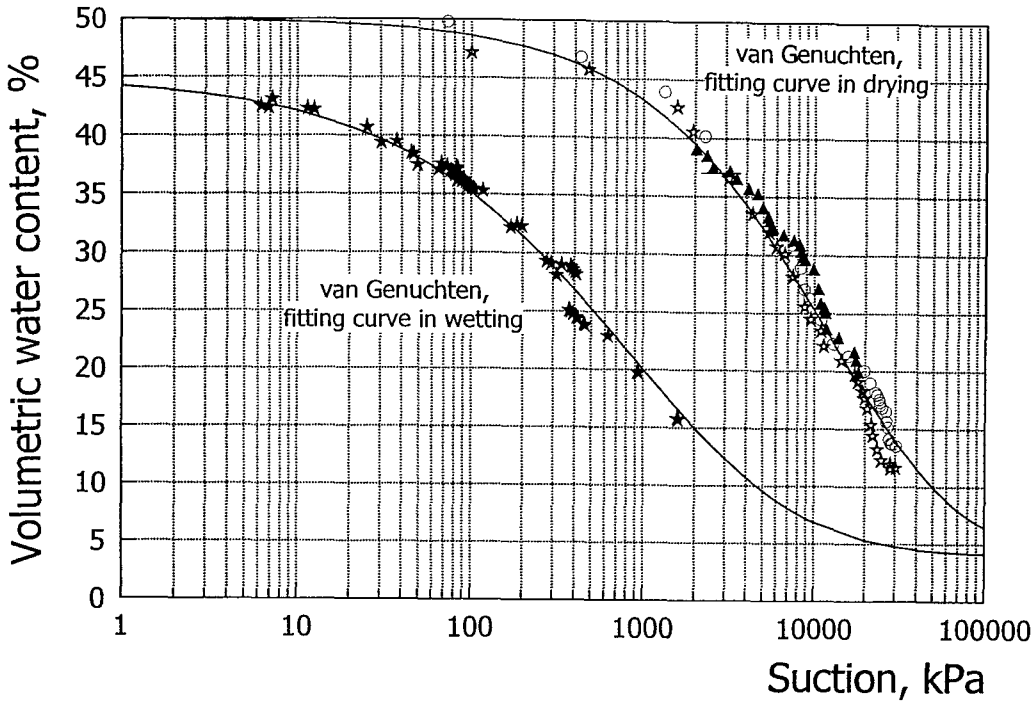

Figure 7.7 van Genuchten curve-fitting for the Embankment Clay data

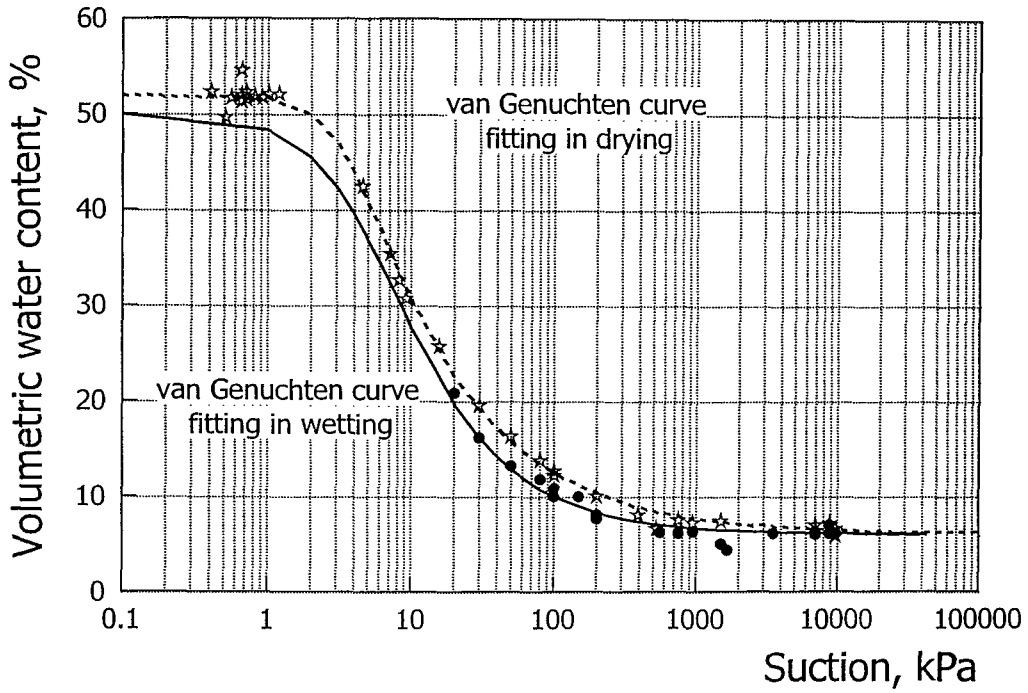

Figure 7.8 van Genuchten curve-fitting for the Ash material data

Table 7.2 Summary of parameters for characterising the bi-modal SWRC of the residual soil from Hong Kong

Parameter	α_d (kPa)	n_d	m_d	θ_s	θ_f
Initial part	850	0.701	13.958	0.29	0.18
Final part	16,945	1.265	14.021	0.18	0.01

The equations that express Luckner's model are as follows

$$\Theta = \frac{(\theta - A)}{(\phi - A - B)} = \left[\frac{1}{1+\left(\frac{\alpha}{\psi}\right)^{n}}\right]^{m} \quad \text{for drying and wetting} \qquad (7.2)$$

$$A_w = \frac{\phi - \theta_{ar} - \theta_{wo}\left[1+\left(\frac{\alpha_w}{\psi_o}\right)^{n_w}\right]^{m_w}}{\left\{1-\left[1+\left(\frac{\alpha_w}{\psi_0}\right)^{n_w}\right]^{m_w}\right\}} \quad , B_d = \phi - \theta_f - (\theta_{w,0} - \theta_f)\left[1+\left(\frac{\alpha_d}{\psi_0}\right)^{n_d}\right]^{m_d} \qquad (7.3)$$

	MDC	PDC	MWC	PWC	SDC	SWC
A	θ_f	θ_f	θ_f	0	θ_f	A_w
B	θ_{ar}	0	θ_{ar}	θ_{ar}	B_d	θ_{ar}

where:

Θ normalized volumetric water content

A, B dimensionless scaling factors (defined in the above table for the different type of curves and Appendix A2.5)

θ_f terminal residual volumetric water content for the wetting fluid (water)

θ_{ar} initial residual volumetric water content for the non-wetting fluid (air) α, n, m constants affecting the shape of the SWRC

ϕ porosity

θ_w volumetric fluid content (water and air)

SDC, SWC scanning curves in drying and wetting respectively.

Further details of Luckner's model which describes the hysteretic nature of the SWRC are given in Appendix 2. The model is based on the van Genuchten equation and so can define the PDC and PWC. Once the $\alpha, n.m$ parameters for drying and wetting processes and θ_s, θ_a and θ_f have been determined from the curve-fitting exercise and an appraisal of the experimental data, they can be implemented in Luckner's model to define the SWRC for that particular soil. Additionally if scanning curves are required these can also be generated by inputting the initial point of the curve in terms of suction and volumetric water content (details are given in Appendix 2). This operation needs to be carried out for each individual scanning curve.

In Luckner's model the PWC does not start from the same point at which the PDC ends. It is the MWC in the model that starts from this point, i.e. the PDC and the MWC converge to a point at the high suction range. The scanning curves in drying all head for this same point of convergence, regardless of where they start (see Figure A2.24 in Appendix 2). In the case of wetting, similarly they all travel towards the θ_a value of volumetric water content at very low suction (see Figure A2.25).

In the following figures, the curves generated for each of the soils are presented. It should be noted that the curves presented in the previous section form part of the SWRCs shown here, representing the PDC and the MWC or the PWC.

Data from three of the study materials have not been analysed using Luckner's model. The data from the residual soil from Colombia was not modelled because of the lack of data. The experimental data for the Hong Kong soil relates to a compacted material and so it was thought not to be appropriate to use the Luckner model (as discussed earlier it was necessary to model the data using a bimodal fit with the van Genuchten equation). In the case of the Ash material the data were not hysteretic and so there was little point in analysing it with the hysteretic model.

Kaolin. The data and the modelled curves for Kaolin sample kB are shown in Figure 7.9(a) (the data are also shown in Figure 6.9(b)). The PDC and the MWC are the same as those shown in Figure 7.1. There are three scanning curves that have been modelled using Luckner's formulation. The curve representing the wetting scanning curve (PSC)1W (representing the primary scanning curve on first wetting) which starts about half-way down the PDC lies above the experimental data (open diamond symbols) for most of the points. This is a consequence of the fact that the MWC and also the PWC lie above the experimental data at low suctions values, i.e. less than about $200kPa$ (as discussed in the previous section when Figure 7.1 was described) and the scanning curves in wetting always converge to the MWC at low suctions. However the shape of the generated scanning curve models the trend of the data well. The drying scanning curve (PSC)1D (which starts from the end of the (PSC)1W with open star symbols) is over-predicted by the generated curve up to about $2{,}000kPa$ suction (i.e. the curve indicates higher water contents than were measured). Beyond this point the generated curve under-predicts as a consequence of it heading for the θ_f value. Drying was continued to a suction of about 5,000kPa $5{,}000kPa$ from which point another scanning curve in wetting was started ((PSC)2W with solid star symbols). The curve generated using Luckner's formulation over-predicts the volumetric water content initially but then joins the data and has the right form.

The data and the modelled curves for Kaolin sample kC are shown in Figures 7.9(b) and (c). Two figures have been used as two hysteretic scanning curves were followed during the experimental programme. Figure 7.9(b) describes the first part of the hysteretic loop. The sample was wetted from close to the end of the PDC (solid diamonds symbols defining (PSC)1W) up to volumetric water content of about 28%. The generated Luckner curve only converges to the data at the end of the wetting path, prior to this it first under-estimates the volumetric water content and then over-estimates it.

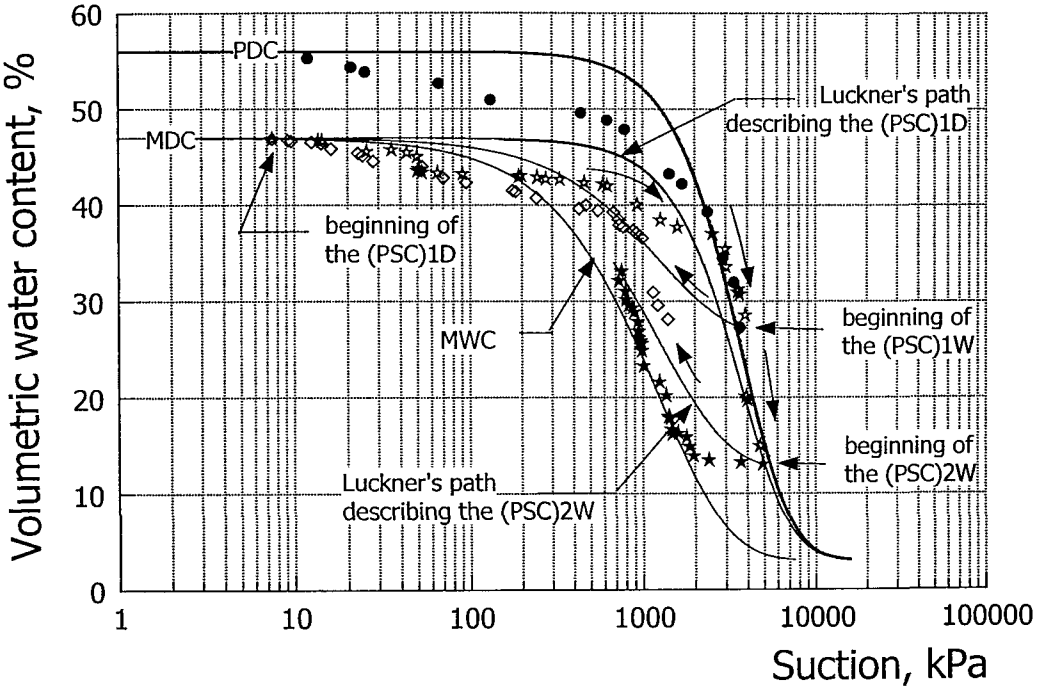

Figure 7.9(a) Luckner's model formulation for sample kB

The sample was then dried (open star symbols defining (PSC)1D), but drying was stopped before the path reached the MDC. In this case the path given by the Luckner model lies close to the data for about the initial half of the path and then falls well below the data, heading towards the point where the PDC and the MWC converge.

The sample was then wetted once more (see Figure 7.9(c)), forming a secondary scanning curve (solid star symbols defining (SSC)2W) which did not quite reach the MWC. In this case the path given by Luckner's model only coincides with the data at the very beginning and then over-predicts the volumetric water content as it heads towards the θ_a value. Finally a drying path was followed forming a tertiary scanning curve (open circle symbols defining (TSC)2D). In this case the Luckner curve models most of the data reasonably well, although the experimental data shows greater curvature than the model path. It should be noted that the main reason that

the model curve intercepts the lower part of the data is because these points lie close to the PDC towards which the model curve converges. The test was terminated at the end of (TSC)2D.

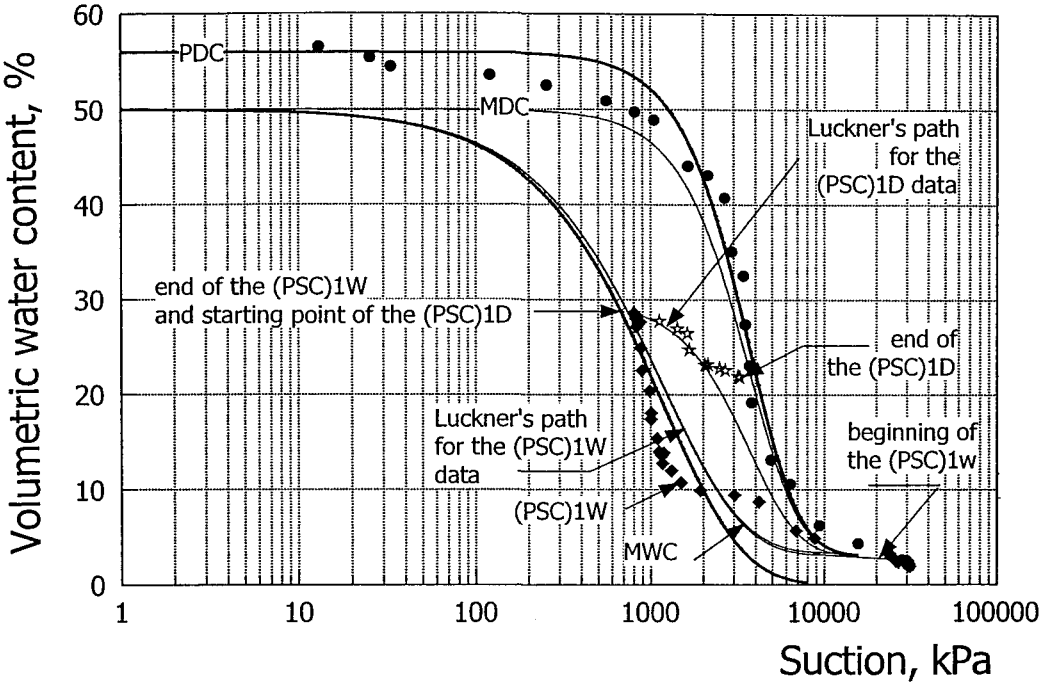

Figure 7.9(b) Luckner's model formulation for sample kC, first hysteretic scanning curve

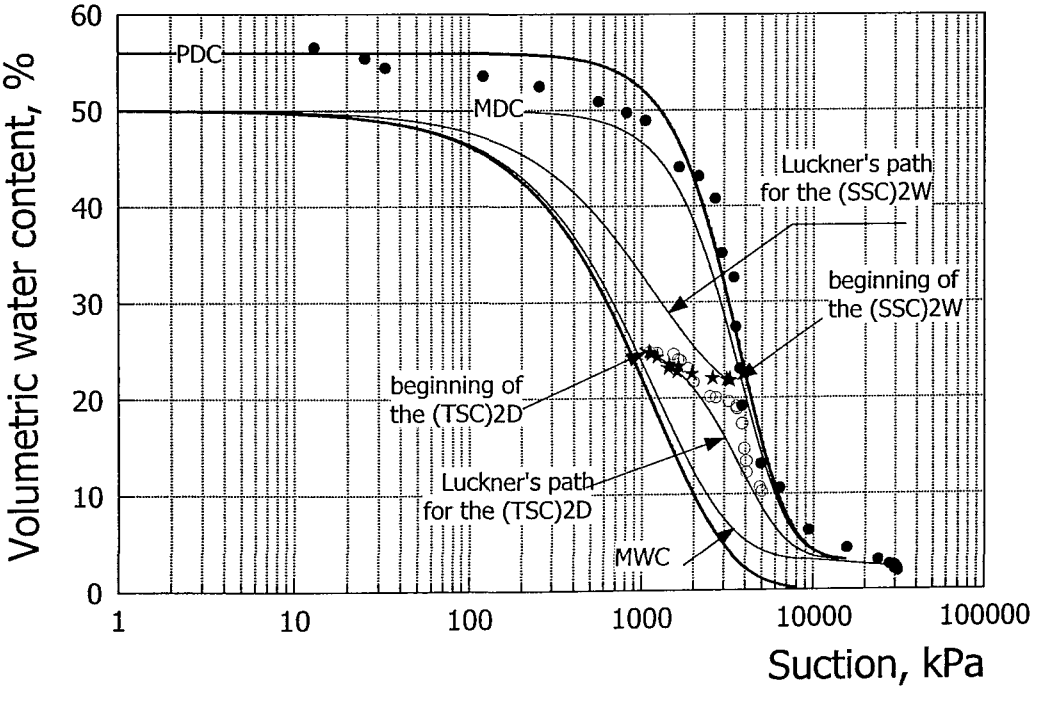

Figure 7.9(c) Luckner's model formulation for sample kC, second hysteretic scanning curve

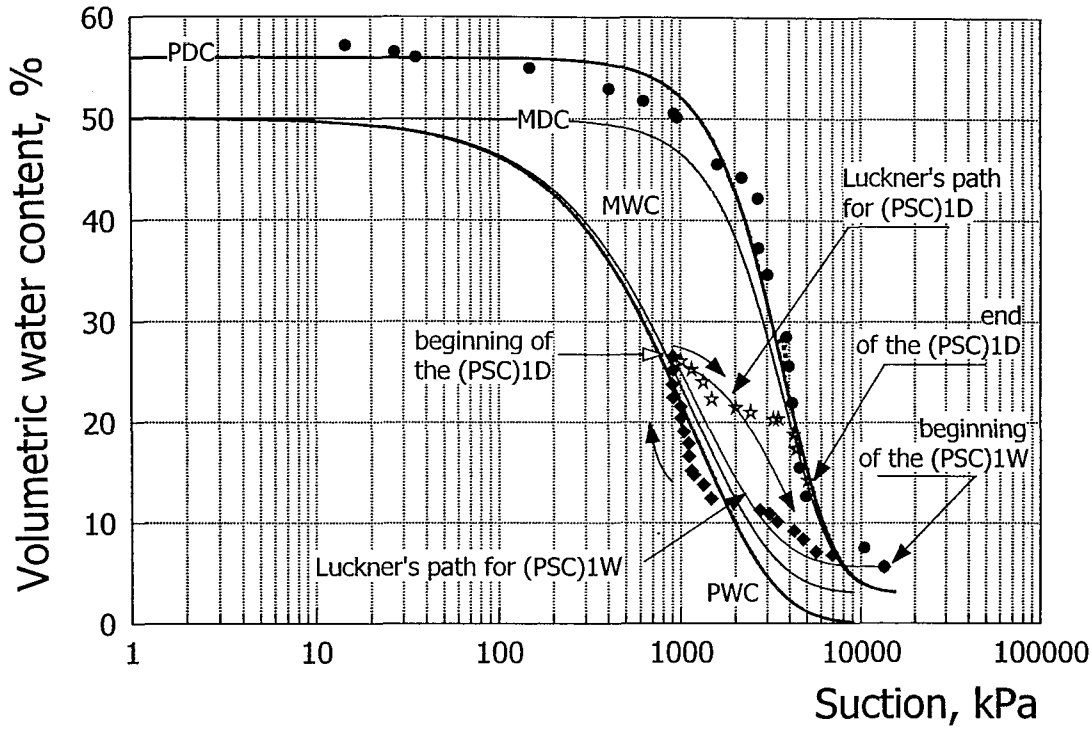

Figure 7.9(d) Luckner's model formulation for sample kD, first hysteretic loop

It can be observed in Figure 7.9(c) that, for the curves generated for this data set, that the PWC lies below the MWC and does not converge with the PDC. This is a characteristic of the Luckner formulation as discussed earlier.

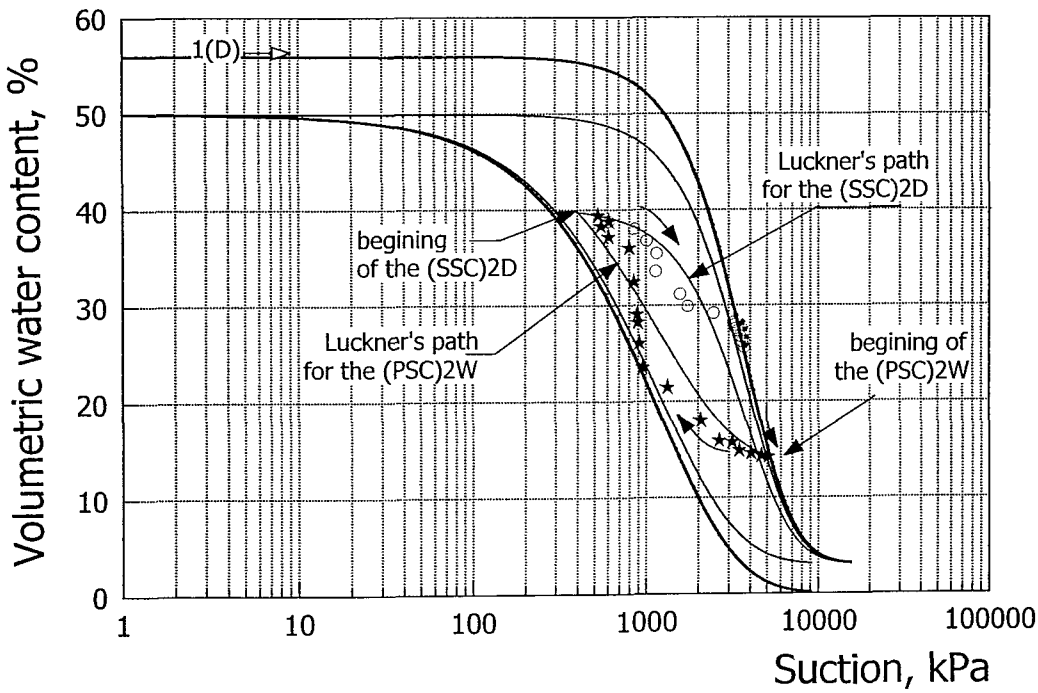

Figure 7.9(e) Luckner's model formulation for sample kD, second hysteretic loop

In the case of sample kD as for sample kC the initial scanning curve in wetting was started from towards the end of the PDC (solid diamond symbols defining (PSC)1W,

see Figure 7.9(d). The Luckner curve models the data reasonable well initially but then over-predicts the volumetric water content. From this point the sample was dried forming a primary scanning curve (open star symbols defining (PSC)1D). After the inflection point the data converge to the MDC (which is collinear with the PDC). The generated curve joins the MDC at a lower value of volumetric water content than the measured data.

The second hysteretic scanning curves (see Figure 7.9(e)) were therefore started from the MDC (solid star symbols defining the (PSC)2W). Wetting was continued to a volumetric water content of almost 40%, prior to the data converging to the MWC. The Luckner path only coincides with the data at the start and the end of this scanning curve, initially over-predicting and then under-predicting the volumetric water content.

The final scanning curves in drying was therefore a secondary scanning curve (open circle symbols defining (SSC)2D). As for the path (PSC)1D (shown in Figure 7.9(d)) the data rapidly converge to the MDC. Once again the Luckner path only fits the data at the very beginning and then over-predicts as it heads down towards the point where the PDC and the MWC converge.

In summary neither the van Genuchten formulation for the PDC and PWC nor the Luckner formulation for the hysteretic response fit the Kaolin experimental data well, despite the fact that the data are generally very well conditioned.

Weald Clay. The data for the initial drying of the two samples to form the PDC for the soil are shown in Figure 7.10 and it can be seen that the two paths are essentially coincident (refer also to Figure 6.12). The modelled PDC fits the data extremely well (see Figure 7.2). Both samples were then wetted from this point, eventually converging towards the MWC or PWC. The PSC in wetting modelled by the Luckner formulation lies well below the data during the initial stages as would be expected and converges onto it at a suction of about $3{,}000kPa$. The MDC generated from the Luckner model which starts from the end of this wetting curve at a suction of about $10kPa$ initially lies below the modelled PWC before crossing it at a suction of about $1{,}000kPa$ after which it lies above it and converges towards the PDC. Clearly this initial behaviour is completely contradictory to what would be expected given the definitions of the MDC and the PWC. It probably results from the fact that the experimental data for this soil exhibits a very narrow hysteretic loop.

One of the samples was wetted to a suction of about $800kPa$ before a drying path started. The data from this drying path eventually converge onto the PDC (black

diamond symbols defining (PSC)1D). The Luckner curve modelling the initial wetting path only coincides with the initial data point, thereafter it is almost parallel to the PWC, lying just above it. The sample was then wetted (open diamond symbols defining (PSC)1W) to the point where the data just join the MWC. The Luckner path intended to model these data once again only coincides with the data at the very beginning. In this instance the modelled path lies above the data as it heads towards the θ_a value.

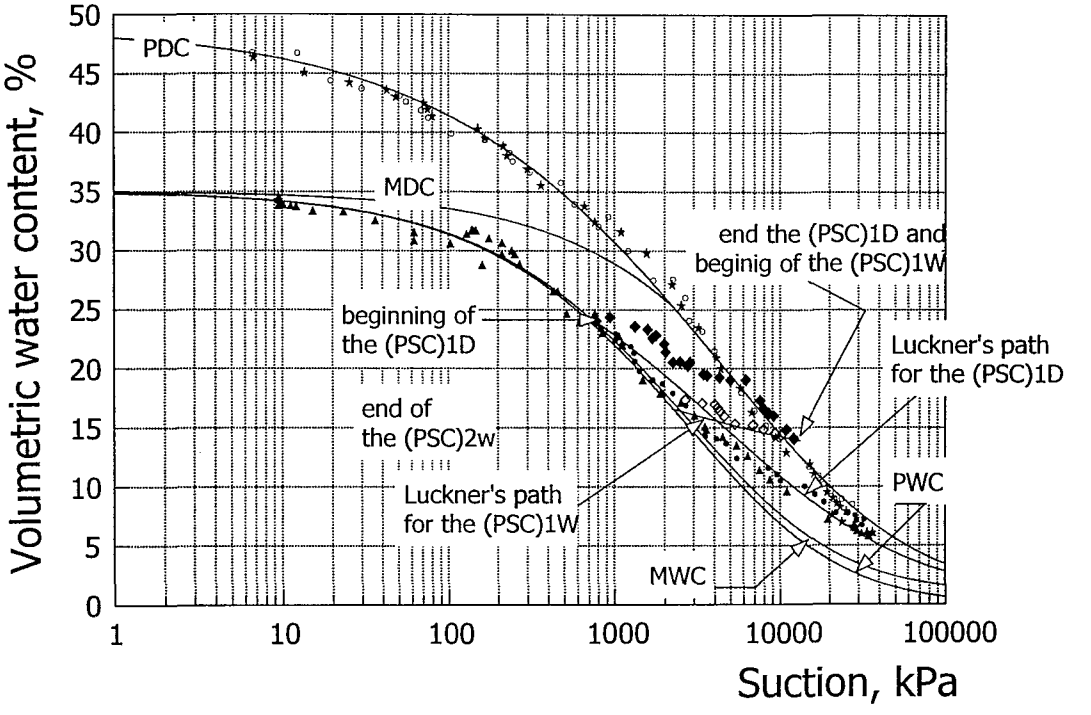

Figure 7.10 Luckner's model formulation for the Weald Clay

Once again, as for the Kaolin data, the scanning curves for Weald Clay are very poorly modelled by the Luckner formulation.

UN-Bogotá Clay. Two samples of reconstituted clay were dried to form the PDC. One of them was taken to high suction values and then wetted to form the MWC (refer to Figure 6.13). The curves representing these two parts of the data shown in Figure 7.11, i.e. the PDC and the MWC, are the same as those in Figure 7.3. The other reconstituted sample was wetted from a suction of just under $10{,}000kPa$ to form a primary scanning curve in wetting, (PSC)1W (open diamond symbols), which was continued to a very low suction value. The curve generated using Luckner's model fits the data very well for most of the range, the only difference being that the experimental data join the MWC slightly earlier than the curve does, although they eventually converge.

Luckner's model can also be used to generate the MDC. Two intact samples were dried constituting primary scanning curves that almost start from the MDC generated by the Luckner formulation (solid star and circle symbols). However, the data from one sample fall outside the generated MDC. Luckner's model cannot generate scanning curves outside the MDC (as the scanning curves, converge to the MDC at high suctions) and so the curve generated for this intact sample is almost coincident with the MDC. Data from the other sample lie just below the MDC and the curve generated does too, although it is also very close to the MDC.

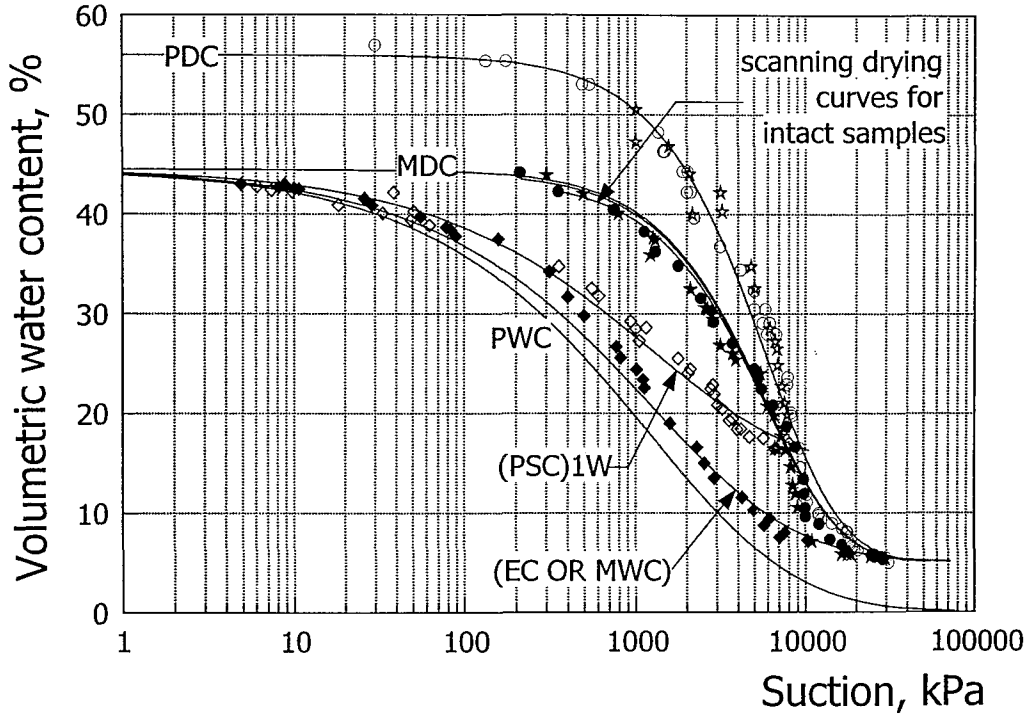

Figure 7.11 Luckner formulation for the UN-Bogotá Clay

Residual soil from Brazil. The PDC and the MWC generated from the drying and wetting data of one of the reconstituted samples in Figure 7.12(a) are the same as those shown in Figure 7.4 (refer also to Figure 6.14). After wetting to a very low suction the sample was then dried again to form the MDC (open square symbols). The MDC generated by the Luckner model fits the data very well.

The other reconstituted sample was wetted after an initial drying stage to form a primary scanning curve in wetting (PSC)1W, see Figure 7.12(b) (solid triangle symbols). The generated curve fits the experimental data well, although there is some scatter of the data points about the curve. From very low suctions this sample was then dried again also to form the MDC ((PSC)2D defined by solid circle symbols), similar to the first reconstituted sample. In this case there are many more data points that emphasise that the generated MDC fits the experimental data very well.

Additionally, two *intact* samples were dried. One of these, as discussed in Chapter 6, cracked on several occasions and required re-trimming, resulting in a scanning curve that did not follow a typical form (see Figure 7.12(b), (SC)1D defined by open circle symbols). For this reason the generated curve from Luckner does not match well the data relating to this sample. It was then wetted ((SC)1W defined by open square symbols) and can be seen to be well matched by the generated PWC.

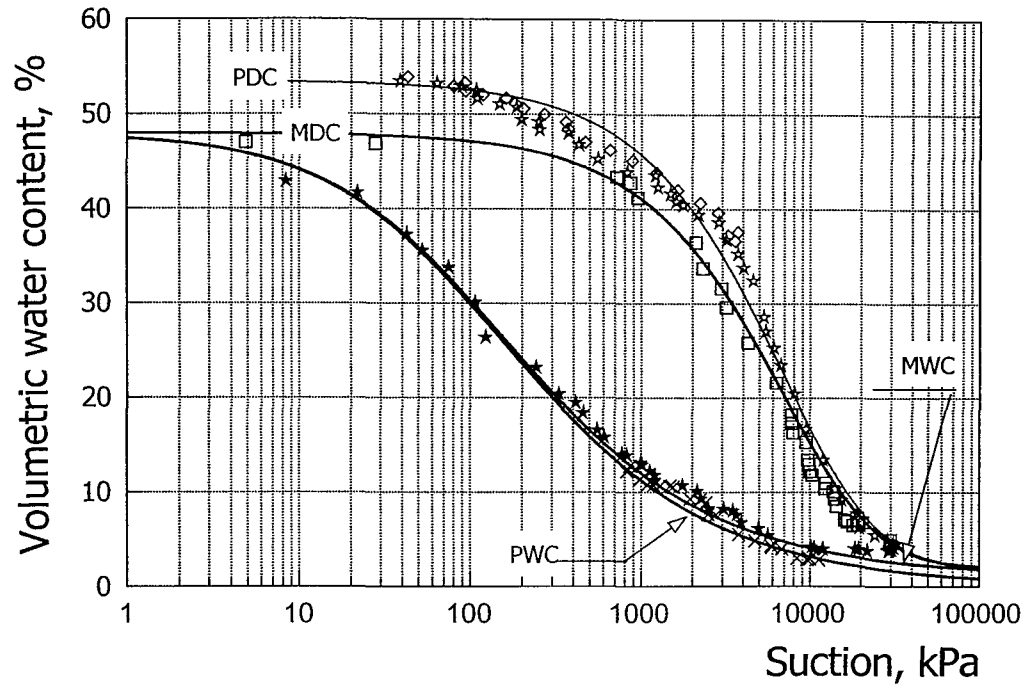

Figure 7.12(a) Luckner formulation for the residual soil from Brazil describing the PDC, MDC, PWC and MWC data

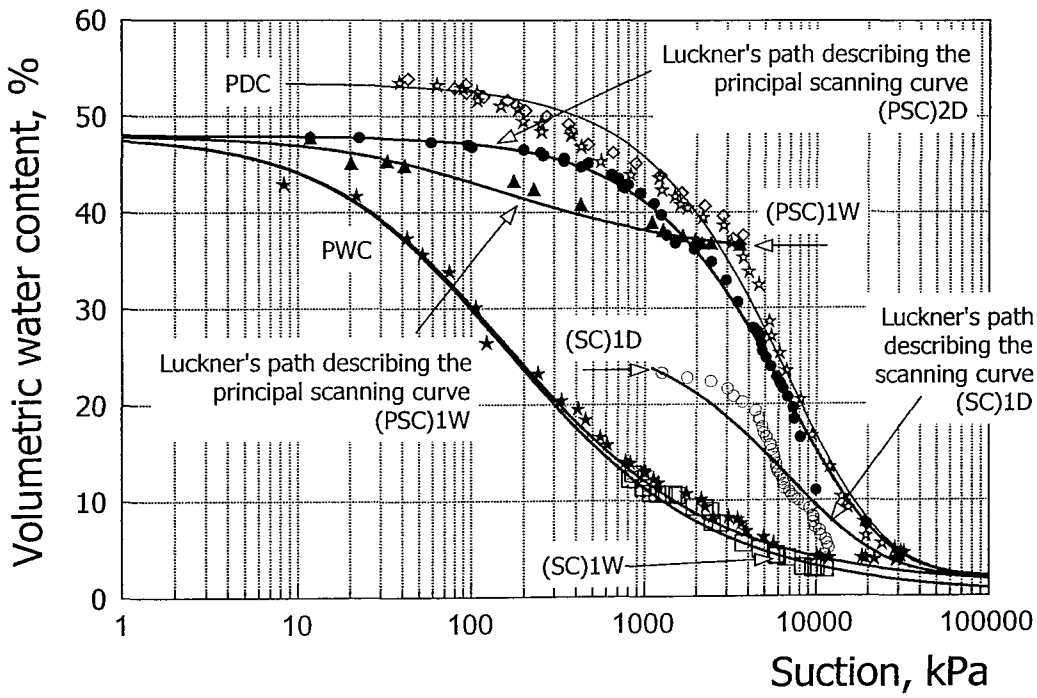

Figure 7.12(b) Luckner formulation for the residual soil from Brazil describing the scanning curve (C) and the principal scanning curve (B)

The initial point of the other intact sample starts on the steep part of the MDC (see Figure 7.12(c)). It was dried and continued to follow the generated MDC ((SC)1D defined by solid circle symbols). It was then wetted from just over halfway down the MDC to form (SC)1W (open inverted triangle symbols). The generated scanning curve fits the data extremely well, both converging to the end of the MWC.

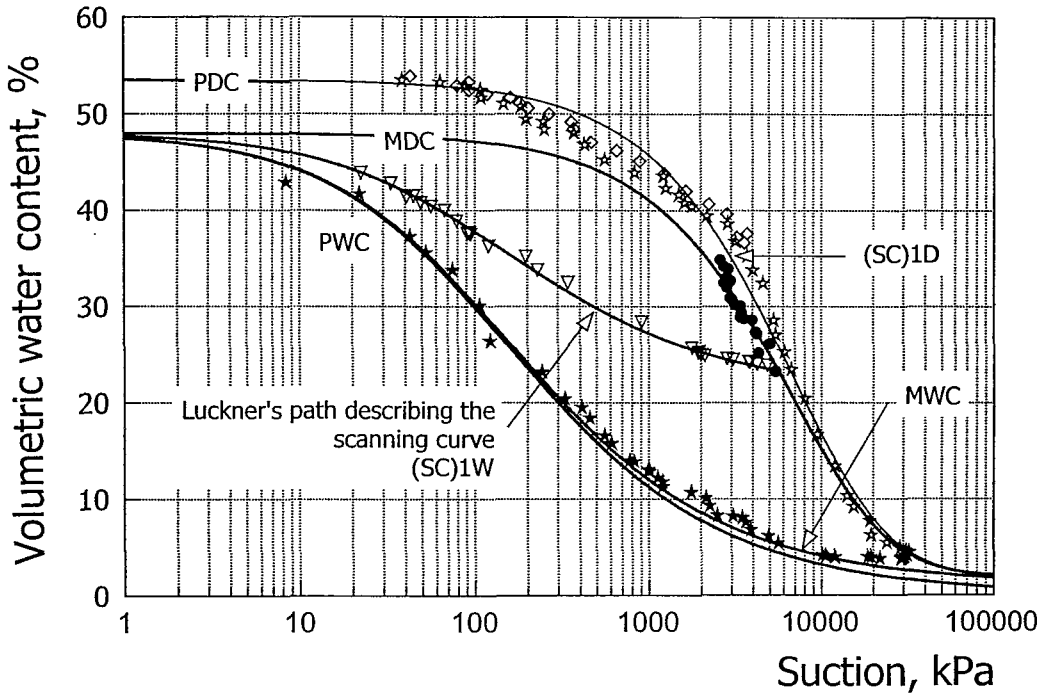

Figure 7.12(c) Luckner formulation for the residual soil from Brazil describing the scanning curve (D)

Embankment Clay. The data from the reconstituted samples and the PDC and the PWC curves fitted to them are shown in Figure 7.7. In Figure 7.13 the PDC and PWC along with the MDC and MWC generated by the Luckner model are shown. It should be recalled that it was not possible to generate the entire PDC experimentally because of the high values of suction that existed in the soil (beyond the filter paper technique range). Therefore, the final volumetric water content had to be estimated. It is perhaps as a consequence of this that the PWC and MWC have a form indicating considerable hysteresis in the SWRC. Because of the lack of data at the lower end of the PDC it is not possible to confirm the initial shape of the generated MWC and PWC. However, from the end of drying one of the reconstituted samples was wetted up to form a primary scanning curve, which does eventually converge to the generated MWC and PWC. The curve modelling the scanning curve (PSC)1W fits the data very well as can be seen in Figure 7.13.

One intact sample (recalling that the 'intact' samples were trimmed from a block of compacted clay fill) was dried from a point lying on the generated MDC. However it did not follow the MDC for very long before joining the PDC obtained from the

reconstituted samples (solid triangle symbols). The other intact sample, starting from just inside the MWC (at a volumetric water content of 35%), was dried to a suction in excess of $10{,}000kPa$, forming a primary scanning curve (PSC)1D (open diamond symbols), but did not converge to the PDC or the MDC. It was then wetted to form a secondary scanning curve in wetting (SSC)1W (solid diamond symbols). The curve generated to model this path fits the data very well. Wetting was continued to a suction of about $300kPa$ and the data did not converge even close to the generated MWC. Drying was then recommenced to form a tertiary scanning curve in wetting (TSC)2D (spherical symbols). Again the generated scanning curve fits the data extremely well.

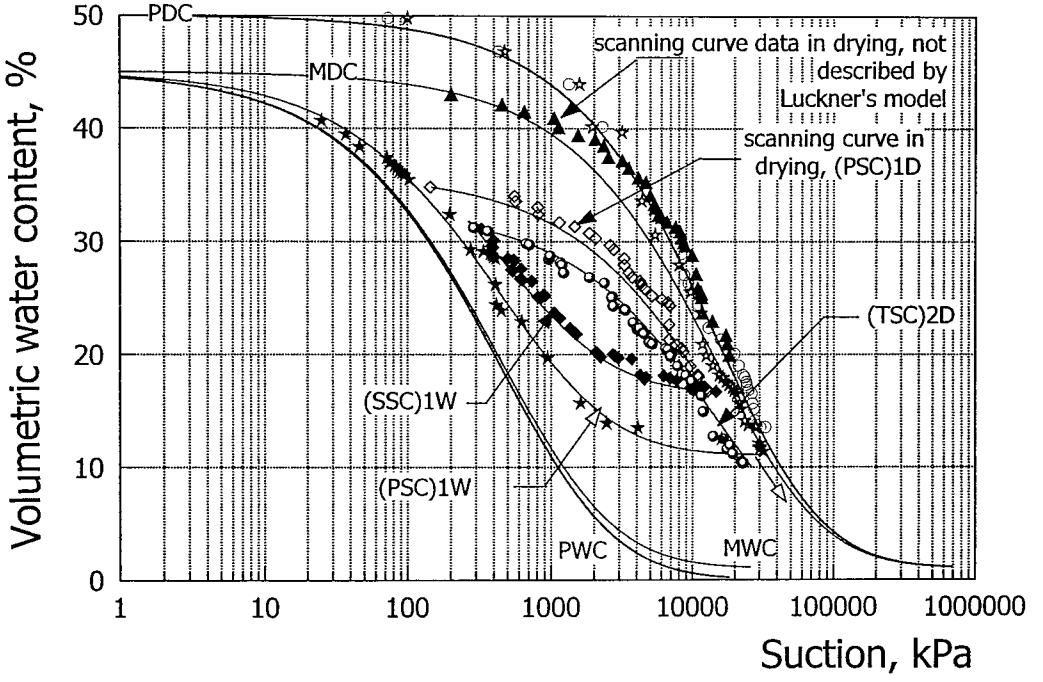

Figure 7.13 Luckner formulation for the Embankment Clay

RELATING VAN GENUCHTEN PARAMETERS TO SOIL CHARACTERISTICS 7.3

Some clear trends in the shape and location of the SWRCs were discussed at the end of Chapter 6 after appraising the experimental data. Having carried out the curve fitting of the boundary curves using the van Genuchten equation, it was decided to investigate potential relations between the parameters required in the equation and basic soil characteristics such as the Atterberg limits. Clearly, it would be very beneficial to be able to predict an SWRC using such basic characteristics without having to carry out a lengthy experimental study, even if only to gain a rough idea of its form. With this in mind the van Genuchten parameters have been plotted

against some of these basic quantities. It should be noted that the parameters discussed are based on those given in Table 7.1 which relate to the SWRCs plotted as volumetric water content versus suction. A similar exercise was carried out for van Genuchten parameters relating to curves expressed in terms of degree of saturation versus suction, but there was little difference in the trends.

Results of Atterberg limits and activity for the soils investigated were presented in Table 6.4. An initial check was performed on the relation between activity and plasticity index by plotting these together. Generally they would be expected to be related, and this can be seen to be the case from the data plotted in Figure 7.14. It was therefore decided to just look for relationships between plasticity index (as the primary quantity) and the van Genuchten parameters.

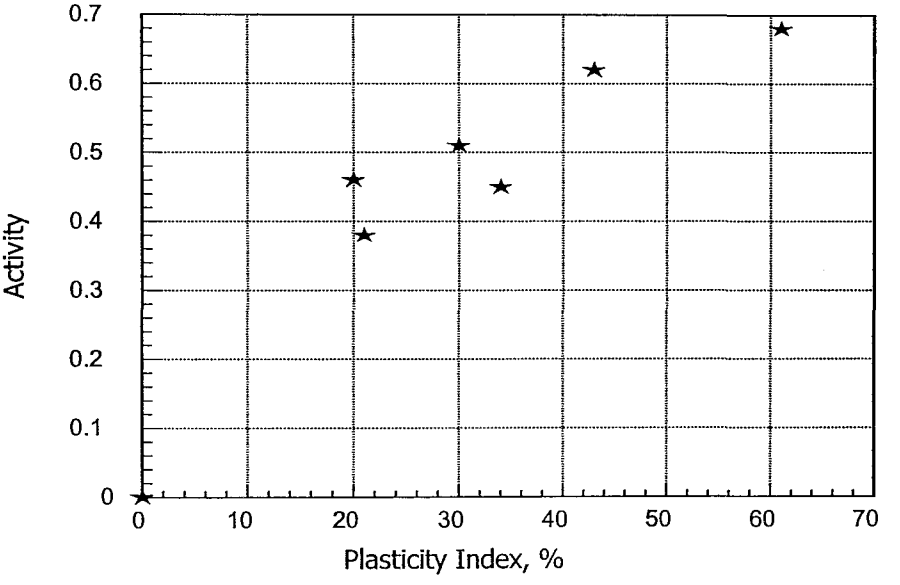

Figure 7.14 Relationship between activity and plasticity index for soils investigated in research (based on data given in Table 6.4)

The van Genuchten α parameter, which controls the position of the SWRC is plotted against plasticity index and liquid limit for both the wetting and drying parts of the SWRC in Figure 7.15. The van Genuchten parameters are the same as those given in Table 7.1. A rough trend of increasing α value with both plasticity index and liquid limit is evident. Lines forming boundaries to most of the data are marked on the figures. The fact that these boundaries extend over a significant range means that a well defined line cannot be justified with any great accuracy.

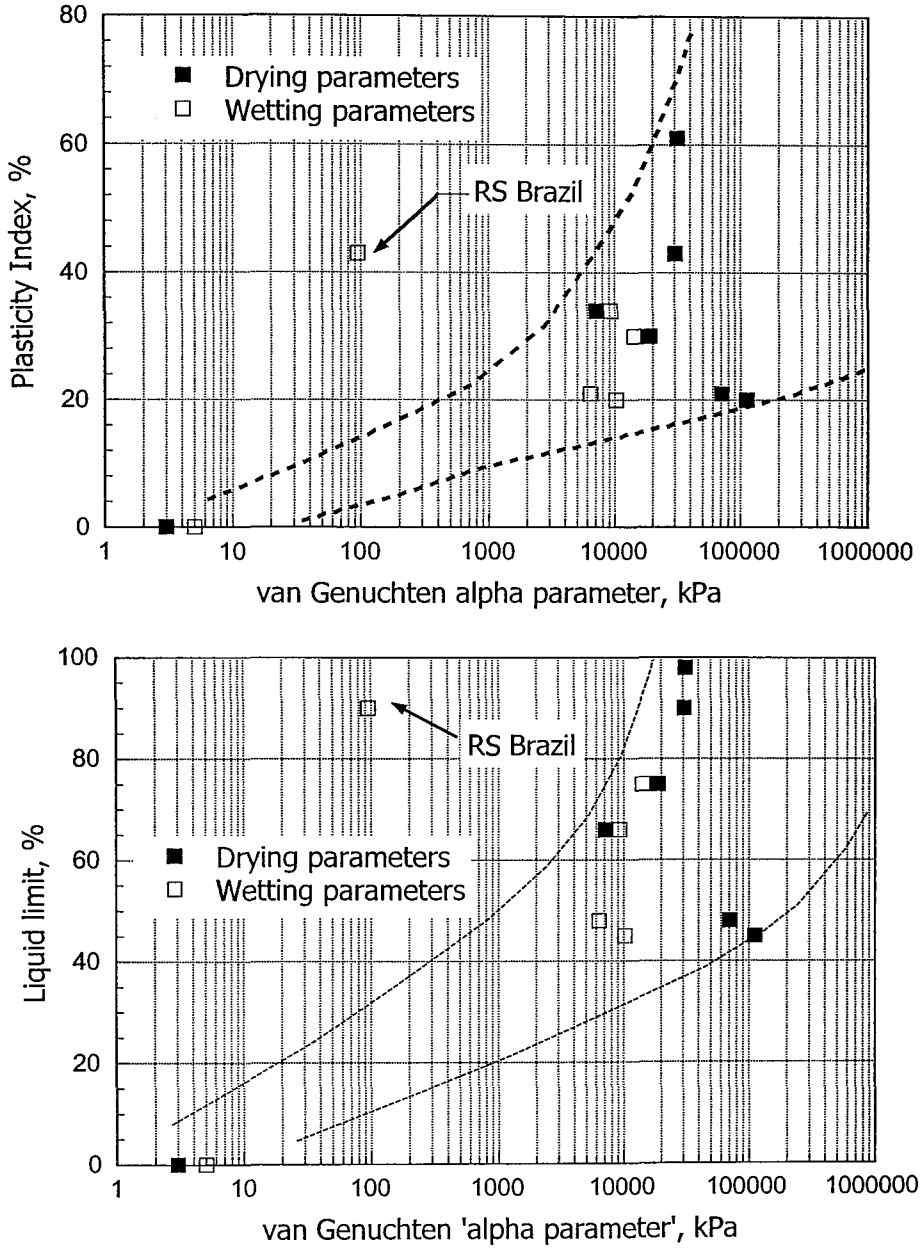

Figure 7.15 Relationships between plasticity index and liquid limit and the drying and wetting van Genuchten α parameters

The point relating to the wetting curve for the residual soil from Brazil falls well outside the range. It is possible that this can be explained by the fact that the plasticity of residual soils has been found to reduce after drying (even to moderate levels), the clayey components clumping together to form silt sized peds. This process is irreversible and would certainly have taken place to some degree given that the soil was dried to a very low degree of saturation. Unfortunately, it was not possible to generate wetting curves for the residual soil from Colombia to corroborate this idea.

Another interesting point to note from Figure 7.15 is that generally the α values in wetting are less than those in drying. This is not surprising as α is usually expected to shift the SWRC laterally to the higher suction range as it increases in value. The one exception in the figure relates to the Kaolin parameters, for which α in wetting is greater than that in drying (by a small amount). This illustrates the fact that the shape of the curve, governed by the n and m values, also has an influence on the α value.

As the trends between plasticity index and liquid limit against α are very similar, comparisons with the van Genuchten n and m parameters have only been made with the former quantity. These are shown in Figure 7.16.

Once again, as for α, the general trend indicated by the plots is that n and m increase (by different degrees) with plasticity index, but with a wide scatter of the data. The parameter n, which controls the slope of the steep part of the SWRC has values within a range of about 0.5 to 3 for the soils investigated in the present study. The values relating to the non-plastic ash material do not fall within the general trend and neither does that for the residual soil from Colombia (only a drying point is available).

The parameter m, which controls the transition of the curve at either end of the steep part of the SWRC has a greater range of values than n, extending from almost zero to about 5. Most of the data points fall within a narrower area than for the n parameter, with the exception of the residual soil from Colombia and the wetting point relating to the residual soil from Brazil.

In conclusion, although trends are evident between the van Genuchten parameters and plasticity index (the primary quantity used here to characterise the soil) they are not defined well enough to generate accurate and reliable relationships. Other factors probably need to be taken into account. In particular it is felt that the particle size distribution curve plays an important role. For instance, although the Kaolin investigated is a clay, it has a very uniform particle size distribution (i.e. is poorly graded) and so when it is dried it has a much steeper SWRC, and hence higher n value, than might be expected for a natural clay.

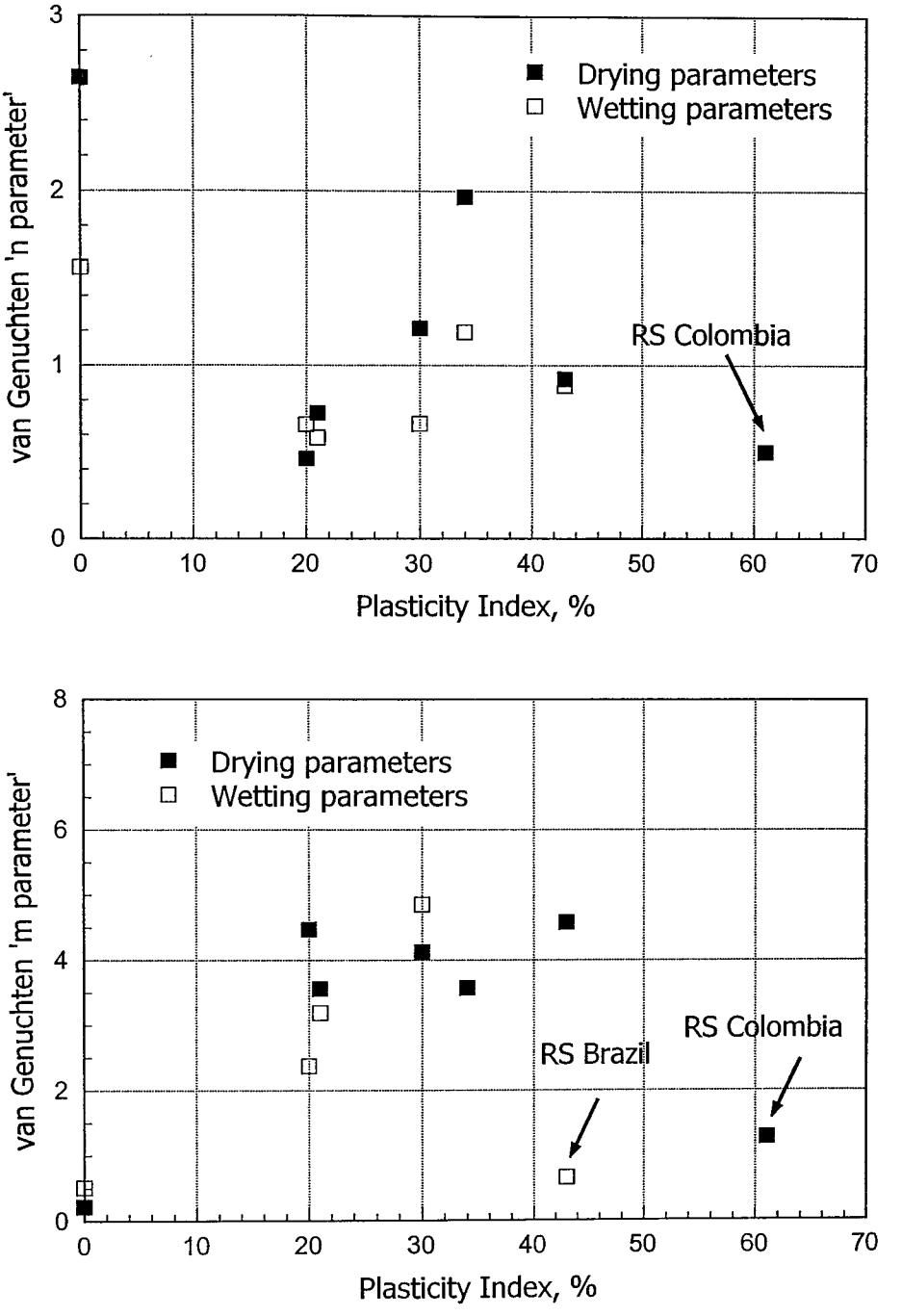

Figure 7.16 Relationships between plasticity index and the drying and wetting van Genuchten n and m parameters

7.4 CONCLUSIONS ON MODELLING COMPONENTS OF THE SWRC

In conclusion the van Genuchten equation fits the data well in most cases except towards the upper and lower ends of the steeply sloping path of the PDC. As mentioned earlier this feature of the curve is controlled by the m parameter. The equation seems particularly good at modelling the PWC, perhaps because it has a

much smoother and shallower curve. Excellent fits to the data were observed for the Weald Clay, the UN-Bogotá Clay, the residual soil from Brazil, the Embankment Clay and the Ash material.

It was not possible to test the equation for the residual soil from Colombia, which has the highest clay content and plasticity, because of the lack of data due to the limitations of measuring high suctions.

Ironically, the data produced from the Kaolin samples, which were very well conditioned, were not modelled well by the van Genuchten formulation. This was particularly the case at the upper and lower parts of the steeply sloping section of the SWRC, despite attempts at adjusting the generated curve by varying the m parameter.

During the course of the modelling of the hysteretic behaviour, one of the limitations of Luckner's formulation became evident. If a wetting path (scanning curve) starts above the θ_a value (to which the PWC and MWC converge at low suctions) the generated path travels towards the θ_a value implying that the volumetric water content decreases, while for wetting it would be expected to increase.

In the case of the Luckner model, the scanning curves and the MDC are reasonably well represented. However, it cannot model scanning curves well if the experimental data lie outside the MWC or PWC (as was the case for the Kaolin, kB sample) as scanning curves generated converge to either the MWC or MDC.

In addition to the reasons given above, the Luckner formulation probably did not model the scanning curves for kaolin well because it is based on the van Genuchten equation and this did not fit the PDC and PWC well for this material. It is therefore unlikely that the more intricate scanning curves could be modelled accurately. This should be born in mind when modelling detailed cyclic behaviour of any soil. It is necessary as a first step to achieve a good match to the boundary curves (PDC and PWC) using the van Genuchten equation, if the scanning curves are to be successfully modelled.

As was stated in Chapter 2, the MWC and PWC in many cases are almost collinear. In the Luckner model it should be noted that these two curves start at different values of volumetric water content and generally are not consistent with the PWC generated using just the van Genuchten formulation.

In conclusion the Luckner model has been observed in most cases to provide a good fit for the MWC and MDC and most of the scanning curves (except for the

Kaolin data). However, as discussed above, care needs to be taken where wetting takes place at high degrees of saturation (this is relevant for many situations encountered in practice).

Relationships between the soil types and the shape and position of the SWRCs became evident when the experimental curves were discussed in Chapter 6. However, expressing the soil characteristics in terms of plasticity index (primarily) and the shape and position of the SWRCs in terms of the van Genuchten equation parameters α, n and m has not produced trends that are defined well enough to be used to generate SWRCs reliably or accurately. Other parameters, for example relating to the particle size distribution curve, also probably need to be taken into account.

CHAPTER 8

F.E. ANALYSIS IMPLEMENTATION

In this chapter the equation describing the SWRC is implemented in numerical analysis to simulate observations made during the course of a field project carried out in Brazil. Initially the field work is described and then details are given of the numerical analysis performed, including parametric studies, and the results presented and discussed.

DETAILS OF FIELD WORK TO BE ANALYSED 8.1

Rodriguez (1998) compared data from field tests and numerical analysis in order to establish the flow characteristics within a slope in Rio de Janeiro (Brazil). Falling head tests and a constant head test were performed in an open standpipe around which Imperial College suction sensors were installed, measuring continuously suction changes. The numerical analyses were performed using a model based on Richard's equation and van Genuchten's equation for describing the flow and the SWRC concepts in a partly saturated soil.

The field works were carried out in the PUC's Campus (Pontificial Catholic University) located in the South of Rio de Janeiro (Brazil). The PUC's campus has an experimental site where significant geological and geotechnical research has taken place for several years.

The tests made by Rodriguez (1998) used a pre-existing 3m deep pit that was already characterised (see Figure 8.1). The pit location was selected because of the ground homogeneity to a depth of 8m (Rodriguez, 1998). The tests were performed at the bottom of the pit. Between the depths of 3 to 8m the ground showed no presence of roots and no evidence of structure from the parent rock (Rodriguez, 1998). The ground conditions at the test site are also described in Figure 8.1. Rodriguez also stated that no ground water table was found during the field works.

However there are some disadvantages with the site. The vegetation that surrounded the pit had roots that reached to a depth of 2m and it is thought that these can affect the measurements of the suction at 5m depth (Rodriguez, 1998). Another disadvantage of the site is the wet weather. During the initial periods of suction measurements in the ground, heavy rain occurred for several days, delaying the in-situ suction measurements since suction took a long time to stabilise.

It should be noted that the two tested intact samples of the residual soil from Brazil in the present research project were taken from a block trimmed from this pit that had an initial suction measurement of $210kPa$ and a gravimetric water content of 26.4%.

At a depth of about 2m (with respect to the bottom of the pit) five Imperial College suction sensors were installed around a standpipe as is shown in Figure 8.2 Rodriguez notes that the depth of the standpipe and probes were selected to ensure that they were located in the middle of the very homogeneous stratum. The figure illustrates that sensors BH1 to BH4 were located assuming that the maximum distance of influence of the wetting front due to an infiltration test is 20 times the diameter of the standpipe, the arrangement for the standpipe and the suction sensors was determined by Rodriguez (1998). BH5 was installed as a reference sensor for indicating the suctions in the ground away from the standpipe (it was located just outside the pit shown in Figure 8.2).

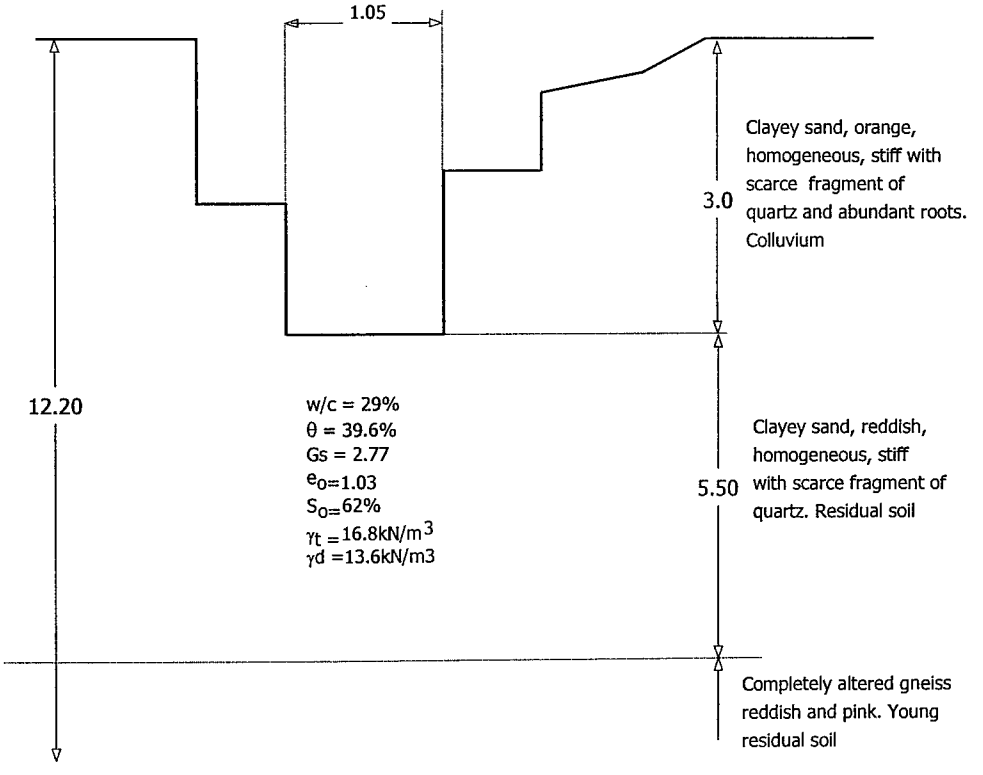

Figure 8.1 Profile of the ground at the infiltration tests site (from Rodriguez, 1998). Not to scale, dimensions in metres

Two falling head tests were carried out by Rodriguez in the open standpipe (BH0) and the response of the ground in terms of suction was recorded using five different Imperial College suction sensors in BH1 to BH5 located around the open standpipe, as is shown in Figure 8.2. The results from BH2 were considered to not be reliable (because no substantial changes in the soil suctions were measured) and so have

not been used. Equally the response from the sensor in BH5, which would have been expected to be constant (as it was outside the zone of influence of the infiltration test) was found to drift erroneously and so has also been ignored.

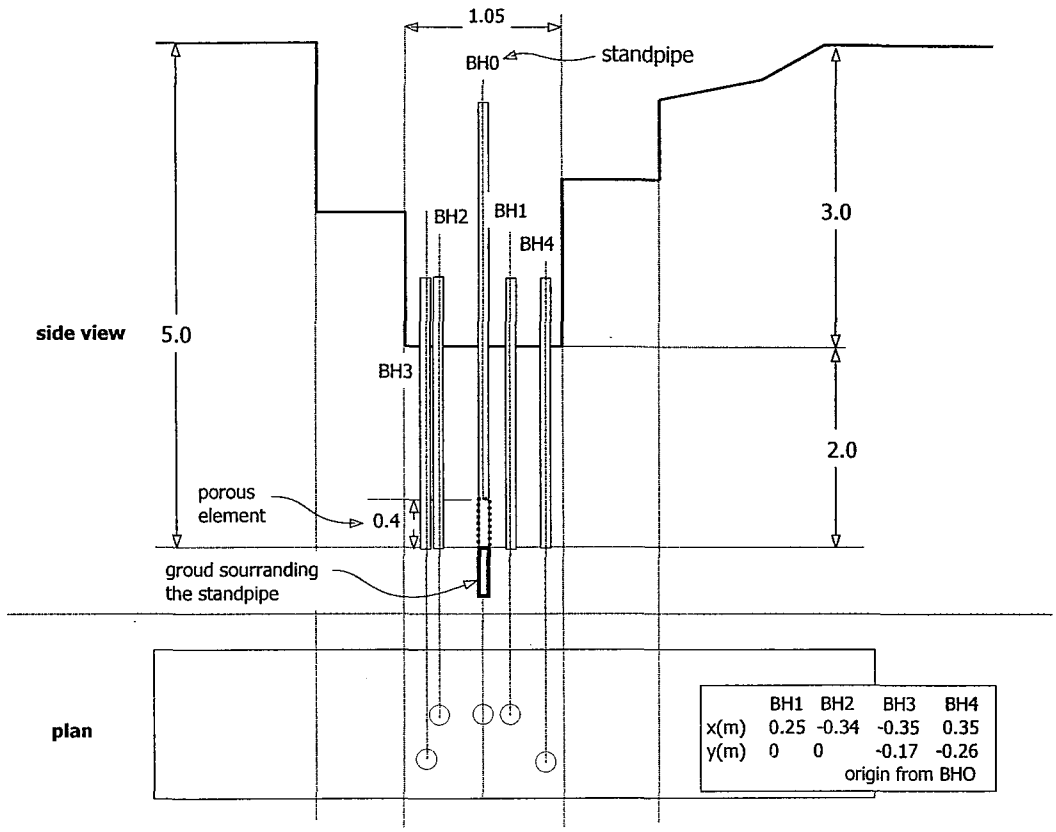

Figure 8.2 Geometry of the infiltration tests on site. Not to scale, dimensions in metres (from Rodriguez, 1998)

The IC suction sensors used were sealed piezometers with the ability to measure small pore water suctions up to $70kPa$ (details can be found in Ridley and Burland, 1996). The sensors were screwed in to each open standpipe with small ceramic tips at the base, see Figure 8.3. The ceramic tips are capable of sustaining a pore water tension of $100kPa$.

The first falling head test was performed with an initial head of 2.12m and the second one with an initial head of 3.48m (tests 1 and 2 respectively, see Figure 8.4). In the subsequent analyses to be discussed mainly data from test 2 will be used (this being considered the most reliable test). The recorded pore water pressure in boreholes BH1, BH3 and BH4 are shown in Figure 8.5 for falling head test 2.

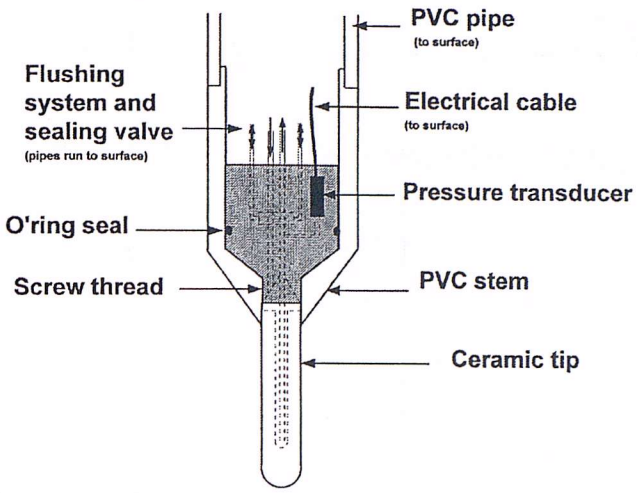

Figure 8.3 Porous tip and IC sensor used by Rodriguez, 1998. Not to scale

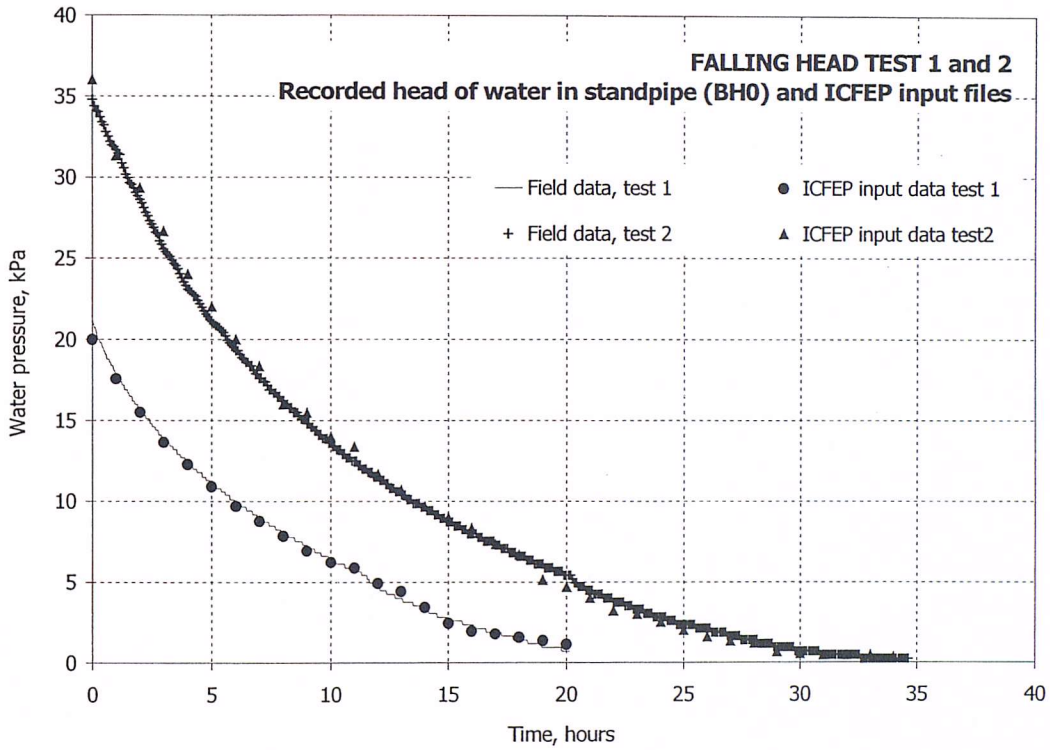

Figure 8.4 Head of water for falling head tests 1 and 2 recorded in the standpipe (BH0)

The suction change measurements recorded in the three boreholes are shown in Figure 8.5. The initial suction measurements in the boreholes are very similar, being between 17 and $14kPa$. This is what would be expected given that the sensors are at the same level. It should be noted that the resolution of the sensors is about $0.7kPa$, evident from the step changes seen in the plots.

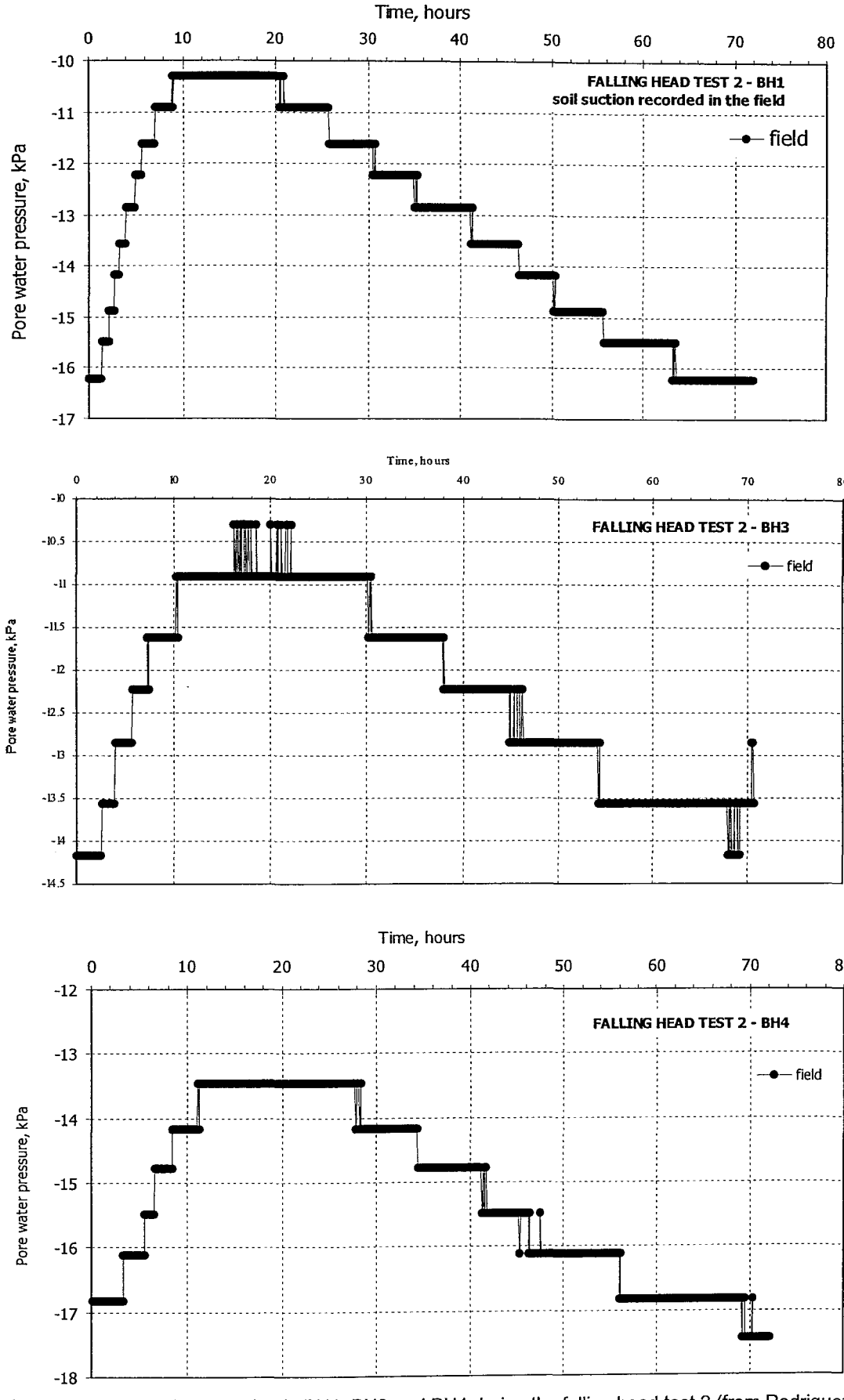

Figure 8.5 Recorded soil suction in BH1, BH3 and BH4 during the falling head test 2 (from Rodriguez, 1998)

In response to the falling head test, a reduction in suction can be observed from each sensor as the ground wets up, followed by a gradual increase back to an equilibrium condition. It can be seen that the initial response time is a function of the distance of the sensor from BH0, the closest sensor (BH1) having the fastest response and the furthest (BH4) the slowest. Also generally the maximum change in suction reduces with increasing distance from the standpipe (BH0). The period over which the minimum suction was sustained was shorter for the closest instrument. In all cases the final suction was within $1kPa$ of the initial suction.

In the constant head test, a head of 1.6m was applied to the standpipe and suction changes in the ground were recorded in BH1 as shown in Figure 8.6.

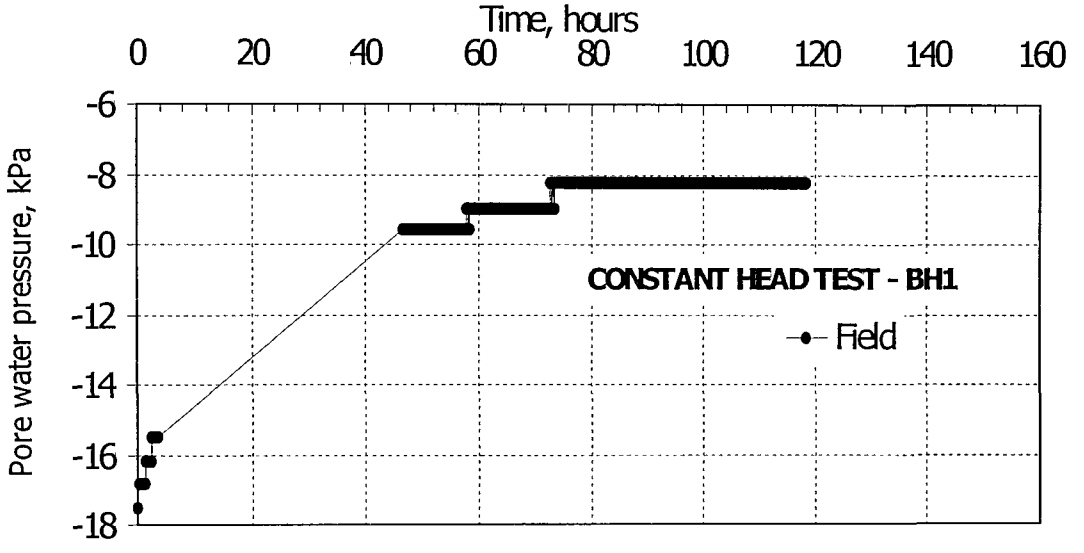

Figure 8.6 Recorded soil suction in BH1 during the constant head test (from Rodriguez, 1998)

In Figure 8.6 it can be seen that the initial suction was about $17.5kPa$ similar to the values measured prior to the falling head test. During the constant head test the suction decreased as wetting up of the ground took place, reaching a final steady state suction of just over $8kPa$. No reason for the gap in the data is given by Rodriguez, but it is probably associated with a temporary fault in the data logging system.

APPRAISAL OF INITIAL GROUND CONDITIONS 8.2

As stated above, the initial suction at level of the sensors was between 14 and $17kPa$. A profile of gravimetric water content with depth given by Rodriguez (1998) indicates that $\omega/c = 29\%$ at the level of the sensors. This implies that the volumetric water content is 39.6% (for a specific gravity equal to 2.77 and void ratio $e_0 = 1.03$).

In Figure 8.7 the boundary curves of the SWRC for this soil are reproduced (from Figure 7.12(b)) along with the data from the initial drying of one of the intact samples (open circle symbols). Also marked is the point representing the initial state of the soil at the level of the sensors (solid spherical symbol) and data points from Daylac (1994) given by Rodriguez (open square symbols).

It can be seen that some of these points lie just outside the PWC and the one data point relating to the infiltration tests is essentially on the PWC. As discussed in Chapter 2, natural soils lie between the boundary curves and so follow scanning curves during seasonal cyclic wetting and drying. Clearly there is no information relating to the scanning curve followed by the soil at this location prior to it reaching its current state. However, the path followed must have been a wetting path. The reason for this is that drying of the soil would have resulted in movement of the path to the right of the PWC. In fact the data relating to the intact sample are at much higher suctions and lower volumetric water contents indicating that the sample must have dried out to some degree in the period between sampling and testing (which was at least two years). The anticipated scanning path that would have been followed from in-situ conditions to the dried state is also marked on Figure 8.7.

During the course of the infiltration test the soil in all cases initially wets up. This would imply that the path followed on the SWRC would continue up the PWC. In the case of the falling head test, after the suction had reduced to a minimum value it then started to increase again towards its initial equilibrium value (refer again to Figure 8.5). The path followed during this time would have been a scanning curve in drying.

As the three boreholes were at different distances from the open standpipe (BH0), the magnitude of suction change decreased with increasing distance. Therefore the path relating to BH1 would have moved further up the PWC than the paths for the other two locations. The drying paths would therefore start from different values of volumetric water content and because of the hysteretic nature of the SWRC scanning curves these move away from the PWC. This idea is given schematically in Figure 8.8 which shows an enlarged section of the PWC in the vicinity of the in-situ state wetting presented in Figure 7.23.

The above example illustrates the complexity of trying to follow the scanning path of natural soils under cyclic conditions in the field. In the following section the measured data are analysed using ICFEP with a single SWRC. At this stage the hysteretic behaviour cannot be modelled as a continuous process.

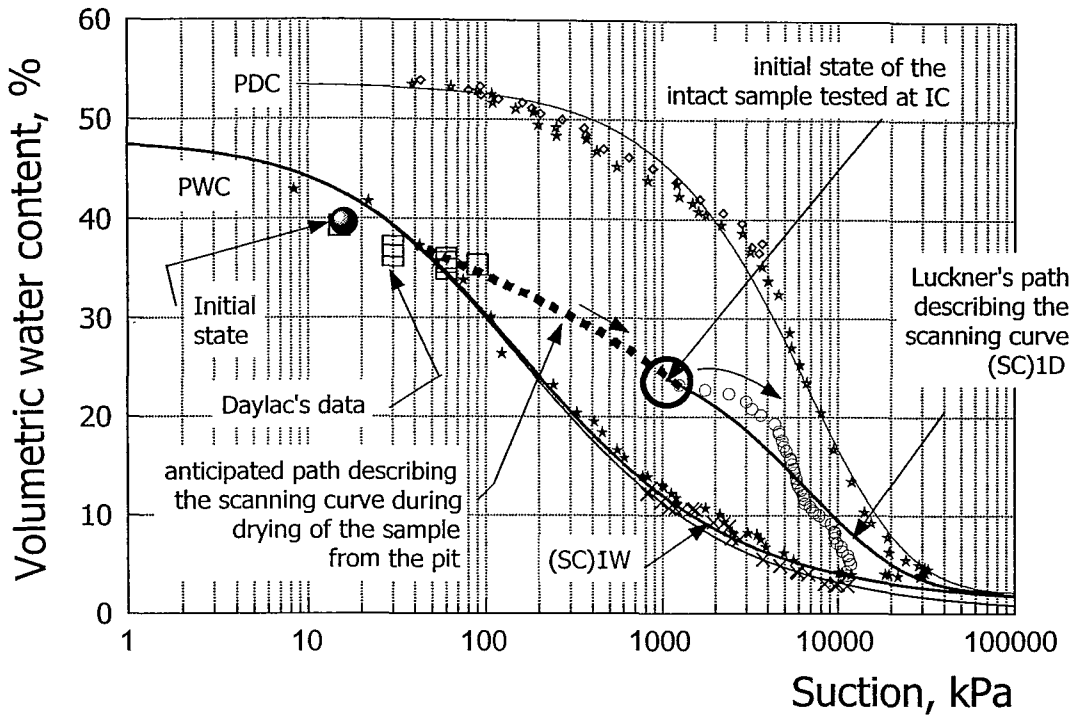

Figure 8.7 Boundary curves (PDC and PWC) for residual soil from Brazil and scanning curve for intact sample, initial state prior to infiltration test and data from Rodriguez (1998)

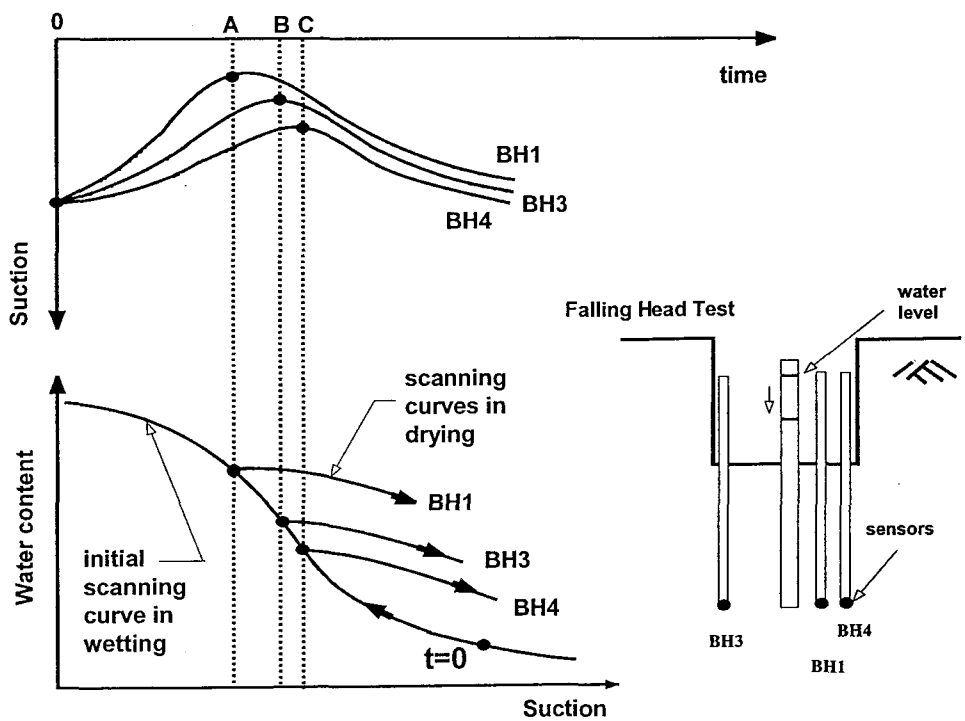

Figure 8.8 Schematic diagram of the hysteretic path followed by the soil at the three borehole locations during the falling head test

The aim of the FE analyses performed by Rodriguez was to model the particular wetting path followed by the soil in the infiltration process. The FE analysis used the SWMS-2D program (version 1.21) developed by Simunek, Vogel and van Genuchten (1994). The results from Rodriguez's analyses using the van Genuchten formulation were reasonably successful. However none of the results from the analyses are presented here because of the lack of information concerning the program used (for further information see Rodriguez (1998)). The purpose of undertaking the numerical analysis with ICFEP was to investigate the analyses made by Rodriguez, using a parametric study approach to obtain a best fit to the field data, i.e. to investigate the influence of the various parameters on the accuracy of the results. Additionally in the future it is anticipated that ICFEP analyses with a hysteretic model will be possible.

Similar analyses to those performed by Rodriguez (1998) were therefore carried out using ICFEP. The aim of these ICFEP analyses was to model the particular scanning wetting curve followed in situ when performing falling and constant head tests on site. A non-hysteretic SWRC was implemented in ICFEP (see Chapter 3, ICFEP SWRC model 3) using the most appropriate parameters to provide the best match to the field data. This was achieved by first considering the wetting response observed in BH1 bearing in mind the parameters that Rodriguez (1998) established. In the first instance this was done using a single element analysis and then once the model had been validated a mesh encompassing the area of interest was implemented (as described below). Following from this a parametric study was carried out to assess the influence of varying a number of parameters on the analysed response of the ground around BH1. Final refined analyses relating to the falling head test and constant head test were then performed.

Mesh. The numerical analyses to model the tests were based on an axisymmetric mesh generated using ICFEP. The mesh describes a geometry as is shown in Figure 8.9. The mesh used comprised 58 blocks and 338 elements.

The extent of the mesh used encompasses the soil from 1.2m to 2.86m below the lower level of the pit (see Figure 8.10) and extends laterally a distance in excess of twenty times the standpipe diameter (just under 50mm), which is considered to be the outer extent of the zone of influence of the infiltration test (from BH0). These dimensions are the same as those used by Rodriguez (1998) in his numerical analysis. The mesh also describes the standpipe's porous element for the water infiltration which is 0.4m length (the standpipe, BH0 extends to a depth of 2.0m, see Figures 8.9 and 8.10).

Ground and boundary conditions. The ground characteristics used in the analyses were taken from Rodriguez and are given in Figure 8.10 ($S_0 = 62\%, e_0 = 1.03, \phi = 51\%, \theta_s = 51\%, \gamma_t = 16.8 kN/m^3, \gamma_d = 13.6 kN/m^3, k = 6*10^{-8} m/s$). Additionally the ground was assumed to be homogeneous, isotropic and rigid. As the primarily objective of the analysis was to investigate the changes of suction during the infiltration test, the assumption was made that the soil does not swell or shrink if wetted or dried for the range of suction recorded during the tests.

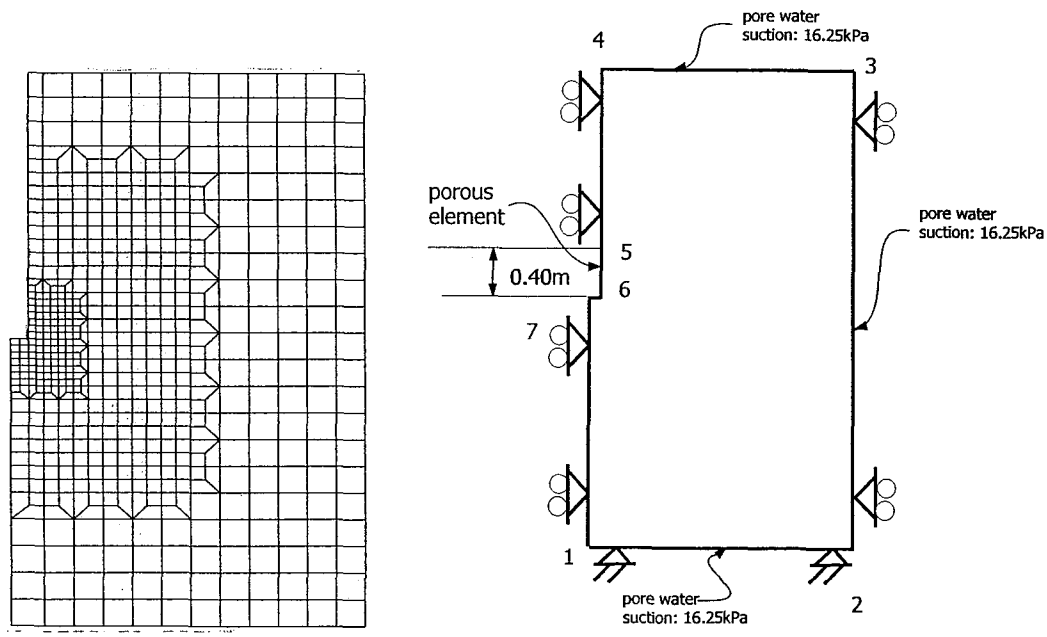

Figure 8.9 Geometry of the mesh used and the boundary conditions imposed to model the falling and constant head test

A number of soil parameters remain *constant* throughout all of the runs. In terms of the linear material properties, ICFEP model 1.0 was used which assumes isotropic behaviour with values of Young's modulus ($10{,}000 kPa$) and Poisson's ratio (0.2). Additionally the cards expressing material density and the thickness for plane stress problems were set at unity. The non-linear material properties were defined by ICFEP model 82 (see Appendix A3) which considers partly saturated 3D Mohr Coulomb conditions. During all the runs the following values were adopted: cohesion of 1000kPa, effective angle of shearing resistant of 30° and angle of dilation of zero. The high value of cohesion was adopted so that the soil behaviour remained elastic. A constant value of Bulk modulus of 166,667kPa was adopted (note that a variable bulk modulus can be implemented as discussed in Chapter 3, but was not applied in any of the analyses). Equally constant values of suction at the air entry value and in the long term of 40 and $100{,}000 kPa$ respectively were used.

The input parameters that were *varied* during the parametric study were the terminal residual suction, the saturated permeability and the ratio of the maximum to minimum permeabilities. The saturated permeability was used for modelling steady state seepage conditions when there are no changes in suction in the field, i.e. as a consequence of performing the infiltration test. This parameter is input under 'Seepage Properties' required in ICFEP (model 2.0, see Appendix A3). The variable permeability was used for modelling transient conditions during the infiltration test when suctions in the field are changing. This quantity is expressed using the ratio of maximum to minimum values of permeability relating to the permeability at the air entry suction (i.e. saturated permeability) and at the initial residual suction respectively. This parameter is input under 'Variable Permeability' in ICFEP (model 1.0, see Appendix A3).

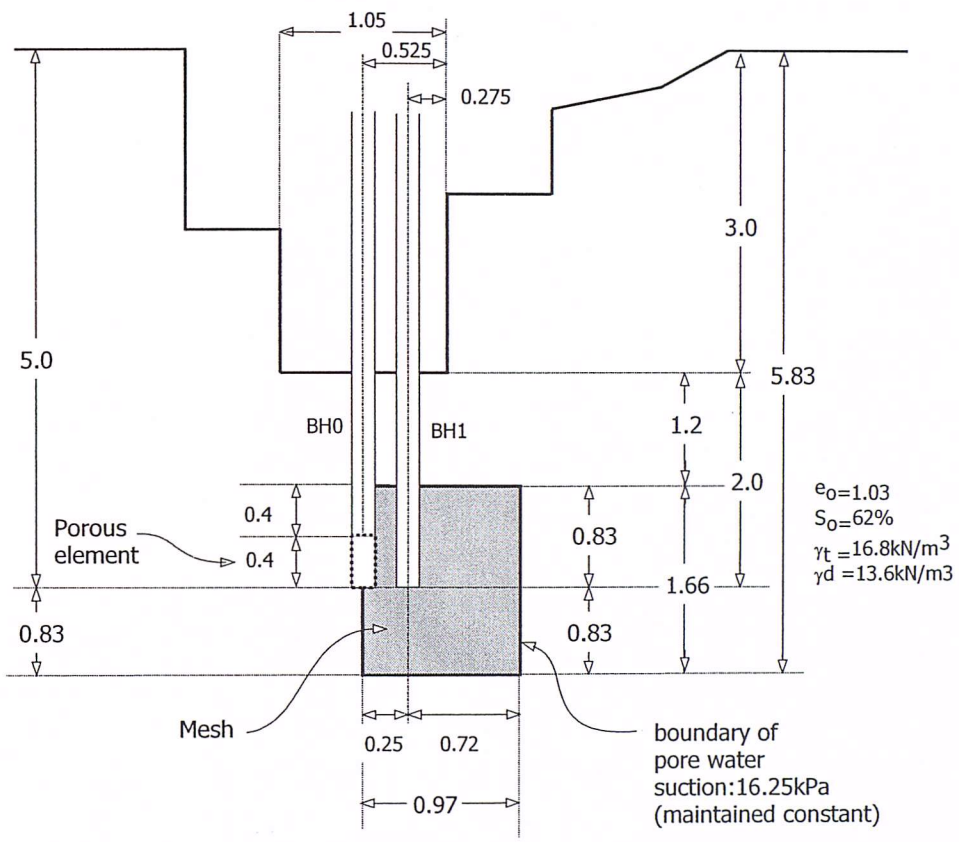

Figure 8.10 Extent of the mesh within the ground profile of the test site. Not to scale, measurements in metres

The parameters defining the SWRC were also varied. ICFEP model 3 was used (see Chapter 3) which requires suction values at desaturation, air entry value, the shrinkage limit (initial residual value), the point at which parameter Ω becomes zero and in the long term (see Chapter 3), along with degree of saturation in the long term and the van Genuchten parameters. The values initially chosen were similar to those given in Table 8.1, which were initially based on those given by Rodriguez (1998). These original values were varied to obtain a best fit to the field data as described below in Section 8.4.

In Figure 8.10 an average value of initial suction of 16.25kPa is shown and the suction at the mesh boundary was kept at the same value. In fact this value was varied slightly to reflect the initial suction registered in the borehole being modelled (see Figure 8.5).

Conditions of zero horizontal displacement were imposed at all boundaries of the mesh and zero vertical displacement at the bottom boundary (see Figure 8.9). The initial pore water suction measured in BH1 ($16.25kPa$) was imposed at the upper and lower boundaries of the mesh and the far boundary (i.e. from points 2 to 3 as shown in Figure 8.9).

The conditions of the falling head tests were modelled by imposing the change in water pressure at the base of the standpipe in BH0 to follow the field observations (see Figure 8.4). This was done over a number of increments (typically 20 and 35 for tests 1 and 2) where generally the maximum change in water pressure was less than 2kPa per increment.

The program requires a period of consolidation for each increment to be defined. It was generally set at one hour.

8.4 PRELIMINARY CURVE-FITTING ANALYSIS

The initial stage of the analysis involved a series of computer runs where the input parameters discussed above were varied to provide a match to the data from falling head test 2 as observed in BH1. Initially only the wetting stage was modelled. The two primary objectives of the curve fitting were to model (i) the rate of change of suction with time and (ii) to achieve the maximum change in suction. As stated earlier, these runs were performed using a single element analysis. After several runs, where the influence of varying the original parameters individually and in groups were investigated, it was found to be impossible to achieve both of these criteria with a single set of parameters (which although varied were generally kept close to those used by Rodriguez).

The best curve fitting data are shown in Figure 8.11. It can be seen that the analyses, using the model described above in Section 8.3 and Chapter 3, provides good results: the form of the field data, with a decrease in suction to a minimum value followed by an increase back towards an equilibrium condition, is well modelled. The data set that matches the rate of change of suction best does not reach the maximum change in suction measured (this data set is referred to as set

1). The analysis that does replicate the maximum change in suction over-predicts the rate of change (set 2). The parameters that were used in sets 1 and 2 are given in Table 8.1. It should be noted that the van Genuchten parameters are different to those given in Table 7.1. This is because the values in Table 7.1 relate to the boundary principal curves while those in Table 8.1 relate to specific scanning curves (even though the scanning curves do ultimately converge to the boundary curves).

It can also be seen that the point at which the suction starts to increase again occurs sooner than that indicated by the measurements. This could result from the fact that the soil parameters are not accurately modelled (particularly permeability). Another factor to consider is that the resolution of the measuring sensor is slightly less than $1kPa$ and so a well defined field curve is not produced.

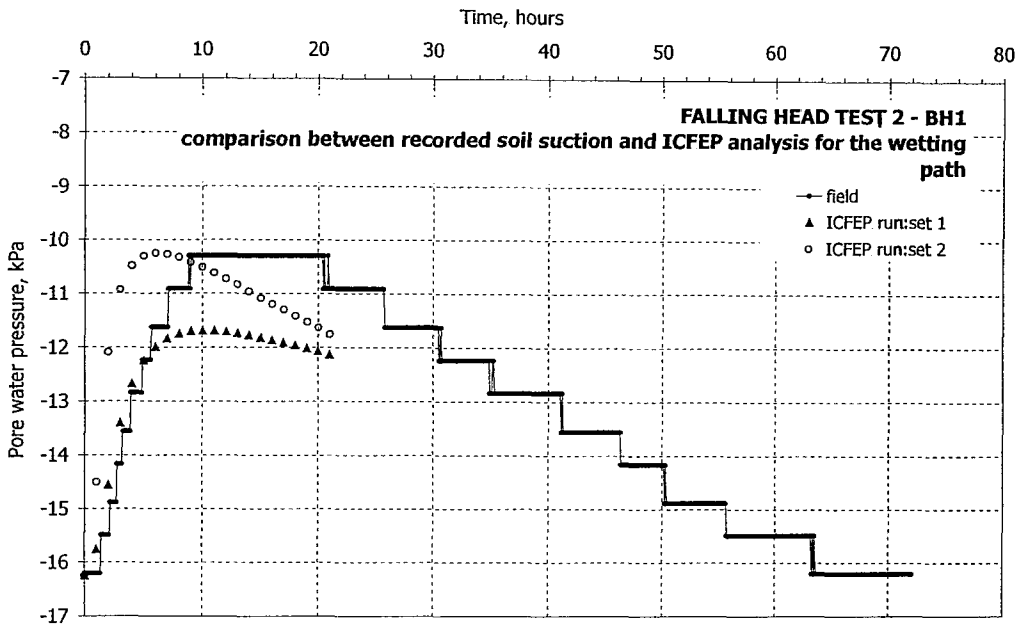

Figure 8.11 Set 1 and 2 from the initial curve fitting analyses

Table 8.1 Parameters of the sets of data

Set	Suction at desa-turation (kPa)	Suction at the AEV (kPa)	Suction in long term (kPa)	S_f (%)	α (kPa)	n	m	Suction at $\Omega \rightarrow 0$ (kPa)	Suction at Sr (kPa)	k_{max}/k_{min}	k_{max} (m/s)
1	10	40	100,000	8.0	340	1.35	0.95	1800	3,800	1,000	$5*10^{-9}$
2	100	150	100,000	8.0	330	2.00	0.5	450	1,800	1,000	$1*10^{-9}$

Following the initial analyses described above, a parametric study was performed in order to analyse the effect of varying some parameters in ICFEP when describing the changes in soil suction for this particular field test (response observed in BH1 during falling head test 2). It soon became evident that performing the parametric analyses on both sets 1 and 2 resulted in very similar trends. Therefore in the following figures and discussion, only the parametric data relating to set 1 are presented.

Figures 8.12 to 8.17 show the effect of changing various parameters describing the SWRC and the permeability function. In each case the values used in the analyses are the same as those given in Table 8.1 except the one being varied. These analyses are now presented and discussed individually.

Varying. α Figures 8.12 shows the effect that α has on the soil suction response during the falling head test 2 recorded in BH1. It can be recalled that α controls the position of the SWRC, moving it to the right as α increases. The range of α values investigated was from 250 to $628kPa$. It can be seen that as α increases the maximum change in suction and the rate of change of suction both increase.

Varying n. Figure 8.13 describes the effect of varying n, which controls the slope of the SWRC. A range of values from 0.8 to 1.8 was investigated. A much greater influence on the results than was observed for varying α is evident, although the trend is the same with the maximum change and the rate of change of suction increasing as n increases.

Varying m. The effect of varying m can be seen from the data set shown in Figure 8.14. Parameter m changes the rate at which the steep part of the SWRC is approached, the larger the m value the sharper the corner. A range of values of m from 0.68 to 1 was investigated. The resulting paths show little variation although it is evident that the maximum change in suction and the rate of change of suction increase with decreasing m value.

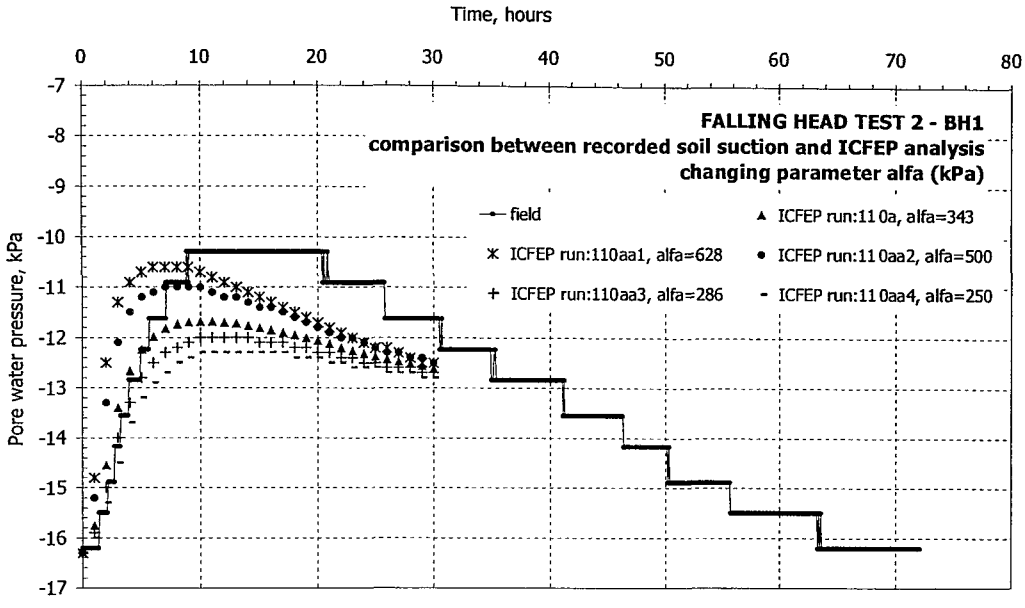

Figure 8.12 Effect of varying α when analysing set 1 using ICFEP

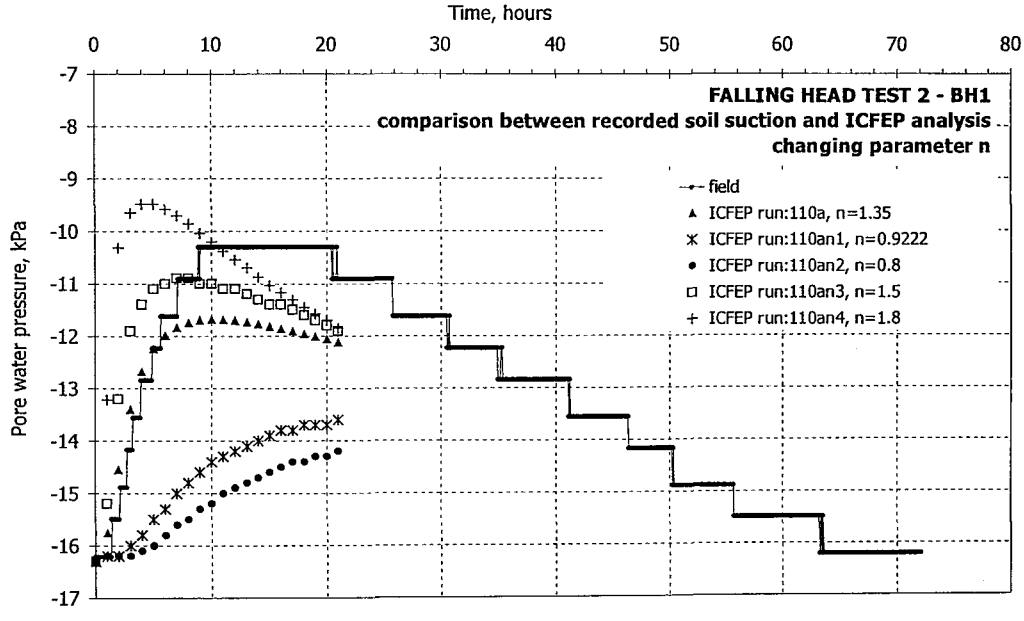

Figure 8.13 Effect of varying n when analysing set 1 using ICFEP

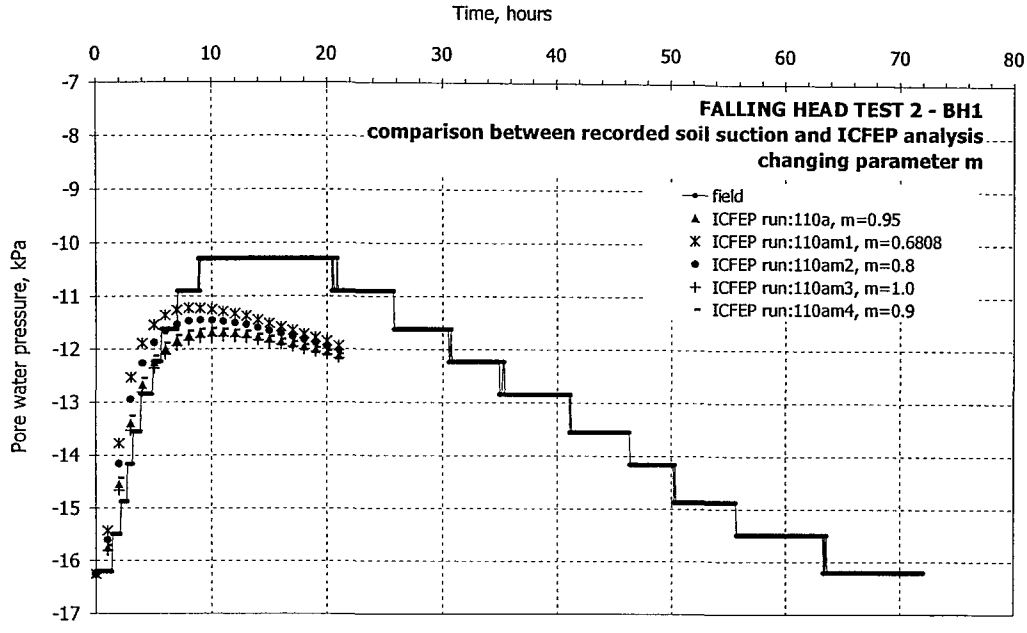

Figure 8.14 Effect of varying m when analysing set 1 using ICFEP

Varying S_r. A range of initial residual degree of saturation values from 4 to 60% vas investigated and the results from the analyses are shown in Figure 8.15. Most of the curves are very similar, only the curve at S_r equal to 60% being markedly different. The overall trend is the same as that for α and n with the maximum change and the rate of change of suction increasing with increasing S_r.

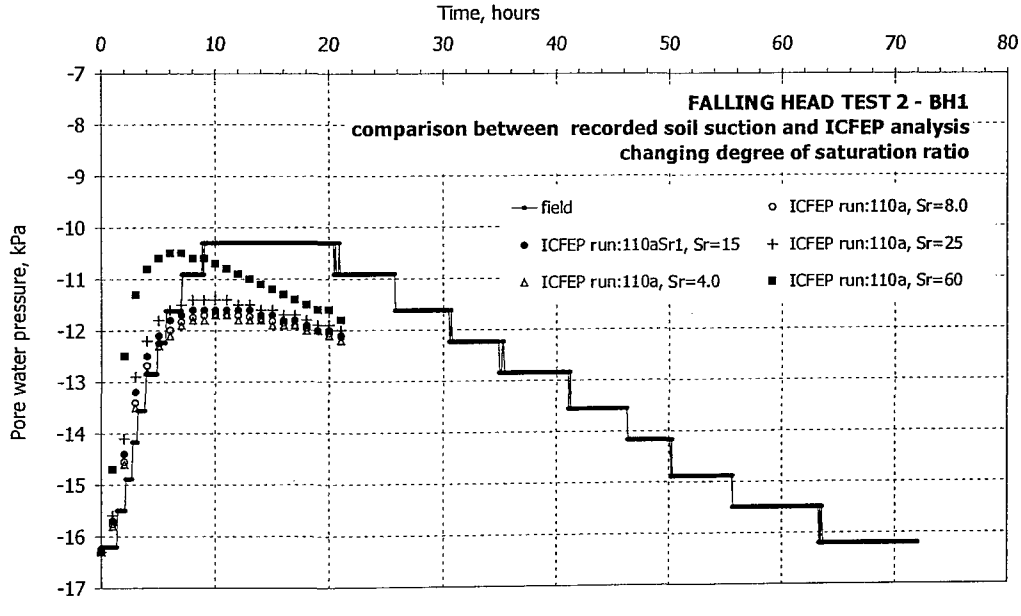

Figure 8.15 Effect of varying S_r when analysing set 1 using ICFEP

Varying k_{max}/k_{min}. There is no discernible difference when changing the ratio of maximum to minimum permeability, even though a large range was investigated, varying k_{max}/k_{min} between 1 and 100,000. The result from the analyses are shown in Figure 8.16.

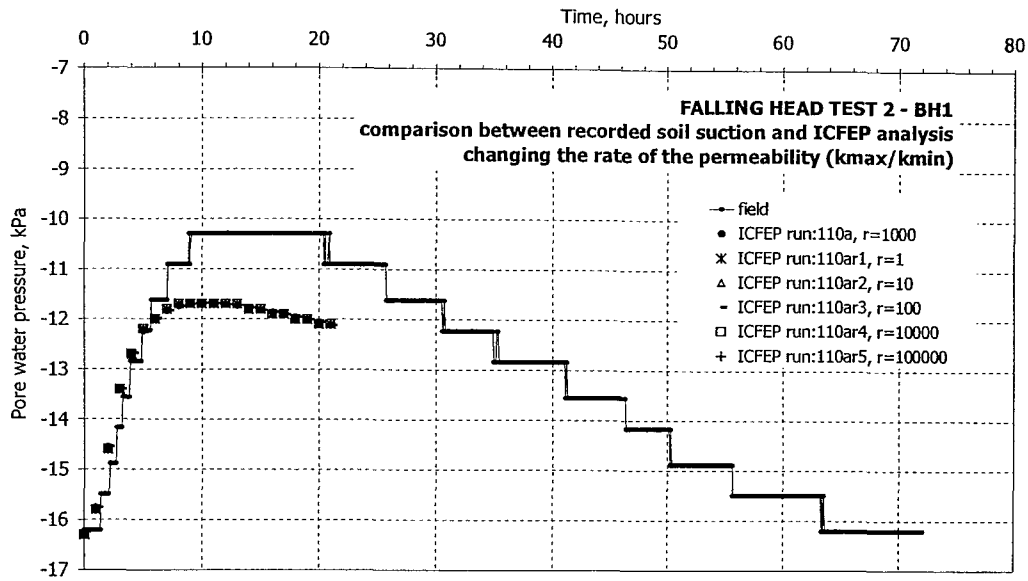

Figure 8.16 Effect of varying the rate (k_{max}/k_{min}) in the permeability function when analysing set 1 using ICFEP

Varying k_{max}. A range of values of permeability from $1*10^{-10}$ to $3*10^{-8}$ m/s was investigated corresponding to the suction at the air entry value. A dramatic variation in curves is evident from Figure 8.17. In the case of the lowest permeability used the curve indicates that the soil is still wetting up at the end of the analysis while the highest value rapidly reaches the end of the wetting cycle and starts drying. The maximum change in suction increases with increasing permeability.

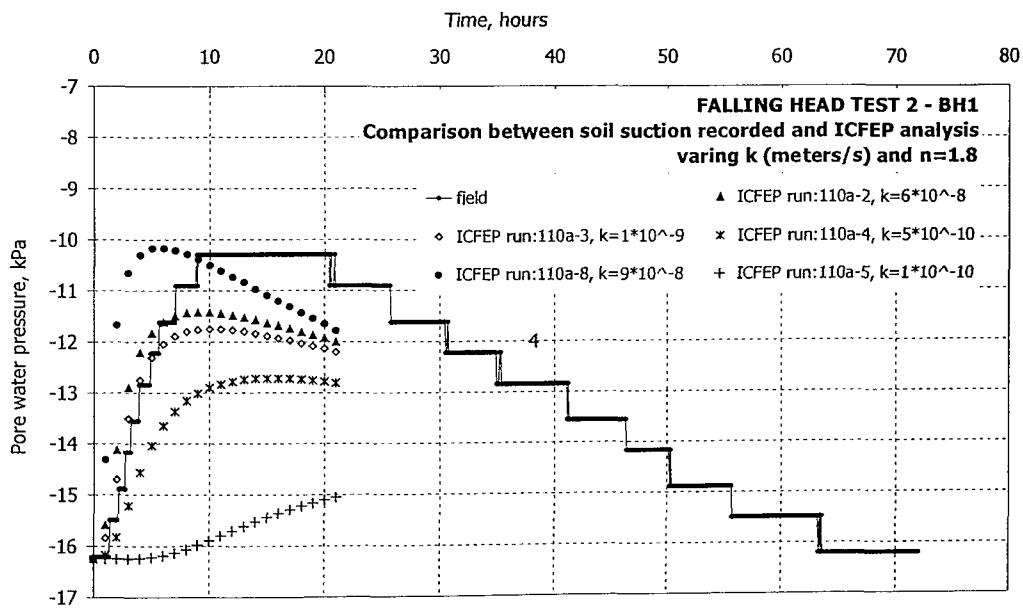

Figure 8.17 Effect of varying the saturated permeability (k_{max}) when analysing set 1 using ICFEP

Of all the parameters investigated k_{max} appears to have the greatest influence on the modelled response for the ranges of the values investigated.

FINAL REFINED ANALYSES 8.6

Following the initial curve fitting and parametric analyses a final refined analyses was performed using soil parameters from Rodriguez but modified to improve the fit accounting for the behaviour observed in the parametric study. The values used and those given by Rodriguez are shown in Table 8.2. The full mesh shown in Figure 8.9 was used for these analyses.

Table 8.2 Parameters used for wetting for the final refined analyses

Set	Suct. at desa-turation (kPa)	Suct. at the AEV (kPa)	Suct. in long term (kPa)	S_f (%)	α (kPa)	n	m	Suct. at $\Omega \rightarrow 0$ (kPa)	Suct. at Sr (kPa)	k_{max}/k_{min}	k_{max} (m/s)
Rodriguez	-----	10	-----	62	22.2	2.65	0.62	-----	-----	-----	$6*10^{-8}$
This study	10	100	100,000	62	47.6	2.65	0.62	8,900	46	8900	$6*10^{-9}$

The first exercise was to model falling head test 2, which is the test which has been analysed so far, looking at the response in BH1. In these analyses only the wetting parameters were used.

The results from this analysis are shown in Figure 8.18. It can be seen that the wetting data are modelled well. At the point when the suction measurements start to increase again there is a sharp change in the results from the analysis. This is because another set of parameters, relating to the drying part of the SWRC, is implemented at this point, i.e. from the time when the field data for BH1 showed suctions starting to increase again, heading towards equilibrium conditions. This corresponds to the time at which water within the standpipe falls to its minimum level and consequently there is no further change in water pressure in the standpipe (BH0). A reasonably match to the measured drying data is obtained. In drying the analysis initially over-predicts suctions and then under-predicts them, with a more gradual response. The output from the analysis relating to BH3 are shown in Figure 8.19. Once again an extremely good match to the wetting response and a reasonably good match to the drying measurements was achieved, although the rate of increase of suction is slightly under-predicted by the analysis.

The same data set was used to model the response measured within BH1 for falling head test 1, implementing the relevant change in water level observed in the standpipe (see Figure 8.4). The results from the analysis are shown in Figure 8.20 and once again excellent agreement is achieved between the field data and the numerical analysis in both wetting and drying.

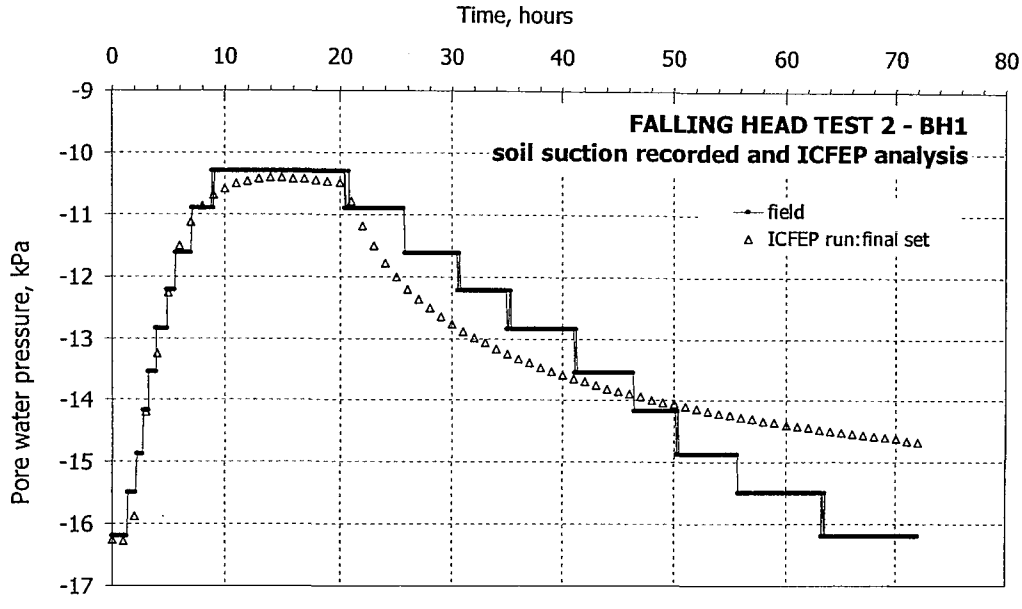

Figure 8.18 Comparison between soil suction recorded and ICFEP analysis using final set

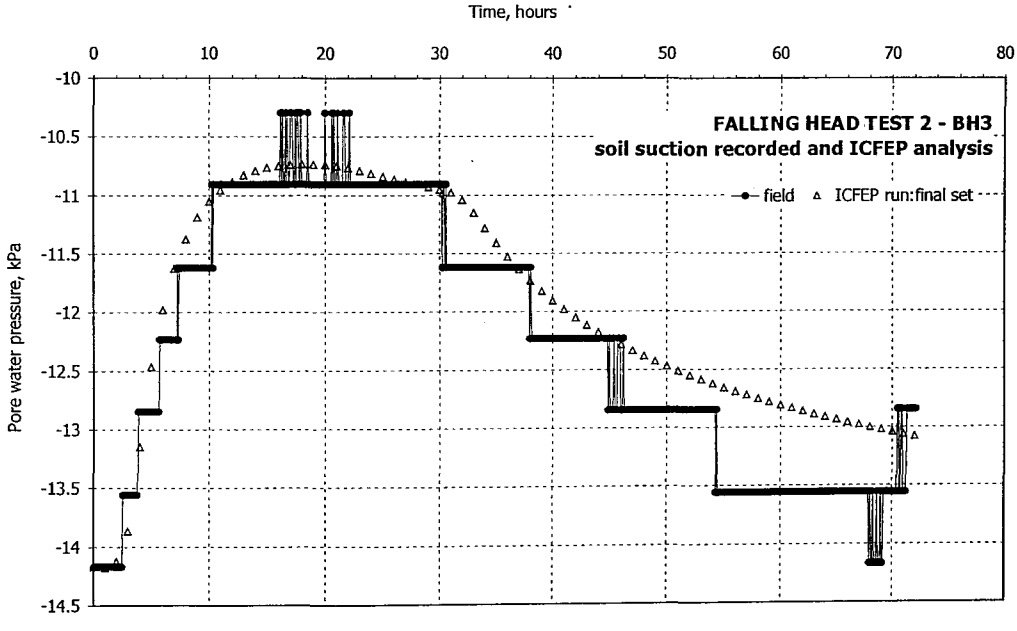

Figure 8.19 Comparison between soil suction recorded and ICFEP analysis using final set

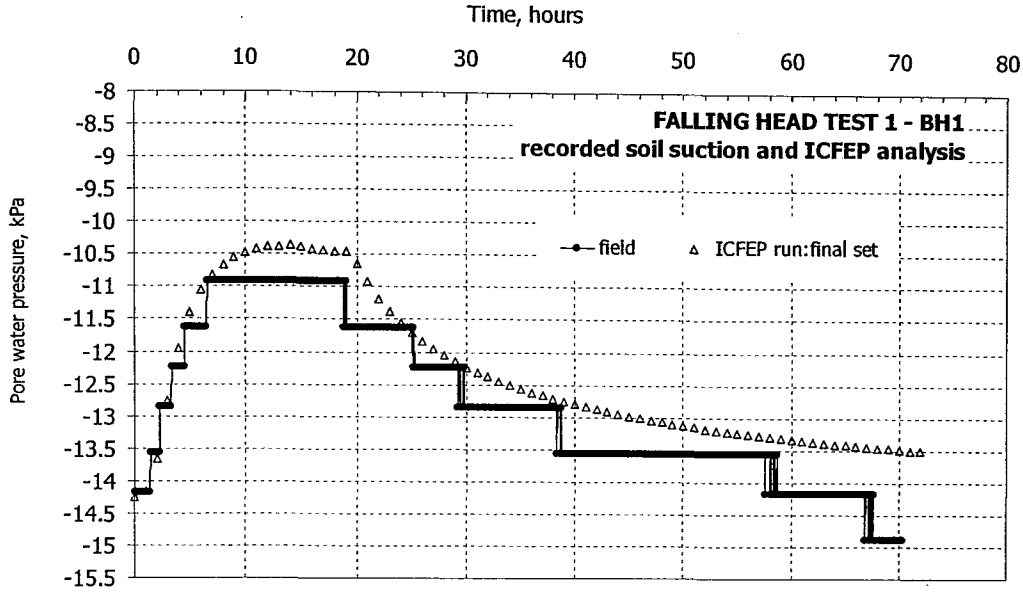

Figure 8.20. Falling head test 1 when analysing final set in ICFEP

Finally the constant head test was analysed using the same refined wetting data given in Table 8.2. The field measurements and the result from the numerical analysis relating to borehole BH1 are shown in Figure 8.21. Once again there is excellent agreement.

The same data set also provided an excellent simulation of the field data from another falling head test and also a constant head test, giving confidence that the parameters used are applicable to these field and test conditions.

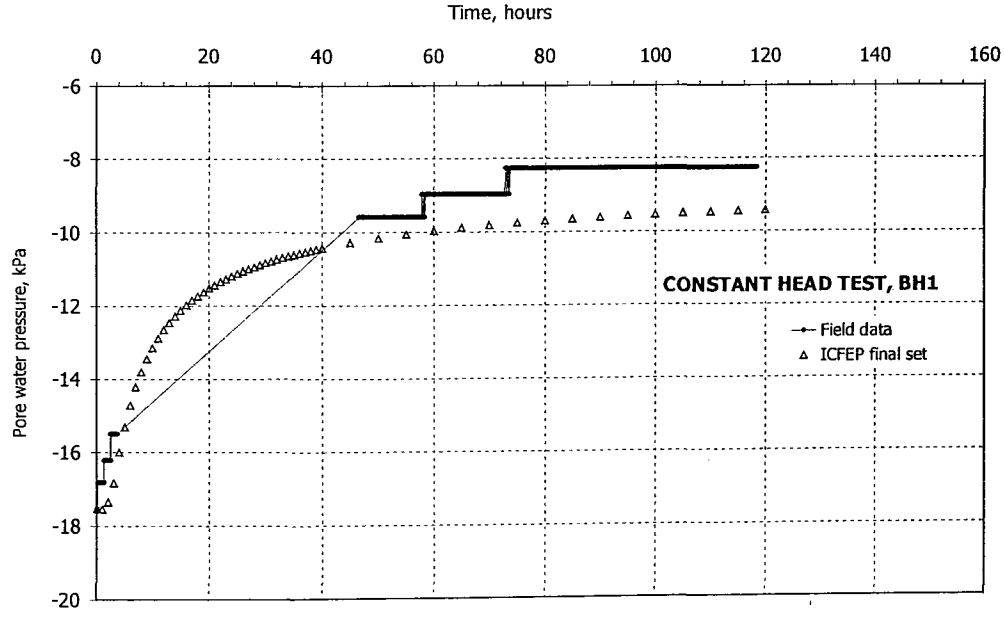

Figure 8.21. Constant head test when analysing final set in ICFEP

CONCLUSIONS FROM F.E. ANALYSES 8.7

It has been found to be possible to obtain a good fit to the field data but so far this has only been achieved by curve fitting. A refined set of parameters that provide very good simulations of the field data from the sensor of closest to the falling head test were found to also give an excellent match with data from the other sensors.

The numerical parametric study performed indicates that the van Genuchten *n* value and the saturated permeability (i.e. that at the air entry value suction) have the greatest influence on the results. Therefore, it is important to determine these values as accurately as possible. However, it is well recognised that measuring permeability in situ is very difficult. The value of permeability that was used in the final refined analysis was an order of magnitude less than that quoted by Rodriguez (1998).

In the analyses performed and described in this chapter only one path has been followed without taking into account the hysteretic nature of the SWRC and its components. Although the results from the analyses give a good match to the field data, it must be remembered that only very small changes in suction took place during the test. Also the degree of saturation was quite high. If conditions were being modelled where significant suction changes were expected, it would be necessary to model the hysteretic response using a formulation similar to that given by Luckner.

The example used in this chapter, where the response of a falling head test at several different locations was measured by individual sensors, illustrates well the complexity of the ground response. It was observed that the response monitored by the different sensors was a function of their offset from the standpipe in which the test was performed. At any one time the ground around one sensor might be wetting up, while at another, drying may have already commenced. This means that different locations within the ground are represented by different points along the hysteresis path (see Figure 8.8).

CHAPTER 9

CONCLUSIONS AND RECOMMENDATIONS FOR FUTURE RESEARCH

Throughout the world many near-surface soils exist in a partly saturated state and as a consequence often have a very different behaviour to fully saturated soils. This is particularly relevant in the analysis of slopes where stability is largely controlled by pore pressure. Smith (2003) has shown that the variation of pore pressure is very sensitive to the relationship between suction and degree of saturation, as represented by the soil water retention curve (SWRC).

The main objective of this thesis has been to investigate the SWRC and in particular its hysteretic response and how to model it most realistically so that it can be incorporated into numerical analyses. A number of findings have emerged during the course of the research. These are now presented as conclusions under different headings.

MEASUREMENT OF SUCTION 9.1

Total suction is the sum of matrix and osmotic suctions. A number of experimental techniques have been used to measure matrix suction, $\psi = u_a - u_w$, representing the component of suction generated by surface tension effects (or capillarity) of the water. Osmotic suction, the other component of total suction, is generated by the different concentration of salts in the pore water. It is generally considered that the osmotic component becomes negligible at high total suction values associated with low degrees of saturation.

Of the techniques available, the filter paper test was performed for the majority of measurements made in the present research and found to be the most reliable, easy to perform and cost–effective test method. Simplistic analyses have been carried out to investigate the likely range of errors that might occur with the measurements. This indicated that accuracy reduces with increasing suction, e.g. accuracies of $\pm 1kPa, \pm 60kPa, \pm 600kPa$ being associated with suctions of about $70kPa$, $1{,}300kPa$ and $14{,}000kPa$ respectively. Also a simplistic parametric study was undertaken to asses the 7-day equilibration period usually allowed. This indicated that seven days is appropriate for most soil types, although it might be

possible to reduce the period significantly for clayey soils within the low suction range (less than $1{,}000kPa$). The permeability of coarser soils reduces much more rapidly with decreasing degree of saturation and in such cases longer test periods might be necessary.

Based on the large number of measurements made and the experience gained, suggestions are made on how to improve the accuracy of measurements with the filter paper technique, particularly in relation to developing the SWRC. The main points are as follows (these should be read in conjunction with the recommendations given by Marinho (1994)).

- The thickness of the sample disk should not be greater than about $20mm$ to avoid excessive equilibration times.
- The diameter of the sample disk should be almost the same size as the filter paper to ensure a uniform moisture content. Equally, the larger the disk diameter, the more accurate the measurement of volume, which is better for defining the SWRC in terms of volumetric water content.
- Although it is important to define adequately the steeply curving parts of the SWRC in wetting, sufficient water should be added to produce definite changes in suction and minimize scatter (caused by evaporation).
- Ideally the sample disks should be stored and the filter papers weighed under conditions of constant temperature and humidity.
- Particular care is needed in the preparation of the more granular reconstituted soils to ensure homogeneous samples and avoid segregation of different particle sizes.

Although recommendations are given here, it should be noted that the quality of the data from the measurements made during the course of the research is generally very good and perhaps better than data sets presented in earlier literature. This most likely arises from the modified procedures described above that were developed and also because of the number of measurements made. This has allowed many behavioural aspects of the SWRC for the different materials tested to be discussed with confidence.

9.2 PROFILES OF THE SWRC AND ITS COMPONENTS

Soil-water retention curves were determined for eight materials comprising artificial and natural soils. Classed within the artificial soils are Kaolin, Embankment Clay (as this came in the form of a block sample of compacted fill) and Ash. The natural soils covered a wide range of Atterberg limits and gradings from UN-Bogota Clay, Weald Clay to residual soils from Brazil, Colombia and Hong Kong. In some cases the SWRC was determined from intact samples, but the resulting curves are primarily

scanning curves. Reconstituted samples are required for the full determination of all components of the SWRC. Except for the Ash material the reconstituted samples were formed from slurry at $1.5(\omega/c)_L$.

The SWRCs have been expressed in terms of log suction plotted against volumetric water content, degree of saturation and void ratio. The error analysis indicated that a more accurate definition of the slope of the curves is likely to be achieved in terms of volumetric water content. This is therefore the quantity discussed in most cases and it is recommended for the best definition of the SWRC.

The main components of the SWRC can be summarized as follows:

- The outer limits of the SWRC, formed by the principal drying and wetting curves (PDC and PWC), are observed to be sigmoidal in shape and hysteretic. To define these, the soil must start from a fully saturated state at a very low suction, i.e. a reconstituted sample formed from a slurry. The soil must be dried sufficiently to reach the terminal residual volumetric water content, prior to wetting.
- If the soil is not dried sufficiently the *main wetting* curve (MWC) is formed which lies just inside the PWC and is sometimes almost coincident with it. As wetting is continued the PWC and the MWC converge. They do not return to the same volumetric water content at which they started, but have a lower value.
- The *main drying* curve (MDC) is formed by drying from this point. Usually the MDC is well below the PDC although it tends to converge towards it during the steep part of the curve when there are large changes in volumetric water content for moderate changes in suction.
- Any paths within the bounds of the MDC and MWC are termed *scanning* curves and can be either wetting or drying. If the paths start from the *main* curves they are primary scanning curves (PSC) while paths issuing from the PSCs are secondary scanning curves (SSC) and from the SSCs are tertiary scanning curves (TSC). Whether drying or wetting, if any scanning curve is continued to a sufficient degree, it will eventually join a main curve (MDC or MWC respectively). Some or all of these various components of the SWRC were observed from the experimental test data from the eight materials, confirming the existence and the hierarchy of their development.

In a number of cases, particularly for the Kaolin a number of almost identical reconstituted samples were formed and these were found to follow the same paths.

The general form of the PDC (or MDC), plotted in terms of void ratio against log suction, is very similar to that observed for a fully saturated sample undergoing consolidation in a oedometer test up to the residual effect point (i.e. the inflection point of the SWRC). This is perhaps not completely surprising. The effective stress

in the fully saturated soil sample, induced by an externally applied total stress is in some respects synonymous to the suction induced in the partly saturated soil by drying but under conditions of zero total stress (in the cases of drying and measuring suction using the filter paper technique). The main differences are that the SWRC in drying or wetting (loading or unloading in the oedometer) has an inflection point; that suction values are much greater than typical effective stresses imposed in the oedometer test and; three-dimensional conditions are relevant to the SWRC compared with the one dimensional oedometer test.

The inflection point along with the parts of the curve where marked changes in degree of saturation or suction occur have significance in terms of the partly saturated state. As the soil dries the air entry value (AEV) roughly corresponds to the point from which significant amounts of air enters the sample and marks the start of the SWRCs transition stage. The inflection point marks the point where the greatest changes in volumetric water content occur.

At the lower end of the curve there is another transition into what is known as the residual effective stage. At this end of the curve large suctions are required to induce relatively small changes in volumetric water content. Although it has not been possible to observe physically the manner in which the air enters the soil, the expected trends in behaviour (as reported by others) are observed in most of the samples.

As a variety of soil types has been investigated it is possible to make some observation about the form and position of the SWRC in terms of soil characteristics.

- Generally samples with high clay content have greater initial void ratios.
- The AEV increases with clay content.
- The slope of the PDC becomes less steep with increasing clay content and activity.
- On wetting from the lower end of the PDC the hysteresis between the PDC and the PWC or MWC also increases with increasing clay content and activity.
- There was essentially no hysteresis for the granular ash material.
- The PWC and the MWC are generally coincident.
- In cases where the clay content is very high (UN-Bogotá Clay and Embankment Clay fill) it was not possible to develop the full SWRC because of the limitation of suction measurements with the filter paper technique (i.e. suction of 30,000kPa).
- The starting point of the intact samples always lies between the PDC and PWC and their subsequent paths, represented by scanning curves, do not cross these boundaries but usually converge to one of the main curves (MDC or MWC), depending on whether the soil is drying or wetting).
- The form of the scanning curves are similar to that of the PDC, MDC, PWC or MWC with double curvature and a point of inflection.

- The response of the intact residual samples, which are likely to have some degree of bonding and structure, was essentially similar to that of the intact and reconstituted sedimented samples (i.e. their SWRCs were of the same form).
- Two of the materials tested were of compacted soil. The Embankment Clay, though compacted, had been in place for several decades and was likely to have a reasonably uniform distribution of suction within it (its response in terms of the SWRC was similar to that of the reconstituted sample made from the same material).
- The residual soil from Hong Kong was initially in a desiccated condition and it was not possible to trim intact samples. The soil was of quite a granular nature and it was not possible to form homogeneous reconstituted soil samples. Two samples were therefore compacted. The resulting SWRCs were not consistent in either their position or shape. One of the PDCs exhibited what appeared to be a bi-modal form. It was concluded that a reliable repeatable SWRC was unlikely to be achieved with dynamically compacted soils of this nature.

9.3 CURVE FITTING THE PDC AND THE PWC

Several techniques have been suggested in the literature for curve-fitting the boundary curves of the SWRC (i.e. the PDC and the PWC). The equation given by van Genuchten (1980) was adopted in this study. It has similarities to some of the other formulations and was chosen because of its simplicity and because it was one of the earlier models that is well proven. The nature of the equation is such that it can be used to model any of the components of the SWRC. Only the boundary curves were modelled in the first stage to obtain the three unknowns of the equation for both drying and wetting. The three unknowns, denoted α, n and m control the position of the SWRC, its slope and the transitions at each end of the steep part of the curve respectively.

The van Genuchten equation was found to fit the data well in most cases except at the upper and lower of the steeply sloping part of the PDC. The main exception was the data from the Kaolin samples, which is surprising given that the data from the four samples were very consistent.

The next stage was to implement the van Genuchten equation into a hysteretic model that can then follow the entire path of an SWRC. This was done using Luckner's formulation. To implement this additional quantities are required, namely the volumetric water contents at the start and end of the curve being modelled (e.g. scanning curves).

Luckner's model was applied to the data from five of the samples tested. It was found that generally this model provided a good fit to the scanning curves and the MDC. However, the following disadvantages of the model need to be considered.

- The scanning curves in wetting and drying head towards the volumetric water contents θ_a and θ_f respectively. In practice the data often join the MWC or MDC sooner.
- Wetting paths above θ_a head for this value, implying a decrease in volumetric water content while in fact wetting results in the opposite effect.

The relationship between the van Genuchten parameters and the liquid limit and plasticity index were investigated. It has not been possible to establish any strong trends. This is surprising as generally the soil type was found to control the shape and position of the SWRC (as discussed above) which are controlled by these parameters. Expressing the soil characteristics in terms of plasticity index (primarily) and the shape and position of the SWRC in terms of the van Genuchten equation parameters α, n and m has not produced trends that are defined well enough to be used to generate SWRCs reliably or accurately. Other parameters, for example relating to the particle size distribution curve need also to be taken into account.

9.4 IMPLEMENTING THE SWRC INTO F.E. ANALYSIS

F.E. analyses using ICFEP were performed to model conditions in the ground around a standpipe in which falling head tests and a constant head test were carried out. In the field the ground response was monitored using suction probes devices.

The data from one of these sensors were used to generate a best fit curve and the required van Genuchten parameters. A parametric study was then performed varying each component of the model one at a time while holding the others constant. This exercise showed that the critical variables are the saturated permeability and the van Genuchten n value (that controls the slope of the steep part of the SWRC).

With the information gained from the parametric study, the initial analysis was repeated to achieve an excellent fit. Additionally the responses observed at the other sensor locations and for other tests were found to be very well modelled. Although this gives confidence that the parameters used were appropriate to the ground and test conditions at this site it must be remembered that the modelling was based on a curve fitting exercise.

Additionally, the modelling was performed using only data for a wetting scanning curve, even though the ground response was a combination of wetting followed by

drying. This was probably acceptable as the suction changes were very small. For cases where significant suction changes are expected it would be necessary to implement a hysteretic model, such as that described by Luckner.

9.5 RECOMMENDATIONS FOR FUTURE RESEARCH

The subject of this thesis is part of the newly developing area of soil mechanics involving partly saturated soils. Although much work and progress has been made in the study of partly saturated soils, there is still much to be learnt and understood because it is still comparatively new and perhaps more importantly because the behaviour of partly saturated soils is very complex!

The research and conclusions discussed in this thesis aim to contribute towards this developing subject, both in providing new experimental SWRC data and discussing their mathematical representation for implementation in numerical analysis. The following topics suggested for further research are based around some of the specific areas covered in this thesis.

The SWRCs for eight soil types have been investigated in this thesis, covering a wide range of soil types. For a better understanding of the SWRC relationships, further experimental data are required. This is particularly relevant for investigating relationships between soil characteristics such as plasticity index and parameters used to define the SWRC mathematically (e.g. the van Genuchten parameters).

The experimental determination of the SWRC can be a very time-consuming exercise, taking in some cases a period of years. Further research is required to optimise this process and time period as efficiently as possible. For example, a method for obtaining the SWRC for coarse, i.e. granular, soils in a matter of days from a continuously monitored drying sample has been recently been suggested by Toker et al (2004).

Partly saturated soil mechanics is particularly relevant to residual soils which are usually found near-surface and are affected by wetting-drying cycles and prevalent in many vast regions of the world. The behaviour of these soils is additionally complex because of their structure and bonding but also because of their propensity to change in terms of plasticity index, permeability etc. on drying. Three residual soils from Brazil, Colombia and Hong Kong have been investigated in this study and the need to gain a better understanding of their behaviour in this respect is clear from some of the results.

Most of the suction measurements reported in this thesis are based on the filter paper technique. Although this technique is well recognised as being reliable and accurate, in its present form it only allows measurements to be made at atmospheric conditions. The dependence of partly saturated soil behaviour on the level of net normal stress has been established by other researchers and needs further investigation to provide a more comprehensive framework of behaviour.

The time required for filter paper measurements can probably be minimised by taking into account the soil type and thickness of the sample. It might be possible to base the former on easily established quantities such as the Atterberg limits. Both areas need further investigation in order to facilitate the compiling of a greater database of SWRCs.

The direct measurement of matrix suction using devices such as the Imperial College suction probe is the key to efficiently producing SWRCs at various total net stress levels. At present these devices have a maximum suction capacity of about $1{,}500kPa$. There is a need and potential to develop devices that can operate at higher suction levels without cavitation and that equilibrate more quickly.

A number of expressions are available for modelling the basic shape and position of the SWRC and its hysteretic response. In this thesis, those proposed by van Genuchten and Luckner, for these two components of behaviour, have been investigated and found generally to model conditions well. There is still scope to improve these models.

In the field, the response of partly saturated soils is frequently controlled by a complex series of wetting and drying cycles. One of the most promising and effective ways of modelling this behaviour is to use advanced numerical analysis (FEA), implementing the hysteretic nature described by the boundary and scanning curves of the SWRC. A numerical analysis using ICFEP was performed in this study with a simplified model for the SWRC. However, a hysteretic model needs to be implemented to achieve a full and continuous soil response for the elements within the soil mass.

In the numerical analysis performed a series of data from field tests and monitoring were modelled. This was achieved using a curve-fitting exercise. It became evident that the suction range covered in these tests was very small and towards the top of the SWRC. An important aspect of in-situ field behaviour, about which a better understanding is required, relates to the realistic range of suctions that a typical soil is subjected to. Although it is important to establish the entire SWRC for an overall understanding of the drying and wetting processes of a partly saturated soil, in practice perhaps a much smaller range would suffice. This would mean that the

relevant part of the SWRC could be investigated experimentally much more quickly using for instance suction measuring devices like the Imperial College suction probe. It might also be possible to optimise the range of the SWRC that needs to be modelled, thus improving on the accuracy of the mathematical simulation of the SWRC and its hysteresis. Establishing typical operating suctions and their variation in situ requires more field monitoring of a range of soils with reliable suction measuring devices that can provide reasonably continuous data.

REFERENCES

Adams, B.A., Wulfson, D. And Fredlund, D.G. (1996) *Air volume change measurement in unsaturated soil testing using digital pressure-volume controller,* Geotechnical Testing Journal, GTJODJ, Vol. 19, No. 1, pp 12-21.

Aitchinson, G.D. (1961) *Relationship of moisture and effective stress functions in unsaturated soils.* Proceedings of Pore Pressure and Suction in Soils Conference, London: England, Butterworths ed., pp. 7-21 [Reported in Fredlund and Rahardjo (1993)].

Aitchinson, G.D. (1965) *Moisture equilibria and moisture changes in soils beneath covered areas.* A symposium in print, Aitchinson, G.D. ed, Australia: Butterworths, 278p [Reported in Fredlund and Rahardjo (1993)].

Alonso, E.E.; Gens, A. and Hight, D.W. (1987) *Special problems soils. General report.* Proceedings of 9th European Conference on Soil Mechanics, Dublin, pp. 1087-1146.

Alonso, E.E., Gens, A., and Josa, A. (1990) *A constitutive model for partially saturated soils.* Géotechnique, Vol. 40, pp.405-430.

ASTM Standard D421-85 Practice for dry preparation of soil samples for particle-size analysis of soils.

ASTM Standard D422-63 Method for particle-size analysis of soils.

ASTM Standard D3152-72 Test method for capillary-moisture relationships for fine-textured soils by pressure membrane apparatus.

Barden, L.; Madedor, A.O. and Sides, G.R. (1969) *Volume change characteristics of Unsaturated clays.* ASCE Journal of Soil Mechanics and Foundation Engineering Division, Vol. 95, S.M. 1, pp. 33-52 [Reported in Fredlund and Rahardjo (1993)].

Barry, B.A., (1978) *Errors in practical measurement in Science, engineering & technology.* Ed. MD Morris. Wiley, New York.

Baver, L.D., Gardner, W.L. and Gardner, W.R. (1972) *Soil physics.* Fourth Edition. John Wiley and Sons, Inc. New York.

Biot, M.A. (1941) *General theory of tri-dimensional consolidation.* Journal of App. Physics [Reported in Fredlund and Rahardjo (1993)].

Bishop, A.W (1959) *The Principle of effective stress.* Teknish Ukeblad, Vol. 106, No. 39, pp. 859-863 [Reported in Fredlund and Rahardjo (1993)].

Bishop, A.W. and Blight, G.E. (1963) *Some aspects of effective stress in saturated and partly saturated soils.* Vol. 13, No.3, pp 177-197.

Bishop, A.W.; Alpan, I.; Blight, G.E. and Donald, I.B. (1960) *Factors controlling the shear strength of partially saturated cohesive soils.* ASCE Conference of Shear Srength of Cohesive Soils, University of Colorado, Boulder, pp.503-532 [Reported in Fredlund and Rahardjo (1993)].

Bolzon, G.; Screfler, B.A. and Zienkiewics, O.C. (1996) *Elastoplastic soil constitutive laws generalized to partially saturated states.* Geotechnique, Vol. 46, No. 2, pp. 279-289.

Brooks, R.H. and Corey, A.T. (1964) *Hydraulic properties of porous media.* Colorado State University Hydrol. Paper, No. 3, pp. 27 [Reported in Fredlund and Rahardjo (1993)].

British Standards Institution (1990) *British Standard Methods of test for Soils for Civil Engineering purposes.* London. BS 1377: Part 2:1990:3.2, *Oven-drying method for water content.* BS 1377: Part 2:1990:9.2, *Wet sieving method for particle size distribution.* BS 1377: Part 2:1990:8.3, *Small pyknometer method for specific gravity.* BS 1377: Part 2:1990:4.3, *Cone penetrometer method (definitive method) for liquid limit.* BS 1377: Part 2:1990:5.3, Method for plastic limit.

Burland, J.B. (1964) *Effective stresses in partially saturated soils.* Geotechnique, Vol. 14, pp. 65-68.

Burland, J.B. (1965) *Some aspects of the mechanical behaviour of partially saturated soils.* Proocedings: Moisture Equilibria and Moisture Changes in Soils Beneath Covered Areas. A symposium in print, Aitchinson, G.D. ed, Australia: Butterworths, pp. 270-278 [Reported in Fredlund and Rahardjo (1993)].

Burland, J.B. (1990) *On the compressibility and shear strength of natural clays,* Geotechnique, Vol. 40, No. 3, pp 329-378.

Burland, J.B. and Ridley, A.M. (1996) *The importance of suction in soil mechanics.* Keynote address. Proceedings of the Twelfth Southeast Asian Geotechnical Conference. Vol. 2, pp.27-49.

Cabarkapa, Z. (2001) *Mechanical behaviour and modelling of unsaturated soils.* PhD Thesis, South Bank University.

Chandler, R.J.; Crilly, M.S. and Montgomery-Smith, G. (1992) *A low-cost method for assessing clay desiccation for low-rise buildings.* Proceedings of Institution of Civil Engineers, Vol. 92, No.2, pp. 82-89.

Chen, Z.H.; Fredlund, D.G. and Gan, J.K.M. (1999) *Overall volume change, water volume change and yield associated with an unsaturated compacted loess.* Canadian Geotechnical Journal, Vol. 36, pp. 321-329.

Childs, E.C. (1969) *An introduction to the physical basis of soil water phenomena.* London: Wiley-Interscience, 493p [Reported in Fredlund and Rahardjo (1993)].

Childs, E.C. and Collis-George, N. (1950) *The permeability of Porous Materials.* Proceedings of the Royal Society. Vol. 201A, pp. 392-405.

Coleman, J.D. (1962) *Stress/strain relations for partially saturated soils.* Geotechnique, Vol.12, No.4, pp. 348-350.

Corey, A.T. (1957) *Measurement of water and air permeability in unsaturated soil.* Proceedings of Soils Science Soc. Amer. Vol. 21, No.1, pp. 7-10.

Craig, R.F. (1992) *Soil Mechanics.* Fifth Edition. Chapman and Hall. London.

Croney, D.; Coleman, J.D. and Black, W.P.M. (1958) *Movement and distribution of water in soil in relation to highway design and performance.* Water and its conduction in soils, Highway research board, special report, Washington D.C., No. 40, pp. 226-252 [Reported in Fredlund and Rahardjo (1993)].

Cui, Y.J. and Delage, P. (1993) *On the elasto-plastic behaviour of unsaturated silt,* Geotechnique, Vol. 47, No. 3 [Reported in Fredlund and Rahardjo (1993)].

Cui, Y.J. and Delage, P. (1996) *Yielding and plastic behaviour of an unsaturated compacted silt,* Geotechnique, Vol. 46, No. 2 [Reported in Fredlund and Rahardjo (1993)].

Dineen, K. (1997) The Influence of Soil Suction on Compressibility and Swelling. PhD Thesis, University of London.

Duddley, J.H. (1970) *Review of collapsing soils.* Journal of Soil Mechanics and Foundation Division, ASCE 96, pp. 925-947.

Escario, V. and Saez, J. (1986) *The shear strength of partially saturated soils.* Geotechnique, Vol. 36, No. 3., pp. 453-456.

Fredlund, D.G. (1964). *Comparison of Soil Suction and One-Dimensional Consolidation Characteristics of a Highly Plastic Clay.* Nat. Res. Council. Tech. Report No. 245. V, Div. of Building Res. , Ottawa, Ont., Canada, 26 pp.

Fredlund, D.G. (1978) *Appropriated concepts and technology for unsaturated soils.* Canadian Geotechnical Journal, Vol. 16, No. 1, pp. 121-139.

Fredlund, D.G. (1985) *Soil mechanics principles that embrace unsaturated soils.* Proceedings of 11th International Society for Soil Mechanics and Foundation Engineering, San Francisco, USA, August 11-15, A.A. Balkena, Rotterdam, Vol. 2, pp. 465-473.

Fredlund, D.G. (1997) *From theory to the practice of unsaturated soil mechanics.* Proceedings of 3rd Brazilian Symposium on Unsaturated Soils, NSAT'97, Freitas Bastos ed., Rio de Janeiro, April 21-25, Vol.2.

Fredlund, D.G. and Morgenstern, N.R. (1976) *Constitutive relations for volume change in unsaturate soils,* Canadian Geotechnical Journal, Vol. 13, No. 2, pp. 262-255.

Fredlund, D.G.; Morgenstern, N.R. and Widger, R.S. (1978) *The shear strength of Unsaturated soils.* Canadian Geotechnical Journal, Vol. 15, No. 3, pp. 313-321.

Fredlund, D.G. and Rahardjo, H. (1988) *State-of-development in the measurement of soil suction.* Proceedings of the international Conference on Engineering Problems of Regional Soils, August 11-15, Beijing, China, pp. 582-588.

Fredlund, D.G. and Rahardjo, H. (1993) *Soil mechanics for unsaturated soils.* John Wiley and Sons, Inc. New York.

Fredlund, D.G. and Rahardjo, H. (1995) *Non-linearity of strength envelope for unsaturated soils*, Proceedings of the 6th International Conference on Expansive soils, New Delhi, pp.45-59.

Fredlund, M.D.; Fredlund, D.G. and Wilson, G.W (1997) *Prediction of the soil-water characteristic curve from grain-size distribution and volume-mass properties.* Proceedings of 3rd Brazilian Symposium on Unsaturated Soils, NSAT'97, Freitas Bastos ed., Rio de Janeiro, April 21-25.

Fredlund, M.D.; Sillers, W.S.; Fredlund, D.G. and Wilson, G.W. (1996). *Design of a knowledge-based system for unsaturated soil properties.* Proceedings 3rd Canadian Conference on Computing in Civil and Building engineering, Montreal, Que., Canada, April 26-28, Canadian Society for Civil Engineering, pp. 659-677.

Fredlund, D.G. and Xing, H. (1994) *Equations for the soil water characteristic curve.*Canadian Geotechnical Journal, Vol. 31, pp. 521-532.

Fredlund, D.G., Xing, A. and Huang, S. (1994) *Predicting the permeability function for unsaturated soils using the soil-water characteristic curve.* Canadian Geotechnical Journal, Vol. 31, No. 3, pp 533-546.

Fredlund, M.D.; Fredlund, D.G. and Wilson, G.W (1997) *Prediction of the soil-water characteristic curve from grain-size distribution and volume-mass properties.* Proceedings of 3rd Brazilian Symposium on Unsaturated Soils, NSAT'97, Freitas Bastos ed., Rio de Janeiro, April 21-25.

Freeze, R.A. and Cherry, J.A. (1979) *Groundwater.* Englewood Cliffs, NJ: Prentice-Hall, 604 pp [Reported in Fredlund and Rahardjo (1993)].

Fung, Y.C. (1965) *Foundations of Solid Mechanics.* Englewood Cliffs, NJ: Prentice-Hall, 525 pp [Reported in Fredlund and Rahardjo (1993)].

Gardner, W.R. (1958) Some steady state solutions of the moisture flow equation with application to evaporation from the water table. Soil Science, Vol. 85, pp. 228-232.

Georgiadis, K. (2003) Development, Implementation and application of partially saturated soil models in finite element analysis. PhD thesis. University of London.

Hilf, J.W. (1956) *An investigation of pore-water pressure in compacted cohesive soils.* Ph.D. Thesis, U.S. Dep. Of the Interior, Bureau of Reclamation, Design and Construction Div., Denver, CO, 654 pp [Reported in Fredlund and Rahardjo (1993)].

Hillel, D. (1998) *Environmental Soil Physics.* Academic Press, San Diego, CA.

Hogarth, W.L.; Hopmans, J.; Parlange, J.-Y. and Haverkamp, R. (1988) *Application of a simple soil-water hysteresis model.* Journal of Hydrology, vol. 98, pp. 21-29.

Houlsby, G.T. (1997) *The work input to an unsaturated granular material.* Geotechnique, Vol. 47, No.1, pp. 193-196.

Jaynes, D.B. (1984) *Comparison of soil-water hysteresis models.* Journal of Hydrology, Vol. 75, pp. 287-299.

Jennings, J.E. (1960) *A revised effective stress law for use in the prediction of the behaviour of unsaturated soils.* Prodeedings: Conference on Pore Pressure and Suction in Soils, Butterworths, London, pp. 26-30.

Jennings, J.E.B. and Burland, J.B. (1962) *Limitations to the use of effective stresses in partly saturated soils.* Géotechnique 12 (2), pp 125-144.

Karube, D. (1988) *New concept of effective stress in unsaturated soil and its proving test.* Proceedings Advanced Triaxial Test on Soil and Rock (eds. R.T. Donaghe, R.C. Chaney and M.L. Silver), ASTM STP 977, pp. 539-552.

Kohgo, Y.; Nakano, M. and Miyazaki, T. (1993) *Theoretical aspects of constitutive modelling for unsaturated soils.* Soils and Foundations, Vol. 33, No.4, pp. 49-63.

Koorevaar, P.; Menelik, G. and Dirksen, C. (1983) *Elements of soil physics.* Amsterdam, The Netherlands: Elsevier, 228pp.

Lambe, T.W. (1960) *A mechanistic picture of shear strength in clay.* Proceedings, ASCE Research Conference on Shear Strength of Cohesive Soils, Boulder, CO. pp. 555-580.

Lloret, A. and Alonso, E.E. (1985) *State surfaces for partially saturated soils.* Proceedings of 11th International Conference on Soil Mechanics and Foundation Engineering, San Francisco, vol. 2, pp. 557-562.

Luckner, L, van Genutchten, M. Th., and Nielsen, D.R. (1989) *A consistent set of parametric models for the two phase flow of immiscible fluids in the subsurface.* Water Resources Research. Vol.25, No. 10, pp.2187-2193.

Maatouk, A.; Leroueil, S. and La Rochelle, P. (1995) *Yielding and critical state of a collapsible unsaturated silty soil.* Geotechnique, Vol. 45, pp. 465-477.

MacNought, (1998). *Final year dissertation,* Dept. Of Civil &Environmental Engineering. Imperial College of Science Technology and Medicine, London (personal communication from Dr. A.M. Ridley).

Mahamoud, M. (1989) Aspects of the measurement of soil strength using rotating shear devices, with particular reference to the Vane test. PhD. Thesis, University of London.

Maksimovic, M. (1993) *Non-linear failure envelope for the limit state design, limit state design in geotechnical engineering.* International symposium, Danish Geotechnical Society, Bui. 10, Copenhagen. [Reported in Cabarkapa (2001)].

Mallants, D.; Tseng, P.-H; Toride, N.; Timmerman, A. and Feyen, J. (1997) *Evaluation of multimodal hydraulic functions in characterizing a heterogeneous field soil.* Journal of Hydrology, Vol. 195, pp. 172-199.

Marinho, F.A.M. (1994) *Shrinkage behaviour of some plastic soils.* Ph.D. Thesis, University of London.

Matyas, E.L. (1967) *Air and water permeability of compacted soils.* In: Permeability and Capillarity of Soils, ASTM STP 417, American Society of Testing and Materials, pp. 160-175 [Reported in Fredlund and Rahardjo (1993)].

Matyas, E.L. and Radhakrishna, H.S. (1968) *Volume change characteristics of partially saturated soils.* Geotechnique, Vol. 18, pp. 432-448.

Modaressi, A. and Abou-Bekr, N. (1994). *A unified approach to model the behaviour of saturated and unsaturated soils.* Proceedings of 8th Int. Conference Computer Methods and Advances in Geomechanics. Balkema, pp. 1507-1513.

Mualem, Y. (1976a) Hysteretical models for prediction of the hydraulic conductivity of unsaturated porous media. Water resources research, Vol. 12, No. 6, pp. 513-522.

Mualem, Y. (1984) *Prediction of the soil boundary wetting curve.* Soil Science, Vol. 137, No. 6, pp. 379-390.

Mualem, Y. and Miller, E.E. (1979) *A hysteresis model based on an explicit domain dependence function.* Soils Science Society of America, Vol. 43, No.6, pp. 1067-1073.

Ng, C.W.W. and Pang, Y.W. (2000) Experimental investigations of the soil-water characteristics of a volcanic soil. Canadian Geotechnical Journal, Vol. 37, No. 6, pp. 1252-1264.

Oberg, A.L. and Sallfords, G. (1997) Determination of shear strength parameters of unsaturated silts and sands based on the water retention curve. Geotechnical Testing Journal, vol. 20, pp. 40-48.

Parlange, J.-Y. (1976) *Capillary hysteresis and the relationship between drying and wetting curves.* Water Resources Research, Vol. 12, No. 2, pp. 224-228.

Potts, D.M. and Zdravkovic, L. (1999) *Finite element analysis in geotechnical engineering : theory.* Thomas Telford, London.

Poulovassilis, A. (1970) *Hysteresis of pore water in granular porous bodies.* Soil Science, Vol. 109, No.1, pp. 5-12

Rampino, C.; Mancuso, C. and Vinale, F. (1999) *Laboratory testing on an unsaturated soil: equipment, procedures, and first experimental results.* Canadian Geotechnical Journal, Vol. 36, pp. 1-12.

Rampino, C.; Mancuso, C. and Vinale, F. (2001) *Experimental behaviourand modelling of an unsaturated compacted soil.* Canadian Geotechnical Journal, Vol. 37, pp. 748-763.

Richards, B.G. (1966) The significance of moisture flow and equilibria in unsaturated soils in relation to the design of engineering structures built on shallow foundations in Australia. Proceedings: Symposium on Permeability and Capillary, ASTM, Atlantic City, NJ [Reported in Fredlund and Rahardjo (1993)].

Ridley, A.M. (1993) *The measurement of soil moisture suction.* PhD thesis. University of London.

Ridley, A.M. and Burland, J.B. (1993) *A new instrument for the measurement of soil moisture suction.* Géotechnique, Vol. 43, No. 2, pp. 321-324.

Ridley, A.M. and Edenmosun, E.O. (1999) *The influence of pore water salt concentration on the measurement of soil suction using the filter paper method.* In Geotechnics for Developing Africa (eds. G.R. Wardle, G.E. Blight and A.B. Fourie). Rotterdam: Balkema.

Ridley, A.M. and Wray, W.K. (1996) *Suction measurement: A review of current theory and practices.* Unsaturated Soils, Alonso & Delage (eds), pp.1293-1322.

Ridley, A.M.; Dineen, K.; Burland, J.B. and Vaughan, P.R. (2003) *Soil matrix suction: some examples of its measurement and application in geotechnical engineering.* Geotechnique, Vol. 53, No.2, pp. 241-253.

Rodriguez, J.J. (1998) Field Measurement of flow in a partly saturated residual soil. M.Sc. Thesis, University of London.

Smith, P.G.C. (2003) Numerical Analysis of infiltration into partially saturated soil slopes. PhD thesis, University of London.

Toker, N.K.; Germaine, J.T.; Sjoblom, K.J. and Culligan, P.J. (2004) *A new technique for rapid measurement of continuous soil moisture characteristic curves.* Geotechnique, Vol. 54, No.3, pp. 179-186.

Toll, D.G. (1990) *A framework for unsaturated soil behaviour.* Geotechnique, Vol. 40, No.1, pp. 31-44.

Toll, D.G. (1995) *A conceptual model for the drying and wetting of soil.* Proceedings of the First International Conference on Unsaturated Soils. Vol. 2, pp. 805-810. Alonso, E.E. and Delage, P. (Editors). Balkema.

Van Genuchten, M.T. (1980) *A closed-form equation for predicting the hydraulic conductivity of unsaturated soils.* Soil Science Society of America Journal. Vol. 44, pp. 892-898.

Vanapalli, S.K., Fredlund, D.G., Pufahl, D.E. and Clifton, A.W. (1996) *Model for the prediction of shear strength with respect to soil suction.* Canadian Geotechnical Journal, Vol. 33, No. 3, pp 379-392.

Vanapalli, S.K.; Fredlund, D.G. and Barbour, S.L. (1996) *A rationale for an extended soil-water characteristic curve.* Proceedings 49th Canadian Geotechnical Conference, St John's, New foundland, September 23-25, Vol.1, pp. 457-464.

Vanapalli, S.K., Fredlund, D.G. and Pufahl, D.E. (1999) The influence of soil structure and stress history on the soil-water characteristics of a compacted till. Geotechnique, Vol. 49, No. 2, pp. 143-159.

Viaene, P.; Vereecken, H.; Diels, J. and Feyen, J. (1994) *A statistical analysis of six hysteresis models for the moisture retention characteristic.* Soil Science, Vol. 157, No. 6, pp. 345-356.

Wagner, L.E. and Ding, D. (1994) *Representing aggregate size distributions as modified lognormal distributions.* American Society of Agricultural Engineers, Vol. 37, No.3, pp. 815-821.

Wheeler, S.J. and Karube, D. (1996) *Constitutive modelling: state of the art report.* Unsaturated soils, (eds. Alonso and Delage). Balkema, Rotterdam, pp. 1179-1200.

Wheeler, S.J. (1991) *An alternative framework for unsaturated soil behaviour.* Geotechnique, Vol. 41, No. 2, pp. 257-261.

Wheeler, S.J. and Sivakumar, V. (1995) *An elastoplastic critical state framework for unsaturated soil.* Geotechnique, Vol. 45, No. 1, pp. 35-53.

Wheeler, S.J.; Sharma, R.S. and Buisson, M.S.R. (2003) *Coupling of hydraulic hysteresis and stress-strain behaviour in unsaturated soils.* Geotechnique, Vol. 53, No.1, pp. 41-54.

Wong, T.T.; Fredlund, D.G.; Krahn, J. (1998) *A numerical study of coupled consolidation in unsaturated soils.* Canadian Geotechnical Journal, Vol. 35, pp. 926-937.

APPENDIX 1

SURFACE TENSION AND CAPILLARY PHENOMENON

The air-water interface (interface between soil-water and air or contractile skin) is a surface between two immiscible phases. The physical properties of this interface are markedly different from those of the bulk phases on either side. In relation to stresses in soils, the most important characteristic of the interface is the ***surface tension*** (T_s). The surface tension results from the greater attraction of water molecules for each other than for the air above (see Figure A1.(a)). It means that (T_s) results from the intermolecular forces acting on molecules in a contractile skin, which are different from those, that act in the interior of the water mass. The net effect is an inward force at the surface that causes water to behave as if its surface were covered with a stretched elastic membrane or a sort of compressed film.

The pressure difference across the curved surface (Figure A1.1 (b) and (c)) can be related to the surface tension and the radius of curvature of the surface by considering equilibrium across the membrane. In a two dimensional membrane (Figure A1.1 (c)) the equilibrium forces in the vertical direction require that: $2T_s \sin\beta = 2\Delta u R_s \sin\beta$, where $2\Delta u R_s \sin\beta$ is the projection of the membrane on to the horizontal plane. Rearranging gives the pressure difference as $T_s/R_s = \Delta u$. In a three-dimensional membrane (Figure A1.1 (b)), the previous equation can be written using the Laplace equation as: $\left(1/R_1 + 1/R_2\right)T_s = \Delta u$ where, R_1 and R_2, are the radius of curvature of a warped membrane in two orthogonal principal planes (which are equivalent to R_s). If the ratio of curvature is the same in all directions, the previous equation will be $\Delta u = 2T_s/R_s$.

In an unsaturated soil, the contractile skin is called the meniscus, and the contractile skin would be subjected to an air pressure (u_a). This pressure is greater than the water pressure (u_w). The matrix suction is referred to the pressure difference between pore air pressure and pore water pressure $(u_a - u_w)$ acting on the

contractile skin as $(u_a - u_w) = {}^{2T_s}/_{R_s}$. As a result, the radius of curvature of the meniscus decreases if the matrix suction of a soil increases. When the difference between pore air and pore water pressures tend to zero, the radius of curvature tends to infinity, however the air-water interface still exists.

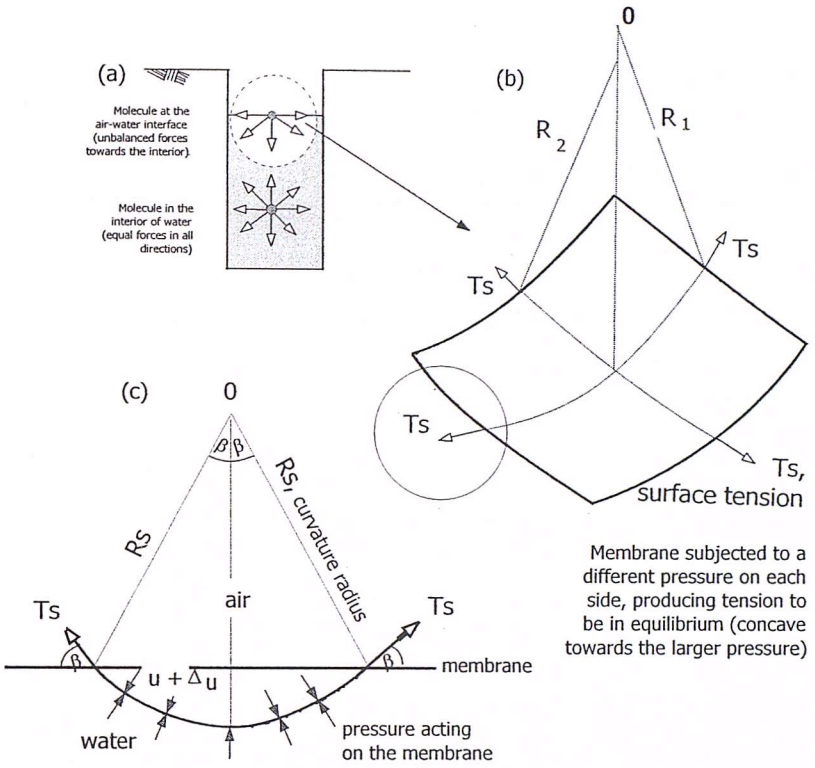

Figure A1.1. Surface tension phenomenon at the air-entry interface (a) molecular forces on the contractile skin and water, (b) surface tension in a three-dimensional warped membrane, (c) pressures and surface tension acting on a curve two-dimensional surface.

On the other hand, capillary pressure is a direct result of surface tension (T_s) and so matrix suction is associated with the ***capillary phenomenon*** from the surface tension. The capillary phenomenon is usually illustrated by the rise of a water surface in a capillary tube (Figure A1.2). Capillarity is due to two forces: the attractive force of water towards on the walls of the channels through which it moves and the surface tension of water which may have any form (i.e. radius) except that of a flat plane at the air-water interface (or contractile skin).

The water rises up in a tube because of the surface tension in the contractile skin and the tendency of the water to wet surfaces because of their hygroscopic properties. From Figure A1.2(a), the surface tension (T_s) acts at a contact angle (β)

from the vertical. The magnitude of β depends on the adhesion between the molecules in the meniscus (contractile skin or air-water interface) and the material of the tube. From Figure A1.2(a) the vertical equilibrium of the capillary water in the tube requires that $(2\pi r T_s \cos\beta) = (\pi r^2 h_c \rho_w g)$, meaning that the vertical component of the surface tension is responsible for holding the water column's weight with height h_c.

Considering the analogy of a capillary rise of water in a small tube (see Figure A1.2(a)), the radius of the tube is analogous to the pore radius in soils. The smaller the pore radius in the soil, the higher will be the capillary height. The weight of the water column is transferred to the tube through the contractile skin. The surface tension associated with the contractile skin results in a reaction force on the wall of the capillary tube (Figure A1-2b) the vertical component produces compressive stresses on the wall of the tube. In the case of a soil having a capillary zone, the contractile skin results in an increased compression of the soil structure (i.e. an increased effective stress). As result, the presence of matrix suction in an unsaturated soil increases the shear strength of the soil.

The surface of the soil-water will be curved (called meniscus) in a capillary tube filled with soil water (Figure A1.2). The partial pressure of the water vapour above the meniscus of soil water (u_a), is less than the partial pressure of the water vapour (relative humidity) above a flat surface of the same water. Accordingly, as the relative humidity in a soil decreases due to the presence of curved water surfaces, the relative humidity decreases as the radius of curvature of the water surface decreases. Therefore, the radius of curvature is inversely proportional to matrix suction $(u_a - u_w)$ across the surface, so the matrix suction contributes to a reduction in a relative humidity.

Figure A1.2(c) shows that at points A and B, the water pressure is the same and equal to the atmospheric pressure (i.e. $u_w = 0$). Additionally, because of the hydrostatic equilibrium, the total head at points A, B, and C is equal to zero. At point C, the pressure head is equal to the negative value of the elevation head at the same point. Accordingly, the water pressure is $u_w = -\rho_w g h_c$. Below point A, water pressures are positive due to hydrostatic pressure, and above point A are negative in the capillary tube. At point C, the air pressure is atmospheric and the water pressure

is negative. Therefore, the matrix suction (or capillary pressure) can be expressed as $(u_a - u_w) = \rho_w g h_c$ which can be expressed as $(u_a - u_w) = {}^{2T_s}/_{R_s}$. In soils, the radius of curvature R_s, can be considered to be the pore radius, r, by assuming zero contact angle. Consequently, the smaller pore radius of a soil, the higher the soil matrix suction.

In soils, pores with small radii, act as capillary tubes, causing the ascent of water above the water table (Figure A1.2(a)). Capillary water pressure (u_w) has a negative pressure with reference to the air pressure (u_a), which is generally zero in the field (Figure A1.2(c)).

The rate of movement of water above the phreatic surface and the amount it rises in soil from the capillary phenomenon is strongly influenced by soil pore size. However, the fact that the soil pores are not straight, uniform openings as is the case with the capillary glass tubes, and additionally because of the fact that some soil pore are filled with air which may be entrapped, the rise and the movement of pore water by capillarity in the soil is slowed down or prevented. The height of rise resulting from capillarity is greater in fine textured soils if sufficient time is allowed and the pores are not too small. With sandy soils, the movement of pore-water is rapid but as many of the pores are not of a capillary size, the height of rise cannot be great.

In the case of salt water T_s will be different hence, the capillary pressure $(u_a - u_w)$, will be affected. In soils, the capillary geometry is more complex than a single symmetrical tube. At any given water content, the matrix suction represents the equivalent capillary pressure that is representative of the particle size distribution of the soil. If it is assumed that surface tension is relatively unaffected by salt concentration the soil matrix for a given soil at a given water content should not be significantly affected by changes in salt concentration.

The height of the water rise and the radius of curvature have direct implication on the water content versus matrix suction relationship in soils (i.e., the soil-water retention curve). This relationship is different for wetting and drying portions of the curve, and these differences can be explained with the capillary model.

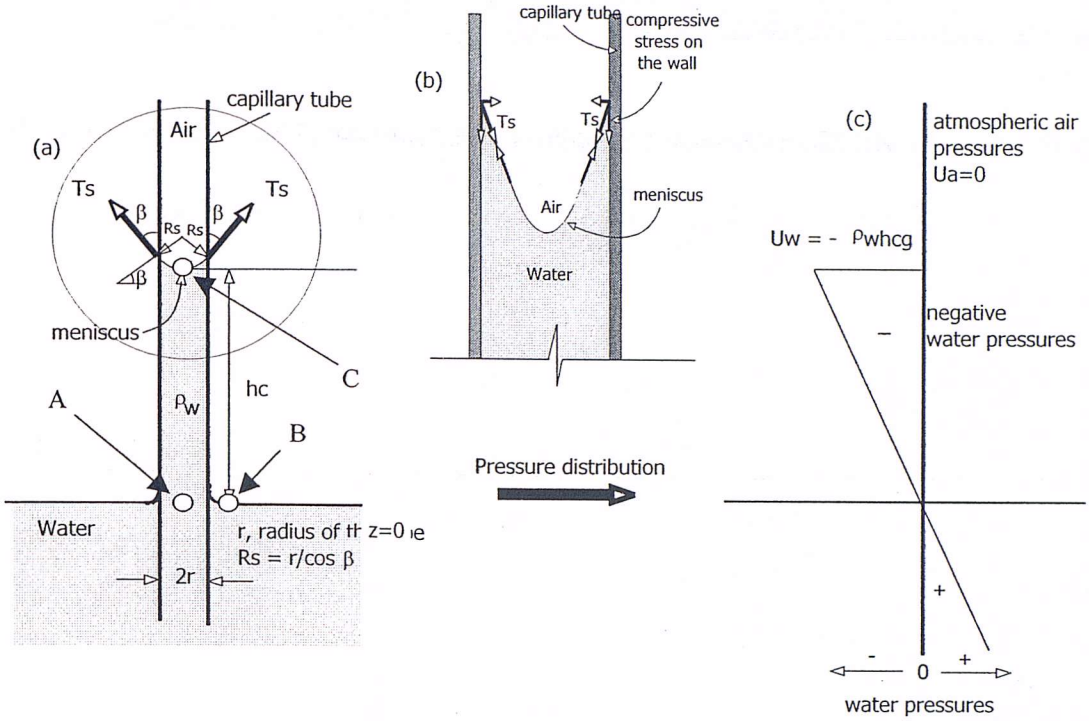

Figure A1-2 (Not to scale). (a) Forces acting on capillary tube (b) Capillary phenomenon (c) physical model

APPENDIX 2

HYSTERETIC MODELS

LINEAR METHOD A2.1

Jaynes, D.B. (1984) first used this two-branch model in 1969. The linear model is characterized by the way it approximates the primary and higher order scanning curves by straight lines spanning the main wetting and drying curves. The scheme calculates the slope based on the shape of the main curves and the initial point of departure from the main curves, these therefore need to be established at the outset. The drying and wetting curves are calculated directly from the equations described in Table A2.1.

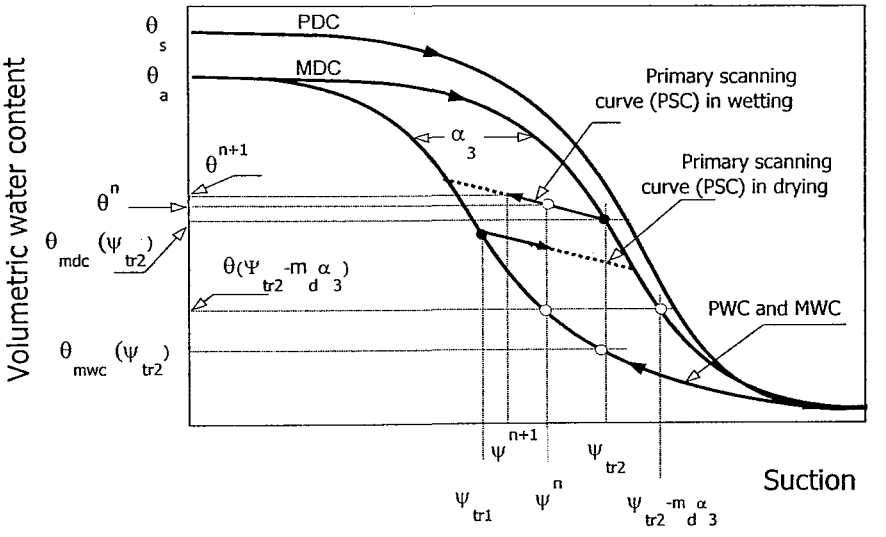

Figure A2.1 Features in the linear method

The method obtains the new value of the volumetric water content, θ^{n+1} for the new scanning curve, from the information given by the main curves. The important features of the linear model are shown in Figure A2.1. These are:

ψ^{n+1} suction at the new volumetric water content, θ^{n+1}

ψ^{n+1}, θ^{n} suction and volumetric water content at a previous calculated point on the primary scanning curve

ψ_{tr1} transition suction pressure at which the soil changes from wetting to drying

ψ_{tr2} transition suction pressure at which the soil changes from drying to wetting

ψ_{AEV} suction at the graphic air entry value

θ_{mwc} and θ_{mdc} volumetric water contents on the main wetting curve and on the main drying curve (volumetric water contents at the suctions (ψ_{tr1}), $(\psi_{tr1} + m_w \alpha_3 \psi_{tr2})$ and $(\psi_{tr2} - m_d \alpha_3)$).

m_w or m_d slope of the scanning curve depending on the process of wetting or drying with the only constraint that it should be less than the slope of the main curves at intersection

α_3 maximum suction difference between the main wetting and drying curves at the same moisture content.

Typical primary scanning curves in wetting and drying of the SWRC from several starting points (named suction at transition point, ψ_{tr}) are shown in Figures A2.2 and A2.3 respectively . The figures show sets of PSCs with a particular constant value of m, which determines the slope of the scanning curves. Figure A2.2 illustrates PSCs in wetting where m is m_w and Figure A2.3 shows PSCs for a particular value of m_d for the drying process.

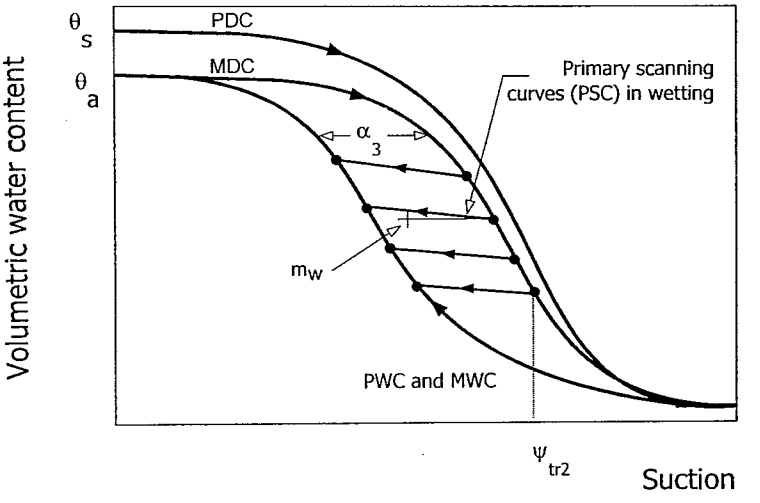

Figure A2.2 Primary scanning curves in wetting defined by the linear method

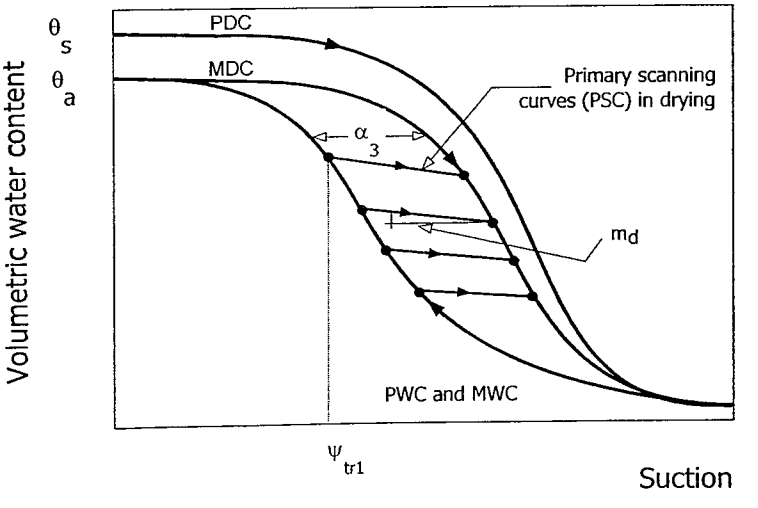

Figure A2.3 Primary scanning curves in drying defined by the linear method

The linear model is constructed such that the primary and the higher order scanning curves must travel along the same path. Figure A2.4 illustrates this property of the method. The linear method assumes that when a scanning curve subsequently changes from wetting to drying or vice versa, it initially follows a single linear curve (i.e. the loop for the scanning curves is closed and they follow a single line). The entire path of each of the primary scanning curves is defined by the equations given in Table A2.1, and the secondary and higher order scanning curves remain on the same line as the primary curves until intersecting one of the main hysteresis curves (i.e. wetting or drying).

The linear method is classified as a 2-branch model, as it describes the scanning curves within two known boundaries (main drying and wetting curves). The method is easy to use, once the m_d and m_w constants are established.

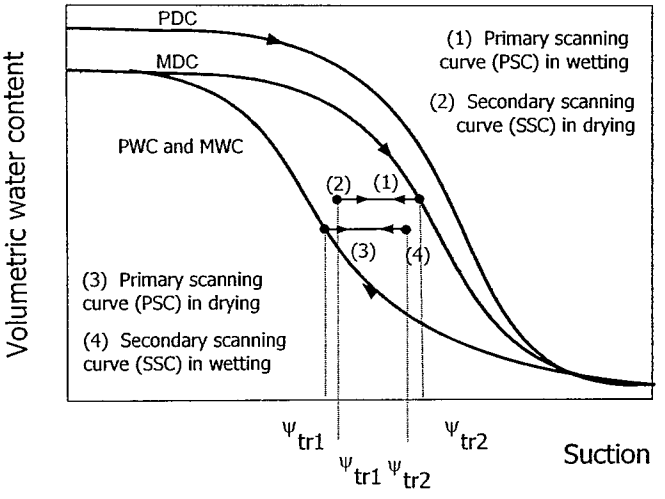

Figure A2.4 Hysteretic loop described by the linear method

PARLANGE'S MODEL A2.2

In this model, knowing one main curve, either the drying or the wetting curve (MDC, θ_{mdc} or MWC, θ_{mwc}), allows the other main curve to be calculated. The model can also be used to calculate the primary and secondary scanning curves[1]. The main parameters used for calculating the new curve using the model are shown in Figure A2.5, where:

θ_d and θ_w volumetric water contents in drying and wetting processes

[1] Note in the literature Parlange refers to primary scanning curves as secondary. In order to avoid confusion and be systematic, the terminology described in Section 2.5 is adhered to.

$\theta_{1w}, \theta_{2w}, \theta_{3w}$ volumetric water contents on primary, secondary and tertiary wetting curves

θ_{ew} volumetric water content at the effective wetting curve (which is the wetting curve starting before reaching the suction at the final residual volumetric water content).

θ_{AEV} volumetric water content at the air entry value, ψ_{AEV}

$\theta_{AEV,mwc}$ and $\theta_{AEV,mdc}$ volumetric water contents at a suction equal to the air-entry value ψ_{AEV} on the main wetting and drying curves respectively

θ_1^* highest volumetric water content of a primary drying curve (for the ψ_{tr1} of a PSC on the effective wetting curve or the PWC)

θ_2^* lowest volumetric water content of effective wetting curve (for the ψ_{tr2} of the effective curve on the MDC)

ψ_{tr1}^* suction on a primary scanning curve in drying for θ_1^*

ψ_{tr2}^* suction on the effective wetting curve for θ_2^*

ψ_u suction on main and effective wetting curves for θ_a

λ Brooks and Corey (1964) coefficient[2]

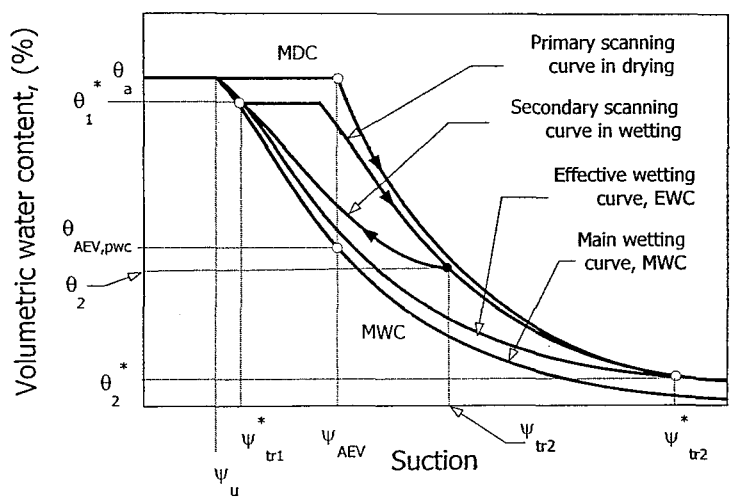

Figure A2.5 Sketch of features of the SWRC defined by Parlange's model

In the model only the MDC is considered without taking into account the PDC. The MDC used has a simplified form compared with that observed in practice (i.e. the form of the curve shown in Figure A2.4). The simplified form is based on the construction used for obtaining the AEV suction, so the initial volumetric water content is constant up to ψ_{AEV} whose location is fixed by extrapolating backwards the linear part of the main drying curve (as described in Section 2.2, Figure 2.6 in the main text). Additionally, the terminal residual volumetric water content is considered to be zero (refer to Figure 2.7 in the main text for terminal residual degree of

[2] The λ coefficient is discussed in Chapter 2 (Section 2.2). It is a pore size distribution index given by the negative slope of the effective degree of saturation versus matrix suction curve.

saturation, the terminal residual volumetric water content corresponds to the same final state). The authors consider that the terminal residual volumetric water content does not have a real physical meaning and it is used in practice as a curve-fitting parameter. Therefore, the model reduces to that of Brooks and Corey (1964) equation by considering θ_f as zero.

The drying and wetting scanning curves can be related following Parlange (1976) and Hogarth et al. (1988) using the equations in Table A2.1. Knowing one curve MDC or MWC, the other can be calculated (MWC or MDC respectively).

Using the Brooks and Corey (1964) equation, the model proposed the MWC (θ_{mwc}), (see Figures A2.5, A2.6 and Table A2.1) joined at the points $(\theta_{AEV,mwc}, \psi_{AEV})$ and $(\theta_a, \psi_u)$where θ_a is also considered as the maximum moisture content defined under natural conditions (see Figure A2.6). Equally, the model describes the MDC, and scanning curves. The equations for defining the SWRC are given in Table A2.1 and sketches of various sets of curves generated with this hysteretic model are shown in Figures A2.7, A2.8 and A2.9.

The constants ψ_{AEV} and ψ_u are fitting parameters associated with the initial choice of the Brooks and Corey formulation (1964) rather than true physical air and water entry suction values.

With reference to the secondary scanning curves, SSC, in drying, they issue from the MWC at any suction ψ_{tr1} and volumetric water content θ_{mwc}, as can be seen in Figure A2.7 and are characterised by $\frac{\delta\theta}{\delta\psi} = 0$ at $\psi = \psi_{tr1}$ (see Table A2.1). The highest primary scanning curves in drying defined by the model, starts at a volumetric water content of θ_1^* and suction ψ_{tr1}^* (see Figure A2.5) and it is called by Parlange as a primary scanning curve.

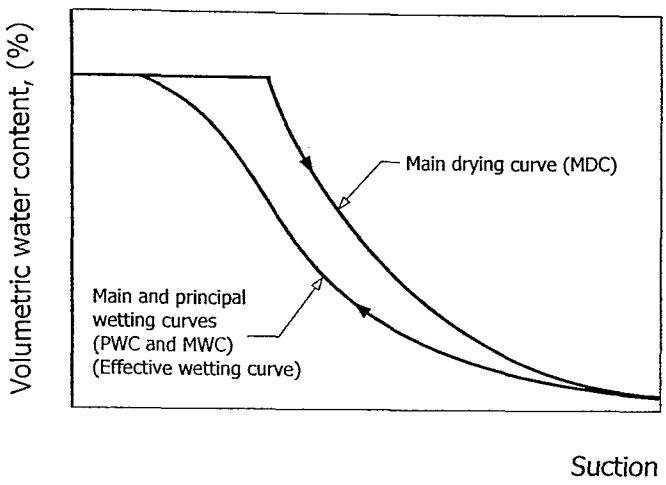

Figure A2.6 Main, principal drying and wetting curves and the effective wetting curve of the SWRC defined by Parlange's model

The MWC is rarely measured, even for a completely dry soil. The model defines an effective wetting curve (EWC) which starts at θ_2^* (see Figure A2.5) and is a lower limit for θ. The θ_2^* plays a role similar to the terminal residual volumetric water content, except that it is considered as a starting point of the wetting curve in an incomplete set of measured data on the initial drying curve. Nevertheless, as can be seen from Figure A2.6 to A2.9, the EWC will be the same as the MWC when the measured set of data in drying is completed. The EWC is not considered to relate to a specific physical state.

The effective wetting curve starts from the point $(\theta_2^*, \psi_{tr2}^*)$ (see Figure A2.5). If the EWC is considered as the natural MWC, then the drying curves issuing from the EWC at any point (θ_1, ψ_{tr1}) are secondary scanning curves (SSC) since the EWC is a primary wetting curve equivalent to the MWC (Figure A2.7 and see Table A2.1).

The primary scanning drying curves are used to generate secondary scanning wetting curves (SSC). The starting point for the latter is (θ_2, ψ_{tr2}), the curves can be described as shown in Figure A2.8.

In order to use the hysteretic model defined by Parlange (1976) either the MDC or MWC must be known. The Parlange equations can then be applied to describe either the MDC or MWC (depending on which was used initially) along with primary, secondary and tertiary scanning wetting and drying curves. Normally the initial curve-fit is done for the drying curve (i.e. the MDC) for which experimental data are available. Four parameters are then required, $\theta_a, \psi_u, \psi_{AEV}$ and λ for the

determination of any of the curves. In principle from one single curve any other curve can be obtained by applying this model.

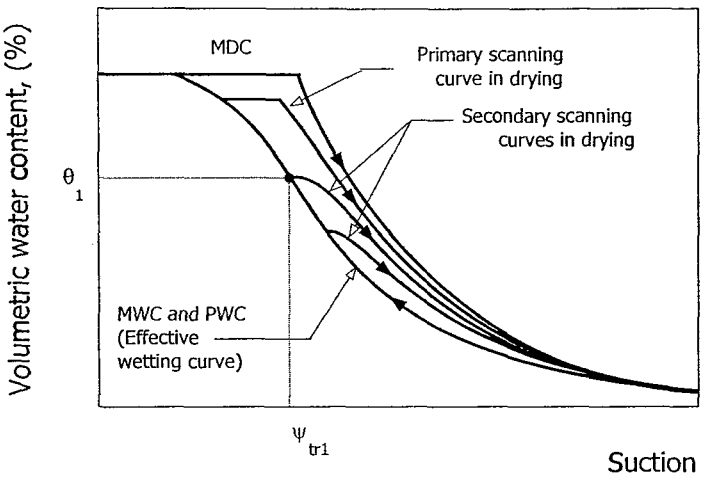

Figure A2.7 Scanning curves in drying process

The author defined the primary, secondary and the tertiary scanning wetting or drying curves as being essentially of the same form as the main wetting and drying curves.

Figure A2.9 illustrates two sets of hysteretic loops starting from particular volumetric water contents on the primary and effective wetting curves. Therefore, hysteretic loops are formed from secondary and tertiary scanning curves. The loops described by Parlange are closed curves that move towards the main drying curve in the direction of θ_a or θ_2^* depending on the sequence of wetting and drying.

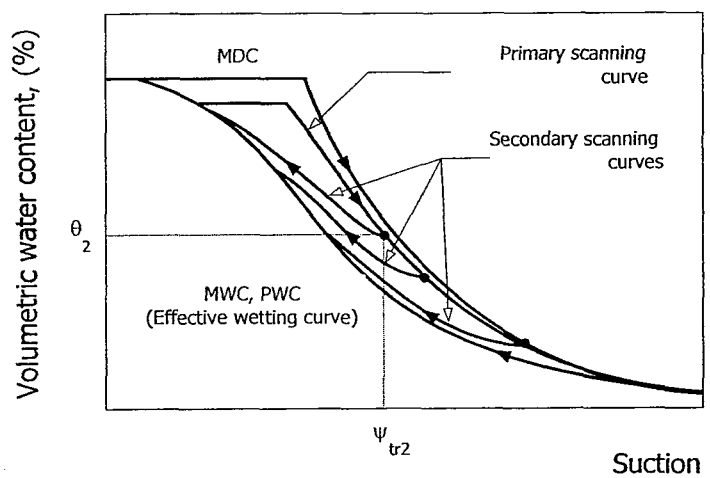

Figure A2.8 Scanning curves in wetting processes defined by the Parlange models

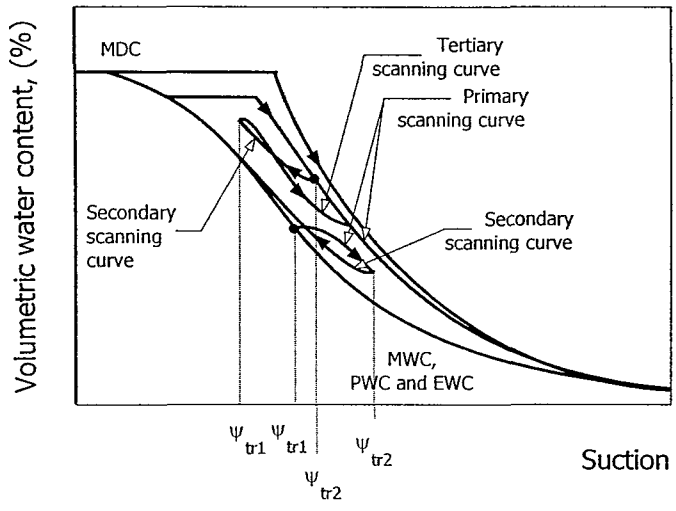

Figure A2.9 Hysteretic loop in the SWCC defined by Parlange et al. (1976)

THE POINT METHOD A2.3

Dane and Weirenga described this method in 1974. The method calculates the value of θ at the new soil-water suction $\left(\psi^{n+1}\right)$ from the volumetric water content values of the main wetting and drying curves, θ_{mwc} and θ_{mdc} in a similar manner as the linear method does. The model is classified as empirical and as a two-branch model. The Point method offers an improvement on the Linear method as the scanning curves produced are more realistic than the straight lines given in the latter.

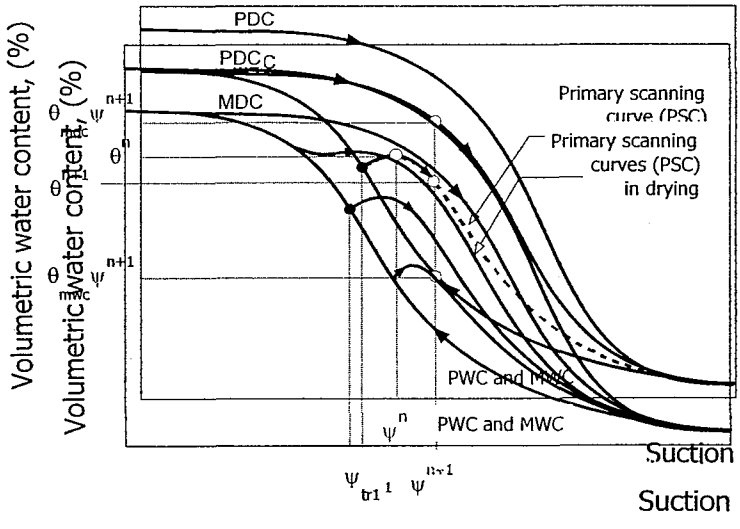

Figure A2.10 Principal feature applying the point method

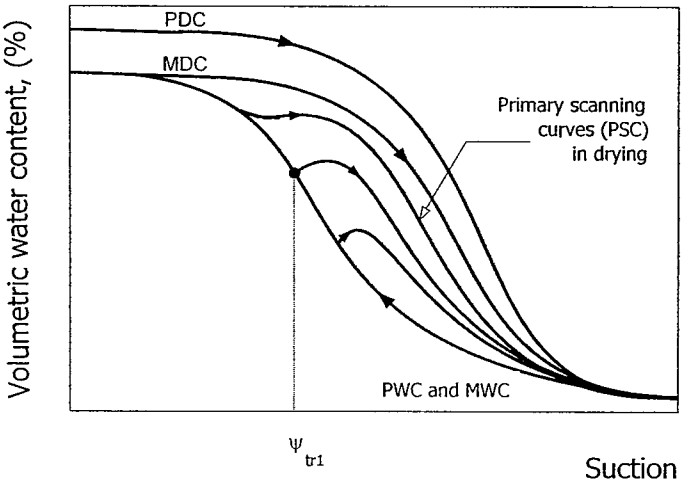

Figure A2.11 Principal scanning drying curves defined by the point method

For wetting processes and the drying processes, Dane and Weirenga (1975) defined the new volumetric water content value, θ^{n+1} as described in Table A2.1 and the formulation is illustrated in Figures A2.10 to A2.13. Figure A2.10 describes the main features for calculating a new curve applying the point method. From Figure A2.10 and Table A2.1, w_w and w_d depend on the volumetric water contents at the transition pressure, ψ_{tr}, and are required for the secondary or higher order scanning curves. C_d and C_w determine the influence of the main drying and wetting curves on the calculated volumetric water content and α_w and α_d determine the rate at which the scanning curves approach the main hysteresis curves for a wetting and drying processes respectively, they are found by trial and error for any soil. The values of α_w and α_d would best be calculated from the information contained in the main wetting and drying curves. However, as the $\alpha-$values vary with the transition suction a first approximation for them can be calculated using the method suggested by Dane and Weirenga (1975).

Figures A2.11 and A2.12 show a typical SWRC and illustrate the PSC in wetting and drying processes respectively starting at different moisture content values on the MDC and MWC.

The Point method creates an unrealistic description in predicting the scanning curves when the sense of changing suction is reversed. That is, the predicted soil moisture content tends at first to increase or decrease when a particular scanning curve is describing drying or wetting respectively (i.e. continue to change in the same sense rather than reverse, like the suction, as would be expected) during the initial fluctuations in suction until some stable volumetric water content value is reached (see Figures A2.11 to A2.13). This effect results from a deviation of the algorithm and is not a real property of soils. In reality, as has been shown in earlier figures, the

volumetric water content and suction both start changing in the opposite sense on a reversal of suction change.

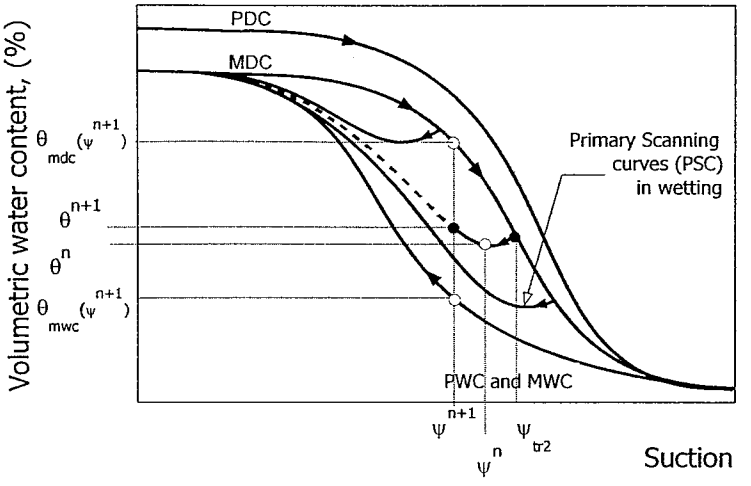

Figure A2.12 Principal scanning wetting curves defined by the point method

Additionally, primary scanning curves in drying described by the point method exaggerate this unrealistic behaviour when they start at relatively high suctions (see Figure A2.11). Conversely, the point method produces the most unrealistic effect when the scanning curves in wetting start at relatively low suctions (see Figure A2.12).

The Point method takes no special precaution to create scanning curves that close, resulting in an unrealistic description of the scanning curves, which significantly affects the performance of the algorithm when it is used to simulate a number of wetting and drying cycles in soils (see Figures A2.13 and A2.14).

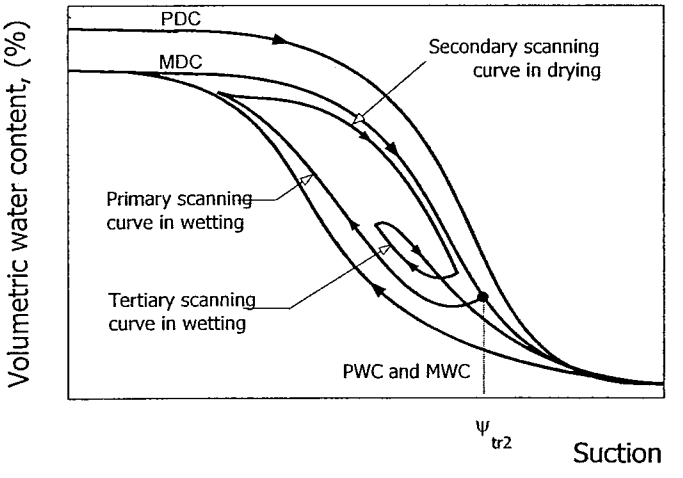

Figure A2.13 Loop of hysteresis defined by point method with PSC in wetting

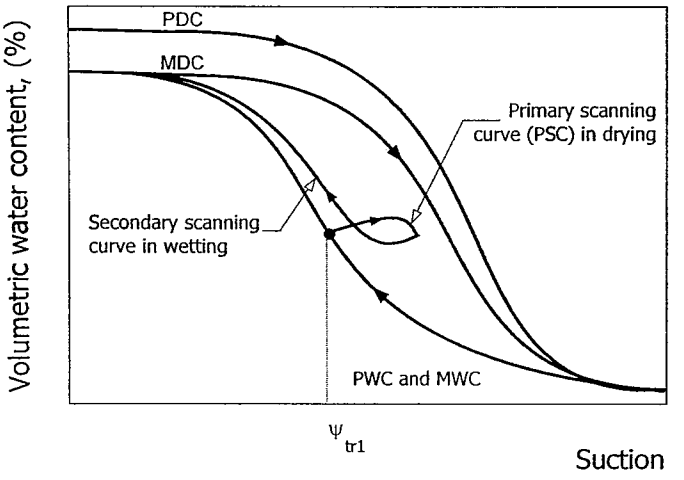

Figure A2.14 Loop of hysteresis defined by the point method with PSC in drying

THE SLOPE METHOD A2.4

This method, given by Jaynes (1984), is a modification of the Point method. In this approach the scanning curves are calculated from the slopes of the main drying and wetting curves ($\delta\theta_{mdc}/\delta\psi$ and $\delta\theta_{mwc}/\delta\psi$) rather than from the volumetric water contents as with the Point method (see Figure A2.15).

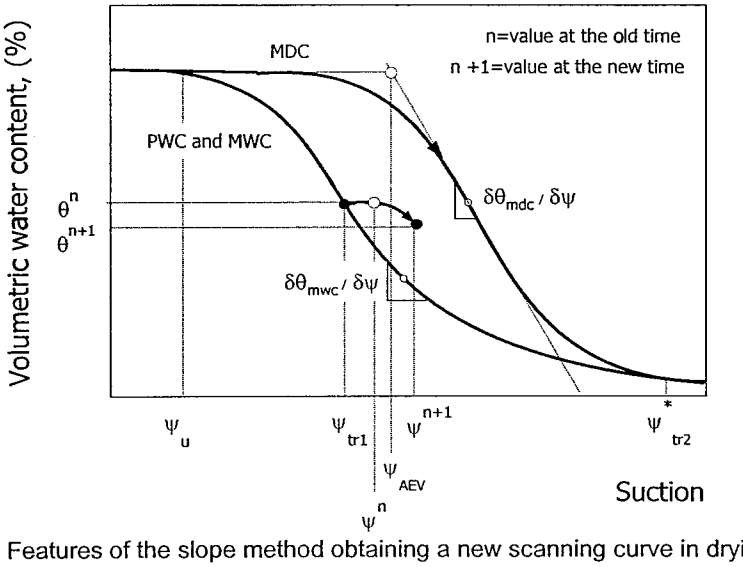

Figure A2.15 Features of the slope method obtaining a new scanning curve in drying processes

The equations for calculating the scanning curves in drying and in wetting are shown in Table A2.1. Primary scanning curves in wetting and drying, issuing from the MDC and MWC respectively, formulated using the slope method, are shown in Figures 2.16 and A2.17

In the same manner as the point method, the slope model does not take special precautions to create scanning curves that close as is seen in Figures A2.18 to A2.20 resulting in a significant effect on the second and third cycle (describing the

secondary and tertiary scanning drying curves). The slope method gives the worst effect when the volumetric water content of the scanning curves in drying is such that they go out of the main boundary loop (see Figure 2.20). Therefore, this model would not be satisfactory for use in situations where numerous wetting–drying cycles are to be modelled.

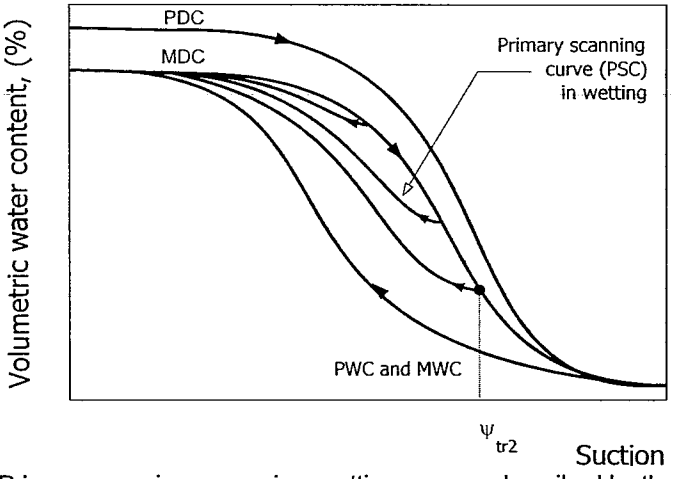

Figure A2.16 Primary scanning curves in a wetting process described by the slope method

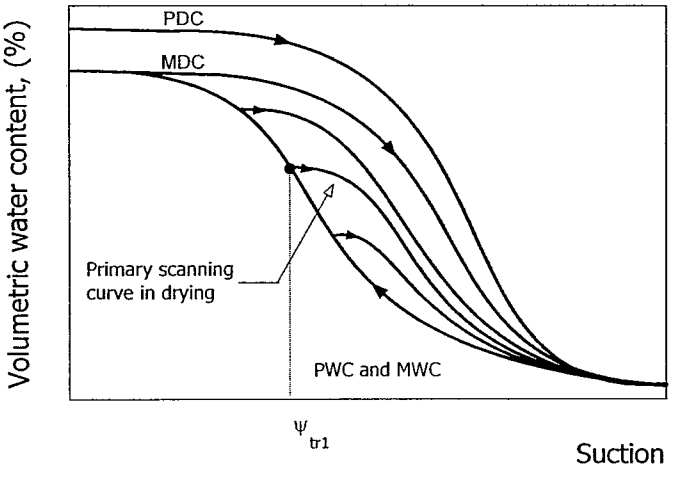

Figure A2.17 Primary scanning curves in a drying process described by the slope method

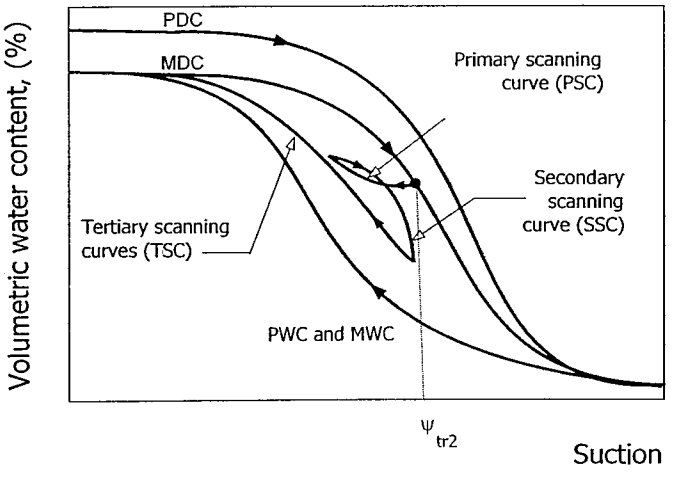

Figure A2.18 Hysteresis described by the slope method

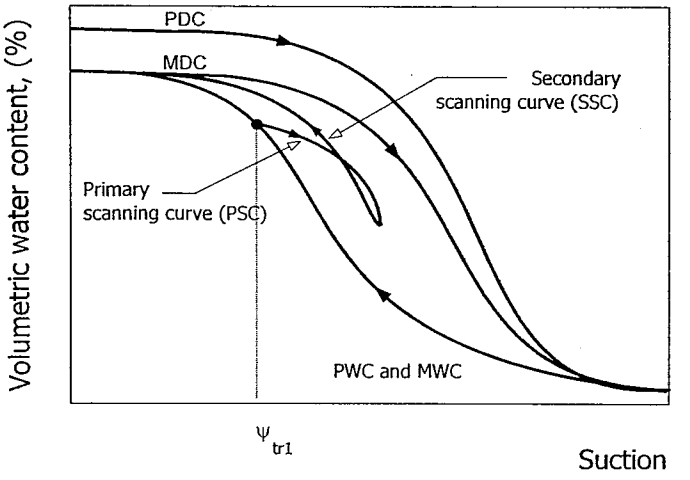

Figure A2.19 Hysteretic loop starting in drying process described by the slope method

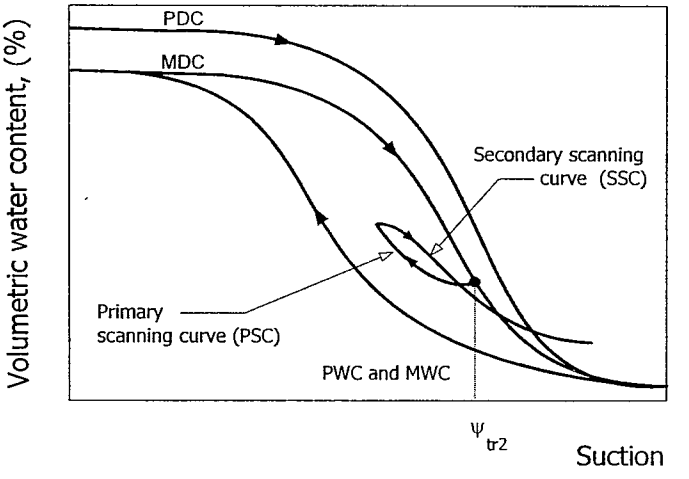

Figure A2.20 Hysteretic loop starting in wetting process described by the slope method

LUCKNER'S MODEL A2.5

A consistent set of parametric models for hysteretic unsaturated fluid phase content and hydraulic conductivity functions of a three-phase system (water and air as fluids and solids) was described by Luckner et al. (1989).

The model defines the hysteretic fluid phase distribution (air and water) as a function of the capillary pressure $\psi_a - \psi_w$ (or matrix suction). However, the model originally employed the pressure head equivalent rather than using suction. The SWRC model is given by the equation described in Table A2.1 and is related to:

Θ normalized volumetric water content

A, B dimensionless scaling factors which depend on θ_f and θ_{ar} (where θ_f is the terminal residual volumetric water content for the wetting fluid (water)

and θ_{ar} is the residual volumetric water content for the non-wetting fluid (air) which is equal to the volumetric water content at saturation θ_s at the maximum volumetric water content for water ($S = 100\%$))

α, m, n experimental constants which affect the shape of the SWRC

ϕ porosity (it should be estimated separately)

θ_w volumetric fluid content (water and air).

The parameters used for applying the model are shown in Figure A2.21.

The Luckner equation contains four unknown parameters θ_f, θ_{ar} and α_d, α_w where the subscripts *w* and *d* on α represent wetting and drying respectively. Luckner et al. (1989) defines θ_a as the volumetric water content of the non-wetting fluid (air), which increases when the degree of saturation decreases. In addition, the model initially assumes that *n* is independent of the saturation history (wetting and drying): an assumption made in many studies of hysteretic fluid flow.

Data in the literature suggest that: $1.25 < n < 4.0, \theta_f \approx 2\theta_{ar}, \alpha_w < \alpha_d$ are suitable for an approximation of the unknown model parameters. Using the latter two relationships, the number of unknown parameters can be reduced to three. However, it may sometimes be necessary to use, different values for ***n***, during wetting (n_w) and drying (n_d as in the case for α) thus leading to an additional unknown in the fluid retention model.

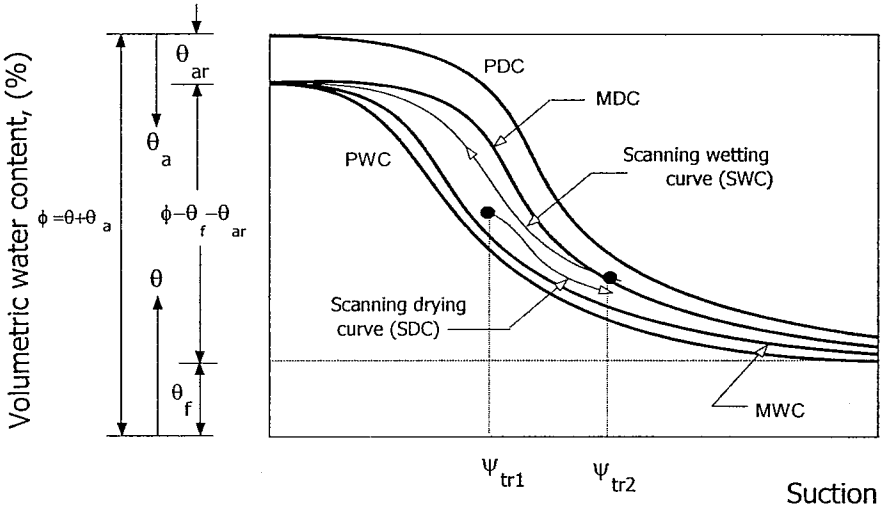

Figure A2.21 Parameters used for applying Luckner's model for the hysteresis in SWRC

Each of the different curves in the SWRC is defined by *A*, *B*, α, m and n. The main drying curve (MDC) is characterised with $A = \theta_f$, $B = \theta_{ar}$, α_d and n_d, and the main wetting curve (MWC) by the parameters $A = \theta_f$; $B = \theta_{ar}$; α_w; and n_w (see Figure A2.21).

The MDC and MWC curves form geohydraulic limits of the hysteretic fluid distribution domain and approach each other asymptotically when $\psi \to 0$ and $\psi \to \infty$. It is only possible to obtain fluid contents outside this domain by normal geohydraulic fluid flow (Luckner et al. 1989). Therefore, if a fully saturated soil sample is generated first by dissolving the randomly distributed non-wetting fluid (air) in the wetting fluid (water) and then removing dissolved air with the flowing wetting fluid, a principal drying curve (PDC) is produced (see Figures A2.22 and A2.23).

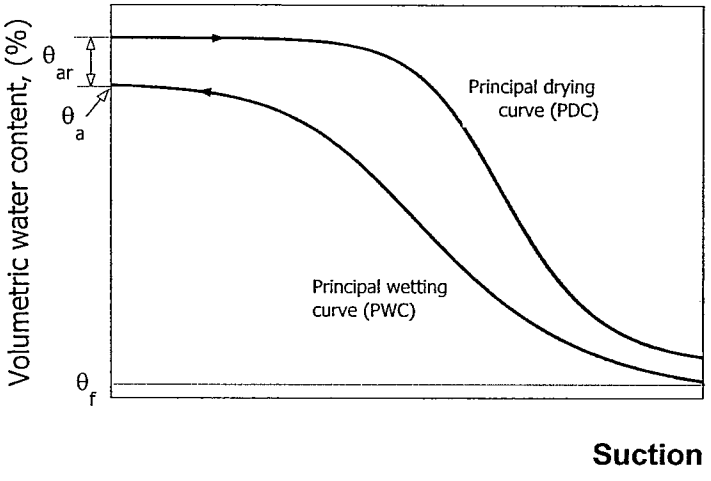

Figure A2.22 Principal drying and wetting curves for a particular SWRC

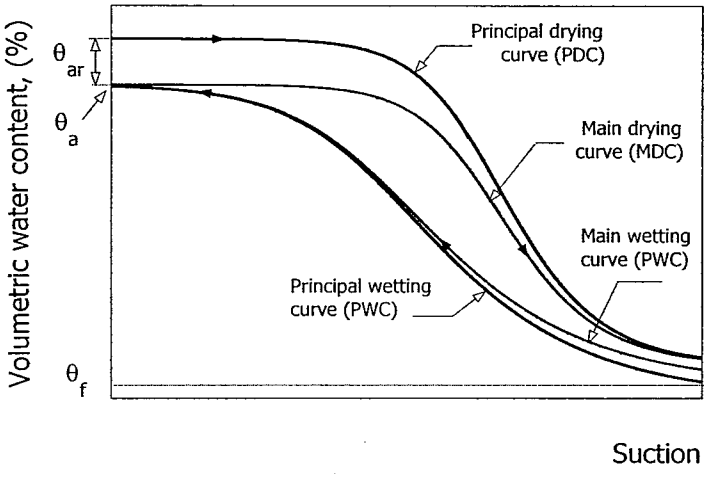

Figure A2.23 Principal and main drying and wetting curves for a particular SWRC

The PDC is used to estimate the parameters from laboratory derived data. The parameters which describe the PDC are $A = \theta_f$, $B = 0, \alpha_d$; and n_d (see Figure A2.23). Similarly, a soil sample which has first been saturated only with the non-wetting fluid (air-evaporating all residual soil water and later removing water vapour) and secondly saturated by wetting (first perhaps, with water vapour and later with liquid water) will generate a principal wetting curve (PWC). The parameters of the PWC curve are defined by $A = 0$, $B = \theta_{ar}, \alpha_w$; and n_w (see Figure A2.23).

The scanning curves can start at any point (θ_{w0}, ψ_0) within the limits of the PDC and PWC curves (see Figures A2.21, A2.24 and A2.25). The scanning wetting curves (SWC) are characterised by the parameters $A = A_w$ (see Table A2.1); $B = \theta_{ar}, \alpha_w$; and n_w, additionally the scanning curves during drying processes (SDC) are defined by the parameters $A = \theta_f$, $B = B_d, \alpha_d$ and n_d respectively (see Figures A2.24 and A2.25).

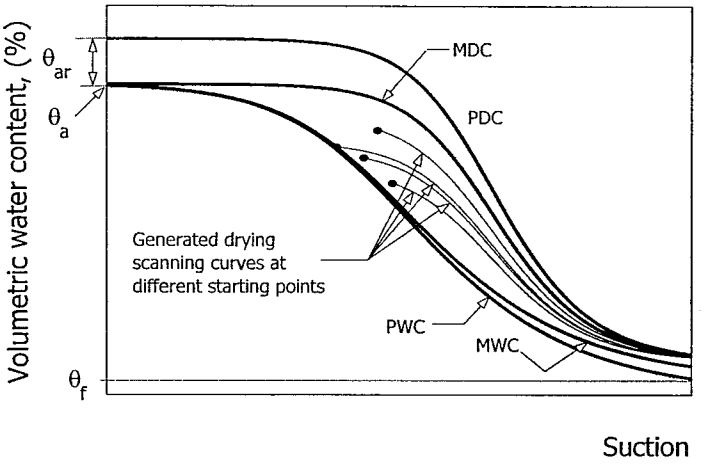

Figure A2.24 Scanning curves in drying processes for a particular SWRC defined by Luckner et. al. (1989)

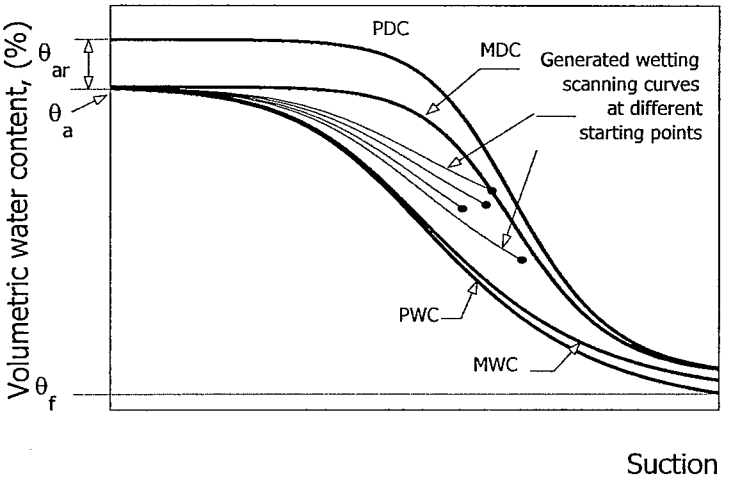

Figure A2.25 Scanning curves in wetting processes for a particular SWRC defined by Luckner et. al. (1989)

As can be seen from Figures A2.24 and A2.25 Luckner et al. (1989) define scanning curves as asymptotic lines at θ_a for the wetting processes and at θ_f for the drying processes respectively. The model also defines hysteretic loops for several drying and wetting processes which are enclosed by the main loop as shown in Figure A2.26.

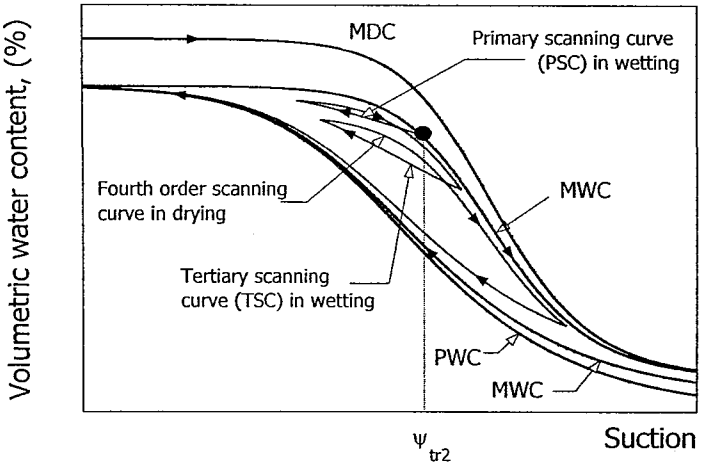

Figure A2.26 Hysteresis described for Luckner's model (1989)

Table A2.1 Proposed equations for describing the SWRC

AUTHOR	WETTING CURVES	DRYING CURVES
Linear	$\theta^{n+1} = \frac{\theta_{mwc}(\psi_{tr1} + m_w\alpha_3) - \theta_{mdc}(\psi_{tr1})}{m_w\alpha_3}\left[\psi^{n+1} - \psi^n\right] + \theta^n$	$\theta^{n+1} = \frac{\theta_{mwc}(\psi_{tr2}) - \theta_{mdc}(\psi_{tr2} - m_d\alpha_3)}{m_d\alpha_3}\left[\psi^{n+1} - \psi^n\right] + \theta^n$
	where: θ^{n+1} new volumetric water content, ψ_{tr} transition pressure, m_w, m_d empirical constants for wetting and drying processes	
Point	$\theta^{n+1} = C_w\theta_{mdc}(\psi^{n+1}) + (1-C_w)\theta_{mwc}(\psi^{n+1})$ $C_w = \frac{\alpha_w}{(\psi^{n+1} - \psi_{tr1} + \alpha_w)}w_w$ $w_w = \frac{[\theta(\psi_{tr1}) - \theta_{mwc}(\psi_{tr1})]}{[\theta_{mdc}(\psi_{tr1}) - \theta_{mwc}(\psi_{tr1})]}$ $\alpha_w = \exp\left(9 + \frac{\psi_{tr1}}{(\psi_{AEV} - \psi_c)}\right)$	$\theta^{n+1} = C_d\theta_w(\psi^{n+1}) + (1-C_d)\theta_d(\psi^{n+1})$ $C_d = \frac{\alpha_d}{(\psi_{tr} - \psi^{n+1} + \alpha_d)}w_d$ $w_d = \frac{[\theta_d(\psi_{tr}) - \theta(\psi_{tr})]}{[\theta_d(\psi_{tr}) - \theta_w(\psi_{tr})]}$ $\alpha_d = (\psi_u - \psi_{tr2})$
	where: w_w, w_d and C_w C_d are weighting factors, α_d, α_w are empirical factors	
Slope	$\theta^{n+1} = w_w\left[\psi^{n+1} - \psi^n\right]\frac{\partial\theta_{mwc}}{\partial\psi} + \theta^n$ $w_w = \frac{\theta_{mdc}(\psi^{n+1}) - \theta(\psi^{n+1})}{\theta_{mdc}(\psi^{n+1}) - \theta_{mwc}(\psi^{n+1})}$	$\theta^{n+1} = w_d\left[\psi^{n+1} - \psi^n\right]\frac{\partial\theta_{mdc}}{\partial\psi} + \theta^n$ $w_d = \frac{\theta(\psi^{n+1}) - \theta_{mwc}(\psi^{n+1})}{\theta_{mdc}(\psi^{n+1}) - \theta_{mwc}(\psi^{n+1})}$ When $\psi \geq 1.5\psi_{AEV}$, θ^{n+1} will be the maximum of the value either the previous equation or the value calculated from the equation: $\theta^{n+1} = \frac{\partial\theta_{mdc}}{\partial\psi} + \frac{\partial\theta_{mwc}}{\partial\psi}^n\alpha_4$ where $\alpha_4 = \frac{\left\lfloor\theta_s - \theta^{n+1}\right\rfloor}{0.1\theta_s}$ if $\alpha_4 \leq 1.0$

Parlange

MWC,(θ_{mwc}):

$$\left(\frac{\theta_{mwc}}{\theta_{AEV,mwc}}\right)=\left(\frac{\psi_{AEV}}{\psi}\right)^{\lambda} \quad \text{for } \psi \geq \psi_{AEV} \text{ and}$$

$$\left(\frac{\theta_{mwc}}{\theta_{AEV,mwc}}\right)=\left(1+\lambda-\lambda\frac{\psi}{\psi_{AEV}}\right) \quad \text{for } \psi_u \leq \psi \leq \psi_{AEV} \text{ and}$$

$$\theta_{mwc}=\theta_a \quad \text{for } \psi \leq \psi_u$$

PSC,(θ_{1w}):

$$\left(\frac{\theta_{1w}}{\theta_{AEV,mwc}}\right)=\left(\frac{\psi_{AEV}}{\psi}\right)^{\lambda}+\frac{\lambda}{\psi_{tr1}}\left(\frac{\psi_{AEV}}{\psi_{tr1}}\right)^{\lambda}\left(\psi-\psi_u\right) \quad \text{for } \psi \geq \psi_{AEV}$$

$$\left(\frac{\theta_{1w}}{\theta_{AEV,mwc}}\right)=\left(1+\lambda-\lambda\frac{\psi}{\psi_{AEV}}\right)+\frac{\lambda}{\psi_{tr1}}\left(\frac{\psi_{AEV}}{\psi_{tr1}}\right)^{\lambda}\left(\psi-\psi_u\right) \quad \text{for } \psi_u \leq \psi \leq \psi_{AEV}$$

$$\theta_{1w} \leq \theta_a \quad \text{for } \psi \leq \psi_u$$

TSC(θ_{3d}):

$$\left(\frac{\theta_{3w}}{\theta_{AEV,mwc}}\right)=\left(\frac{\psi_{AEV}}{\psi}\right)^{\lambda}+\frac{\lambda}{\psi_{tr2}}\left(\frac{\psi_{AEV}}{\psi_{tr2}}\right)^{\lambda}\left(\psi-\psi_{tr1}^{*}\right)+\frac{\lambda}{\psi_{tr1}^{*}}\left(\frac{\psi_{AEV}}{\psi_{tr1}^{*}}\right)^{\lambda}\left(\psi_{tr2}^{*}-\psi_u\right)$$

for $\psi > \psi_{AEV}$

$$\left(\frac{\theta_{3w}}{\theta_{AEV,mwc}}\right)=\left(1+\lambda-\lambda\frac{\psi}{\psi_{AEV}}\right)+\frac{\lambda}{\psi_{tr1}}\left(\frac{\psi_{AEV}}{\psi_{tr1}}\right)^{\lambda}\left(\psi-\psi_{tr2}^{*}\right)+\frac{\lambda}{\psi_{tr1}^{*}}\left(\frac{\psi_{AEV}}{\psi_{tr1}^{*}}\right)^{\lambda}\left(\psi_{tr2}^{*}-\psi_u\right)$$

for $\psi_{tr2}^{*} < \psi \leq \psi_{AEV}$

MDC (θ_{mdc}):

$$\left(\frac{\theta_{mdc}}{\theta_{AEV,mwc}}\right)=\left(\frac{\psi_{AEV}}{\psi}\right)^{\lambda}\left(1+\lambda-\lambda\frac{\psi_{we}}{\psi}\right) \quad \text{for } \psi \geq \psi_{we} \text{ and}$$

$$\theta_{mdc}=\theta_s \quad \text{for } \psi \leq \psi_{AEV}$$

SSC (θ_{2d}):

$$\left(\frac{\theta_{2d}}{\theta_{AEV,mwc}}\right)=\left(\frac{\psi_{AEV}}{\psi}\right)^{\lambda}\left(1+\lambda-\lambda\frac{\psi_{tr2}}{\psi}\right)+\frac{\lambda}{\psi_{tr2}^{*}}\left(\frac{\psi_{AEV}}{\psi_{tr2}^{*}}\right)^{\lambda}\left(\psi_{tr2}-\psi_{we}\right)$$

for $\psi \geq \psi_{AEV}$ and

$$\theta_2=\theta_1 \quad \text{for } \psi_{tr2} \leq \psi \leq \psi_{AEV} \quad \text{if } \psi < \psi_{AEV}$$

Parlange

EWC (θ_{ew}):

$$\left(\frac{\theta_{ew}}{\theta_{AEV,mwc}}\right)=\left(\frac{\psi_{AEV}}{\psi}\right)^{\lambda}+\frac{\lambda}{\psi_1{}^*}\left(\frac{\psi_{AEV}}{\psi_1{}^*}\right)^{\lambda}(\psi-\psi_u) \qquad \text{for } \psi \geq \psi_{AEV}$$

$$\left(\frac{\theta_{ew}}{\theta_{AEV,mwc}}\right)=\left(1+\lambda-\lambda\frac{\psi}{\psi_{AEV}}\right)+\frac{\lambda}{\psi_1^{*}}\left(\frac{\psi_{AEV}}{\psi_1^{*}}\right)^{\lambda}(\psi-\psi_u) \qquad \text{for } \psi_u \leq \psi \leq \psi_{AEV}$$

Where:

λ constant defined by Brooks and Corey, ψ_u water entry pressure and the moisture content at the air entry value can be defined as:

$\theta_{AEV}=\dfrac{\theta_s}{\left(1+\lambda-\lambda\dfrac{\psi_{wAEV}}{\psi_{AEV}}\right)}$, $\theta_{AEV,mwc}$ water content on the MWC corresponding to the pressure as the AEV

Luckner

$$\Theta=\frac{(\theta-A)}{(\phi-A-B)}=\left[\frac{1}{1+(\alpha\psi)^{n}}\right]^{m}, \quad m_w = 1-\frac{1}{n_w}$$

$$\mathrm{A}_w=\frac{\phi-\theta_{ar}-\theta_{w0}\left[1+(\alpha_w\psi_0)^{n_w}\right]^{m_w}}{\left\{1-\left[+(\alpha_w\psi_0)^{n_w}\right]^{m_w}\right\}}$$

$$\Theta=\frac{(\theta-A)}{(\phi-A-B)}=\left[\frac{1}{1+(\alpha\psi)^{n}}\right]^{m}, \quad m_d=1-\frac{1}{n_d}$$

$$B_d=\phi-\theta_f-(\theta_{w,0}-\theta_f)\left[1+(\alpha_d\psi_0)^{n_d}\right]^{m_d}$$

where:

Θ normalized volumetric water content, dimensionless *A, B* scaling factors, θ_f terminal residual volumetric water content for the wetting fluid (water), θ_{ar} residual volumetric water content for the non-wetting fluid (air) , α, n, m constants affecting the shape of the SWRC, ϕ porosity, θ_w volumetric fluid content (water and air).

APPENDIX 3

RELEVANT PAGES FROM ICFEP USER'S MANUAL

MODEL 82 : Partially Saturated 3D Mohr Coulomb

YIELD SURFACE

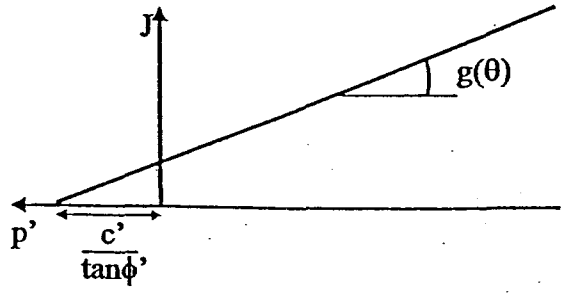

Note: Tension +ve convention

$$F(\sigma) = \frac{J}{(\frac{c'}{\tan\phi'} - p').g(\vartheta)} - 1 = 0 \qquad g(\vartheta) = \frac{\sin\phi'}{\cos\vartheta + \frac{\sin\vartheta.\sin\phi'}{\sqrt{3}}}$$

PLASTIC POTENTIAL (FLOW RULE)

An angle of dilation is specified and the shape of the plastic potential in the deviatoric plane is again given by a hexagon.

BULK MODULUS ASSOCIATED WITH SUCTION CHANGES

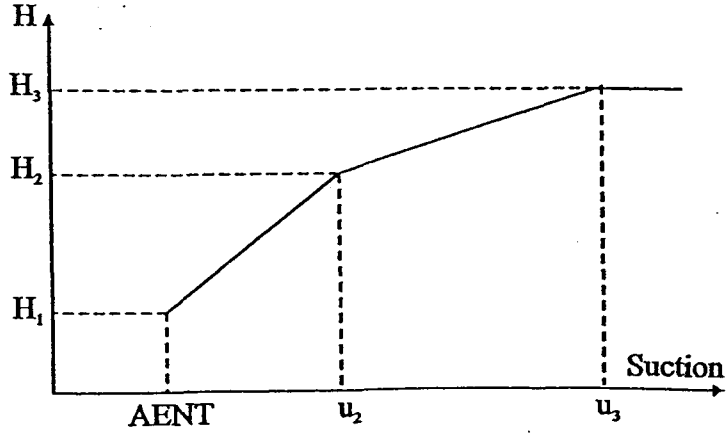

DATA CARD ENTRIES

MNOS	82.0		
P2	c'	Cohesion	
P3	ϕ'	Angle of shearing resistance	
P4	υ	Angle of dilation	
P5	AENT	Air entry suction	
P6	H1	Bulk modulus at AENT	≥0
P7	U2	Suction value 2	>AENT
P8	H2	Bulk modulus at U2	>0
P9	U3	Suction value 3	>U2
P10	H3	Bulk modulus at U3	>0
P11	TIPTOL	Apex tolerance	

Note: A minimum of ten parameters must be specified

ADDITIONAL PARAMETERS CALCULATED BY ICFEP

P27	cos(ϕ')
P28	sin(v)
P29	sin(ϕ')
P30	tan(ϕ')

NOTES

1. A tension positive convention is adopted in the program, i.e. +ve values refer to tensile quantities. However parameters should be input assuming a compression +ve sign convention. The program will make the appropriate conversions necessary for the tension +ve sign convention that it adopts.

3. If the stress state approaches the apex of the yield surface it will be pushed back to the point A in the diagram below (i.e it will be pushed back a distance of TIPTOL from the apex). This prevents:
   a) the singularity of the apex causing problems, especially with the flow steps.
   b) the stress state flipping onto the mirror image of the yield surface.

   TOL is not specified or is set to 0.0 a default TIPTOL=TOLY*J_{inc} is assumed.

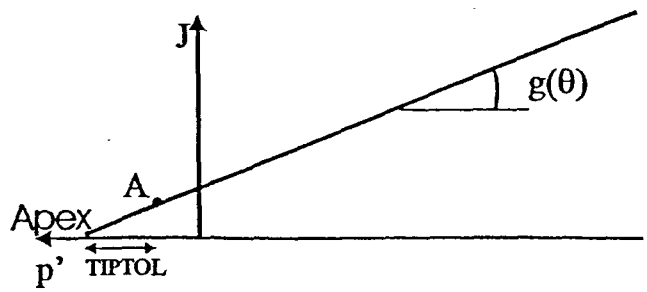

MODEL 1 : NO VARIABLE PERMEABILITIES - De-saturation and/or Dessication

If a particular material belongs to elements that are not consolidating then this option should be chosen. Likewise, for a consolidating element in which the permeabilities are constant and given in the *SEEPAGE PROPERTIES module then this option is appropriate. For consolidating solid elements this option also allows the permeabilities to be changed when de-saturation (i.e. tensile pore pressures (suctions) are encountered) and/or dessication(i.e. tensile principal total stresses are encountered) occurs. This enables the program to deal with 'phreatic surfaces' and/or tensile cracks.

De-Saturation

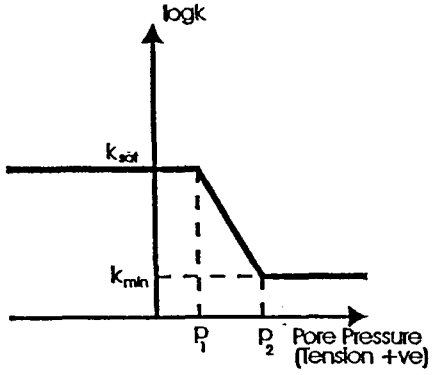

$$\log k = \log k_{sat} - \frac{(p-p_1)}{(p_2-p_1)} \log \frac{k_{sat}}{k_{min}}$$

Dessication

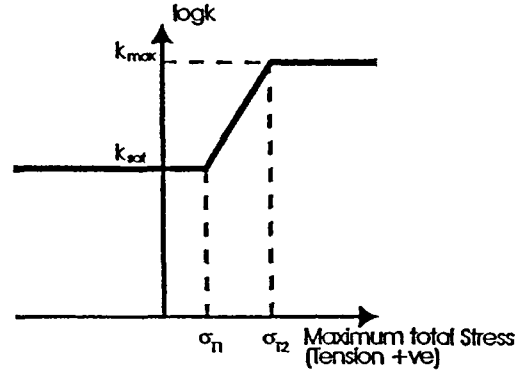

$$\log k = \log k_{sat} + \frac{(\sigma_t-\sigma_{t1})}{(\sigma_{t2}-\sigma_{t1})} \log \frac{k_{max}}{k_{sat}}$$

DATA CARD ENTRIES

Basic Model : For joint, beam, bar and membrane elements and for non-consolidating solid elements. Also for consolidating solid elements which have constant permeabilities (given in *SEEPAGE PROPERTIES module)

MNOS = 1.0 model number

De-saturation Model: For consolidating solid elements having an abrupt change in permeability when tensile pore water pressures encountered.

MNOS	= 1.0	model number
P2	= 1.0	de-saturation switch
P3	= P_1	pore pressures at which permeability begins to change (see figure above)
P4	= P_2	pore pressure at which permeability completes its change (see figure above)
P5	= RATIOS = k_{sat}/k_{min}	(see figure above)

Dessication Model: For consolidating solid elements having an abrupt change in permeability when tensile principal total stresses are encountered

MNOS	= 1.0	model number
P2 - P5	= 0.0	
P6	= 1.0	dessication switch
P7	= σ_{T1}	maximum total principal stress (tension +ve) at which permeability begins to change (see figure above)
P8	= σ_{T2}	maximum total principal stress (tension +ve) at which permeability completes its change (see figure above)
P9	= RATIOT = k_{max}/k_{sat}	(see figure above)

Full Model: For consolidating solid elements having an abrupt change in permeability when either tensile pore water pressures and/or tensile principal total stresses are encountered

MNOS	= 1.0	model number
P2	= 1.0	de-saturation switch
P3	= P_1	pore pressures at which permeability begins to change (see figure above)
P4	= P_2	pore pressure at which permeability completes its change (see figure above)
P5	= RATIOS = k_{sat}/k_{min}	(see figure above)
P6	= 1.0	dessication switch
P7	= σ_{T1}	maximum total principal stress (tension +ve) at which permeability begins to change (see figure above)
P8	= σ_{T2}	maximum total principal stress (tension +ve) at which permeability completes its change (see figure above)
P9	= RATIOT = k_{max}/k_{sat}	(see figure above)

ADDITIONAL NOTES

1. For non-consolidating solid elements and for joint, beam, bar and membrane elements the basic model with only MNOS set to 1.0 should be used.

2. For consolidating solid elements which have constant permeabilities that do not change throughout the analysis the basic model with MNOS set to 1.0 should be used. In this case the permeabilities are taken from the *SEEPAGE PROPERTIES module.

3. If the de-satuartion model is being used (i.e desaturation switch = 1.0) the permeabilities are assumed to be those specified in the *SEEPAGE PROPERTIES module unless the pore

water pressure increases above (tension +ve) P_1. If this occurs then all the components of saturated permeability are reduced in accordance with the equation given above. If the pore water pressure increases above P_2 then all saturated permeability components are *divided* by RATIOS. This option enables the abrupt reduction in permeability that occurs on desaturation to be modelled. Using this option the program can simulate the development of a 'phreatic surface'.

4. If the dessication model is being used (i.e dessication switch = 1.0) the permeabilities are assumed to be those specified in the *SEEPAGE PROPERTIES module unless the maximum total stress (tension +ve) increases above σ_{T1}. If this occurs then all the components of saturated permeability are increased in accordance with the equation given above. If the maximum total stress increases above σ_{T2} then all saturated permeability components are *multiplied* by RATIOT. This option enables the abrupt increase in permeability that occurs on dessication to be modelled. Using this option the program can simulate the behaviour associated with tension cracks.

5. If the full model is being used dessication has preference over de-saturation. That is the program makes the decision on whether or not dessication is occurring before investigating whether de-saturation occurs. This implies that if dessication occurs after de-saturation then the permeability will be increased according to the data input for dessication.

MODEL 2 : SIMPLE NON-HYSTERETIC

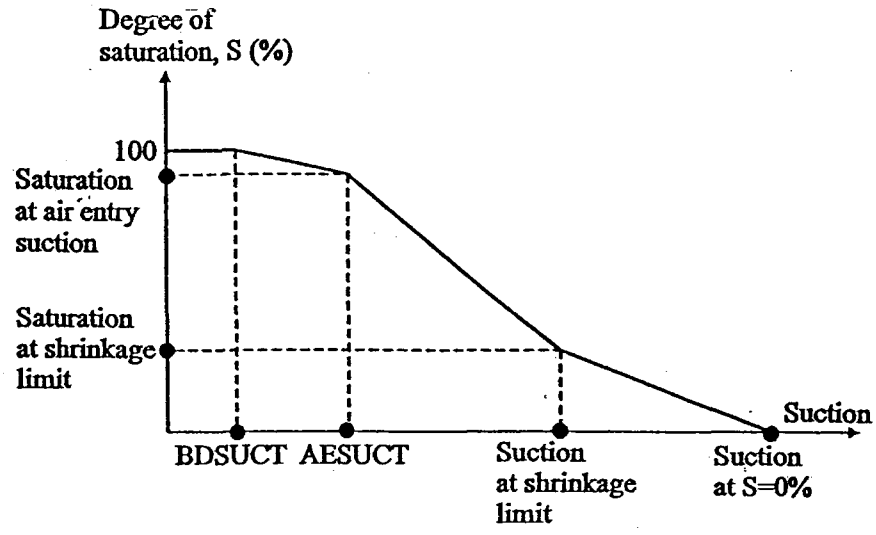

DESCRIPTION

In this model the above non-hysteretic soil characteristic curve is assumed for both drying and wetting.

DATA CARD ENTRIES

MNOS	2.0	model number
P2	BDSUCT	Suction at the beginning of desaturation
P3	S_{ae}	Degree of saturation at air entry
P4	AESUCT	Air entry suction
P5	S_{sl}	Degree of saturation at shrinkage limit
P6	U_{sl}	Suction at shrinkage limit
P7	U_0	Suction in long term (0% saturation)
P8	OMSUCT	Suction at which Ω becomes zero

ADDITIONAL NOTES

1. The parameter Ω appears in the cross coupling (bottom left) and the main consolidation (bottom right) sub matrices of the partly saturated coupled consolidation stiffness matrix. It is assumed to be 1.0 for suctions smaller than the air entry value (AESUCT), to vary linearly from 1.0 at the air entry value (AESUCT) to 0.0 at the transition suction (OMSUCT) for suctions between AESUCT and OMSUCT, and to be 0.0 for suctions grater than OMSUCT. The program checks that OMSUCT>AESUCT.

MODEL 3: SIMPLE NON-HYSTERETIC NON-LINEAR MODEL

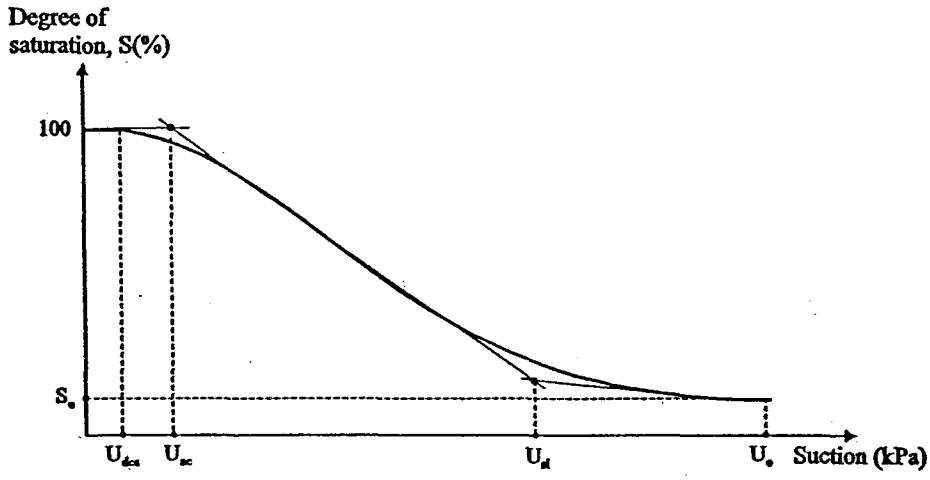

DESCRIPTION

In this model the above non-hysteretic and non-linear soil water characteristic curve is assumed for both drying and wetting. The equation that defines this curve is as follows:

$$S = \left[\frac{1}{1+[(U-U_{des})\alpha]^n}\right]^m \cdot (1-S_o) + S_o$$

The slope of the curve at any point is defined as:

$$R = \frac{\partial S}{\partial U} = -mn\alpha(1-S_o)\frac{[(U-U_{des})\alpha]^{n-1}}{\left[1+[(U-U_{des})\alpha]^n\right]^{m+1}}$$

DATA CARD ENTRIES

MNOS	3.0	Model number
P2	U_{dcs}	Suction at the beginning of de-saturation
P3	U_{ac}	Suction at air-entry value
P4	U_o	Suction in long term
P5	S_o	Degree of saturation in long term
P6	ALFA	α - fitting parameter (see note 2)
P7	N	n - fitting parameter
P8	M	m - fitting parameter
P9	U_Ω	Suction at which Ω becomes zero

Optional:

P10	U_{sl}	Suction at shrinkage limit. If not set, this will be automatically set equal to P4. This may cause a warning message if this value is not compatible with the value set in model 82.

ADDITIONAL NOTES

1. The parameter Ω appears in the cross-coupling (bottom left) and main consolidation (bottom right) sub-matrices of the partially saturated coupled consolidation stiffness matrix. It is assumed to be 1.0 for suctions smaller than the air entry value (U_{ac}), to vary linearly from 1.0 at the air entry value to 0.0 at the transition suction (U_Ω) for suctions between U_{ca} and U_Ω, and to be 0.0 for suction greater than U_Ω. The program checks that $U_\Omega > U_{ac}$.

2. The dimensions of α have to be compatible with the dimensions of pore pressure, so that the product $[(U-U_{dcs})\alpha]$ in the above equation becomes non-dimensional. This implies $\alpha=[m^2/kN]$. The other two fitting parameters n and m are non-dimensional.
If the fitting of data is done in terms of a S-U diagram, then α will automatically have appropriate dimensions. However, if data fitting is done in terms of a S-h diagram (i.e. suction vs. pressure head), then α will have dimensions of [1/length]. This value first has to be converted into units of [1/m] (if the head was not in metres), and then divided by γ_w (i.e. $9.81 kN/m^3$).